CNP-dependent cGMP signalling in vascular smooth muscle cells: from phenotypic plasticity to atherosclerosis

Dissertation
der Mathematisch-Naturwissenschaftlichen Fakultät
der Eberhard Karls Universität Tübingen
zur Erlangung des Grades eines
Doktors der Naturwissenschaften
(Dr. rer. nat.)

vorgelegt von
Moritz Lehners
aus Herrenberg

Tübingen
2022

Gedruckt mit Genehmigung der Mathematisch-Naturwissenschaftlichen Fakultät der Eberhard Karls Universität Tübingen.

Tag der mündlichen Qualifikation:	22.06.2022
Dekan:	Prof. Dr. Thilo Stehle
1. Berichterstatter:	Prof. Dr. Robert Feil
2. Berichterstatter:	Prof. Dr. Robert Lukowski

Zusammenfassung

Atherosklerose ist eine chronische Entzündung der mittelgroßen und großen Arterien mit potenziell tödlichem Ausgang. Sie zeichnet sich durch pathologische Umbildungen der Gefäßwände aus („atherosklerotische Plaques“). Arterielle Gefäßwände bestehen zu großen Teilen aus vaskulären Glattmuskelzellen („vascular smooth muscle cells“, VSMCs). Die Kontraktion und Relaxation von VSMCs ist unverzichtbar für die Regulation von Gefäßtonus und Blutfluss. VSMCs in gesunden Arterien sind ruhende Zellen mit einem stark ausgeprägten Kontraktionsapparat. Werden Gefäße jedoch verletzt oder unterliegen Erkrankungen wie Atherosklerose, verändern VSMCs ihren Phänotyp von einem kontraktilen zu einem modulierten Phänotyp. Modulierte VSMCs besitzen viele Organellen, die an der Proteinsynthese beteiligt sind, exprimieren aber nur geringe Mengen kontraktiler Proteine. Diese Veränderung von einem kontraktilen zu einem modulierten Phänotyp wird als „phänotypische Modulation bezeichnet“ und ist an der Bildung atherosklerotischer Plaques beteiligt.

Atherosklerotische Plaques zeichnen sich durch Anreicherung von Fetten, Immunzellen und modulierten VSMCs unterhalb des Endothels aus. Zum einen stabilisieren VSMCs Plaques, indem sie eine fibrotische Kappe synthetisieren, die reich an extrazellulärer Matrix ist. Zum anderen übernehmen sie Charakteristika anderer Zelltypen (z.B.: Makrophagen, Fibroblasten) und tragen zum Wachstum von Plaques bei. Der sekundäre Botenstoff zyklisches Guanosin-3‘,5‘-Monophosphat (cGMP) spielt eine zentrale Rolle in der (Patho-)Physiologie von VSMCs. Es gibt mehrere Guanylylzyklasen (GCs), die cGMP generieren. NO aktiviert die zytosolische NO-sensitive GC (NO-GC). Atriales natriuretisches Peptid (ANP) und C-Typ natriuretisches Peptid (CNP) hingegen aktivieren membran-gebundene partikuläre GCs. ANP aktiviert GC-A und CNP GC-B. Neben der allgemein anerkannten Funktion von cGMP Glattmuskelzellen zu relaxieren, ist auch beschrieben, dass es die phänotypische Modulation von VSMCs beeinflussen kann. Zum Beispiel wurde mit Hilfe genetisch veränderter Mäuse gezeigt, dass die cGMP-Signalgebung in VSMCs Atherosklerose fördern kann. Es ist bekannt, dass VSMCs in Zellkultur mit der Zeit vom kontraktilen zum modulierten Phänotyp wechseln. In Zellkultur wurde gezeigt, dass VSMCs cGMP erzeugen, wenn sie mit CNP, ANP oder NO stimuliert werden. Das führt zu der Frage, ob dieselbe Glattmuskelzelle auf alle drei Stimuli reagieren kann oder ob sich die cGMP-Antworten einzelner VSMCs aufgrund phänotypischer Modulation verändern und verschiedene Zellen in derselben Kultur schließlich auf verschiedene Stimuli reagieren.

Um die Erzeugung von cGMP in kultivierten VSMCs zu untersuchen, wurden in der vorliegenden Arbeit mit Hilfe des genetisch kodierten Förster-Resonanzenergietransfer (FRET) basierten cGMP-Indikators cGi500 cGMP Messungen durchgeführt. Es wurden VSMCs aus transgenen Mäusen verwendet, die cGi500 entweder global oder selektiv in Glattmuskelzellen exprimieren. NO-, CNP- und ANP-induzierte cGMP Signale wurden in VSMC-Kulturen in Echtzeit mit Einzelzellauflösung gemessen und in Kombination mit Immunfluoreszenzfärbungen und genetischen Ansätzen analysiert. Dadurch konnten wir eine Verbindung zwischen dem Phänotyp von VSMCs und ihren cGMP-Reaktionsmustern aufzeigen. In Kultur haben kontraktile VSMCs stark auf ANP und NO, jedoch nur schwach oder gar nicht auf CNP reagiert. Modulierte VSMCs hingegen haben stark auf CNP, jedoch nur schwach oder gar nicht auf ANP reagiert. Auch die NO-abhängigen cGMP-Antworten waren in diesen Zellen abgeschwächt. Des Weiteren hat ein erhöhtes Alter der Mäuse zu vermehrter Bildung CNP-präferierender VSMCs in Kultur geführt.

Auf Grundlage dieser Entdeckungen haben wir untersucht, ob die Modulation von VSMCs in pathologisch veränderten Arterien die cGMP-Signalgebung auf ähnliche Weise beeinflusst wie in der Zellkultur. Dazu wurden cGMP/FRET-Messungen in isolierten Gefäßen von cGi500-exprimierenden Mäusen durchgeführt. Als Modell für kontraktile bzw. modulierte VSMCs wurden gesunde bzw. atherosklerotische Arterien untersucht. In gesunden Gefäßen wurde die Bildung von cGMP vor allem durch ANP und/oder NO ausgelöst. In atherosklerotischen Arterien wurden zusätzlich deutliche CNP-abhängige cGMP-Signale detektiert. Dies deutet darauf hin, dass sich die cGMP-Erzeugung bei pathologischen Gefäßumbildungen *in vivo*, ähnlich wie in Zellkultur, abhängig vom VSMC-Phänotyp ändert.

Schließlich haben wir die funktionelle Bedeutung der CNP-abhängigen cGMP-Signalgebung in modulierten VSMCs für die Entwicklung von Atherosklerose *in vivo* untersucht. Die genetische Deletion des CNP-Rezeptors GC-B in VSMCs von Mäusen hat die Struktur und Zusammensetzung der atherosklerotischen Plaques verändert. Mit Hilfe eines Reporter-basierten Ansatzes haben wir potenziell CNP-reaktive/modulierte VSMCs (Reporter-positive Zellen) in Plaques nachgewiesen. Das Ausschalten von CNP-abhängiger cGMP-Signalgebung in VSMCs hat zu Läsionen geführt, die mit modulierten (Reporter-positiven) Zellen angereichert waren und deren Kernregion eine verringerte α-Glattmuskelaktin (αSMA)-positive Fläche aufwies.

Zusammenfassend deuten diese Ergebnisse darauf hin, dass die CNP-abhängige cGMP-Signalgebung in VSMCs nicht nur ein neuer Marker für modulierte VSMCs in Kultur, als auch pathologisch veränderten Gefäßen *in vivo* ist, sondern auch den Beitrag von modulierten VSMCs zur Plaque-Entwicklung einschränkt. Die gezielte Manipulation der CNP-induzierten cGMP-Signalgebung in Plaque-assoziierten VSMCs könnte ein neuer Ansatz zur Therapie atherosklerotischer Erkrankungen sein.

Summary

Atherosclerosis is a chronic inflammatory disease of medium and large arteries with potentially deadly consequences. It is characterised by lesions derived from pathological remodelling of the vessel wall known as “atherosclerotic plaques”. The arterial vessel wall consists in large parts of vascular smooth muscle cells (VSMCs). Contraction and relaxation of VSMCs is essential for the regulation of vascular tone and blood flow. VSMCs in healthy arteries are quiescent cells with a well-developed contractile apparatus. Upon vascular injury or during vascular diseases like atherosclerosis they switch from a contractile to a modulated phenotype. Modulated VSMCs are rich in organelles involved in protein synthesis but express only low levels of contractile proteins. This change from a contractile phenotype to a modulated one is called “phenotypic modulation” and is involved in the development of atherosclerotic plaques.

Atherosclerotic plaques are characterised by subendothelial accumulation of lipids, immune cells, and modulated VSMCs. VSMCs stabilise plaques by synthesis of an extracellular matrix-rich fibrous cap but also acquire properties of other cell types (e.g., macrophages, fibroblasts) and thereby contribute to plaque growth. The second messenger 3’,5’-cyclic guanosine monophosphate (cGMP) plays a pivotal role in the (patho-)physiology of VSMCs. Several types of guanylyl cyclases (GCs) generate cGMP. Nitric oxide (NO) activates the cytosolic NO-sensitive GC (NO-GC). Atrial natriuretic peptide (ANP) and C-type natriuretic peptide (CNP) activate the membrane-bound particulate GC-A and GC-B, respectively. In addition to the well-established function of cGMP to induce smooth muscle relaxation, cGMP was also reported to influence phenotypic modulation of VSMCs. For instance, it was demonstrated via genetic mouse models that cGMP signalling in VSMCs can promote atherosclerosis. During cell culture, contractile VSMCs convert towards the modulated phenotype over time. It was demonstrated that cultured VSMCs generate cGMP upon stimulation with CNP, ANP, and NO. This raises the question as to whether an individual VSMC can respond to all three stimuli or whether VSMCs change their cGMP responses due to phenotypic modulation, and, in consequence, different cells in the same population react to different stimuli.

To investigate cGMP generation in cultured VSMCs, the genetically encoded Förster resonance energy transfer (FRET)-based cGMP indicator cGi500 was used in this work to perform cGMP measurements. VSMCs from transgenic mice that expressed cGi500 either globally or selectively in smooth muscle cells, were used. NO-, CNP- and ANP-induced cGMP signalling in VSMC cultures was analysed in real time with single-cell resolution in combination with immunofluorescence stainings and genetic approaches. This allowed us to draw connections between VSMC phenotypes and their cGMP response patterns. In culture, contractile VSMCs responded strongly to ANP and NO, but only weakly or not at all to CNP. Modulated VSMCs, in contrast, responded strongly to CNP but only weakly or not at all to ANP. These cells also exhibited attenuated NO-dependent cGMP responses. Furthermore, increased age of mice led to increased development of CNP-preferring VSMCs in culture.

Based on these findings, we investigated whether the modulation of VSMCs in pathologically remodelled arteries influences cGMP signalling in a similar way as in cell culture. Therefore, we performed cGMP/FRET measurements in isolated arteries of cGi500 expressing mice. As model for contractile and modulated VSMCs, healthy and atherosclerotic arteries were used, respectively. In healthy vessels, cGMP increases were mainly triggered by ANP and/or NO. In atherosclerotic arteries, we could also detect prominent CNP-dependent cGMP signals. This suggests that pathological vascular

remodelling *in vivo* leads to a similar phenotype-dependent modulation of cGMP in VSMCs as seen during cell culture.

Finally, we investigated the functional relevance of CNP-dependent cGMP signalling in VSMCs for development of atherosclerosis *in vivo*. Genetic deletion of the CNP receptor GC-B in murine VSMCs altered the structure and composition of atherosclerotic plaques. A reporter-based approach allowed us to identify potentially CNP-responsive/modulated VSMCs (reporter-positive cells) in plaques. Silencing of CNP-dependent cGMP signalling in VSMCs led to lesions with an increased number of modulated (reporter-positive) VSMCs and a reduced α-smooth muscle actin (αSMA)-positive area in the plaque core.

Altogether, these results imply that CNP-dependent cGMP signalling in VSMCs is not only a new marker for modulated VSMCs in culture as well as pathologically remodelled vessels *in vivo*, but also attenuates the contribution of modulated VSMCs to plaque development. Manipulation of CNP-induced cGMP signalling in plaque-associated VSMCs could be a new therapeutical approach to treat atherosclerotic disease.

Table of Contents

List of Abbreviations

αSMA	α-smooth muscle actin
aa	amino acid
a.u.	arbitrary unit
ANOVA	Analysis of variance
ANP	Atrial natriuretic peptide
ApoE	Apolipoprotein E
APS	Ammonium persulfate
ATP	Adenosine triphosphate
BF	Brightfield
BNP	B-type natriuretic peptide
BP	Band pass
bp	base pairs
BSA	Bovine serum albumin
BSA-PBS-T	BSA-PBS-Triton
CAG	Cytomegalovirus immediate early enhancer/chicken β actin/rabbit β-globin
cAMP	3',5'-cyclic adenosine monophosphate
CCD	Charge-coupled device
CFP	Cyan fluorescent protein
cGi	cGMP indicator
cGi500	cGMP indicator with an apparent EC_{50} of 500 nM
cGK	cGMP-dependent protein kinase
cGMP	3',5'-cyclic guanosine monophosphate
CNG	Cyclic nucleotide-gated
CNP	C-type natriuretic peptide
CRBP-1	Cellular retinol binding protein-1
Cre	Cyclisation recombination
DAB	3,3'-diaminobenzidene
dATP	2'-deoxyadenosine triphosphate
DCLP	Dichroic long pass
dCTP	2'-deoxycytosine triphosphate
DEA/NO	Diethylammonium (Z)-1-(N,N-diethylamino)diazen-1-ium-1,2-diolate
dGTP	2'-deoxyguanosine triphosphate
DMEM	Dulbecco's modified Eagle medium
DNA	2'-deoxyribonucleic acid
dNTP	2'-deoxynucleoside triphosphate
DTT	Dithiothreitol
dTTP	2'-deoxythymidine triphosphate
eCFP	enhanced cyan fluorescent protein
ECM	Extracellular matrix
EDTA	Ethylenediamine tetraacetate
EM-CCD	Electron-multiplying charge-coupled device
eNOS	endothelial NOS
eYFP	enhanced yellow fluorescent protein
FCS	Foetal calf serum
FOV	Field of view
FRET	Förster resonance energy transfer
FSP 1	Fibroblast specific protein 1
GAPDH	Glyceraldehyde 3-phosphate dehydrogenase
GC	Guanylyl cyclase
GMP	Guanosine monophosphate
GTP	Guanosine triphosphate
HDL	High density lipoprotein
HEPES	4-(2-hydroxyethyl)-1-piperazineethanesulfonic acid
HRP	Horseradish peroxidase
IB	Imaging buffer
IF	Immunofluorescence
IHC	Immunohistochemistry
iNOS	inducible NOS
KHD	Kinase homology domain
LDL	Low density lipoprotein
loxP	locus of crossing-over [X] of P1
LP	Long pass
MLC	Myosin light chain
mRNA	messenger RNA
na	not analysed
NDS	Normal donkey serum
NGS	Normal goat serum
nNOS	neuronal NOS
NO	Nitric oxide
NO-GC	NO-sensitive guanylyl cyclase
NOS	Nitric oxide synthase
NP	Natriuretic peptide
4-OHT	4-hydroxytamoxifen
pAb	primary antibody
PBS	Phosphate-buffered saline
PCR	Polymerase chain reaction
PDE	Phosphodiesterase
PDGFRα	Platelet-derived growth factor receptor α
PDMS	Polydimethylsiloxane
pGC	particulate gualnylyl cyclase
PMSF	Phenylmethylsulfonylfluoride
PVDF	Polyvinylidene fluoride
rcf	relative centrifugal force
RNA	Ribonucleic acid
ROI	Region of interest
Rosa26	Reverse orientation splice acceptor clone 26
RT	Room temperature
sAb	secondary antibody
SDS	Sodium dodecyl sulphate
SEM	Standard error of the mean

SM-MHC	Smooth muscle-myosin heavy chain
SM22α	Smooth muscle protein 22-α
SMC	Smooth muscle cell
SMemb	Smooth muscle embryonic
Smko	Smooth muscle knockout
SNR	Signal-to-noise ratio
TAE	Tris-acetate-EDTA
TBE	Tris-borate-EDTA
TBS	Tris-buffered saline
TBS-T	TBS-Tween
TE	Tris-EDTA
TEMED	N,N,N',N'-Tetramethylethylendiamin
Tris	Tris(hydroxymethyl)-aminomethane
VSMC	Vascular smooth muscle cell
X-gal	5-Bromo-4-chloro-3-indolyl-β-D-galactopyranoside
YFP	Yellow fluorescent protein

1 Introduction

1.1 cGMP signalling with a focus on the vascular system

3',5'-cyclic guanosine monophosphate (cGMP) is an intracellular second messenger with diverse (patho-)physiological functions. It was first discovered in mammals [1] and a functional role of cGMP has also been reported in insects, parasites [2] and even plants [3]. In mammals it exerts its functions via various cell types, including but not limited to smooth muscle cells (SMCs), platelets, neurons and fibroblasts [2]. In the vascular system, cGMP regulates SMC contractility, blood pressure and thrombus formation [2; 4]. In the nervous system, it is important for phototransduction and nociception [2]. In the kidney and intestine, it controls secretory processes, and for various cell types an influence on proliferation and differentiation was described [2; 5].

Despite its pivotal role in mammalian physiology and its plethora of functions, cGMP was discovered just about 60 years ago and it took several decades to identify further key components of this pathway [1]. In mammals, two types of guanylyl cyclases (GCs) are known to generate cGMP from GTP: the cytosolic nitric oxide (NO)-sensitive GCs (NO-GCs, formerly known as "soluble GCs" or "sGCs") and the transmembrane "particulate" GCs (pGCs) [1; 6]. NO-GCs generate cGMP upon binding of NO [7-9] that can be generated by NO synthases (NOSs) [10]. In mammals, seven cGMP-generating pGCs (GC-A to GC-G) are known that can be stimulated by various intra- and extracellular stimuli [1]. The most important pGCs in the cardiovascular system (GC-A and GC-B) are stimulated by peptide hormones that can be secreted from the heart and various other tissues. GC-A (gene name: Npr1) binds preferentially atrial (ANP) and B-type natriuretic peptide (BNP, formerly known as "brain natriuretic peptide"). GC-B (gene name: Npr2), in contrast, is selectively activated by C-type natriuretic peptide (CNP) [11; 12]. For the remaining pGCs (GC-C to GC-G), intracellular proteins, bicarbonate or even temperature were described to stimulate cGMP generation in addition to peptide hormones [1]. cGMP exerts its effects upon binding to three classes of proteins: cyclic nucleotide-gated (CNG) cation channels [13], cGMP-dependent protein kinases (cGKs) [14] and cGMP-regulated phosphodiesterases (PDEs) [15]. While the latter two are expressed in various mammalian tissues [14; 15], convincing evidence for a function of CNG channels outside of the sensory system is lacking [13]. The actions of cGMP are terminated by its degradation to 5'-GMP via cGMP-hydrolysing PDEs [16] or via export of cGMP into the extracellular space [17-19].

Many mechanistic details and physiological functions of the cGMP signalling pathway were investigated *in vitro* or in various animal models. Especially the genetic or pharmacological manipulation of the cGMP signalling pathway in animals indicated a pivotal role of cGMP in the development and therapy of various diseases [20]. Nonetheless, there are known differences in disease development between animals and humans (e.g., atherosclerosis [21]) and even in the cGMP signalling pathway itself [22; 23]. For example, in murine platelets weak expression of the cGKIα isoform was detected in addition to the cGKIβ isoform while human platelets only express the latter [22]. Therefore, the translation of findings from animal models to the human situation is essential.

Nevertheless, the pivotal role of cGMP in human (patho-)physiology is widely accepted. This is reflected by the vast number of clinically used drugs that target different components of the cGMP signalling pathway [24]. All started with the treatment of angina pectoris by the NO-generating drug nitro-glycerine (increases cGMP in the vessel wall) more than one hundred years ago [25]. Nowadays,

the cGMP signalling pathway is not only manipulated via NO-generating compounds. For more than two decades, selective PDE 5 inhibitors like sildenafil (later also tadalafil and other -afils) have been used to treat erectile dysfunction [26; 27]. PDE 5 inhibitors are also used to treat pulmonary hypertension, but their efficiency is limited when NO-induced cGMP production is low [28]. Since 2013, riociguat, a NO-GC stimulator, has been used to treat various forms of pulmonary hypertension, including situations of low NO bioavailability [28; 29]. Not only NO-dependent cGMP signalling is targeted to treat cardiovascular diseases. The combination drug LZC696 was approved a few years ago for treatment of patients with heart failure [30]. LZC696 combines an angiotensin receptor blocker (valsartan) with an inhibitor of the neutral endopeptidase neprilysin (sacubitril) [31]. As the ectoenzyme neprilysin degrades natriuretic peptides (NPs) [32], its inhibition increases NP-dependent cGMP. While best known for their cardiovascular effects, cGMP-elevating drugs are also used to treat other diseases. The CNP analogue vosoritide, for instance, had a positive effect on annual growth velocity in children with achondroplasia [33; 34] and was recently approved for treatment of this disease [35]. Several other cGMP manipulating drugs are currently used in the clinics and considering the huge quantity of clinical trials [24; 27; 36], the number of diseases treated by cGMP-modulating drugs will certainly increase in the near future.

One reason for the successful treatment of vascular diseases with drugs that manipulate the cGMP signalling pathway is the pivotal role of vascular smooth muscle cells (VSMCs) in these diseases.

1.2 cGMP signalling in VSMCs

The cGMP signalling system is a key player in VSMC physiology. For instance, NO-dependent cGMP generation is an important regulator of vascular tone via relaxation of VSMCs [4]. VSMCs are reported to express many components of the cGMP signalling pathway. The most robust data suggests that VSMCs can express **GC-A** [37], **GC-B** [38], **NO-GC** [39], **cGKIα/β** [40] and their major cGMP-degrading PDE is **PDE 5** [17] (**Figure 1**). Except for PDE 5, this data is based on studies that investigated the (functional) expression of cGMP signalling components in healthy murine vessels, optimally by SMC-selective genetic ablation experiments. It is likely that the exact composition of the cGMP signalling tool kit can differ between VSMCs of different vascular beds (e.g., see reference [41]) or possibly even between individual VSMCs of the same vascular bed (see this work). Interestingly, functional expression of GC-A in murine VSMCs was proven in various vascular beds [37], whereas functional expression of GC-B in murine VSMCs was only investigated in mesenteric arteries [38]. In the latter study, the only indications for expression of GC-B in aortic VSMCs was provided at the mRNA level [38].

1.2.1 Generation of cGMP

The cGMP-inducing molecule NO is an important signalling molecule in the vasculature [4], but the exact physiological concentration range is still not clear [42]. Most likely the physiologically functional concentration of NO lies between 100 pM and 5 nM [42]. NO generated by the endothelial NOS (eNOS) and neuronal NOS (nNOS) is important for vascular physiology [10; 43]. These constitutively expressed isoforms of NOS generate NO from L-Arginine in a Ca^{2+}/Calmodulin-dependent manner [10]. Under inflammatory conditions the constitutively active inducible NOS (iNOS) [44] can be expressed in a plethora of cell types (e.g., SMCs, leukocytes, and fibroblasts) [45] and thereby contribute to NO synthesis. It should be noted that the different isoforms of NOS do not only differ in their expression pattern and regulation but also in their catalytic activity [46] and NO output [45].

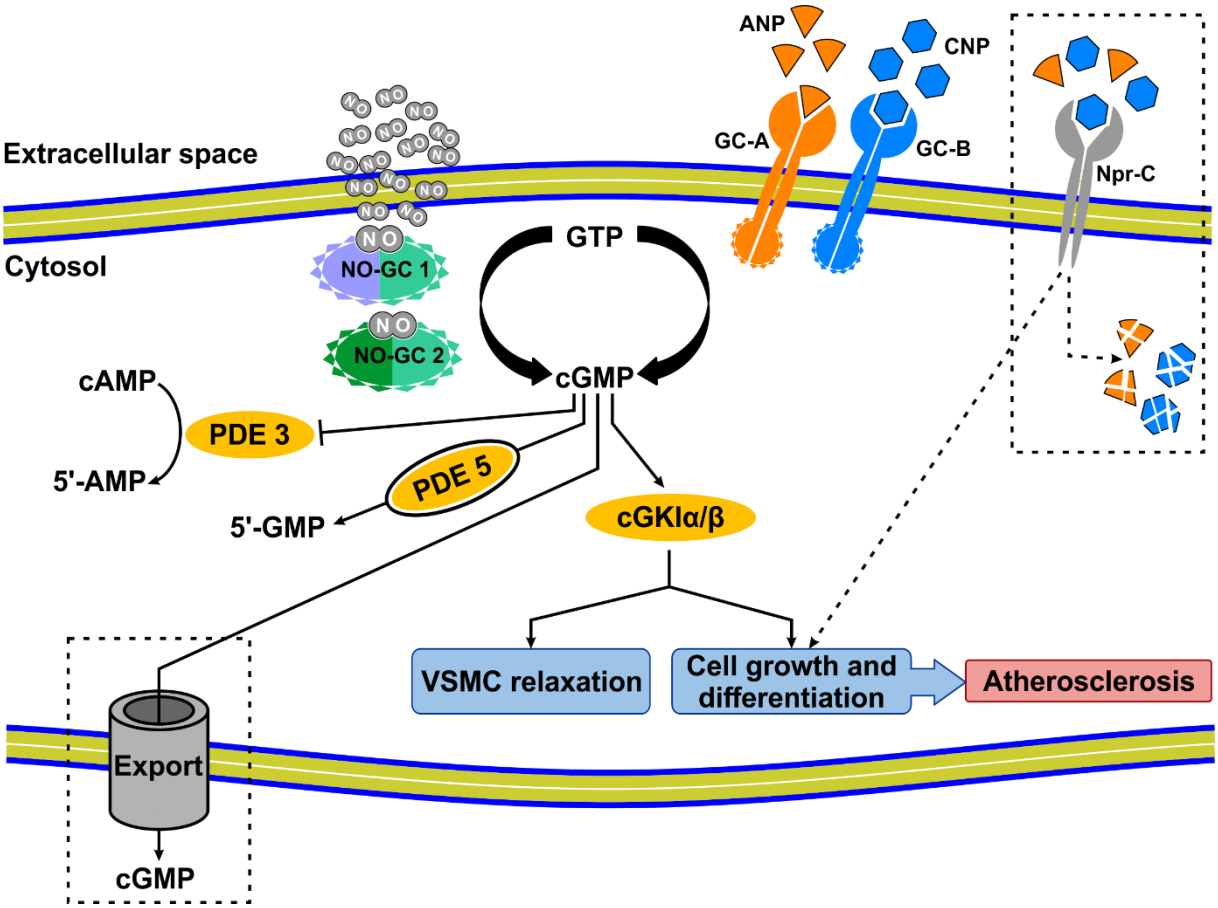

Figure 1: cGMP signalling in VSMCs. *Shown are components that are involved in cGMP signalling in VSMCs. Pointed arrowheads indicate stimulatory actions, flat arrowheads indicate inhibitory actions, and dashed lines indicate that expression or function in VSMCs of healthy arteries in vivo needs to be validated. ANP: atrial natriuretic peptide, 5'-AMP: 5'-adenosine monophosphate, cAMP: 3',5'-cycic adenosine monophosphate, cGKIα/β: cGMP-dependent protein kinase α/β, cGMP: 3',5'-cyclic guanosine monophosphate, CNP: C-type natriuretic peptide, GC-A/B: guanylyl cyclase-A/B, 5'-GMP: 5'-guanosine monophosphate, NO: nitric oxide, NO-GC 1/2: NO-sensitive guanylyl cyclase 1/2, Npr-C: natriuretic peptide receptor-C. PDE 3/5: phosphodiesterase 3/5, VSMC: vascular smooth muscle cell, For details see text.*

As soon as NO is generated it can diffuse freely through cells and tissues. It should be noted that the diffusion distance is limited by various NO-consuming processes leading to a half-life in the range of milliseconds to seconds *in vivo* [42]. The main receptors for NO are the cytosolic NO-GCs which generate cGMP from GTP. These receptors are expressed in the vasculature, lung, brain, and heart, to name a few [47]. NO-GCs are heterodimers, comprised of an α and β subunit which are both required for a catalytically active enzyme [48]. In mammals, two isoforms of the α and β subunit are known (α1, α2, β1, β2) that can build two different NO-GCs [49]; NO-GC 1 (α1β1) and NO-GC 2 (α2β1). The β2 subunit could not be detected at the protein level *in vivo* [48]. Functional characterisation of NO-GC 1 and NO-GC 2 led to the conclusion that their catalytical properties are similar [50]. They even co-exist in the vasculature with NO-GC 1 as the predominant form [51]. Upon binding of NO, the activity of NO-GC increases more than 100-fold [8]. The subsequent cGMP generation influences a wide range of processes. Most prominent in the vascular system are the induction of SMC relaxation [39], control of blood pressure [39] and inhibition of platelet aggregation [52].

Studies with genetically modified mice lacking one of the three physiologically relevant subunits (α1, α2, β1) led to interesting insights concerning the function and physiological relevance of NO-GC for

vascular homeostasis. Dimerization seems to be essential for the stability of NO-GCs. Ablation of one of the α subunits decreases the quantity of the β1 subunit and ablation of the β1 subunit leads to a complete loss of both α subunits [51; 53]. Global [53] or SMC-selective [39] NO-GC-deficient mice as achieved by ablation of the β1 subunit, are hypertensive and their vessels are unable to relax upon stimulation with NO. It was reported that global ablation of the NO-GC 1 or NO-GC 2 isoform, leads only to mild [51] or no hypertension [51], respectively. Interestingly, loss of NO-GC 1 can be partially compensated by NO-GC 2 as shown by relaxation experiments with aortic rings [51]. While it is still possible to relax aortic rings of NO-GC 1 knockout mice completely, the required amount of NO is significantly increased [51]. Importantly, several lines of evidence indicate that NO-dependent cGMP signalling is involved in the development of cardiovascular diseases [54-62] (see also 1.4). Nonetheless, when investigating NO-dependent cGMP signalling, one should be aware that NO can also act independently of cGMP, e.g. by S-nitrosylation of cysteine residues [63].

The most important membrane-bound cGMP generating pGCs in the cardiovascular system are GC-A and GC-B. Three different NPs – ANP, BNP, and CNP – can bind and stimulate cGMP generation by these pGCs with different affinities. ANP, BNP, and CNP have in common that they are synthesized as a full length "prepro" form that is cleaved several times to generate the biologically active mature form [64]. The processing of immature ANP and BNP requires the transmembrane ectoenzyme corin [1], whereas processing of immature CNP most likely involves the intracellular peptidase furin [65]. The mature NPs are composed of a 17 amino acids (aa) ring that is closed by a disulphide bond and is extended by short N- and C-terminal tails [66]. Mature ANP and CNP are highly conserved between species with CNP being the most conserved one [12; 66]. The mature forms in mice are α-ANP (28 aa), BNP-45 (45 aa) and CNP-22/CNP-53 (22 aa and 53 aa, respectively) [64; 67]. CNP-53 is the predominant form in tissues, whereas CNP-22 is the major circulating form [66]. Both forms of CNP show a similar biological activity [68]. To ease understanding, we will refer to the mature forms simply as "ANP", "BNP" and "CNP".

ANP and BNP are secreted mainly from the atrium under physiological conditions [1]. Muscle stretch or neurohormones lead to an increased release of these peptides [69]. While both peptides can act in an endocrine manner [70], there are indications for a paracrine function in the aorta and some further tissues [1]. CNP, in contrast, most likely acts primarily in a para- or autocrine manner [71]. This is supported by data showing that tissue levels of CNP can exceed plasma levels by several orders of magnitude [72]. The release of CNP is most likely regulated directly by its expression which was reported to be increased by inflammatory stimuli or shear stress [73]. Concerning the cardiovascular system, CNP expression was reported in cell culture models at least for endothelial cells [74-77], fibroblasts [78], and VSMCs [79-81]. At least for the first two cell types expression of CNP *in vivo* is validated by analysis of fibroblast-selective [82], and endothelial-selective [38; 83] CNP knockout mice. Interestingly, the studies investigating the effect of endothelial-selective CNP ablation on blood pressure and vessel relaxation came to similar but slightly different results. Both groups detected an increased blood pressure and reduced acetylcholine-induced relaxation of mesenteric arteries in female mice as well as decreased plasma CNP levels. Only the group of Nakao and colleagues detected an increased blood pressure in male mice [38]. As Moyes and colleagues measured the mean arterial blood pressure and Nakao and colleagues the mean systolic blood pressure, this might serve as an explanation. Together, these results indicate that endothelial cells, at least in female mice, are involved in CNP generation. For VSMCs, CNP expression in intact vessels was confirmed by immunohistochemical stainings of vessel sections from coronary artery bypass patients [79]. Therefore,

this data might not adequately reflect the physiological situation. Furthermore, to our knowledge no reliable antibodies for CNP detection in tissue sections exist.

ANP, BNP, and CNP are inactivated mainly via two different pathways. Either they are directly degraded by the ectopic neutral endopeptidase neprylisin [32] or they bind to the natriuretic peptide receptor-C (Npr-C, also called "clearance receptor") which leads to internalisation and subsequent degradation [84; 85]. These clearing mechanisms lead to a plasma half-life of the three peptides in the range of minutes [66]. Concerning Npr-C, there are indications that it is not only involved in the clearance of NPs but also in cGMP-independent signalling [86]. For instance, fragments of its cytoplasmic tail were shown to stimulate G-proteins (increased binding of radioactively labelled GTP by $G_i\alpha$ subunits) [87].

The three NPs can induce cGMP generation by binding to GC-A or GC-B. GC-A is the canonical receptor for ANP and BNP, whereas GC-B is the canonical receptor for CNP. Despite a high selectivity of GC-A/-B for the respective peptides, CNP can also activate GC-A, while ANP/BNP can also activate GC-B [11; 12; 88]. According to Suga and colleagues, the selectivity of the natriuretic peptide receptors for their peptides can be summarised as follows: GC-A: ANP ≥ BNP >> CNP, GC-B: CNP > ANP ≥ BNP [12]. The clearance receptor Npr-C binds all three peptides with high affinity but does not generate cGMP. **Table 1** summarises the dissociation constants as well as the EC_{50} values for GC-A, GC-B and Npr-C.

Table 1: Binding affinities and cGMP generation potential of natriuretic peptides for their physiological receptors. *The binding affinities are indicated by the dissociation constants (K_d, taken from [88]) and the cGMP generation potential by the EC_{50} values (taken from [12]). Lower values mean higher affinities/potentials. Values assessed for the human peptide are marked with "h", and values assessed with the rat peptide are marked with "r". If not otherwise indicated, receptors and peptides were species matched.*

	ANP		**BNP**		**CNP**	
Receptor	K_d	EC_{50}	K_d	EC_{50}	K_d	EC_{50}
GC-A	1.9 pM (h)	1.7 nM (h)[1] 2.9 nM (r)	7.3 pM (h)	1.5 nM (h)[1] 17.4 nM (r)	>0.5 µM (h)	>1 µM (h)[1] >1 µM (r)
GC-B	5.4 nM (h)	>1 µM (h) 926 nM (r)	30 nM (h)	>1 µM (h) >1 µM (r)	7 pM (h)	34.1 nM (h) 97 nM (r)
Npr-C	2.6 pM (h)	-	13 pM (h)	-	10.8 pM (h)	-

1) Data was acquired with the human peptide but a bovine cell line [12].

GC-A and GC-B act as homodimers. Each monomer of GC-A/B consists of an N-terminal extracellular ligand-binding domain, a transmembrane domain, an intracellular kinase homology domain (KHD) with regulatory functions, a homodimerization domain, and a C-terminal guanylyl cyclase domain [1]. The KHD is usually heavily phosphorylated at several serine (S) and threonine (T) residues which is a pre-requisite for NP-dependent activation of the dimeric receptors [89; 90]. Conversely, dephosphorylation of GC-A/B, caused by binding of their endogenous ligands [90; 91], artificial dephosphorylation [90; 91], or the mutation of S/T residues to alanine in the respective KHD [89; 92], desensitises the receptors. Experiments with genetically modified mice indicated that this regulatory mechanism, at least for GC-B, is relevant in (patho-)physiology [93; 94]. For instance, mice were generated that express a mutated GC-B that mimics the phosphorylated state of GC-B but cannot be dephosphorylated. To achieve this, seven regulatory S/T residues in the KHD of GC-B were mutated to the phosphomimetic amino acid glutamate (E) (Npr2-7E) [93]. Processes where dephosphorylation of GC-B is known to occur were altered in homozygous Npr2-7E mice [93; 94], indicating that this phosphomimetic mutant of GC-B is resistant to desensitisation.

GC-A is expressed in the cardiovascular system, the kidneys, adipose tissue, various glomerular cells, podocytes, SMCs, and endothelial cells of kidney, lung and heart [1; 37; 95]. GC-B is expressed in the cardiovascular system, the reproductive system, bone, brain, chondrocytes, fibroblasts, SMCs, and pericytes [1; 96-99]. GC-A/-B and Npr-C were detected in intact vessels [100; 101] or cultured VSMCs [17; 102; 103] either by responses to ANP and CNP or on the mRNA level. Nonetheless, the exact expression patterns of GC-A/-B and Npr-C are still not completely understood.

The ANP/GC-A system controls blood pressure and volume chronically (e.g., via natriuresis and diuresis). It can induce acute blood pressure drops via SMC relaxation and attenuates cardiac hypertrophy [1]. Mice lacking either ANP or GC-A globally are chronically hypertensive and show cardiac hypertrophy [104; 105]. Interestingly, these effects are not based on ANP-dependent cGMP signalling in SMCs. Endothelial-selective ablation of GC-A is sufficient to induce chronic hypertension and cardiac hypertrophy without affecting vessel relaxation [95]. Deletion of GC-A in SMCs, in contrast, impairs relaxation of aortas, pulmonary arteries and renal resistance arteries, without affecting chronic blood pressure [37]. As acute drops in blood pressure due to ANP infusion or volume overload are prevented in mice that lack GC-A in SMCs, GC-A dependent cGMP signalling in SMCs seems to be important for acute adaptations of blood pressure.

CNP can cause vasodilation and regulate blood pressure as well, but whether this is GC-B dependent or not seems to change with species and vessel type [1; 71]. A chronic GC-B-dependent increase of systolic blood pressure in mice has been reported after deletion of GC-B in pericytes and precapillary arteriolar SMCs [99]. The chronic elevation in blood pressure of female mice after genetic ablation of CNP in the endothelium [38; 83] appears to be unrelated to GC-B in SMCs as mice with SMC-selective ablation of GC-B are normotensive [38]. Interestingly, CNP-induced relaxation of mesenteric arteries and acute drops in blood pressure involve GC-B expression in SMCs [38]. CNP-induced relaxation of capillaries and pre-arteriolar capillaries relies on GC-B as well [99]. In contrast to cell type-selective deletions of CNP/GC-B, no altered blood pressure has been reported after systemic deletion of CNP [106] or GC-B [97]. A pathologically changed blood pressure in mice that lack CNP or GC-B globally might be occluded by the severe phenotypes of these mice (e.g., dwarfism, reduced life span). CNP-dependent effects that cannot be attributed to GC-B, might be mediated via Npr-C. For example, a recent elaborate study combined pharmacological approaches with genetic mouse technology to demonstrate that the pro-angiogenic effect of CNP relies on Npr-C and not GC-B [107].

Together with pharmacological studies, these studies corroborate an important role of NPs in the vascular system. ANP and CNP exert vasodilating effects throughout the vascular tree (resistance and conduit arteries) [37; 71; 108], either via GC-A/B or potentially via Npr-C. In mice, GC-A and GC-B can be functionally expressed in SMCs of healthy vessels (GC-A: renal resistance arteries, pulmonary arteries, aorta; GC-B: mesenteric arteries) [37; 38; 108] and in cultured VSMCs [17; 102]. Notably, various variants of genes of the NP/pGC system or mutations in their promoter regions were associated with hypertension and heart disease in humans [1].

1.2.2 Mediation of cGMP effects

In VSMCs, cGMP exerts its effects mainly via cGKs and cGMP-regulated PDEs. There are indications that the third class of cGMP effector proteins, CNG cation channels, might play a role in VSMCs [109; 110], but convincing evidence for a function of CNG cation channels outside of the sensory system is

lacking [13]. CNG cation channels allow cations like Na^+, K^+ and/or Ca^{2+} to pass upon binding of cyclic nucleotides, thereby transducing cyclic nucleotide levels into ion currents [13].

cGKs (also known as PKGs) belong to the class of serine/threonine kinases, hence mediate cGMP effects via phosphorylation of their target proteins [14]. In mammals there exist three different cGKs: Two isoforms of cGKI (cGKIα, cGKIβ) and cGKII. All three enzymes act as homodimers. They dimerise via an N-terminal leucine zipper, contain a tandem cGMP-binding domain and a C-terminal catalytic domain [14; 111]. In their cGMP-free state, an autoinhibitory/pseudo substrate domain inhibits catalytic activity [14]. Upon binding of cGMP, the enzymes are activated and increase their activity. cGKIα/β are cytosolic enzymes that only differ in their N-terminal part [112; 113]. The N-terminus has an important function in dimerization [14; 114]. Additionally, the N-terminus interacts with substrates and therefore contributes to substrate specificity of the isozymes [115; 116]. The different N-termini also affect the affinity of cGKIα/β for cGMP [117]. This results in a 20-fold higher activation constant of cGKIβ vs. cGKIα (1748 nM vs. 77 nM) for cGMP [118]. Interestingly, in SMCs which express high levels of both isoforms, cGKIα/β can compensate for each other at the functional level [40]. In the cardiovascular system, expression of cGKI was also reported in the heart, endothelium, and platelets [14]. The contribution of each isoform to the cGKI pool varies strongly between different tissues/cell types [119]. To our knowledge, cGKII is not expressed in VSMCs. In the vasculature, cGKI plays an essential role in the acute cGMP-dependent SMC relaxation (**Figure 2**) [40].

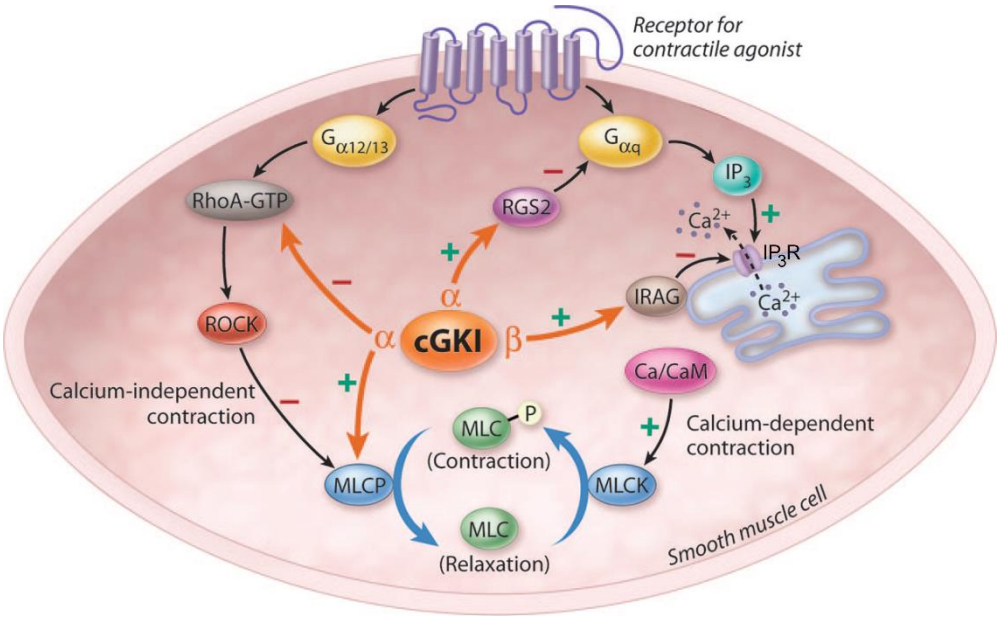

Figure 2: Mechanisms of cGKI-dependent SMC relaxation. *cGKI induces SMC relaxation via inhibition of Ca^{2+} release from the sarcoplasmic reticulum, promotion of MLCP activity, inhibition of Ca^{2+} release from the extracellular space (not shown) and promotion of active export of Ca^{2+} from the cytosol (not shown). Stimulatory actions are indicated by a "+" and inhibitory by a "-". ROCK: rho-associated, coiled-coil-containing protein kinase, cGKI: cGMP-dependent protein kinase I, MLC: myosin light chain, MLCK: MLC kinase, MLCP: MLC phosphatase, CaM: calmodulin, RGS 2: regulator of G protein signalling 2, IP_3: inositol 1,4,5-trisphosphate, IP_3R: inositol 1,4,5-trisphosphate receptor, IRAG: IP_3R-associated cGK substrate. Adapted from [120].*

SMC relaxation is essentially the reversal of contraction [121]. The contraction of SMCs revolves around the phosphorylation state of the regulatory myosin light chain (MLC) [122]. Ca^{2+}-dependent phosphorylation of MLC by MLC kinase allows ATP-dependent cross-bridge cycling between actin and myosin which leads to contraction. Conversely, Ca^{2+}-independent dephosphorylation of MLC by

MLC phosphatase leads to relaxation of SMCs. Therefore, a decrease of intracellular Ca^{2+} levels and/or an increase in MLC phosphatase activity via cGKI can induce relaxation of SMCs.

In addition to SMC relaxation, cGKI in the vasculature is involved in the shear-dependent inhibition of thrombus formation [52], regulates growth of VSMCs [123], and was even shown to promote atherosclerosis via VSMCs [124].

The (patho-)physiological relevance of cGKs in the vasculature and their essential role for proper SMC function was elucidated by studies with mice lacking cGKI [14]. Systemic ablation of cGKI in mice impairs cGMP-dependent vasorelaxation [125-127] and vascular growth under pathological conditions [128; 129]. SMC-selective deletion of cGKI reduces development of atherosclerosis [124] but does not affect injury-dependent restenosis [130]. Interestingly, SMC-selective cGKI rescue mice show normal vasorelaxation and a significantly increased life span in comparison to systemic knockout mice [40; 126].

Today, 11 families of PDEs are known that hydrolyse cGMP and/or 3',5'-cyclic adenosine monophosphate (cAMP) to their non-cyclic 5'-monophosphates [36]. These families can be grouped into three types of PDEs: PDEs specifically degrading cGMP (PDE 5, 6, 9), PDEs specifically degrading cAMP (PDE 4, 7, 8), and bispecific PDEs that can degrade cGMP and cAMP with varying preferences (PDE 1, 2, 3, 10, 11) [16; 36]. For VSMCs, expression and/or functional activity of PDE 1/3/4/5/9/10 is supported by the literature [24; 36; 131], but it is likely that not all isoforms are present in the same cell, at the same time. PDEs can modulate/mediate cGMP-dependent effects in VSMCs in various ways. cGMP-hydrolysing PDEs can stop/attenuate cGMP signalling via degradation of cGMP. The major cGMP-hydrolysing PDE in VSMCs is PDE 5 [17]. The activity of PDE 5 is heavily regulated by its substrate cGMP. Phosphorylation of PDE 5 by cGKI or binding of cGMP to PDE 5 increase its catalytic activity as well as its binding affinity for cGMP [16]. These mechanisms allow for a fast and tight control of cGMP levels in VSMCs. The pivotal role of PDE 5 for the regulation of cGMP signalling in VSMCs led to the use of PDE 5 inhibitors for the treatment of cardiovascular diseases. Sildenafil and tadalafil, for example, are used to treat erectile dysfunction and pulmonary arterial hypertension [36].

cGMP-regulated bispecific PDEs allow cGMP to modulate cAMP-dependent signalling [15]. For instance, binding of cGMP to PDE 3 can competitively inhibit the ability of PDE 3 to degrade cAMP [15], thereby increasing cAMP levels in VSMCs [132]. Conversely, cGMP can lower cAMP levels via PDE 2 as the catalytic activity of PDE 2 is increased by allosteric binding of cGMP to its regulatory domain [15]. To our knowledge, functionally relevant expression of PDE 2 is not reported for VSMCs.

There exists the hypothesis that cGMP-hydrolysing PDEs could compartmentalise cGMP within a cell by creating locally restricted cGMP pools ("subcellular cGMP microdomains") [24]. For instance, cGMP generated by different GCs (e.g., GC-A, NO-GC) could be restricted to distinct subcellular cGMP microdomains within the same cell. Depending on the proteins present in these microdomains, ANP-induced and NO-induced cGMP might lead to different effects. Just recently, Zhang and colleagues reported that cGMP generated by GC-A, GC-B, and NO-GC in VSMCs could be compartmentalised by PDEs [102]. Nonetheless, due to technical limitations (see section **4.1.4**) of their and a similar study [17], definite proof for the existence of cGMP microdomains in VSMCs is still lacking. A detailed discussion of cGMP microdomains, whether they exist or how they might be established, can be found elsewhere [24].

In addition to degradation of cGMP by PDEs [16], cells can clear their cGMP levels by export of cGMP into the extracellular space [17-19], or direct transfer to neighbouring cells via gap junctions [133; 134]. At least the first two mechanisms are known to be important in VSMCs [17].

1.3 The vascular system and VSMCs

The heart pumps blood through the whole body via the vascular system. This does not only provide cells with nutrients, oxygen, and metabolites but also allows cells to clear metabolic by-products, exchange information via hormones, and dissipate heat [135]. To fulfil these tasks, different types of vessels exist that are optimised for their respective function. When blood leaves the heart, it is pumped through large elastic arteries like the aorta and carotid arteries (conductance vessels) which branch several times thereby decreasing in size [135]. Simultaneously they get less elastic while their muscle content increases (muscular arteries) allowing them to regulate blood flow/pressure via contraction/ relaxation of their smooth muscle layers (resistance vessels) [135]. They finally end in capillaries that allow exchange of molecules between cells and the blood stream. From capillaries, blood is returned to the heart via venules and veins [135]. The distinct functions of different vessel types are reflected by structural differences of their vessel wall. For instance, capillaries are mainly composed of endothelial cells and pericytes whereas arteries contain multiple layers of VSMCs [136].

The vessel wall of arteries is comprised of three distinct layers (**Figure 3**). The layer closest to the vessel lumen is called tunica intima [137]. It is comprised by a monolayer of endothelial cells attached to a basement membrane. Besides its function as a barrier between blood and tissue it is essential for the regulation of vascular tone [136].

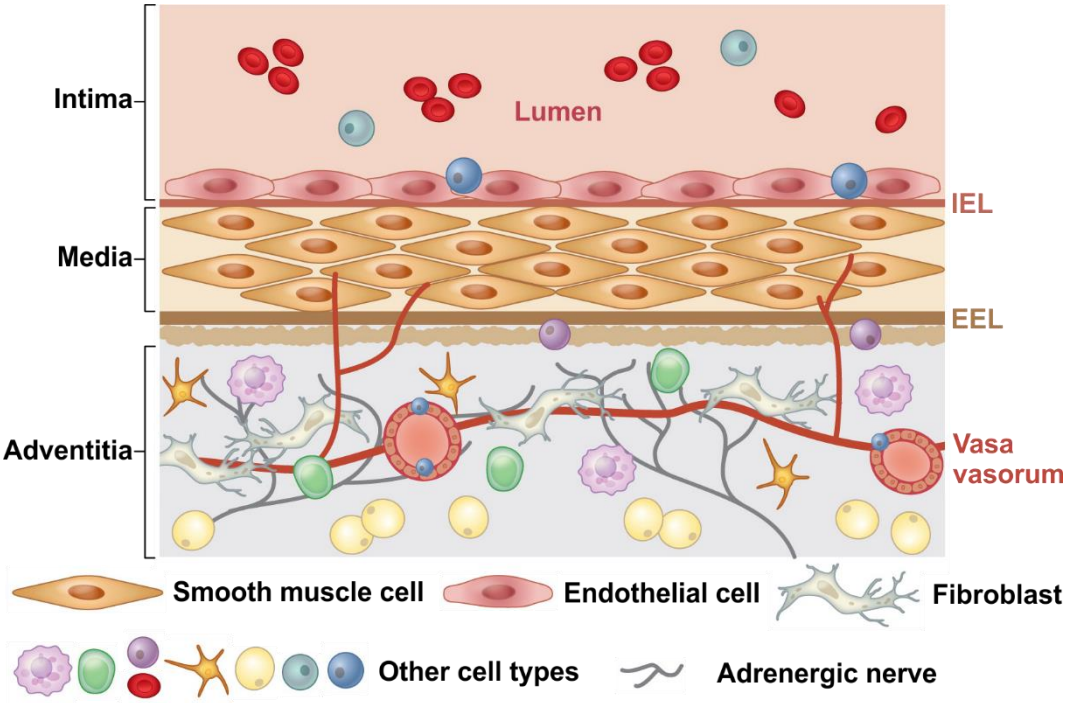

Figure 3: Structure of the murine arterial vessel wall. *The arterial vessel wall is composed of three layers. The tunica intima is composed of endothelial cells. The internal elastic lamina separates the tunica intima from the tunica media. The tunica media is composed of VSMCs and separated from the tunica adventitia by the external elastic lamina. The tunica adventitia is composed of various cell types, can be innervated, and can contain small blood vessels (vasa vasorum). For details see text. IEL: internal elastic lamina, EEL: external elastic lamina. Adapted from [138]*

The tunica intima is separated from the tunica media by an extracellular matrix (ECM) rich layer, the so-called internal elastic lamina [137]. The media is formed by several layers of VSMCs which are separated by layers of elastin (elastic lamellae) [139]. In contrast to elastic arteries where the elastic ECM forms a major part of the vessel (in the aorta elastin and collagen make up ~50 % of the dry weight [137]), the media of muscular arteries is mainly composed of VSMCs [136]. The media regulates the vessel diameter via contraction and relaxation of VSMCs [139]. Even though the media is comprised of a single cell type – VSMCs – it is an unexpectedly heterogeneous layer of the vessel wall. VSMCs of different vessels or even different parts of the same vessel can have different developmental origins [140] (**Supplementary figure I**). It appears that the developmental origin of medial VSMCs can influence their gene expression profile or even their function (e.g., response to growth factors) [140; 141]. The outermost layer (tunica adventitia) is separated from the tunica media by the external elastic lamina. The adventitia contains multiple cell types including various immune cells, (myo-)fibroblasts and adipocytes [138]. Furthermore, the adventitia is innervated by neurons and even contains small vessels (vasa vasorum) which provide nutrients to large vessels from the outside.

This structure of the vessel wall is shared by most animals that are used as model organism for atherosclerosis research. An important difference between arteries of small animal models like mice and human arteries is that the intimal layer of human arteries can develop prominent diffuse intimal thickenings that contain VSMCs in the subendothelial space [142; 143]. These diffuse intimal thickenings are thought to play an important role in the development of human atherosclerosis [143].

1.3.1 Phenotypic modulation/transdifferentiation of VSMCs in culture

In healthy arteries during homeostasis, VSMCs are highly contractile but quiescent cells with low migratory and proliferative potential [144]. They regulate blood flow via vasoconstriction and vasodilation of muscular arteries [135]. In addition, VSMCs contribute substantially to the development of new vessels [145] and the pathological remodelling of the vessel wall in cardiovascular diseases like atherosclerosis [144; 146] and restenosis [147]. The contribution of VSMCs to developmental/remodelling processes involves major cellular adaptions of VSMCs [144; 148; 149]. These include increased migration, proliferation, and enrichment in organelles (e.g., rough endoplasmic reticulum, free ribosomes) [148] that are involved in ECM synthesis and deposition. Similar changes as observed between VSMCs of healthy and developing/pathologically remodelled arteries were already described decades ago for VSMCs in culture [150]. When VSMCs from healthy arteries are cultured, they change from a quiescent cell that is manly comprised of its contractile apparatus to a cell with high migratory and proliferative potential [148]. These two states of VSMCs were called the “contractile” and the “synthetic” phenotype, respectively [151]. Since then, a plethora of studies characterised these phenotypes in more detail concerning their function and their gene expression profile. While the contractile phenotype is well characterised by expression of several marker proteins, the synthetic one is often characterised by their loss [151]. The proteins used to identify the synthetic phenotype by an increased expression often change from study to study (see below). Furthermore, it was discovered that different factors (e.g., inflammatory signalling molecules, ECM components) can favour the development of a certain phenotype [152]. Since these early discoveries, our understanding of the phenotypic modulation as well as the underlying mechanisms has grown. Nowadays, it is widely accepted that rather than a binary switch from contractile to synthetic phenotype, the transition is a continuous non-terminal process [151], called phenotypic modulation. Therefore, we will use the term “modulated VSMC” rather than “synthetic VSMC” in this work. The contractile and modulated/synthetic phenotype might build the extreme ends of the

phenotypic spectrum during physiological processes, but during pathological remodelling of the vessel wall, as it happens in atherosclerosis, VSMCs can change their phenotype to an extent that they resemble other cell types as demonstrated by lineage marker expression and functional changes (e.g., chondrocytes, macrophages) [153-155]. This extent of phenotypic modulation is often referred to as "transdifferentiation" [153].

A lot of effort has been invested into the characterisation of SMC phenotypes, including identification of marker proteins to verify SMC lineage and to determine their actual phenotypic state. VSMCs with a contractile phenotype have a spindle shaped morphology and are densely packed with contractile filaments [144; 148; 151]. Intuitively, the contractile phenotype can be identified by high expression of proteins involved in contraction. Markers to define the contractile state of VSMCs are α-smooth muscle actin (αSMA), smooth muscle protein 22-α (SM22α, also referred to as transgelin), smooth muscle-myosin heavy chain (SM-MHC), smoothelin-B, heavy-caldesmon and calponin 1, to name a few [144]. These proteins are either components of contractile structures in VSMCs or are involved in the regulation of contraction [156-161]. Importantly, the expression of some of these proteins or their isoforms can vary between vessels [158], individual VSMCs [159], or developmental stage [160]. Furthermore, most of these marker proteins are at least temporarily expressed in other cell types [144]. Therefore, identification of the contractile VSMC phenotype or SMC lineage identity should rely on a combination of these markers.

Upon modulation towards the modulated phenotype in culture, SMCs lose their contractile potential [148]. Modulated VSMCs in culture have a rhomboid morphology and contain few contractile filaments (**Figure 4**) [148; 151]. Concerning marker proteins for the modulated phenotype(s) the situation is less clear than for the contractile phenotype. One reason might be the various states of phenotypic modulation and the various models that are used to analyse modulated VSMCs. In most cases either VSMCs of developing vessels [162; 163], of pathologically remodelled vessels [163-166] (atherosclerotic or restenotic), or cultured VSMCs [164; 167; 168] are investigated. Based on such studies, non-muscle myosin heavy chain B (also referred to as smooth muscle embryonic "SMemb"), cellular retinol binding protein-1 (CRBP-1) and vimentin are recommended, to name a few [144; 151; 152]. These proteins have in common that they are frequently found in non-SMCs like cardiac myocytes (SMemb [169]), hepatocytes (CRBP-1 [170]), or fibroblasts (vimentin [171]). For some potential modulated VSMC markers contradictory results are found in the literature. For instance, vimentin was used as a marker for modulated VSMCs in several studies where it was upregulated in VSMCs with low contractile marker expression [167; 172; 173]. There are also indications that vimentin expression can be downregulated together with contractile marker proteins in VSMCs [174]. In an early study, vimentin was found to be upregulated in passaged modulated VSMCs [168]. Interestingly, it was already strongly upregulated after three days in culture when most contractile markers were still high [168]. All in all, various proteins were found under conditions where modulated VSMCs were present, but the use of them as markers might be highly context specific. The lack of a "general" marker for modulated VSMCs in combination with their similarity to fibroblasts (see below), makes unambiguous identification of modulated VSMCs difficult.

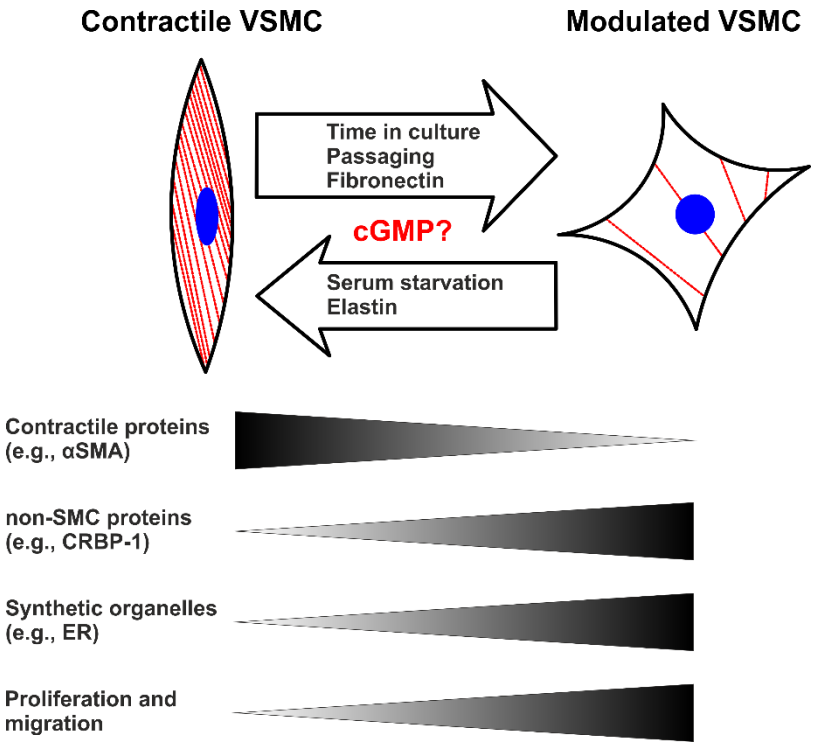

Figure 4: Phenotypic modulation of VSMCs in culture. *In culture, VSMCs change from a contractile towards a modulated ("synthetic") phenotype. Factors that can influence this process are indicated within the arrows. Contractile filaments are indicated as red lines within the cells. Characteristics of contractile and modulated VSMCs are indicated at the bottom. The triangles indicate whether protein expression or function in the respective phenotype is low (pointed end) or high (blunt end). cGMP is reported to affect phenotypic modulation but whether it promotes or inhibits phenotypic modulation is still controversially discussed. αSMA: α-smooth muscle actin, cGMP: 3',5'-cyclic guanosine monophosphate, CRBP-1: cellular retinol binding protein-1, ER: endoplasmic reticulum, SMC: smooth muscle cell, VSMC: vascular smooth muscle cell. For details see text.*

Fibroblasts are located in the adventitial layer which surrounds the media [138]. As modulated VSMCs in culture show similarities to fibroblasts [148], the potential contribution of fibroblasts to VSMC cultures should be considered in experiments with cultured VSMCs. Furthermore, VSMCs were reported to express several markers that are usually applied to identify (adventitial) fibroblasts like collagen1a1, fibroblast specific protein 1 (FSP 1, also referred to as S100A4), transcription factor 21 or vimentin [171; 175]. In contrast to its name, FSP 1 is all but specific for fibroblasts [171; 175]. It was detected in pathologically remodelled arteries and several cell types, including cultured modulated [176-178] and transdifferentiated [179] VSMCs. Platelet-derived growth factor receptor α (PDGFRα) is another fibroblast marker which was also reported in other cell types (e.g., mesenchymal stem cells [180], Müller cells [181]) but rarely in VSMCs [182; 183]. All in all, the proximity of cells that resemble VSMCs with different degree of phenotypic modulation to "original" VSMCs within the vessel wall requires careful interpretation of results that are obtained in VSMC cultures. The best way to avoid misidentification of modulated VSMCs as other cell types are lineage tracing approaches and/or characterisation of cells by large arrays of different markers (e.g., by single-cell transcriptomics). Today, there are an increasing number of studies employing these two techniques to characterise cells in healthy [141] and diseased arteries, e.g. in atherosclerotic lesions [179; 184-188].

Today, several factors/procedures are known that can influence phenotypic modulation of VSMCs in culture (**Figure 4**). When VSMCs are enzymatically isolated and cultured, phenotypic modulation gets apparent after few days in culture and proceeds further the longer VSMCs are cultured [148; 189]. If VSMCs are passaged (subcultured), they also adopt a modulated phenotype [148; 190]. Several soluble factors and ECM components were shown to modulate the phenotype of cultured VSMCs. Platelet-derived growth factor [191], basic fibroblast growth factor [191] and the ECM component fibronectin [192] promote a modulated VSMC phenotype in culture [152]. Transforming growth factor β [193]and the ECM component elastin [194], in contrast, promote the contractile phenotype. Incubation of VSMC

cultures with whole blood serum (called “serum” from here on), favours the modulated VSMC phenotype [195; 196], or conversely serum starvation favours the contractile VSMC phenotype [196-198]. Two explanations for this effect were reported in the literature. In an early study selective induction of proliferation of modulated but not of contractile VSMCs by serum incubation was reported [195]. Later works by other groups reported that serum starvation of cultured VSMCs leads to a contractile morphology and/or increased contractile SMC marker expression, hence promotes modulation of VSMCs to a contractile phenotype directly [196-198]. In both cases serum deprivation would lead to a smaller proportion of modulated VSMCs in comparison to contractile ones in the serum-starved cultures. Today, not only factors that influence phenotypic modulation but also factors that can induce transdifferentiation of cultured VSMCs are known. A subset of SMC-derived cells from atherosclerotic lesions can be transdifferentiated to macrophage-like cells by incubation with macrophage colony stimulating factor or to fibroblast-like cells by incubation with connective tissue growth factor [179]. Loading of VSMCs from healthy aortas with cholesterol induces transdifferentiation to macrophage-like foam cells [199]. The macrophage-like foam cells show even some functional similarity to macrophages as indicated by an increased phagocytic activity in comparison to non-transdifferentiated cultured VSMCs [199].

1.3.2 Phenotypic modulation/transdifferentiation of VSMCs in pathological vascular remodelling

While phenotypic modulation/transdifferentiation of VSMCs can be investigated in cell culture at a basic level, cell culture models can only insufficiently mimic the complex environment of VSMCs in intact vessels. To investigate phenotypic modulation/transdifferentiation of VSMCs in a native environment, murine models of restenosis [200] and atherosclerosis [201] can be used. In both diseases the phenotypic plasticity of VSMCs plays a pivotal role [202].

1.3.2.1 Restenosis

Upon vascular injury, VSMCs can transiently adopt a modulated phenotype to assist in injury repair [144; 202]. Thereby, VSMCs can contribute to pathological remodelling of the vasculature. For instance, damage of the arterial wall by surgical interventions can lead to restenosis [147]. While the details of restenosis formation are still unclear, several characteristics have been identified. Inflammatory processes caused by the vascular damage lead to migration of medial VSMCs to the intima where they form a so-called neointima by extensive proliferation and remodelling of the ECM [147]. The contribution of medial VSMCs to neointima formation was recently verified by lineage tracing [203]. Using a murine model of restenosis, Chappell and colleagues demonstrated that few medial VSMCs form the neointima by massive clonal expansion [203]. Migration, proliferation, and ECM remodelling are all processes connected with a modulated phenotype [144]. Interestingly, VSMCs exhibit a rather contractile state in the developed neointima as reflected by the expression of the contractile markers αSMA and SM-MHC in most cells [203]. Synthetic characteristics with maintained expression of contractile markers reminds of VSMCs in the fibrous cap of atherosclerotic plaques (see next section). Concerning the phenotypic state of VSMCs in the neointima, it should be considered that the study by Chappell and colleagues investigated the expression of contractile marker proteins in the established neointima. It is conceivable that VSMCs re-differentiate to a contractile state after repair of the vascular “wound” [202] as a transient downregulation of some contractile markers during neointima formation is reported in the literature [166; 204].

1.3.2.2 Atherosclerosis

Atherosclerosis is a chronic inflammatory disease of medium and large arteries, characterised by extensive remodelling of the vessel wall [205]. As cause of ischaemic heart disease and stroke, it occupies the first and second place of the causes of death worldwide, accounting for approximately 27 % of deaths in 2019 [206]. Atherosclerosis involves complex interactions of modified lipoproteins, the immune system and cells from the vascular media and intima [205; 207].

The development of atherosclerotic lesions is initiated by deposition and retention of low-density lipoprotein (LDL) and other lipoprotein particles in the intimal ECM [208-210]. This is normally prevented by a functionally intact endothelium [211]. While LDL is widely accepted as the main causative agent for atherosclerosis development, recent research indicates that other lipoproteins like triglyceride-rich lipoproteins are also important contributors [212]. LDL undergoes various modifications like oxidation, lipolysis and aggregation while retained in the ECM [213]. These processes trigger inflammatory responses of the vascular endothelium leading to recruitment of leukocytes into the intima. The other major cell type in atherosclerotic lesion formation are media-derived VSMCs [203; 214]. The uptake of modified LDL by macrophages and VSMCs leads to foam cell formation [215-217], characterised by intracellular accumulation of lipids [218]. It seems that modulated VSMCs are more prone to foam cell formation than contractile ones [219]. This might be connected to the reduced potential of modulated VSMCs to clear cholesterol [220]. Macrophage-derived and VSMC-derived foam cells, together with other types of transdifferentiated VSMCs form a lipid-rich core (**Figure 5**). With further progression of plaque development, foam cells undergo apoptosis and secondary necrosis which leads to the accumulation of extracellular lipids and cell debris, building the necrotic core [221]. As efferocytosis (clearance of dead cells) is impaired in atherosclerotic lesions [222; 223], the necrotic core continues to grow [223]. Lesions can be further modified by calcification [207], a process depending on macrophages [224] and VSMC-derived cells [225]. Depending on the type of calcification, the lesion is thought to be destabilised (micro-calcification) or stabilised (macro-calcification) [212; 226]. At the luminal side of the plaque, SMCs form a fibrous cap directly below the endothelium [221; 227]. Even though these SMCs largely retain their contractile marker protein expression [203], they are different from VSMCs found in the media of healthy arteries [146; 228; 229]. SMCs of the fibrous cap form a plaque stabilising ECM, rich in fibrillar collagens, proteoglycans and hyaluronan [230; 231]. It should be noted that not all αSMA-positive cells in the fibrous cap are of SMC origin [146].

With further plaque development, apoptotic events increase not only in the necrotic core but also in the fibrous cap [232]. Loss of VSMCs and increased degradation of collagen, the main stabilising factor of the fibrous cap, leads to thinning of the fibrous cap [221]. A thin, collagen-poor fibrous cap in combination with a foam cell-rich large necrotic core can lead to plaque rupture [233; 234]. Exposure of thrombogenic stimuli like tissue factor [235] due to plaque rupture leads to thrombus formation [236]. When these thrombi detach, they can clog vessels, leading to death by heart attack or stroke. Besides plaque rupture, plaque erosion can also cause thrombus formation [236]. Eroded plaques are usually rich in SMCs and lack the overlying endothelium.

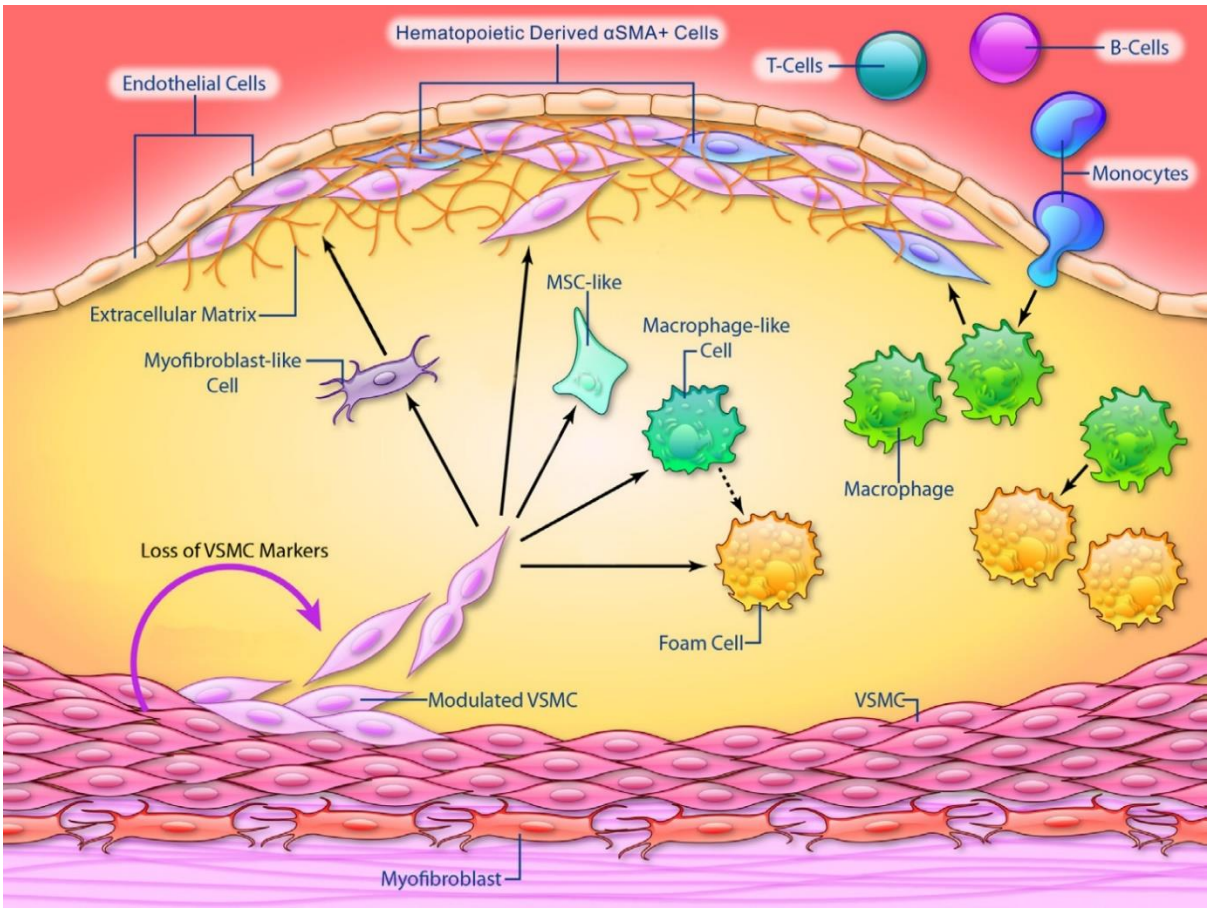

Figure 5: Contribution of VSMCs and immune cells to atherosclerotic plaque formation. *During the formation of atherosclerotic plaques medial VSMCs (bottom) undergo phenotypic modulation and transdifferentiation. Thereby, VSMCs downregulate expression of markers typical for contractile VSMCs and express markers of other lineages (e.g., macrophages). It is estimated that more than 30 % of cells in atherosclerotic plaques are of VSMC origin. Modulated VSMCs contribute to the formation of an ECM-rich fibrous cap (top) whereas transdifferentiated VSMCs are frequently, but not exclusively, found in the lipid rich core (centre) of atherosclerotic plaques. Other cells like bone marrow-derived macrophages contribute to the formation of atherosclerotic plaques as well. αSMA: α-smooth muscle actin, MSC: mesenchymal-stem cell, VSMC: vascular smooth muscle cell. Adapted from [232]. For details see text.*

A major complication in the analysis of atherosclerosis is that up to 80 % of media-derived SMCs in atherosclerotic lesions lose the expression of contractile marker genes [184], for instance by transdifferentiation. Thereby, SMCs in atherosclerotic plaques escape recognition by classical immunohistochemical approaches [146]. In consequence, the contribution of SMCs to foam cell formation as well as lesion formation in general was vastly underestimated for a long time. Only recently definite proof for VSMC transdifferentiation in atherosclerosis *in vivo* was reported by our group [155; 237]. We demonstrated by lineage tracing that VSMCs contribute significantly to plaque formation by clonal expansion and transdifferentiation to macrophage-like cells. In addition, we found indications in this seminal study that these transdifferentiated VSMCs could exert similar functions as conventional macrophages [155]. While the concept of VSMC transdifferentiation in atherosclerosis was questioned in the beginning [238], it was later verified by others [185; 203]. By now, it could be shown that >30 % of cells in advanced atherosclerotic lesions are of SMC origin [184; 203; 239] and that around 30 %-70 % of macrophage-like/foam cells in murine lesions are derived from VSMCs [207]. Besides transdifferentiation of VSMCs to macrophage-like/foam cells [155; 203; 240],

transdifferentiation of VSMCs to chondrocyte-like [188; 241], mesenchymal-stem cell-like [239] or (myo-)fibroblast-like cells [187; 239] based on lineage marker expression, is supported by the literature [153]. Most importantly, in some cases a functional similarity could be demonstrated as well. For instance, there are several indications that osteochondrogenic/chondrocyte-like cells are involved in calcification of atherosclerotic plaques [226]. It should be noted that it is not always clear whether transdifferentiation of VSMCs to a certain cell type is beneficial or detrimental for the outcome of atherosclerosis [226]. The reverse process – non-SMCs acquiring a SMC-like phenotype – was observed as well [146]. Endothelial cells, for instance, can contribute to αSMA+ plaque cells by a process called endothelial-to-mesenchymal transition [186]. The contribution of bone marrow-derived cells to αSMA+ plaque cells is still controversially discussed [146; 185; 242].

In short, atherosclerotic plaques are heterogenous structures that are composed of many different cells. Media-derived SMCs contribute significantly to formation of plaques at various stages of lesion development [207]. While modulated VSMCs of the fibrous cap are generally considered beneficial / plaque stabilising, transdifferentiated VSMCs might stabilise or destabilise atherosclerotic lesions in a context-dependent manner [226].

To predict the outcome of atherosclerosis in patients or to estimate the efficacy of an anti-atherosclerotic treatment, it is important to assess the severity of this disease. Due to the complexity of atherosclerosis, different concepts like plaque burden and vulnerability are used [221]. Plaque burden describes the extent of atherosclerotic lesions ignoring their cellular composition and risk to cause cardiovascular sequelae. It is usually reported as plaque volume or percentage of covered vessel surface [221]. Plaque vulnerability describes the short-term risk of plaques to cause thrombotic events (e.g., by rupture or erosion). It can also describe histological features that are associated with an increased risk for plaque rupture (e.g., thin fibrous cap). Especially in animal models like mice where thrombotic sequelae are rare, the predictive value of plaque vulnerability for the human situation is questionable [243].

1.3.2.3 Apolipoprotein E (ApoE)-deficient mice as murine model of atherosclerosis

Animal studies provide valuable insights into atherosclerosis development and significantly contribute to our current knowledge. Ideally, an animal model for atherosclerosis reflects the human pathophysiology of this disease, including all stages of lesion development, the predilected sites of lesion formation and clinical sequelae [201]. Furthermore, atherosclerosis should develop in a reasonable time frame and not over decades as in humans. Animal models that are frequently used include rabbits, pigs, and mice [244].

In contrast to humans, mice transport cholesterol mainly via high-density lipoproteins, have only low levels of pro-atherogenic low-density / very low-density lipoproteins [201] and do not naturally develop atherosclerosis [245]. To render mice susceptible to atherosclerosis, one can interfere with their lipid metabolism, for instance by genetic ablation of proteins involved in cholesterol transport/ metabolism. One of the most frequently used murine models of atherosclerosis are ApoE-deficient mice [201]. Impaired clearance of lipoproteins leads to increased plasma cholesterol levels in these mice. The increase of plasma cholesterol levels in ApoE-deficient mice can be supported by feeding a cholesterol-/fat-rich diet [246]. ApoE is integrated in all lipoproteins but LDL [247]. It is involved in the clearance of chylomicrons and very low-density lipoprotein remnants. Additionally, ApoE impacts inflammatory processes and SMC migration/proliferation [248]. Therefore, ApoE might influence atherosclerosis development also by other means than changes in cholesterol metabolism. ApoE-

deficient mice develop all types of atherosclerotic lesions within a few months on normal chow and faster when fed a cholesterol-/fat-rich diet [227].

The predilected sites of lesion formation in ApoE-deficient mice are the aortic root, arch, principal branches of the aorta, the pulmonary and carotid arteries [227] (**Figure 6**). In humans, lesions are found in the aorta, cerebral arteries, coronary arteries, and carotid arteries [201], the last two being the major sites of lesion formation.

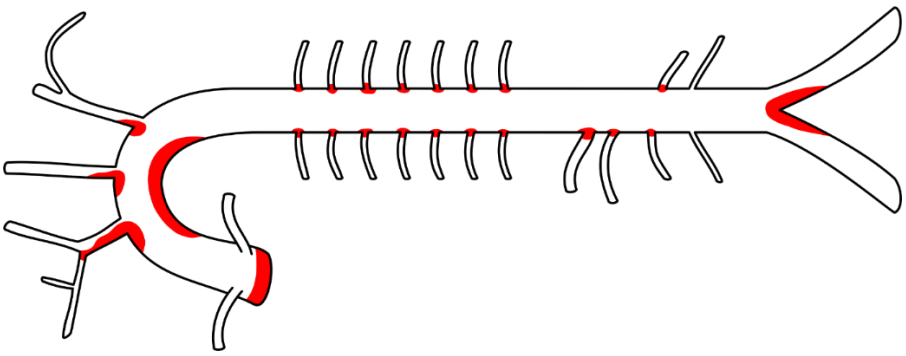

Figure 6: Predilected sites of atherosclerotic lesion formation in the aorta of ApoE-deficient mice. *Sites of lesion formation in the murine aorta are indicated in red. For further information see* ***Supplementary figure I A****. Adapted from [227] with own observations.*

In contrast to human lesions, spontaneous plaque rupture with subsequent thrombotic events is rare in ApoE-deficient mice [21; 201]. Another important difference between human and murine atherosclerotic lesions is the potential contribution of intimal VSMCs to plaque formation. The intimal layer of human arteries contains VSMCs in the subendothelial space[142; 143]. These intimal SMCs are different from medial SMCs in that they can resemble the modulated phenotype [142; 249]. The exact contribution of intimal vs. medial VSMCs in human plaque formation is still incompletely understood [146]. Nonetheless, the earliest event indicating potential plaque formation in humans is diffuse intimal thickening which involves accumulation of VSMCs in the intima. That mice and most other animal models do not develop prominent diffuse intimal thickenings [143], should be considered when using these models to investigate the mechanisms of atherosclerotic lesion development and rupture.

1.4 cGMP signalling and phenotypic plasticity of VSMCs

The pivotal role of cGMP signalling in VSMC physiology and the central role of VSMC phenotype in vascular (patho-)physiology (see sections **1.2** and **1.3.2**, respectively), sparked a multitude of studies investigating if cGMP signalling could impact phenotypic modulation. Despite decades of research, the role of cGMP in phenotypic modulation is still a matter of ongoing debate [54]. One problem with studies that investigate the effect of cGMP signalling on phenotypic modulation of VSMCs is that they are based on different animal models, VSMCs from different vascular beds and experiments performed on whole tissues, primary, or even passaged VSMCs, factors that can potentially influence the expression pattern of cGMP signalling pathway components.

Suga and colleagues, for instance, compared the expression of GC-A, GC-B, and Npr-C at the mRNA level between cultured VSMCs and intact aortas [250]. They detected GC-A and low levels of GC-B in the intact rat aorta but no GC-A and high levels of GC-B and Npr-C in cultured primary and passaged VSMCs. Others reported downregulation of cGKI or NO-GC in higher passages of cultured VSMCs [251; 252]. These changes might be species dependent [252]. Recently, it was reported that expression of

the bispecific PDE 10A increases in cultured modulated VSMCs in comparison to contractile ones [131]. Furthermore, a temporary strong increase in expression of PDE 10A upon growth induction was reported in the same study. In sum, a multitude of factors can impact cGMP-dependent and -independent (e.g., via Npr-C) signalling in VSMCs. These factors must be considered when one interprets the observations of studies that investigate the role of cGMP in phenotypic modulation of VSMCs.

Studies investigating the influence of cGMP signalling on VSMC phenotype in culture agree that cGMP has an impact on phenotypic modulation but disagree whether cGMP signalling promotes or inhibits the modulated VSMC phenotype [54]. The effects on phenotypic modulation are usually assessed by changes in contractile marker protein expression or VSMC proliferation. As phenotypic modulation appears to be a prerequisite for proliferation it is a good but no definite indicator for the modulated phenotype [148; 189; 195]. Studies based on (potentially modulated) **passaged** VSMCs indicate that cGMP promotes the contractile phenotype [54]. These studies report increased expression of contractile marker proteins and/or reduced proliferation upon application of NO donors [253] or NO-GC stimulators [254], direct activation of cGMP effector proteins with membrane-permeable cGMP analogues [253], or overexpression of cGKI [255-257]. Studies based on (potentially contractile) **primary** VSMCs, in contrast, indicate that cGMP promotes the modulated phenotype [54]. These studies report that stimulation of VSMCs with NO donors or membrane-permeable cGMP analogues amplifies growth effects [123; 124; 258; 259] or activates pro-proliferative pathways [260]. These results are in line with a recent study where the NO-GC 1 isoform was genetically ablated in mice [55]. Cultured VSMCs of these mice show reduced proliferation and migration. Another study demonstrates that low concentrations of NO promote the growth of **primary** VSMCs in a cGKI-dependent manner while high concentrations of NO inhibit VSMC growth independent of cGKI [124]. A similar cGMP-independent growth suppressing effect of NO is also reported in the former study [55]. Comparison of cGMP/cGKI-dependent growth effects between **primary** and **passaged** VSMCs by Weinmeister and colleagues shows that the growth-promoting effect of cGMP in **primary** VSMCs is lost in early passages and even slightly reversed in later passages [123]. Most interestingly, the growth-inhibiting effect in **passaged** VSMCs still depends on cGKI. This study also suggests that the underlying mechanism for growth-promotion in **primary** VSMCs is manly based on enhanced adhesion of VSMCs.

Less is known about the impact of NP-dependent cGMP signalling on VSMC phenotype. A few studies report an inhibitory effect of ANP and CNP on growth / DNA synthesis in **passaged** VSMCs [103; 261-263]. While these studies agree about the inhibitory effect of NPs on **passaged** VSMCs, they disagree concerning the mechanism. Depending on the study it is either attributed to cGMP or Npr-C signalling [103; 263]. Nonetheless, as these studies are based on DNA synthesis / cell growth one should be careful with conclusion concerning phenotypic modulation.

All together, these results indicate that NO-dependent cGMP signalling promotes the growth of **primary** (potentially contractile) VSMCs. Growth of **passaged** (potentially modulated) VSMCs, in contrast, appears to be, at least slightly, inhibited by cGMP from various sources. These observations would fit a model where cGKI promotes phenotypic modulation of contractile VSMCs towards a modulated phenotype. At the same time, cGKI limits this effect in an autoregulatory fashion by reversing the phenotypic modulation in modulated VSMCs.

The influence of cGMP signalling on cardiovascular remodelling processes that involve phenotypic modulation of VSMCs like restenosis and atherosclerosis is intensely investigated [54]. Due to the

complexity and the various cell types involved in these processes, it is often unclear to what extent cGMP signalling in VSMCs contributes to these processes. Neointima formation during restenosis involves, at least transiently, the phenotypic modulation of VSMCs (see section **1.3.2.1)**. All three NOS isoforms were reported to influence neointima formation in restenosis, but the exact effect depends on the isoform. Genetic ablation of the three isoforms demonstrated that the constitutively expressed e/nNOS limits restenosis [57; 58; 60; 264] while iNOS promotes [265] it. These opposing effects of NOS isoforms indicate that the source of NO could influence whether NO is beneficial or detrimental during restenosis. Studies that investigate the role of NO-GC in restenosis, either by genetic ablation of NO-GC 1 [62], or by isoform-independent stimulation of NO-GC [266-268], report contradicting results. While the former study shows a vasculoproliferative effect of NO-GC, the latter studies show a vasculoprotective effect of NO-GC in restenosis. All these studies have in common that it is unclear whether the observed effects on restenosis are mediated by VSMCs. At least for cGKI in VSMCs, an important role for neointima formation in restenosis could be excluded by analysis of SMC-selective cGKI knockout mice [130]. Looking at the literature as a whole, it appears that NO-cGMP-cGKI signalling in VSMCs is of minor importance in the setting of restenosis. The influence of ANP and CNP on restenosis has been investigated as well. While chronic application of ANP does not influence neointima formation [269], chronic application of CNP seems to reduce neointima formation [270; 271]. Again, it remains to be shown whether these effects are mediated via NP-dependent cGMP signalling in VSMCs.

In addition to phenotypic modulation, transdifferentiation of VSMCs plays a pivotal role in atherosclerosis (see section **1.3.2.2**). Several studies report an effect of cGMP signalling on atherosclerosis, but how exactly cGMP influences disease development remains elusive [54]. This might be in part due to the many processes involved in atherosclerosis that are potentially affected in different ways by cGMP. For instance, cGMP is involved in the regulation of blood pressure [53] and exerts anti-inflammatory effects [272; 273]. Thus, global manipulations of the cGMP pathway by pharmacological treatments or conventional knockouts (e.g., hypertension in eNOS knockout mice [274]) might obfuscate beneficial or detrimental effects exerted by a certain cell type. Similar to restenosis, e/nNOS are reported to be atheroprotective [56; 59], while iNOS promotes atherosclerosis [54; 61]. Again, these results indicate that the effect of NO on disease development is dependent on its source. Whether this effect is based on the exact NO concentration, the time, and/or place of NO release remains to be elucidated. This also reflects the ambivalent role of NO in VSMC cultures, where NO promotes or inhibits VSMC growth via cGMP/cGKI-dependent and -independent mechanisms [124], respectively. A similar discrepancy is reported in the few studies that investigate NO-GC-dependent signalling on atherosclerosis development. Pharmacological stimulation of NO-GC was reported to be atheroprotective in one study [275]. Genetic ablation of the NO-GC 1 isoform in all cells, in contrast, points towards an atheropromoting role of NO-GC 1 as atherosclerosis in knockout mice is attenuated [55]. Experiments with cultured VSMCs from NO-GC 1 knockout mice in the same study suggests that impaired phenotypic modulation of knockout VSMCs might be the underlying mechanism for attenuated lesion development. These results are in line with a study directly investigating the role of cGKI-dependent cGMP signalling in VSMCs for atherosclerosis development. SMC-selective ablation of cGKI does not only attenuate plaque development [124]. SMCs lacking cGKI are nearly exclusively found in the media but do not relevantly contribute to plaque development anymore. Considering these results, it is tempting to speculate that NO-GC 1/cGMP/cGKI signalling promotes phenotypic modulation/transdifferentiation of VSMCs away from the contractile phenotype and thus promotes

atherosclerosis development. Whether atheroprotective effects of pharmacological NO-GC stimulation are based on isoform-independent actions of NO-GC or are based on unspecific actions of the applied drugs, remains to be elucidated.

Little is known about the effects of NPs on atherosclerosis development. In general, an atheroprotective effect is attributed to ANP and CNP. Systemic genetic ablation of GC-A [276] or endothelium-selective ablation of CNP [83] in ApoE-deficient mice, promotes atherosclerotic lesion development. It is possible that the blood pressure lowering effect of GC-A and CNP and the anti-inflammatory effects of CNP that are reported in these studies, are responsible for the atheroprotective actions of ANP/GC-A and CNP. Both studies have in common that it is unclear whether NP-dependent cGMP signalling in VSMCs is involved in the atheroprotective actions.

All in all, there is solid evidence for functional relevance of the cGMP signalling system during vascular remodelling. Whether this function is beneficial or detrimental is still a matter of debate. Most studies investigating the role of this signalling pathway during cardiovascular disease development suffer from a major limitation: the cGMP signalling tool kit, at least in cultured VSMCs seems to change depending on VSMC phenotype. Therefore, the manipulation of this pathway might lead to different outcomes depending on the actual stage of disease. Indeed, there are indications for changes of the cGMP signalling tool kit during disease progression *in vivo*. Two recent studies demonstrated, for example, that the NO-GC/cGKI system or the expression of cGMP-degrading PDE 9A change during development of atherosclerosis in rabbits [277; 278].

1.5 Lineage tracing of VSMCs

To investigate the role of VSMCs in cardiovascular diseases, it is indispensable to identify them reliably in all stages of disease. Due to the extensive changes of VSMCs by phenotypic modulation/ transdifferentiation, identification of VSMCs cannot rely on the acute presence of traditional lineage markers (e.g., αSMA, SM22α, SM-MHC) [184]. Genetic lineage tracing circumvents this problem by stably labelling VSMCs before they lose the expression of lineage markers (**Figure 7 B-C**). This method is based on genetic rearrangements in fully differentiated VSMCs that lead to expression of a marker protein (e.g., a fluorescent protein or β-galactosidase) in these cells as well as all their progeny even after loss of lineage markers. An efficient system for lineage tracing or cell type-selective gene knockout in mice is the Cre/loxP system [279]. Cyclisation recombination (Cre) recombinase is a site-specific tyrosine recombinase [279]. It rearranges genomic DNA at specific sequences, so called locus of crossing-over [X] of P1 (loxP) sites. Thereby, it is possible to excise a DNA sequence (e.g., a complete exon) that is located between two loxP sites. The sequence which is flanked by the two loxP sites is often referred to as “floxed” sequence. For lineage tracing, a reporter gene (e.g., fluorescent protein or β-galactosidase) with a preceding floxed stop cassette is introduced into the mouse genome. The stop cassette blocks transcription of the reporter gene until it is removed by Cre-mediated recombination of the loxP sites (**Figure 7 B**). As the recombination occurs at the genomic level, all progeny cells will express the reporter as well. Cell type selectivity is achieved by expression of the recombinase under the control of a cell type-selective promoter.

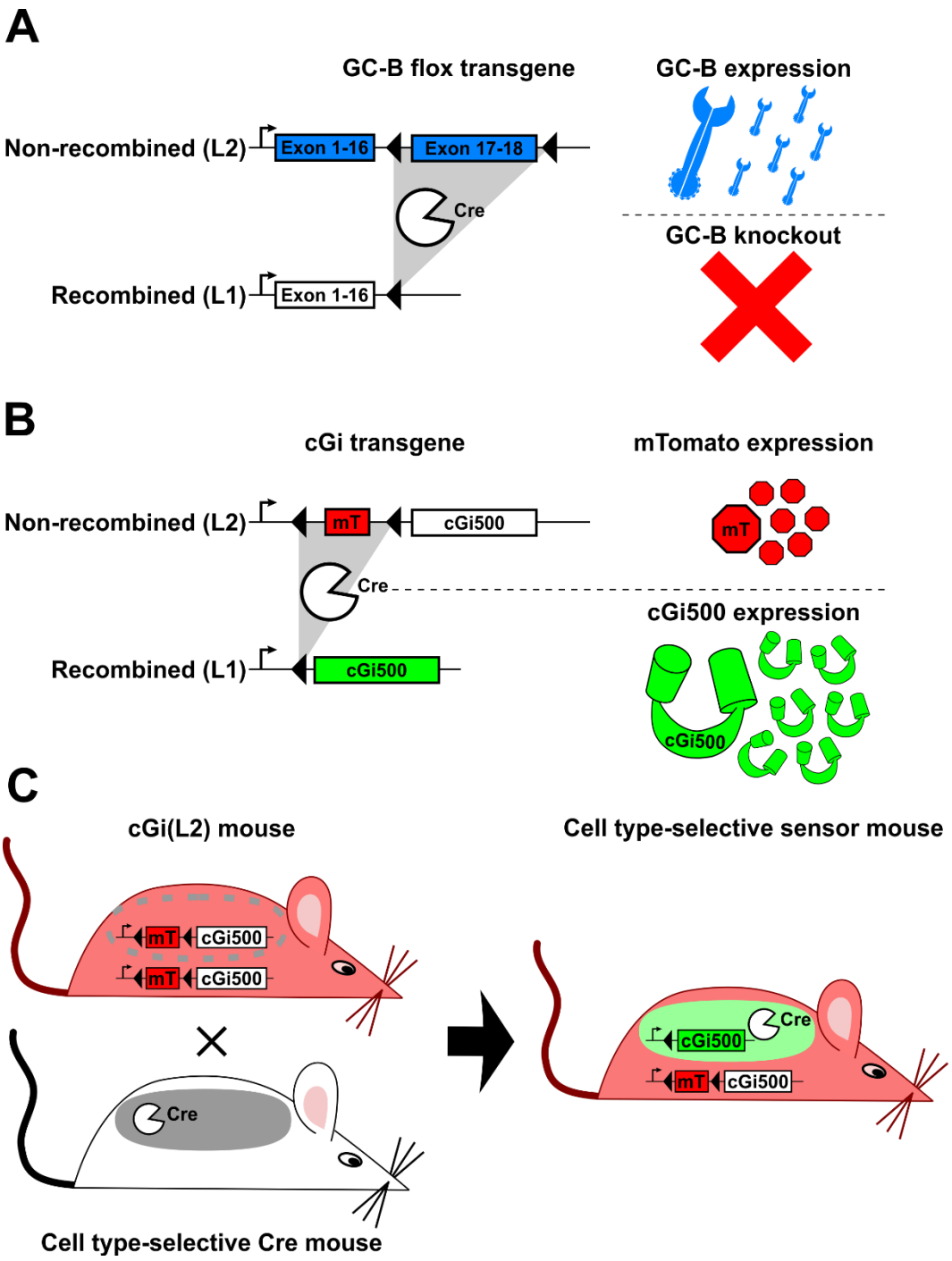

Figure 7: Application of the Cre/loxP system for cell type-selective gene knockout and lineage tracing. *The Cre/loxP system can be used to knock out a gene (A) or to label cells with fluorescent proteins in a cell type-selective manner (B-C, lineage tracing). cGi500 contains a yellow and cyan fluorescent protein. mT is a red fluorescent protein.* ***A:*** *Cre-dependent knockout of GC-B as it occurs in GC-B flox mice that are used in this study. The functionally essential exons 17 and 18 are flanked by two loxP sites (L2). When Cre is present, these exons are excised, and no functional GC-B can be expressed (L1, "one loxP site"). Coloured boxes indicate that a gene is functionally expressed. Triangles indicate loxP sites. GC-B: guanylyl cyclase-B, Cre: cyclisation recombination.* ***B:*** *Cre-dependent expression of the cGMP biosensor cGi500 as it occurs in cGi(L2) mice that are used in this study. Before recombination mT is expressed and serves as stop cassette that prevents expression of cGi500. When Cre is present, the mT gene (stop cassette) is excised, and cGi500 is expressed instead of mT. Coloured boxes indicate that a gene is expressed. Triangles indicate loxP sites. cGi: cGMP indicator, cGi500: cGi with an apparent EC_{50} of 500 nM, Cre: cyclisation recombination, mT: mTomato.* ***C:*** *Application of the Cre/loxP system to achieve cell type-selective expression of cGi500 (lineage tracing). Mice expressing the non-recombined cGi transgene (L2) in all cells*

are bred with mice that express Cre only in the cells of interest. Recombination of the cGi transgene (L2 → L1) occurs only in cells where Cre is present. In consequence, cGi500 is expressed in Cre-expressing cells (and their progeny). These cells can be identified by the yellow and cyan fluorescence of cGi500. Furthermore, cGMP levels can be measured in these cells. Cells that lack Cre expression express mT and can be identified by the red fluorescence of mT. Red and green colour indicate expression of mT and cGi500, respectively. The grey area indicates the cells that express Cre. The grey dashed line indicates the same area without Cre expression. For abbreviations see (B). For details about cGi500 see next section, for details about cGi(L2) mice see ***Table 2****.*

An advantage of this system is the high efficiency of recombination in mice [279]. A disadvantage for lineage tracing is that the time point of recombination cannot be controlled. The latter problem was solved with the invention of CreER^{T2}, a ligand-inducible recombinase that allows time-controlled, cell type-selective recombination. This recombinase exploits the need of Cre to translocate to the nucleus to access and recombine the DNA. CreER^{T2} is a fusion protein of Cre and a triple-mutated ligand binding domain of the human oestrogen receptor (ER^{T2}) [280]. In absence of 4-hydroxytamoxifen (4-OHT), the ligand of ER^{T2}, CreER^{T2} is retained in the cytosol [279]. Upon binding of 4-OHT, but not endogenous oestrogen, the fusion recombinase can translocate into the nucleus and recombine the DNA. Therefore, the time of recombination can be controlled by application of tamoxifen which is metabolised to 4-OHT.

Nonetheless, when using the CreER^{T2} system for experiments one should be aware that tamoxifen itself can influence the experimental outcome by interference with endogenous oestrogen signalling. Tamoxifen is a non-steroidal partial agonist of the oestrogen receptor that can exert agonistic or antagonistic effects in a context-dependent manner [281]. All in all, the inducible CreER^{T2} system is a potent tool for lineage tracing, but requires to control meticulously for potential side effects (e.g., atheroprotective actions of tamoxifen [282]) that might lead to false conclusions.

Several transgenic Cre(ER^{T2}) mouse lines are available to genetically modify SMCs via recombination [283]. In all lines, Cre expression is driven by promoters of contractile lineage markers with varying specificity for SMCs. These lines are the constitutively active SM22-Cre and the inducible SM-MHC-CreER^{T2}, αSMA-CreER^{T2} and SM22-CreER^{T2} line [283]. When using these mice for experiments, one should consider how the corresponding mouse line was created. Some lines were created by a knockin into the endogenous gene locus [284; 285], disrupting endogenous expression of the lineage marker. Some lines were created via random integration [37; 286; 287]. These lines do not disrupt expression of the lineage marker, but therefore might not always reflect the expression pattern of the marker perfectly.

The most specific Cre line for lineage tracing of SMCs in mice is likely the inducible **SM-MHC-CreER^{T2}** line It was generated by **random integration** of the complete murine SM-MHC gene (gene name: Myh11) [286]. Therefore, CreER^{T2} expression is thought to reflect well the endogenous expression of SM-MHC [283]. Expression is reported in SMCs [286] and pericytes in the lung [288]. The downside of this mouse line is that the recombinase transgene was integrated in the male gonosome (Y chromosome) [283]. Thus, studies using these mice can only be performed with male mice. Another widely used inducible Cre line is **αSMA-CreER^{T2}**. To generate this line only a part of the αSMA gene (Acta2) was **randomly integrated** into the mouse genome [287]. Expression is reported in vascular and visceral SMCs, cardiomyocytes [287], and (myo-)fibroblasts [283; 289]. Another inducible Cre line is **SM22-CreER^{T2}**. This line was created by a **targeted knockin** of the CreER^{T2} gene into the murine SM22α locus [285]. It was reported that recombination efficiency (percent recombined SMCs) in these mice is higher in visceral than vascular SMCs [285]. There is also a constitutively active **SM22-Cre** line that is

frequently used. The SM22-Cre line used in this work was created by **random integration** of a 2.8 kb fragment of the murine SM22α promoter together with the Cre recombinase [37]. Besides expression in SMCs, expression in subsets of immune cells [290], megakaryocytes [283] and perivascular adipose tissue [283] are reported. As SM22α can also be expressed by adventitial cells after vascular injury [291], SM22-Cre might lead to recombination in these cells. Potential recombination in the heart due to transient expression of SM22α during embryogenesis should also be considered [292]. While the site of integration of the SM22-Cre transgene is not known, our own observations from breeding suggest that this transgene is integrated in the murine chromosome 4.

The Cre/loxP system cannot only be used to label cells of a certain lineage, but also to inactivate a gene/protein of interest in a lineage-selective manner (**Figure 7 A**). To knock out a gene of interest and thereby ablate the corresponding protein, an essential part of the endogenous gene is flanked by loxP sites. When Cre excises this sequence, no functional product can be translated from the corresponding allele.

1.6 Förster resonance energy transfer (FRET)-based cGMP imaging

To investigate the role of cGMP in (patho-)physiology, it is informative to know when, where, and how much cGMP is present in a given cell, tissue, or organ. Conventional assays like enzyme linked immunosorbent assay provide sensitive tools to measure cGMP levels at a specific time point in culture or whole organs. As these assays are end point assays that are performed with cell/tissue lysates, their spatial and temporal resolution is relatively low. This limits their use for comparing multiple drugs (e.g., different cGMP-stimulating agents) or assessing inhibitor effects, especially in potentially heterogeneous cell cultures. A tool that allows for reversible cGMP detection in real time with a single-cell resolution is provided by genetically encoded cGMP biosensors. cGMP biosensors could allow to compare cGMP generation by various stimuli within an individual cell and between cells within the same culture. For instance, one could distinguish whether an individual cell can generate cGMP upon stimulation with ANP and NO or whether one cell in a culture responds to ANP and another cell of the same culture responds to NO.

cGMP biosensors usually involve fluorescent proteins, and most are based on the principle of FRET (sometimes referred to as “fluorescence resonance energy transfer”). FRET describes the radiationless energy transfer between two fluorophores by dipole-dipole coupling. When a donor fluorophore (shorter wavelength) is excited, it can transfer its emission energy directly to an acceptor fluorophore (longer wavelength) which in turn emits light. Hence, excitation of the donor leads to fluorescence of the acceptor. A prerequisite for FRET to occur is that both fluorophores are spectrally compatible and in close distance (< 10 nm) from each other [293]. The percentage of energy transferred from donor to acceptor fluorophore is called FRET efficiency and depends on the orientation and distance (decreases with increasing distance) of the two fluorophores [293]. The strong dependency of FRET efficiency from distance/orientation of the fluorophores is the reason why many biosensors are based on the FRET principle. cGMP biosensors, for example, translate the binding of cGMP to a change in orientation/distance between the fluorophores (**Figure 8**, top). As this cGMP-dependent change alters the FRET efficiency, the FRET efficiency can be used to determine the cGMP concentration.

Several FRET-based cGMP biosensors are available (e.g., cGi500, red cGES-DE5, Cygnet-2.1) which all have their advantages and disadvantages [24]. Depending on the spectral requirements and the biological question one might be superior to the other. For instance, the low EC_{50} (40 nM) of red cGES-

DE5 might help to image cGMP in cells with unusually low cGMP levels. Cygnet-2.1 with an EC_{50} of 2 µM on the other hand could image strong cGMP elevations that would saturate red cGES-DE5. The properties of an ideal FRET-based cGMP sensor are discussed elsewhere [24]. A cGMP biosensor that proved suitable not only to track cGMP transients in cell cultures from various tissues but also during (patho-)physiological processes in living animals is the "cGMP indicator with an apparent EC_{50} of 500 nM" (cGi500) [24]. This sensor was created by Russwurm and colleagues [294]. Transgenic mice that express this biosensor globally in all cells ("cGMP indicator", cGi(L1)) or in a cell type-selective manner (cGi(L2), based on the Cre/loxP system, **Figure 7 C**) were generated in our laboratory [295] and used throughout this work.

cGi500 is a so-called intramolecular, ratiometric FRET-based cGMP biosensor. It is composed of enhanced cyan fluorescent protein (eCFP, FRET donor) and enhanced yellow fluorescent protein (eYFP, FRET acceptor) which flank the tandem cGMP-binding domain of cGKI (**Figure 8**). It shows maximal FRET efficiency (= maximal energy transfer) in its cGMP-free state (**Figure 8**, left). Hence, in the absence of cGMP, excitation of eCFP leads to strong eYFP fluorescence (F_{535}) and weak eCFP fluorescence (F_{480}). When cGMP binds, a putative conformational change of the cGMP-binding domain reduces the FRET efficiency (**Figure 8**, right). The impaired energy transfer results in increased eCFP fluorescence and decreased eYFP fluorescence. The ratio of eCFP fluorescence over eYFP fluorescence ($R = F_{480}/F_{535}$) reflects the cGMP concentration. The opposite change in eCFP and eYFP fluorescence upon cGMP binding is an important feature of this ratiometric sensor as it allows to distinguish real cGMP/FRET signals from false signals (e.g., caused by tissue movement). Real cGMP/FRET signals are characterized by an increase in eCFP fluorescence and simultaneous decrease in eYFP fluorescence.

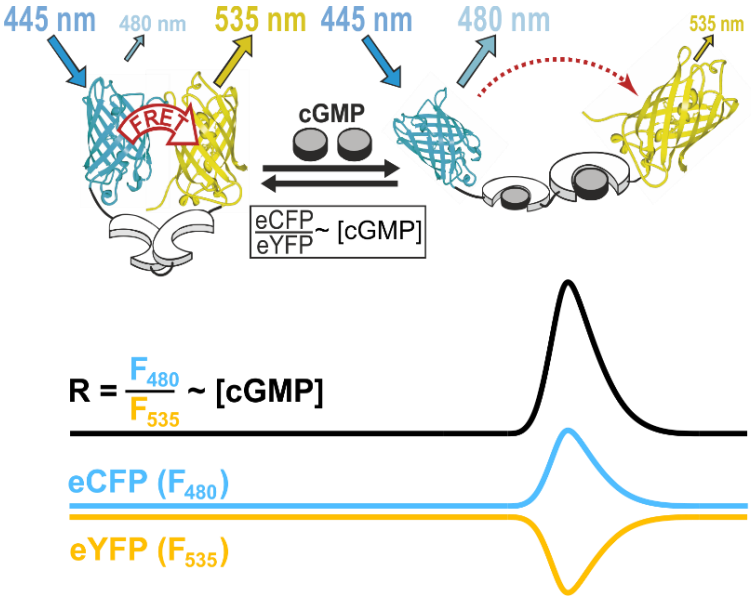

Figure 8: Working principle of the FRET-based ratiometric cGMP biosensor cGi500. *Top: Schematic representation of the sensor in its cGMP-free state (left) and cGMP-bound state (right). The fluorescent proteins are depicted as beta-barrels in cyan (eCFP) and yellow (eYFP). The tandem cGMP-binding domain of cGKI is depicted in white. Bottom: Schematic representation of the eCFP/eYFP fluorescence as well as the calculated ratio trace (R) when no cGMP is bound to the sensor (left part) and the changes when cGMP binds (right part). The ratio trace reflects the cGMP concentration ([cGMP]). In its cGMP-free state excitation of cGi500 at 445 nm leads to radiationless energy transfer from eCFP to eYFP (low eCFP fluorescence, high eYFP fluorescence). Binding of cGMP leads to conformational changes that reduce FRET efficiency (high eCFP fluorescence, low eYFP fluorescence). The antiparallel development of eCFP and eYFP fluorescence verifies real cGMP-dependent FRET signals. cGMP: 3',5'-cyclic guanosine monophosphate, eCFP: enhanced cyan fluorescent protein, eYFP: enhanced yellow fluorescent protein. Modified from [296].*

Cell type-selective expression of cGi500 in transgenic mice provides the possibility to detect dynamic changes of physiological cGMP levels in real time with single-cell resolution in a cell type-selective manner. Thereby, we can analyse the heterogeneity of cGMP signalling in complex cultures, isolated organs and even living animals.

1.7 Aim of the work

The aim of this study was to investigate the role of CNP-dependent cGMP signalling in VSMCs in health and disease. In my diploma thesis, I identified ANP- and CNP-preferring cells in primary VSMC cultures. Based on these results, the first aim of this study was to investigate whether CNP-preferring cells develop due to phenotypic modulation of VSMCs and to further characterise these cells. Next, we sought to identify CNP-dependent cGMP signalling in healthy and atherosclerotic aortas. The final goal of this study was to elucidate the pathophysiological relevance of CNP-dependent cGMP signalling in VSMCs during atherosclerosis *in vivo*.

2 Materials and Methods

2.1 General materials

Common reagents (**Supplementary table I**), common compounds (**Supplementary table II**), and the brands for all materials and devices (**Supplementary table III**) are listed in the supplement. For reagents, compounds, and materials that are not listed in (**Supplementary table I-II**), the brand is indicated in parentheses.

2.1.1 Common buffers and solutions

- **0.5 %** bovine serum albumin (BSA) in phosphate-buffered saline (PBS) (**BSA-PBS**): Dissolve 500 mg BSA in 100 mL PBS, store at 4 °C for up to 1 week
- **Cellfix**: 2 % formaldehyde (27 mL 37 % formaldehyde solution), 0.2 % glutardialdehyde (4 mL 25 % glutardialdehyde), ad 500 mL PBS, store at 4 °C
- Dulbecco's modified Eagle medium (**DMEM**): DMEM (Gibco) with Glutamax^{TM}-I (L-alanyl-L-glutamine), 4.5 g/L D-glucose, sodium pyruvate, phenol red, store at 4 °C
- **0.5 M** ethylenediamine tetraacetate (**EDTA**) pH 8.0: Add 186.1 g EDTA•2 H_2O to 800 mL H_2O on a magnetic stirrer, add NaOH pellets (~20 g) to adjust pH to 8.0, ad 1 L H_2O, autoclave, store at room temperature (RT)
- **3.7 % Formaldehyde-PBS**: 3.7 % formaldehyde (1 mL 37 % formaldehyde solution), ad 10 mL PBS
- Foetal calf serum (**FCS**): heat inactivate FCS 30 min at 56 °C, store at -20 °C
- **37 % formaldehyde solution**: 37 % formaldehyde, 9-11 % methanol (ChemSolute), store at RT
- **Full medium**: 500 mL DMEM, 5 mL 100x Pen/Strep, 50 mL FCS, store at 4 °C
- **Hoechst 33258**: 1 mg/mL Hoechst No. 33258 in H_2O, store at -20 °C protected from light
- **1 M $MgCl_2$**: 101.7 g $MgCl_2$•6 H_2O, ad 500 mL H_2O, store at RT
- **PBS** pH 7.4: 135 mM NaCl (7.9 g NaCl), 3 mM KCl (0.2 g KCl), 8 mM Na_2HPO_4 (1.42 g Na_2HPO_4•2 H_2O), 2 mM KH_2PO_4 (0.24 g KH_2PO_4), ad 1 L H_2O, adjust pH to 7.4 with HCl or NaOH, autoclave, store at RT
- **100x Pen/Strep**: 10 000 U/mL penicillin, 10 000 µg/mL streptomycin (Gibco), store at -20 °C
- **Serum-free medium**: 500 mL DMEM, 5 mL 100x Pen/Strep, store at 4 °C
- **50x** Tris-acetate-EDTA (**TAE**) buffer: 2 M Tris(hydroxymethyl)-aminomethane (Tris, 242 g), 5.71 % acetic acid (57.1 mL acetic acid), 50 mM EDTA pH 8.0 (100 mL 0.5 M EDTA pH 8.0), ad 1 L H_2O, store at RT
- **Tamoxifen** for injection (10 mg/mL): Suspend 100 mg tamoxifen in 200 µL 100 % ethanol, ad 10 mL sunflower oil (Thomy), dissolve completely in an ultrasound water bath, assure that temperature stays below 40 °C, store at 4 °C for up to 3 days
- **10x** Tris-borate-EDTA (**TBE**) buffer: 5 M Tris (605 g Tris), 5 M boric acid (309 g boric acid, ChemSolute), 100 mM EDTA pH 8.0 (200 mL 0.5 M EDTA pH 8.0), ad 1 L H_2O, store at RT
- **10x** Tris-buffered saline (**TBS**) pH 8.0: 1.5 M NaCl (87.7 g NaCl), 100 mM Tris (12.11 g Tris), ad 1 L H_2O, adjust pH to 8.0 with HCl, store at RT
- TBS-Tween (**TBS-T**): 1x TBS (100 mL 10x TBS), 0.1 % Tween-20 (1 mL Tween-20), ad 1 L H_2O, store at RT
- **10x** Tris-EDTA (**TE**) buffer pH 8.0: 100 mM Tris-Cl pH 8.0 (10 mL 1 M Tris-Cl pH 8.0), 10 mM EDTA pH 8.0 (2 mL 0.5 M EDTA pH 8.0), ad 100 mL H_2O, store at RT
- **1 M Tris-Cl** pH 8.0: dissolve 121.1 g Tris in 800 mL H_2O, add 42 mL HCl, cool down to RT for final pH adjustment (pH of Tris buffers is highly temperature sensitive) and adjust pH to 8.0, ad 1 L H_2O
- **40 mg/mL** 5-bromo-4-chloro-3-indolyl-β-D-galactopyranoside (**X-gal**): Dissolve 400 mg X-gal in 10 mL dimethyl sulfoxide, store protected from light at -20 °C

- **X-gal diluent**: 2 mM $MgCl_2$ (0.2 g $MgCl_2$•6 H_2O), 2.5 mM $K_3Fe(CN)_6$ (0.83 g $K_3Fe(CN)_6$), 2.5 mM $K_4Fe(CN)_6$ (1.07 g $K_4Fe(CN)_6$), ad 500 mL PBS, store at RT protected from light
- **X-gal staining solution**: 1 mg/mL X-gal (100 µL 40 mg/mL X-gal), 3.9 mL X-gal diluent, always prepare freshly

2.1.2 Solutions and materials for cGMP/FRET imaging

- **100 µM ANP**: Dissolve 1 mg ANP in 3.27 mL H_2O, store at -20 °C
- **100 µM CNP**: Dissolve 500 µg CNP in 2.28 mL H_2O, store at -20 °C
- **2.5 M D-glucose**: Dissolve 18 g D-glucose in 30 mL H_2O in an ultrasound water bath at 37 °C, ad 40 mL H_2O, sterile filter (0.45 µm pore size, Avantor) and store at RT
- **100 mM** Diethylammonium (Z)-1-(N,N-diethylamino)diazen-1-ium-1,2-diolate (**DEA/NO**): Dissolve 50 mg DEA/NO in 2.42 mL 10 mM ice-cold NaOH, store at -20 °C
- Imaging buffer (**IB**) pH 7.4: 140 mM NaCl (40.9 g NaCl), 5 mM KCl (1.86 g KCl), 1.2 mM $MgCl_2$ (1.22 g $MgCl_2$•$6H_20$), 2 mM $CaCl_2$ (1.11 g $CaCl_2$), 5 mM 4-(2-hydroxyethyl)-1-piperazineethanesulfonic acid (HEPES, 5.96 g), ad 5 L H_2O, adjust pH to 7.4 with NaOH, autoclave and store at RT, add 2 mL 2.5 M D-Glucose (10 mM final concentration) to 500 mL buffer before use
- **10 mM NaOH**: Dissolve 40 mg NaOH in 100 mL H_2O, store at RT
- Polydimethylsiloxan (**PDMS**): Add 1 mL of SYLGARD 184 silicone elastomer curing agent to 9 mL SYLGARD 184 silicone elastomer base (SYLGARD 184 silicone elastomer kit, Dow) in a 15 mL reaction tube, mix by inverting several times and pour into a 100 mm petri dish, let cure at 55 °C overnight, store at RT for several months
- **Silicon grease**: Korasilon (Obermeier)

2.2 Transgenic mice

Transgenic mouse lines that were used in this work are described in **Table 2.** All animal experiments were conform with the directive 2010/63/EU of the European parliament and approved by the local Animal Care and Use Committee (Regierungspräsidium Tübingen, IB 1/15, IB 7/18 G, and IB 2/15). Experiments involving mice used for the isolation of aortae with and without subsequent cultivation of VSMCs were reported to the animal welfare officer of the University of Tübingen ("§4 Mitteilung" of November 25, 2016 and June 17, 2020, IB 01/20M).

Female and male mice were used in experiments. As for some experiments more than two transgenic alleles had to be combined, the generation of experimental animals was performed over several generations. Breeding schemes were optimised to reduce the generation of "non-experimental" mice (if possible, these mice were used in other experiments). If a "floxed" mouse line was combined with the constitutively active SM22-Cre line, this happened in the last breeding step (generation of experimental animals) to avoid the possibility of germline recombination.

2.2.1 Breeding and husbandry

All mice were housed in the animal facility of the Interfaculty Institute for Biochemistry at 20-24 °C and 50-60 % relative humidity during a 12 h light / 12 h dark cycle. Mice were kept in groups in type II (360 cm^2, up to 3 mice) or type III (810 cm^2, up to 8 mice) cages with shredded aspen wood as bedding (J. Rettenmaier & Söhne GmbH + Co KG, Rosenberg, Germany). Wooden tunnels (Tapvei Estonia OÜ, Harjumaa, Estonia) and cellulose for hiding and nest-building, respectively, were provided. Mice had access to standard maintenance chow (ssniff) and tap water (not acidified) *ad libitum*. Pregnant mice and litter (until weaning) received extruded breeding chow (ssniff) instead.

Table 2: Short names, systematic names, alleles, and descriptions of transgenic mouse lines used in this study. *The nomenclature for alleles is as follows: "+" refers to the wild type allele, "tg" indicates random transgenes (site of integration not known), "L2" refers to a targeted knockin before Cre recombination (sequence is flanked by 2 loxP sites), "L1" refers to a targeted knockin after Cre recombination (sequence is excised, so only 1 loxP remains), "-" or "LacZ" refers to a targeted knockin (replacing the endogenous gene by a new one → knockout for the endogenous allele) or a simple knockout. Please note If not otherwise indicated, mice are bred on a C57BL/6N background. For genotyping primers and PCRs, see* ***Supplementary table V and VI****.*

Name	Systematic name	Alleles	Description	Reference
SM22-Cre	B6-Tg(Tagln-cre)1Her	+; tg	Expression of a constitutively active Cre recombinase under control of the SM22α promoter. This mouse line was generated by random integration (no knockout of SM22α). The transgene is probably integrated in chromosome 4 (own observations, see section **1.5**).	[37]
αSMA-CreER^{T2}	B6-Tg(Acta2-cre/ERT2)51Pcn	+; tg	Expression of the inducible CreER^{T2} under control of the αSMA promoter. This mouse line was generated by random integration.	[287]
cGi(L2)	B6;129-Gt(ROSA)26Sor$^{tm4(ACTB-tdTomato,-cGi-500)Feil}$	+; L2; L1	Cre inducible expression of cGi500 under control of the cytomegalovirus immediate early enhancer / chicken β-actin / rabbit β-globin (CAG) promoter. This mouse line was generated by targeted knockin of cGi500 into the Reverse orientation splice acceptor clone 26 (Rosa26) locus. The mTomato gene (flanked by loxP sites) serves as stop cassette and can be excised by Cre mediated recombination (**Figure 7**).	[295]
cGi(L1)	B6;129-Gt(ROSA)26Sor$^{tm4.1(ACTB-tdTomato,-cGi-500)Feil}$	+; L1	Global expression of cGi500 under control of the CAG promoter. This mouse line was generated by targeted knockin of cGi500 into the Rosa26 locus. As the stop cassette was removed in embryonic stem cells by transient transfection with pIC-Cre, the sensor is constitutively expressed in all cells/tissues.	[295]
GC-B LacZ[1]	B6.129Npr2^{tm1Fgr}	+; LacZ	Expression of a nuclear targeted β-galactosidase (LacZ gene) under control of the GC-B promoter. This mouse line was generated by replacing exon 1 of GC-B with LacZ (+ nuclear localisation sequence). This modification leads to expression of β-galactosidase in "originally GC-B positive" cells, while expression of GC-B is impaired from the same chromosome. Homozygous ablation of GC-B leads to reduced body size and a reduced life span.	[297]
GC-B flox[1]	B6;129S7-Npr2$^{tm2.1(flox)Fgr}$	+; L2; L1	Cre inducible ablation of GC-B. This mouse line was generated by inserting loxP sites in the introns upstream of exon 17 and downstream of exon 18. Excision by Cre recombinase leads to a premature stop codon in exon 19 and therefore to ablation of functional GC-B expression.	[298]
ApoE	B6.129P2-Apoe^{tm1Unc}	+; -	Ablation of ApoE by disruption of the ApoE gene. Heterozygous knockout mice are phenotypically unobtrusive. This line was bred on a mixed C57BL/6N and SV129 background.	[299]

[1] As the allele name of the transgenes of GC-B LacZ ("LacZ") and GC-B flox ("L2", "L1") are different, the genotype of these mice clearly indicates which mouse line was used. For better readability, we will indicate the genotype of GC-B LacZ and GC-B flox mice in a short form. Instead of "GC-B LacZ +/LacZ" or "GC-B flox +/L2" we will write "GC-B +/LacZ" and "GC-B +/L2", respectively.

To support the development of young mice, standard maintenance chow was supplemented with extruded breeding chow for the first few days after weaning. For induction of atherosclerosis, mice received an atherogenic diet (modifiziertes Altromin 1324: 20 % fat, 1.5 % cholesterol; Altromin) for 16-18 weeks. For breeding, one male mouse (≥8 weeks) was joined with up to two female mice (≥8 weeks) in a type II cage. Upon verification of pregnancy (visual inspection), female mice were transferred together in a type III cage and chow was changed (see above). Litter was weaned at 3 weeks of age and separated by sex. For identification purposes, mice were marked by ear tagging (**Supplementary figure II**) and ear biopsies were used for genotyping (see section **2.2.4**). Hygiene status of mice was checked by a sentinel system on a regular basis.

2.2.2 SMC-selective sensor expression

In this work, cGMP/FRET measurements with cells/tissues from mice with SMC-selective expression of cGi500 were performed to validate results gained in experiments with mice expressing the sensor globally. Therefore, cGi(L2) mice were mated with SM22-Cre mice. It should be noted that the tissue specificity of sensor expression was limited by the specificity of the Cre line. Information about off-target recombination known for this Cre mouse can be found elsewhere [283].

2.2.3 Knockout mice

In this work, mice lacking ApoE or GC-B globally (constitutive knockout) and mice lacking GC-B in SMCs (conditional knockout) were used. The appropriate control for each knockout was indicated in the respective section.

2.2.3.1 Constitutive knockout mice

To investigate atherosclerosis in mice, ApoE knockout mice (ApoE -/-) in combination with an atherogenic diet were used as mice do not naturally develop atherosclerosis (see section **2.4.5.1** for details). Homozygous GC-B LacZ mice (GC-B LacZ/LacZ x cGi(L1) +/L1) were used as GC-B knockout model to investigate GC-B dependent cGMP signalling in primary cultured VSMCs. Litter matched GC-B LacZ wild type mice (GC-B +/+ x cGi(L1) +/L1) were used as control. Due to the strongly reduced life span of constitutive GC-B knockout mice, these mice must be sacrificed at 3-4 weeks of age.

2.2.3.2 Conditional knockout mice

To investigate GC-B-dependent cGMP signalling in VSMCs of living animals, a conditional SMC-selective GC-B knockout was used (ApoE -/- x GC-B L2/LacZ x αSMA-CreER^{T2} +/tg; referred to as “Smko mice”). αSMA-CreER^{T2} is expressed in SMCs, but can only recombine DNA while tamoxifen is present ([279; 287]). Therefore, upon intraperitoneal tamoxifen injection (5 x 1 mg/mouse/day at 4 weeks and 6 weeks of age), the floxed GC-B allele (“L2”) was recombined in SMCs and therefore inactivated. The inactivated allele was passed on to the progeny cells. In combination with the GC-B LacZ allele, this led to a SMC-selective GC-B knockout. In addition, the GC-B LacZ allele (reporter) allowed to assess by X-gal staining (see section **2.3.4.1**) which cells expressed GC-B in theory. It should be noted that in this model all non-SMCs were heterozygous GC-B knockouts.

2.2.4 Genotyping of mice

- **Agarose**: LE agarose (Biozym)
- **DNA ladder**: 250 µL 1 kb plus DNA ladder (1 µg/µL 1 kb plus DNA ladder, Invitrogen), 8,25 mL 1x DNA loading dye, store at -20 °C (short time storage at 4 °C)
- **6x DNA loading dye**: 30 % glycerol (30 mL glycerol), 0.05 % bromophenol blue (2 mL 25 mg/mL bromophenol blue in H_2O), 0.05 % xylene cyanol (2 mL 25 mg/mL xylene cyanol in H_2O), 66 mL 10x TBE, store at -20 °C
- **dNTPs**: 100 mM dATP/dCTP/dTTP/dGTP (Genaxxon), store at -20 °C
- **50 mM $MgCl_2$**: 50 mM $MgCl_2$ (Invitrogen)
- **Midori green** (Nippon Genetics)
- Polymerase chain reaction (**PCR) lysis buffer**: 1x Reaction buffer (5 µL 10x Reaction buffer), 1 mg/mL proteinase K (1 µL proteinase K), 44 µL H_2O, always prepare freshly
- **10x PCR Rxn buffer** (Invitrogen)
- **Proteinase K**: 50 mg/mL proteinase K (Genaxxon) in 1xTE pH 8.0, store at -20 °C
- **10x Reaction buffer**: Complete II KCl (Bioron), store at -20 °C
- **10x RT buffer**: 500 mM KCl (5 mL 1 M KCl), 100 mM Tris-Cl pH 8.0 (1 mL 1 M Tris-Cl pH 8.0), 15 mM $MgCl_2$ (0.15 mL 1 M $MgCl_2$), 2 mM of each dNTP (4x 0.2 mL 100 mM dATP/dCTP/dTTP/dGTP), 3.05 mL H_2O, store at -20 °C
- **Taq polymerase**: DFS-Taq DNA Polymerase (Bioron) or Taq DNA Polymerase (Invitrogen)

A PCR-based protocol was used to genotype mice. The template DNA was isolated from ear biopsies gained by ear tagging (see section **2.2.1**), tail tips gained during experiments (re-genotyping), or aortas. By selection of appropriate oligonucleotide primers, DNA fragments of a defined length (depending on the present transgene) were amplified from the genomic template DNA by PCR. Agarose gel electrophoresis was used to separate the amplified DNA fragments according to their length ("bands"). The fragment length of PCR products was estimated by comparison with a co-migrating DNA ladder (known fragment lengths) and used to assign every mouse its genotype. See **Supplementary table VI** for a summary of primer combinations and expected fragment lengths for the genotyping PCRs that were used in this work.

2.2.4.1 DNA extraction

1. Incubate tissue samples in PCR lysis buffer (50 µL for ear biopsies / aortas, 150 µL for re-genotyping ear biopsies) overnight at 55 °C
2. Vortex samples until tissue is dissolved, centrifuge 5 min at 18 000 relative centrifugal force (rcf) at RT and transfer supernatant (genomic DNA) to new reaction tubes
3. Inactivate proteinase K for 15 min at 95 °C in a thermocycler and store at -20 °C if not used immediately

2.2.4.2 PCR

For most genotyping PCRs, the Taq polymerase from Bioron was used. PCRs that were problematic were performed with the Taq polymerase from Invitrogen. PCR conditions were determined by the annealing temperature of the primers, the product length and amplification efficiency. The specific conditions for each PCR are listed in **Supplementary table VI**.

1. Prepare master mix (per reaction):
    a. All PCRs but GC-B LacZ: 2.5 µL 10x RT buffer, 0.2 µL Taq polymerase (**Bioron**), primers according to **Supplementary table VI**, ad 22-23 µL H_2O
    b. GC-B LacZ PCR: 2.5 µL 10x PCR Rxn buffer, 0.75 µL 50 mM $MgCl_2$, 0.5 µL 10 mM dNTPs (1:10 dilution from stock), 0.25 µL Taq polymerase (**Invitrogen**), primers according to **Supplementary table VI**, ad 23 µL H_2O

2. Add 22-23 µL master mix to each PCR reaction tube containing 2-3 µL genomic DNA (total volume 25 µL), the positive (DNA sample heterozygous for the transgene) and negative control
3. Place reaction tubes in a thermocycler and run the required PCR program (see **Supplementary table VI**)
4. Analyse PCR products by agarose gel electrophoresis

2.2.4.3 Agarose gel electrophoresis

Agarose gel electrophoresis was performed with 2 % agarose gels. PCR products were visualised by fluorescence of Midori green under UV light and documented as digital images using a gel documentation system (ChemiDoc MP, Bio-Rad).

1. Add 2 g agarose to 100 mL 1x TAE buffer (1x 2 % gel) in a shot flask and boil in a microwave oven until agarose is solved completely (~2 min). Let the solution cool down for 15 min at RT while stirring, then add 3 µL Midori green. Pour into chamber, place combs, and let the gel solidify for 1 h at RT. Add 6x DNA loading dye to samples (1x final concentration, e.g., 5 µL for 25 µL PCR product) in the meantime.
2. Place gel in an electrophoresis chamber filled with 1x TAE buffer, remove combs and load 12-15 µL sample per well. Also load 12 µL DNA ladder in one well. Run agarose gel at 120 V for at least 30 min.
3. Acquire an image of the gel under UV light to document DNA bands (ChemiDoc MP). Estimate fragment sizes by comparison with the DNA ladder and assign genotype accordingly (see **Supplementary table VI**).

2.3 Analysis of murine VSMCs in culture

To analyse cGMP signalling in cultured VSMCs, primary VSMCs were isolated from the thoracic aorta of transgenic and wild type mice. Mice that were 6-12 weeks old were used in general, but the age range was extended for some experiments (e.g., effect of age on cGMP signalling) to 3-50 weeks. Female and male mice were used for VSMC cultures, but each individual culture consisted of VSMCs from female or male mice only. The standard culture time was 5 days but could be extended up to 10 days (until cells were ~90 % confluent). For cGMP/FRET measurements, mice expressing cGi500 heterozygously (cGi(L1) +/L1, SM22-Cre +/tg x cGi(L2) +/L2, cGi(L1) +/L1 x GC-B LacZ/LacZ) were used. For X-gal stainings, mice expressing GC-B LacZ heterozygously were used (GC-B +/LacZ). For western blotting, wild type mice were used. The term “primary” in this work refers to VSMCs that were isolated from an aorta and directly cultured without subculturing (= passaging). For passaged cells, the number of passages is indicated behind a “p” (e.g., “p1” stands for cells that were passaged once). “p0” refers to primary cells. If not otherwise indicated, cells were serum-starved for 12-24 h before the actual experiment.

2.3.1 Isolation and cultivation of (primary) VSMCs from transgenic mice

- **BSA stock**: 100 mg/mL BSA in Ca^{2+}-free medium, sterile filter (0.45 µm pore size, Avantor), store at -20 °C
- **Ca^{2+}-free medium** pH 7.4: 85 mM Na L-glutamate (15.91 g Na L-glutamate•H_2O), 60 mM NaCl (3.5 g NaCl), 10 mM HEPES (2.38 g HEPES), 5.6 mM KCl (0.42 g KCl), 1 mM $MgCl_2$ (0.2 g $MgCl_2$•6 H_2O), ad 1 L H_2O, adjust pH to 7.4 with HCl, autoclave, store at 4 °C
- **Collagenase stock**: 5 mg/mL collagenase from clostridium histolyticum (C7926, Sigma-Aldrich) in Ca^{2+}-free medium, store at -20 °C
- Dithiothreitol (**DTT**) **stock**: 100 mg/mL DTT (Roth) in Ca^{2+}-free medium, sterile filter (0.45 µm pore size, Avantor), store at -20 °C

- **Hyaluronidase stock**: 10 mg/mL hyaluronidase from bovine testes (H3506, Sigma-Aldrich) in Ca^{2+}-free medium, store at -20 °C
- **Lysis buffer A**: 0.7 mg/mL papain (100 µL papain stock), 1 mg/mL DTT (10 µL DTT stock), 1 mg/mL BSA (10 µL BSA stock), 880 µL Ca^{2+}-free medium, prepare freshly
- **Lysis buffer B**: 1 mg/mL hyaluronidase (100 µL hyaluronidase stock), 1 mg/mL collagenase (100 µL collagenase stock), 1 mg/mL BSA (10 µL BSA stock), 790 µL Ca^{2+}-free medium, prepare freshly
- **Papain stock**: 7 mg/mL papain from papaya latex (P4762, Sigma-Aldrich) in Ca^{2+}-free medium, store at -20 °C
- **Trypan blue**: 0.4 % trypan blue (Gibco)
- Instruments: large scissors (F•S•T 91402-12), small bent scissor (F•S•T 14061-09), blunt forceps (F•S•T 11018-12), 2 fine forceps (F•S•T No. 5 [11252-20] and F•S•T No. 5/45 [11253-25]), small spring scissors (F•S•T 15000-08)

The protocol for isolation of VSMCs was modified from Thunemann et al. [300]. 200 000-250 000 VSMCs were isolated per aorta on average. Depending on the age of mice and the duration of the isolation process, this number varied from 100 000-400 000 cells per aorta.

In general, VSMCs were grown on uncoated standard (cGMP/FRET measurement only) or gridded glass coverslips (Photoetched Cover Slips 12 mm round, Dunnlab) for subsequent investigation of marker protein expression (see section **2.3.5.7**). Standard glass coverslips were autoclaved before use, gridded coverslips were incubated with 70 % ethanol overnight, washed twice with H_2O, and dried on a sterile paper towel. To test the effect of fibronectin on VSMC phenotype, VSMCs were grown on glass coverslips coated with fibronectin (see section **2.3.1.3**).

1. Disinfect surgical instruments with 70 % technical ethanol. Pre-heat water bath, full medium and Ca^{2+}-free medium to 37 °C. Thaw papain, DTT and BSA on ice.
2. Sacrifice mice with CO_2 (not more than 2 mice at a time) and verify that inter-toe reflex is gone (blunt forceps). Cut throat with large scissors to assure death (do not perform cervical dislocation as this might rupture the aorta). Spray fur with ethanol and open abdominal cavity completely (caudal to rostral). Cut peritoneum, open thoracic cavity at both sides and bend chest back to expose heart. Cut oesophagus and trachea and remove lungs. Grab liver, cut below, and push liver and gastrointestinal tract aside. Grab heart (blunt forceps!) and pull it slightly upwards. Use bent scissors and cut along the spine caudal until the kidneys are passed. Cut the aorta and store it in PBS on ice. Repeat this step until all mice are processed.
3. Transfer aorta to a 100 mm petri dish with fresh PBS. From here on work under a stereo microscope with fine forceps at RT. Grab aorta at the aortic root and remove the heart with spring scissors. Use fine forceps to remove larger tissue pieces surrounding the aorta. Carefully remove all surrounding tissue at one end of the aorta. Grab the cleaned end firmly with one forceps and loosely with the other forceps directly in front of the non-cleaned part. Pull the second forceps towards the non-cleaned end to remove all surrounding tissue “like a sock”. Remove remaining pieces of surrounding tissue and strike across the aorta once to remove blood.
4. Cut away the aortic arch and the lower part (cut directly above the coeliac artery) and transfer the thoracic/abdominal part to Ca^{2+}-free medium on ice. The cleaning process per aorta should not exceed 15 min and the strain should be kept minimal as both factors heavily impact the cell yield at the end of the cleaning process. Continue with the next aorta from step 3 until all aortas are cleaned.
5. Cut aortas into pieces of 1-2 mm length.
6. From here on work under a cell culture foam hood. Prepare lysis buffer A with the pre-heated Ca^{2+}-free medium in a 15 mL reaction tube (0.25 mL/aorta but at least 0.5 mL). Transfer aortic

pieces to lysis buffer A and incubate 1 h at 37 °C in the water bath. Resuspend tissue pieces every 10-15 min by shaking and thaw collagenase and hyaluronidase on ice in the meantime.
7. Centrifuge digest 3 min at 200 rcf and prepare lysis buffer B (same volume as lysis buffer A) in the meantime. Remove supernatant with a pipette, add lysis buffer B and resuspend by shaking. Incubate 12 min at 37 °C in the water bath. Shake digest every 1-2 min. After ~7 min, pipette digest up and down every minute with a 1000 µL pipette to support digestion. Stop digest as soon as no tissue pieces remain, but latest after 15 min, by adding full medium (3-4x the volume of lysis buffer).
8. Centrifuge digest 8 min at 200 rcf at RT and aspirate supernatant. Resuspend cells in full medium (1 mL for up to 4 aortas) and determine number of viable cells with a Neubauer chamber (18 µL cell suspension, 2 µL trypan blue). Dilute cell suspension to 5 x 10^4 cells/mL with full medium and seed 1 mL per well of a 24-well plate equipped with 12 mm glass coverslips.
9. Culture VSMCs at 37 °C and 6 % CO_2 in a cell culture incubator. If cells are cultured longer than 7 days, renew medium at day 7 (see section **2.3.1.4**)

2.3.1.1 Enzymatic adventitia removal

Enzymatic adventitia removal was performed to assure that no piece of adventitia was co-cultured in VSMC cultures. It was not used for standard cultures as this procedure seemed to reduce the ability of VSMCs to attach/grow in culture. The protocol as described above was used with a **modified** step 3:

3. Transfer aorta to a 100 mm petri dish with fresh PBS. From here on work under a stereo microscope with fine forceps at RT. Grab aorta at the aortic root and remove the heart with spring scissors. Use fine forceps to remove larger tissue pieces surrounding the aorta. **Pre-digest roughly cleaned aorta in lysis buffer B (without hyaluronidase) for 5 min at 37 °C shaking (Thermoshaker). Put aorta back in PBS and use two fine forceps to tear the adventitia open at one end of the aorta. Continue opening the adventitia up to the other end of the aorta and remove it in one piece. Strike across the aorta once to remove blood.**

2.3.1.2 Passaging

- **10x Trypsin/EDTA**: 0.5 % (w/v) trypsin (5 g trypsin, Gibco), 4.8 mM EDTA (2 g EDTA•2 H_2O), 147 mM NaCl (8.5 g NaCl), ad 1 L H_2O, store at -20 °C
- **1x Trypsin/EDTA**: 1 mL Trypsin/EDTA, 9 mL PBS, store at 4 °C for up to 1 month

VSMCs were isolated as described in section **2.3.1**. 800 000 VSMCs were seeded on 100 mm cell culture dishes (8 x 10^4 cells/mL, 10 mL per dish) for passaging and 180 000 cells on 25 mm gridded glass coverslips in 6-well plates for cGMP/FRET measurements (9 x 10^4 cells/mL, 2 mL per well). Cells were passaged up to passage 4 from a 100 mm cell culture dish when they were close to confluency as follows:

1. Pre-heat water bath, full medium and PBS to 37 °C. Bring 1x Trypsin/EDTA to RT.
2. Aspirate medium and wash once with 5 mL PBS. Incubate cells with 3 mL 1x Trypsin/EDTA at 37 °C in a cell culture incubator until cells start to detach. Tap hard against the side of the cell culture dish to completely detach cells.
3. Stop digest by adding 9-12 mL full medium and pipette up and down several times to individualise cells. Transfer cell suspension to a 15 mL reaction tube and centrifuge 5 min at 200 rcf at RT. Aspirate supernatant and resuspend cells in full medium. Join samples if cells are passaged from several cell culture dishes. Determine number of viable cells with a Neubauer chamber (18 µL cell suspension, 2 µL trypan blue) and dilute cell suspension accordingly. Cells are split at a 3:4 ratio. Per passage at least one 100 mm cell culture dish (further passaging) and three 6-wells equipped with glass coverslips for cGMP/FRET measurements are required.

2.3.1.3 Coating of coverslips

- **Fibronectin**: 100 µg/mL fibronectin (Roche) in PBS

1. Work under a cell culture foam hood. Equip a well plate with glass coverslips and add fibronectin (300 µL/24-well or 900 µL/6-well). Incubate coverslips over night at RT.
2. Aspirate fibronectin solution directly before seeding of cells and wash once with PBS.

2.3.1.4 Medium exchange

Medium exchange was either performed to renew nutrients and to get rid of metabolic products (full medium) or to create well-defined conditions before an experiment (serum-free medium).

1. Pre-heat water bath and cell culture medium to 37 °C. Work under a cell culture foam hood.
2. Aspirate old medium and wash twice with fresh medium.
3. Incubate at 37 °C and 6 % CO_2 in a cell culture incubator.

2.3.2 Fixation of cells

2.3.2.1 Fixation for immunofluorescence (IF) staining

This protocol was used to fix adherently growing VSMCs for IF staining. Fixed cells were stained directly or stored for up to 1 month at 4 °C.

1. If cells were incubated with full medium before, wash twice with PBS. If cells were used in a cGMP/FRET measurement, directly continue with next step.
2. Transfer glass coverslips with attached cells to a well plate filled with 3.7 % formaldehyde-PBS and fix for 10 min at RT. Wash once with 0.5 % BSA-PBS and store in 0.5 % BSA-PBS at 4 °C (seal plate with parafilm) or directly continue with IF staining (see section **2.3.3**)

2.3.2.2 Fixation for X-gal staining

To fix cells for X-gal staining a mild fixative and short incubation time were used as the enzymatic activity of β-galactosidase must be preserved. X-gal staining was performed directly after fixation procedure.

1. Wash cells twice with PBS and fix with pre-chilled Cellfix 5 min at RT.
2. Wash cells twice with PBS and continue with X-gal staining (see section **2.3.4.1**)

2.3.3 IF staining of cells

- **Block/Perm solution**: 5 % (v/v) normal donkey serum (NDS) or normal goat serum (NGS) (500 µL NDS/NGS), 9.5 mL BSA-PBS-T, prepare freshly
- BSA-PBS-Triton (**BSA-PBS-T**): 0.1 % Triton X-100 (100 µL 10 % Triton X-100), 9.9 mL 0.5 % BSA-PBS, store at 4 °C for up to 1 week
- Primary antibody (**pAb**) solution: pAb (see **Supplementary table IV**) in BSA-PBS-T
- Secondary antibody (**sAb**) solution: sAb (see **Supplementary table IV**), 0.1 % (v/v) Hoechst 33258 in 0.5 % BSA-PBS
- **10 % Triton X-100**: 10 % (v/v) Triton X-100 (1 mL Triton X-100, Roth), ad 10 mL H_2O, store at RT

With this protocol 1-2 proteins (single/double staining) were detected by indirect IF staining of fixed cells. This allowed to compare the localisation of the respective proteins between samples and to compare relative expression levels within the same sample. A pAb binds the protein of interest while a fluorophore labelled sAb binds the pAb (indirect detection of the antigen). In case of double staining, potential cross reactivity of antibodies had to be considered. To account for unspecific binding of sAbs and other artefacts (e.g., yellow fluorescent protein (YFP) fluorescence of cells that were used in

cGMP/FRET measurements), controls without pAbs were always performed in parallel. The normal serum used for blocking matched the species of the sAb.

1. If cells were stored at 4 °C wait until they reached RT. All washing/blocking steps are performed in well plates with cells facing upwards. Incubation steps with antibodies are performed on parafilm with cells facing towards the parafilm to minimise antibody consumption.
2. Wash cells (fixed according to section **2.3.2.1**) twice with 0.5 % BSA-PBS and block/permeabilise cells with Block/Perm solution for 10 min at RT.
3. Wash cells once with 0.5 % BSA-PBS at RT and centrifuge pAb solution 5 min at 20 817 rcf at 4 °C to reduce precipitates in stainings. Pipette pAb solution on parafilm (~70 µL per 12 mm coverslip or 210 µL per 25 mm coverslip). Carefully add coverslips with cells facing towards the parafilm on top. Incubate overnight at 4 °C (second staining: 2 h at RT) in a closed moist chamber.
4. Wash cells twice with 0.5 % BSA-PBS for 3 min at RT and centrifuge sAb solution 5 min at 20 817 rcf at 4 °C. **From now on keep cells in the dark**. Incubate cells with sAb solution for 1 h at RT on parafilm in a dark moist chamber (see step 3).
5. In case of double staining, wash cells twice with 0.5 % BSA-PBS for 4 min at RT and continue from step 3. Otherwise continue with step 6.
6. Wash cells twice with PBS for 3 min. Add a drop of mounting medium onto a glass slide, dip coverslip with cells twice in H_2O, remove excess liquid with a dry tissue and mount with cells facing the glass slide. Let mounting medium dry for at least 2 h at RT in the dark before documentation according to section **2.3.3.1**.

In combination with gridded coverslips this procedure was used for semi-quantitative analysis of (marker) protein expression in cells that underwent cGMP/FRET measurements (see sections **2.3.5.6** and **2.3.5.7**).

2.3.3.1 Documentation of IF stainings

Immunofluorescence stainings of cells were documented with an inverted epifluorescence microscope using the VisiView® (Visitron) software for image acquisition. The microscope (Axiovert 200, ZEISS) was equipped with a Plan NeoFluar 10x/0.30 objective (ZEISS) and an electron-multiplying charged-coupled device (EM-CCD) camera (Retiga 2000R or Retiga R1 since 08/2017, QImaging). As light source served the computer-controlled Oligochrome (TILL Photonics) equipped with a Xenon short-arc lamp (UXL-S150MO, Ushio) and a set of excitation filters (AHF). Excitation filters were combined with emission filters and dichroic mirrors depending on the fluorophore to be detected according to **Table 3**.

For cGMP/FRET measurements, a beam splitter with 05-EM insert (Micro-Imager DUAL-View, Photometrics) in front of the EM-CCD camera was used to separate cyan fluorescent protein (CFP) and YFP emission for simultaneous recording. It consisted of a dichroic long pass mirror (516 DCLP) and two emission band pass filters (BP 480/50 [for CFP emission] and BP 535/40 [for YFP emission]). Via adjustable mirrors and shutters the light path was manipulated in a way that half of the camera sensor was exposed to YFP emission, and the other half was exposed to CFP emission.

Table 3: Filter combinations that were used to detect the different fluorophores. *BP filters (BP **X/Y**) let only the specified range of the spectrum pass (**X ± Y/2 nm**). Long pass filters (LP **X**) let only light with wavelengths longer than **X** pass. DCLP mirrors (DCLP **Y** or DCXRUV **Y**) reflect wavelengths shorter than **Y** and let pass wavelengths longer than **Y**. DCXRUV: Dichroic long pass, extended reflection including the UV.*

Fluorophore		Excitation filter	Dichroic mirror	Emission filter
Hoechst 33258		BP 387/11	410 DCLP	LP 440
YFP, Alx 488		BP 497/16	516 DCLP	BP 535/22
mTomato, Alx 555, Alx 593		BP 543/22	565 DCLP	BP 610/75
FRET	CFP	BP 445/20	470 DCXRUV + 516 DCLP[1]	BP 480/50[1]
	YFP			BP 535/40[1]

1: Component of the beam splitter "DUAL-View"

1. The microscope is placed in a dark air-conditioned (~21 °C) room.
2. Clean glass slide and coverslip with 70 % technical ethanol and place slide in slide holder.
3. Choose the right filters for the respective fluorophore and inspect the staining through the eye piece to assess quality and overall appearance. Select a region where the staining is intense, take an image, inspect the intensity distribution, and adjust the exposure time accordingly. This cycle should be repeated with the same region until the optimal exposure time is found. The highest intensities should be as close to 12 000 (but not higher) as possible while the exposure time should not exceed 5 seconds. This procedure must be repeated for every protein/fluorophore combination to be documented (only for the first coverslip). All following coverslips are documented using these settings to keep the images comparable.
4. Document 3-5 random regions per coverslip (10x objective).
5. If cells that were analysed by cGMP/FRET measurements before, are documented, the measured region must be documented as well:
    a. Open the brightfield image with the coordinates from the cGMP/FRET measurement.
    b. Locate the same region under brightfield (BF) illumination.
    c. Acquire an image of the coordinates (BF) and of the IF staining (fluorescence).
6. If necessary, relative marker protein expression is quantified using Fiji as described in section **2.3.5.7**.

2.3.4 Analysis of GC-B expression

GC-B LacZ reporter mice were used to follow the development of GC-B expression in primary VSMC cultures over time. The amount of GC-B positive cells (X-gal-stained nuclei) was assessed after 4, 5, 6 and 7 days in culture and normalised to total cell number (Hoechst 33258-stained nuclei).

2.3.4.1 X-gal staining of cells

The β-galactosidase catalyses the hydrolysis of the artificial substrate X-gal which leads to formation of a water insoluble blue indigo dye. As a nuclear localisation sequence is fused to the β-galactosidase of GC-B LacZ reporter mice, the β-galactosidase translocates into the nucleus. Therefore, the nuclei of GC-B expressing cells were stained blue. As only nuclei were stained, the activity of the reporter could be distinguished from endogenous cytosolic β-galactosidase activity. Nonetheless, control stainings with VSMCs from wild type mice were performed in parallel.

1. Incubate cells fixed according to section **2.3.2.2** with X-gal staining solution at 37 °C overnight in the dark. Wash cells twice with PBS next day and store at 4 °C if necessary.
2. Wash cells once with 0.5 % BSA-PBS and incubate 30 min with 0.1 % Hoechst 33258 in 0.5 % BSA-PBS at RT in the dark. Wash once with 0.5 % BSA-PBS. Add a drop of 80 % glycerol to a

glass slide and mount coverslip with the cells facing the glass slide. Seal with transparent nail polish, let dry and document (see section **2.3.4.2**).

2.3.4.2 Documentation and quantification of X-gal-stained cells

X-gal staining of cells was documented in brightfield without phase contrast as blue nuclei were difficult to recognise under phase contrast. The total number of cells in each field of view (FOV) was assessed by the fluorescence of Hoechst 33258 staining. For documentation of cells, an upright epifluorescence microscope (Axioskop 20, ZEISS) equipped with a Plan NeoFluar 20x/0.5 objective (ZEISS) and a colour charge-coupled device (CCD) camera (Marlin F-046C, Allied Vision) mounted with a 0.5x lens was used. For brightfield illumination a tungsten halogen lamp with condenser was used. For fluorescence illumination of Hoechst 33258 staining, an HBO 50 mercury-vapor short-arc lamp was used with a SP 365/LP 420 as excitation/emission filter and a DCLP 395 dichroic mirror.

1. Set up Koehler illumination[301] according to standard procedures [302]. Clean glass slide and coverslips carefully with 70 % technical ethanol and place slide in slide holder. Inspect staining through the eye piece to assess quality and overall appearance. Adjust brightness of the light source and colour balance of the software for optimal image quality. Switch to fluorescence mode and find optimal exposure time for documentation of Hoechst 33258 stained nuclei.
2. Document 5 random regions per coverslip (20x objective) in brightfield and fluorescence mode.
3. Analyse images with Fiji. Use “Cell Counter” to manually count X-gal positive (blue) nuclei per brightfield image and total nuclei per fluorescence image. Calculate the fraction of X-gal positive cells per FOV.

2.3.5 cGMP/FRET measurements in cultured VSMCs

For cGMP/FRET measurements, cells expressing the cGMP biosensor cGi500 were cultured for 5-10 days on glass coverslips. If cells were analysed by subsequent IF staining, they were grown on gridded coverslips that were labelled with coordinates (see section **2.3.1**). Either cells from mice expressing the sensor globally (cGi(L1)) or only in SMCs (cGi(L2) in combination with SMC-selective Cre line) were used. Cells were serum-starved for 12-24 h before the actual measurement. Ratiometric cGMP/FRET signals were recorded with the setup described in section **2.3.3.1** in combination with the superfusion system described below. During the measurement, cells were constantly superfused with IB. This setup allowed to apply drugs during defined time spans, therefore allowing to compare the effect of different drugs on the same cell in a single measurement. The superfusion system consisted of a fast performance liquid chromatography pump (Pharmacia P-500, GE Healthcare), fast performance liquid chromatography injection valves (Pharmacia V-7, GE Healthcare), a vacuum pump (Laboport N86, KNF Neuberger), a 2 mL sample loop, tubing (Tygon S3 E-3603, Saint-Gobain), a superfusion chamber for 12 mm coverslips (RC-25, #64-0232, Warner Instruments) attached to a magnetic chamber holder (PM-1, #64-1526, Warner Instruments), and a heatable pen to pre-warm buffer during superfusion (TC-344C Dual automatic temperature controller, Warner Instruments).

As a typical cGMP/FRET measurement took 45-60 minutes, photobleaching of the biosensor had to be kept minimal. This was achieved by reducing the exposure time and increasing the time between two acquisitions (cycle time). For the relatively slow cGMP signalling a cycle time of 5 seconds was sufficient. Reducing the exposure time also decreased the signal-to-noise ratio (SNR), hence decreased the quality of FRET signals. To improve the SNR at low exposure times, the signal of several pixels was summed up (binning). This improved SNR came at the expense of a reduced spatial resolution. A detailed explanation can be found elsewhere ([303; 304]).

For cell culture cGMP/FRET measurements a **4x4 binning** (sum of 16 pixels), **300 ms exposure**, **5 sec cycle time** and a **flow rate of 1 mL/min** were used. **10x objective** was chosen as it allowed to distinguish individual cells while simultaneously detecting a high number of cells in a single measurement.

1. The microscope is placed in a dark air-conditioned (~21 °C) room. Switch on microscope and light source. The light source should run at least 30 min before the first measurement is started. Thaw drugs on ice, pre-dilute the DEA/NO stock solution 1:1000 in 10 mM NaOH and store on ice. Connect a shot flask with IB (buffer reservoir) with the perfusion system. Flush the perfusion system with IB (1x solvent change ~10 mL) including the sample loops.
2. Align CFP and YFP channel of the beam splitter before the first measurement of the day. If cells from cGi(L2) mice are measured, align the beam splitter before every measurement using a calibration grid (Photometrics).
3. Assemble superfusion chamber:
    a. Add a thin layer of silicon grease to the back of the chamber and the chamber holder using a brush. Remove excess silicon with a cotton bud. Attach coverslip with cells to the chamber with cells facing the inside. Flip chamber upside down, press down onto chamber holder and cover cells immediately with IB. Fix chamber with metal plates and clean coverslip with 70 % technical ethanol from outside.
    b. Place chamber holder onto the microscope stage and attach inlet pen (attached to superfusion) and outlet needle (attached to vacuum pump) to the chamber.
4. Start superfusion and vacuum. Change the level of the outlet needle until a constant buffer flow is achieved. A superfusion velocity of 1 mL/min is used for cell culture cGMP/FRET measurements.
5. Use the YFP filter set (brightest fluorophore of the sensor) and inspect the complete coverslip through the eye piece to find an appropriate FOV for the measurement. The region should comply with the following criteria:
    a. The cell density reflects the density of the culture.
    b. A cell-free region for background correction is present.
    c. Cells look healthy and the various morphologies found in the culture are present (1) in high amounts for investigation of marker protein expression or (2) roughly in the same fractions as found throughout the whole coverslip if the fraction of NP-preferring cells should be calculated.
6. Switch to camera mode and use the YFP filter set to adjust the FOV (only half of the region can be measured due to the beam splitter). If cells are grown on gridded coverslips take a brightfield image of the grid coordinates (1x1 binning).
7. Acquire a snapshot with high resolution (1x1 binning, 2 sec exposure, YFP filter set). Switch to the FRET filter set and adjust settings for the measurement (4x4 binning, 300 ms exposure, 5 sec cycle time). Start measurement and mark ~6 cells with different morphologies and a background region for online analysis. Dilute drugs to their final concentrations in IB and store at RT. DEA/NO is diluted in IB directly before application as it starts to release NO at pH 7.4.
8. Record at least 30 frames before application of the first drug (baseline). Load sample loop with the first drug and apply drug via the injection valve. Note time when drug is applied (in frames). Wash the loop 3 times with IB before loading the next drug. Use the online analysis to identify signals. Wait until signals are back to baseline or for 75 frames if no signal is detected before applying the next drug.
   Record ~30 frames after the last drug application as it simplifies baseline correction during offline analysis. Stop measurement, switch back to YFP filter set and acquire a snapshot series (1x1 binning, 3 sec exposure, 25 images).

9. If cells of cGi(L2) mice are measured, remove the beam splitter and set to bypass mode. Use the YFP and mTomato filter set in addition to document the recombination (1x1 binning, 3 sec exposure for both images) in the measured and at least 3 additional random regions.
10. Remove outlet needle and stop superfusion (do not switch order to avoid drying out of cells). Remove chamber from chamber holder. For subsequent IF staining transfer coverslip to fixation solution (see section **2.3.2.1** for a detailed protocol), otherwise discard coverslip.

2.3.5.1 Offline analysis of cell culture and ex vivo cGMP/FRET measurements

During cGMP/FRET measurements an online analysis was performed with the VisiView® software. Only a few exemplary cells were analysed to allow for coordination of drug applications and to get an overview of cGMP signalling patterns present in the VSMC culture. After a series of measurements, the data of all measurements was analysed in detail (offline analysis). The images that were acquired during measurements were analysed with Fiji to extract the fluorescence data. cGMP/FRET signals were calculated from this data using MS Excel and analysed with the Origin Pro software. The analysis in principle was the same for cGMP/FRET measurements of VSMCs in culture and VSMCs in intact aortas (*ex vivo*). Differences in the analysis of *ex vivo* measurements are highlighted in blue.

The analysis can be broken down into a few simple steps. First, cells/regions of interest were identified. Second, the mean fluorescence intensity in these regions was assessed for every time point in the YFP and CFP image and corrected for background signals. Third, cGMP/FRET signals (CFP/YFP ratio) were calculated from this data and normalised to the baseline. The fluorescence signals of the single channels were normalised to their baseline as well (for representation purposes). Last, cGMP/FRET signals in the ratio trace were verified to be true cGMP/FRET signals. True signals could be distinguished from artefacts by the antiparallel movement of the single channels (YFP decrease and CFP increase). Further criteria were applied to assure the integrity and quality of the data set. A detailed step by step procedure is described below. The first part was performed in Fiji.

1. Open snapshot series (1x1 binning, 25 images) and apply “Z Project: Average Intensity” to create an average image. This simplifies recognition of cell borders.
   Open the image stack of the YFP channel and check how strong the tissue moved during the cGMP/FRET measurement. If tissue moves only slightly, apply “Z Project: Average Intensity” to create an average image and continue with the next step. In most cases tissue movement must be corrected to keep cells/structures of interest at the same position. Use the “MultiStackReg” plugin and perform a stack registration (option: “rigid body”) before creating the average image with “Z Project: Average Intensity”.
2. Adjust brightness/contrast of the average image. Mark the outline of all distinguishable cells with region of interests (ROIs). Increase brightness of the image and mark cells that were not distinguishable/visible before. Repeat until no new cells appear. When all cells are marked, place a circular ROI in a cell-free region and label as background. Save ROI set.
   Mark all structures with a clear border. Due to tissue movement (even after stack registration) it is possible that clusters of cells instead of single cells are marked. When all structures are marked, place several circular ROIs in the remaining regions to get an overview about all signals in the tissue. If possible, place a background ROI. Save ROI set.
3. Cell culture measurements are recorded with a 4x4 binning but the snapshotseries is recorded with a 1x1 binning. Therefore, the ROIs are downscaled using a custom python script. First, ROIs are smoothed to subpixel resolution in Fiji to avoid distortion of the ROIs by downscaling. Next, ROIs are downscaled with a scaling factor of 0.25 and saved. Note: downscaling of ROIs can also be achieved without a script via “Edit -> Selection -> Scale” in Fiji.
   No binning is applied for *ex vivo* measurements.

4. Open CFP and YFP image stacks and open the ROI set matching the binning. Check that cells remain within their ROI during the entire measurement. Use "Multi Measure: mean gray value" to determine the mean fluorescence intensity ($\bar{F}_{480}$ for CFP and $\bar{F}_{535}$for YFP) of all ROIs for all images (= time points).
   Perform a stack registration with the CFP and YFP stack (see step 1) before determining the mean fluorescence intensities.
5. Import "mean gray values" in MS Excel. cGMP/FRET ratios are calculated with a macro kindly provided by Dr. Martin Thunemann. In short, the mean fluorescence intensities ($\bar{F}_{480}, \bar{F}_{535}$) are corrected for background signals. The $\bar{F}_{480}/\bar{F}_{535}$ ratio is built and normalised to the baseline (**R ~ [cGMP]**). This ratio represents the cGMP concentration. The single traces of CFP ($\bar{F}_{480}$) and YFP ($\bar{F}_{535}$) fluorescence are normalised to the baseline as well for representation purposes. These normalised values describe the signal change relative to baseline. Detailed calculations can be found in the appendix (**7.3.1**)
   If no background ROI could be placed, background correction is skipped. If a background ROI could be placed, the evaluation is performed without background correction in addition.

Note that **"R"**, **"F_{480}"** and **"F_{535}"** refer to the normalised values usually annotated as $\Delta R/R$, $\Delta F_{480}/F_{480}$ and $\Delta F_{535}/F_{535}$. This abbreviation was chosen to simplify the understanding of this work.

6. cGMP/FRET signals as well as the single traces are evaluated in the Origin Pro software. First, all ratio traces are plotted in separate graphs together with the corresponding single traces and drug applications. Next, the signals of all cells are inspected for their quality. To avoid misinterpretations, low quality signal traces and "fake signals / measurement artefacts" are excluded from the data set. The following criteria are applied:
   a. Real cGMP/FRET signals are marked by an increase of CFP fluorescence and a concomitant decrease of YFP fluorescence. Changes of the ratio trace that are not based on this antiparallel movement of the single traces are excluded as artefacts.
   b. If the single traces show trace separation but no elevation of the ratio trace can be recognised, it is not accepted as a signal. This can be caused by high noise in the baseline (e.g., very dim cells).
   c. If the fluctuations of the baseline are higher than the elevations caused by cGMP/FRET signals, the complete cell is excluded from analysis. Refocus events as well as focus drift are not counted as "fluctuations".
   d. For measurements in VSMC cultures, the height of signals is assessed. Therefore, further criteria are included. These criteria are estimated by visual inspection:
      i. Extreme noise of the baseline relative to the movement of the ratio trace does not allow to reliably assign signal height. This signal is excluded from analysis.
      ii. The highest signal of a cell is lower than twice the baseline noise. It is likely that further signals are obscured by the noise. The complete cell is excluded from analysis.
      iii. It is **unclear** if a cell responded to any of the NPs. The cell is excluded from analysis to assure the integrity of the "Response to NO only" group (**clear** lack of NP-induced cGMP signals).

Note that in *ex vivo* measurements tissue movement could lead to changes in CFP and/or YFP fluorescence that were not based on cGMP-induced FRET changes. These cGMP-independent changes in CFP/YFP fluorescence could potentially mask the antiparallel CFP/YFP trace separation of real cGMP/FRET signals. Therefore, it was not always possible to validate potential cGMP/FRET signals as "real cGMP-induced signals" in *ex vivo* measurements.

7. Determine the signal height of verified cGMP/FRET signals as described in the following section.
   Only assess which region responded to which stimulus, but do not assess signal height (unreliable due to strong focus drifts in *ex vivo* measurements).

Two different approaches to represent cGMP/FRET signals were used in this work. (1) The signal trace of a single cell representative for a certain response pattern was shown (e.g., **Figure 10 A**). (2) The signal traces of all cells with the same response pattern were averaged (**Figure 17 B**). To indicate the variation of signals from different cells, the standard error of the mean (SEM) of the averaged traces was depicted behind the average trace in a lighter colour.

Note that the approach used within this work was rather conservative. The detection of "false positive" signals was minimised on the expense of a higher "false negative" rate.

2.3.5.2 Classification of cultured VSMCs by NP preference

To investigate whether cultured VSMCs responded stronger to ANP or to CNP, the following sequence of stimuli was applied:

ANP (50 nM) – CNP (50 nM) – ANP (250 nM) – CNP (250 nM) – DEA/NO (500 nM)

First, a low and then a high concentration of NPs was applied. ANP and CNP were applied alternating to optimise the comparability between the respective signals (e.g., desensitisation by multiple stimulation). Only signals induced by the same concentration were compared. DEA/NO was used as NO donor. 1 mol of DEA/NO releases 1.5 mol of NO with a half-life of 16 min (22-25 °C, pH 7.4) or 2 min (37 °C, pH 7.4), respectively [305]. DEA/NO was applied as a control stimulus to differentiate between drug-/receptor-limited and sensor-limited cGMP/FRET signals. The DEA/NO concentration used should lead to sensor-saturating responses (see section **4.1.1** for a detailed discussion of this issue).

To assess the strength of a response, the maximal cGMP generation (= peak height) was assessed using the Origin Pro software. The assignment of peak heights to cGMP/FRET signals was refined over several years to improve speed and robustness of evaluation. The procedure described here is the latest version and was performed by using several custom LabTalk[2] scripts. All scripts are available on reasonable request. In principle, all peak heights of the same measurements could be assessed automatically after initialisation of the parameters. To avoid errors, the analysis was performed semi-automatically with several check points. Check points are indicated in blue. In addition to the short description below, a detailed step by step procedure can be found in the appendix (**7.3.2**).

1. Use the ratio traces that were generated and validated according to the procedure described in the previous section. Correct baseline drift of these ratio traces using an exponential function, if possible. Otherwise, perform a linear baseline correction by interpolation.
   Check that the baseline drift correction worked properly.
2. Smooth ratio traces and plot them on top of the original trace.
   Check that the smoothed and original trace overlay correctly.
3. Assess peak height and centre of all signals using the smoothed traces with the "Peak Analyzer" function by batch processing. Transfer peak heights to an evaluation sheet in MS Excel. Also set all heights to "0" where no (validated) signal was elicited by the corresponding stimulus. The evaluation sheet assigns every ROI the respective NP preference based on their responses (see below for necessary calculations).

[2] LabTalk is the script language of Origin Pro which can be used to automatise evaluations. All evaluations performed with these scripts can also be performed without scripts, manually.

Plot peak positions to the original traces and check that the positions match the maximum of every signal. If a peak is misplaced, assess height manually and correct in the evaluation sheet.

cGMP/FRET responses to NPs were used to group cultured VSMCs in ANP- and CNP-preferring cells. Correction of the baseline drift as well as signal noise led to an uncertainty concerning the exact strength of the cGMP response (signal height). Therefore, a threshold was used to classify cells by their preference. Only cells that responded 1.5 times stronger to one of the NPs were accepted as cells with clear preference. This led to the following 5 groups/classes (indicated in bold) that were assigned to every cell based on the peak heights assessed above. For the calculations "Maximal cGMP response to Substance X at concentration Y" is abbreviated as "Substance X [Concentration Y]":

ANP-preferring cells ("ANP", colour code: orange): Cells that responded to ANP but not to CNP. Cells that responded at least 1.5 times stronger to ANP than to CNP (concentration range 50-250 nM).

$$\frac{ANP\ [50\ nM]}{CNP\ [50\ nM]} \geq 1.5\ \boldsymbol{AND}\ \frac{ANP\ [250\ nM]}{CNP\ [250\ nM]} \geq 1.5$$

Cells without clear/stable preference ("ANP~CNP", colour code: green): Cells that responded equally to ANP and CNP. Cells with a slightly stronger response to ANP or CNP (concentration range 50-250 nM).

$$\frac{2}{3} \leq \frac{ANP\ [50\ nM]}{CNP\ [50\ nM]} \leq 1.5\ \boldsymbol{OR}\ \frac{2}{3} \leq \frac{ANP\ [250\ nM]}{CNP\ [250\ nM]} \leq 1.5$$

CNP-preferring cells ("CNP", colour code: cyan): Cells that responded to CNP but not to ANP. Cells that responded at least 1.5 times stronger to CNP than to ANP (concentration range 50-250 nM).

$$\frac{CNP\ [50\ nM]}{ANP\ [50\ nM]} \geq 1.5\ \boldsymbol{AND}\ \frac{CNP\ [250\ nM]}{ANP\ [250\ nM]} \geq 1.5$$

NO-only cells ("NO-only", colour code: grey): Cells that responded to DEA/NO but neither to ANP nor to CNP at any concentration.

Excluded cells (not analysed: "na", not shown): All cells that did not respond at all or were excluded from analysis to assure data quality.

To mark the position of cells with a certain preference in the measured region, ROIs were colour coded after classification with the colours that are indicated above. This can be achieved by selecting a colour for each individual ROI in Fiji.

2.3.5.3 Quantification of cGMP responses to NO

For cell culture experiments, the strength of the NO-induced cGMP/FRET response was quantified in addition to the NP preference. As the strength of the NO response was assessed during the classification procedure, this data was used. To compare the NO response between cells of the same measurement or between measurements, it was normalised. As cells were further processed (IF staining) after the measurements, no permeabilization could be done to normalise on a defined cGMP concentration (cells round up and can detach due to permeabilization). Therefore, NO signals were normalised to the highest response that was induced by one of the NPs (ANP for ANP-preferring cells and CNP for CNP-preferring cells).

$$NO\ response\ [\%\ of\ \max\ NP\ response] = \frac{DEA/NO[500\ nM]}{\max(ANP\ [50\ nM], ANP\ [250\ nM], CNP\ [50\ nM], CNP\ [250\ nM])} \times 100\ [\%]$$

2.3.5.4 Quantification of cells with a certain NP preference

To analyse the heterogeneity of VSMC cultures, the number of cells belonging to one of the 3 groups (ANP-preferring, ANP~CNP, CNP-preferring; "na" was excluded from analysis) was counted and normalised to all cells belonging to these 3 groups. For VSMC cultures from GC-B knockout mice (**Figure 12**, **Supplementary figure V**) "NO-only" cells were included in the analysis as well. Thereby, the relative contribution of cells with different preferences to VSMC cultures under various conditions could be compared. If data from different measurements were pooled (e.g., all measurements performed with the same conditions), all cells belonging to the same group were counted across all measurements. The necessary calculations are shown exemplary for ANP-preferring cells:

$$Fraction\ of\ ANP-preferring\ cells\ [\%] = \frac{(ANP-preferring\ cells)}{(ANP-preferring\ cells) + (CNP-preferring\ cells) + (ANP\sim CNP\ cells) + (NO\ only\ cells)}^{3} \times 100\ [\%]$$

2.3.5.5 Quantification of responsive cells

When it was of interest how many cells responded to ANP, for instance, but not how many cells preferred ANP over CNP, the fraction of "responsive cells" was calculated. Therefore, the number of cells that reacted to ANP, CNP, or DEA/NO was quantified instead of the number of cells belonging to one of the 4 groups. All cells that reacted to the respective stimulus at least once were counted and normalised to all analysed cells ("na" was excluded from analysis). The same analysis was performed for *ex vivo* measurements.

2.3.5.6 Correlation of marker protein expression and NP preference

The cGMP response patterns of cells were assessed by cGMP/FRET measurements. The protein expression of the same cells was assessed by a subsequent IF staining. To correlate both, the position of the cells during the FRET measurement had to match the position of the cells in the IF staining. This was achieved by exploiting the coordinates that were etched into the coverslip. As described in section **2.3.3.1**, the coordinates were used to document the IF staining in the FOV of the measurement. Now the images of the coordinates were used to reorient the image of the IF staining to match the FOV of the cGMP/FRET measurement. All required steps (same numbering as in the description below) are illustrated in **Supplementary figure III** schematically and exemplarily with images of an evaluation that was performed for this work.

1. Open the BF images of the coordinate grid for the cGMP/FRET measurement and the IF staining in Fiji. Rotate the BF image of the staining until both grids show the same orientation ("Enlarge Image" must be checked in the rotation tool). Note the rotation angle.
2. Apply "Enhance contrast: Saturated pixels 0.3 %, Equalize histogram" to both BF images. Copy the BF image of the measurement and paste it into the rotated BF image of the staining. Use "Paste control: Transfer mode Blend" to create a transparent overlay.
3. Move the image of the measurement until both grids match as good as possible (sharp non-blurry overlay). Note position of the pasted image.

[3] NO-only cells were only included in experiments with VSMCs from GC-B knockout mice.

4. Open the snapshot of the measurement and the IF image of the nuclear staining. Apply “Enhance contrast: Saturated pixels 0.3 %, Normalize” to both images to get images with a comparable brightness. Rotate the image of the nuclear staining by the angle determined in step (1). Copy the snapshot and paste it in the staining at the same position as in step 3. Use “Paste control: Transfer mode Blend” to create a transparent overlay.
5. Check if the nuclei of the staining match the nuclei of the cells in the snapshot. If there is a significant mismatch move snapshot until both images match. If the angle does not match, repeat step (4) with an adjusted angle. Note new position and/or angle.
6. Close all images, then open all images of the IF staining that belong to the region of this measurement. Rotate all images by the refined angle. Use “Specify” to create a selection at the refined coordinates with the dimensions of the snapshot. Crop images and safe the cropped images. Now all cells of the IF staining are at the exact same position as the cells during the cGMP/FRET measurement.

Sometimes not the entire FOV of the cGMP/FRET measurement was documented in the IF staining. This was caused by the different orientation of the coverslip. The protein expression of cells that lied (partially) outside of the documented region could not be analysed.

2.3.5.7 Relative quantification of protein expression

To quantify the expression of proteins without loss of spatial resolution, IF stainings for the respective proteins were used. The fluorescence intensity should correlate with the amount of protein. Therefore, the fluorescence intensity was used as an indicator for protein expression. This analysis was only semi-quantitative as the exact intensities depended on several factors (e.g., quality of the antibodies, fluorophores, staining procedure, exposure time). It was not possible to compare the expression levels of different proteins with each other. This method was applied to compare the average expression (mean fluorescence intensity = “mean gray value”) of a marker protein (e.g., αSMA) between cells of the same measurement or between cells of different measurements that were stained and documented at the same day, respectively.

1. Align the IF staining for the protein of interest with its cGMP/FRET measurement as described in the previous section. Open IF staining and the ROI set of this measurement (1x1 binning) in Fiji. Note which ROIs lie (partially) outside of the staining, contain staining artefacts or parts of other cells. These ROIs are excluded from analysis.
2. Use “Multi Measure: mean gray value” to determine the mean fluorescence intensity. Save data and import into MS Excel. Correct the mean fluorescence intensity values by subtraction of the unspecific signal of the background ROI.
3. Group values according to the NP preference of the corresponding cell. If measurements were performed with the same conditions and stained and documented in parallel, expression values can be pooled for further analysis.

2.4 *Ex vivo* analysis of murine tissues

2.4.1 cGMP/FRET measurements in healthy aortas and atherosclerotic plaques

Ex vivo cGMP/FRET measurements in murine tissues were performed with a confocal spinning disk setup (Visitron), controlled by the VisiView® (Visitron) software for image acquisition. An upright microscope (Examiner.Z1, ZEISS) in combination with a spinning disk unit (CSU-X1, Yokogawa) was equipped with an EC Plan-NeoFluar 2.5x/0.085 air objective (ZEISS) and 3 water immersion objectives (W N-Achromat 10x/0.3, W Plan-Apochromat 20x/1.0, W Plan-Apochromat 40x/1.0, ZEISS). For excitation of fluorophores, 3 diode lasers (445 nm 100 mW, 488 nm 100 mW and 561 nm 75 mW) were used. To record high resolution images, a monochrome CCD camera (SPOT Pursuit Monochrome, SPOT

Imaging) was used. The combinations of di-/polychroic mirrors and emission filters (Chroma) for the respective fluorophores are summarised in **Table 4**. For detection of cGMP/FRET signals, a more sensitive EM-CCD camera (QuantEM 512SC, Photometrics) was used. A movable mirror was used to switch the light path between both cameras. Similar to cell culture measurements, a beam splitter (Dual-View DV2) with insert (Micro-Imager DUAL-View, Photometrics) was used to allow simultaneous detection of CFP and YFP emission. It contained a dichroic mirror (505 DCLP) and two emission filters (BP 470/24 [for CFP emission]) and BP 535/30 [for YFP emission]).

Table 4: Filter and laser combinations that were used to detect the different fluorophores. *Band pass filters (ET **X/Y**) let only the specified range of the spectrum pass (**X ± Y/2 nm**). Multi pass filters (**ZET X/Y/Z**) let the indicated centre wavelength (**X, Y, Z ± several nm**) pass. DCLP mirrors (DCLP **Y**) reflect wavelengths shorter than **Y** and let pass wavelengths longer than **Y**. Polychroic mirrors (T **X/Y/Z**) let the indicated wavelengths pass (**X/Y/Z ± several nm**) and reflect the remaining part of the spectrum. The transmission spectrum of the respective mirrors/filters can be inspected following the given links. ET: magnetron sputtered emission filter, T: magnetron sputtered polychroic mirror, ZET: magnetron sputtered emission filter specifically designed for laser use.*

Fluorophore		Camera	Laser	Di-/polychroic mirror	Emission filter
YFP		SPOT Pursuit	488 nm	T405/488/568/647	ET525/50[1]
YFP		QuantEM	488 nm	T405/488/561 + 505 DCLP[2]	ET535/30[2, 3]
CFP		SPOT Pursuit	445 nm	T445/515/561	ET470/24[4]
mTomato		SPOT Pursuit	561 nm	T405/488/568/647	ZET405/488/561/640[5]
FRET	CFP	QuantEM	445 nm	T445/515/561 + 505 DCLP[2]	ET470/24[2, 4]
	YFP				ET535/30[2, 3]

1: https://www.chroma.com/products/custom-inventory/nc460228-et525-50m700lp, 2: Component of the beam splitter "DUAL-View DV2", 3: https://www.chroma.com/products/parts/et535-30m, 4: https://www.chroma.com/products/parts/et470-24m, 5: https://www.chroma.com/products/parts/zet405-488-561-640m

A similar superfusion system as described in section **2.3.5** was used for *ex vivo* cGMP/FRET measurements. Instead of the superfusion chamber RC-25, the chamber RC-26 (#64-0234, Warner Instruments) was used. This chamber was sealed with a 24 x 40 mm square coverslip from below. It was wide enough for the water immersion objectives to enter from above (upright microscope!). Tissues were fixed on the coverslip either by a block of PDMS with needles or with a mesh and a slice hold-down (SHD-26H/10, Warner Instruments). Buffer/drugs were heated to 37 °C by a heatable pen directly before chamber entry.

2.4.1.1 Healthy aorta

- Instruments: large scissors (F•S•T 91402-12), small bent scissor (F•S•T 14061-09), blunt forceps (F•S•T 11018-12), 2 fine forceps (F•S•T No. 5 [11252-20] and F•S•T No. 5/45 [11253-25]), small spring scissors (F•S•T 15000-08)
- Needles (Minuten pins No.10, Entosphinx)

For cGMP/FRET measurements, aortas of mice expressing the cGMP biosensor cGi500 either globally (cGi(L1)) or selectively in SMCs (cGi(L2) in combination with SM22-Cre mice) were isolated with a modified version of the protocol described in section **2.3.1** to match the different needs. The evaluation of cGMP/FRET measurements is described in sections **2.3.5.1** and **2.3.5.5**.

For isolation of VSMCs it was important to remove any other cell type as good as possible during the isolation process. Therefore, tissue damage was acceptable to a certain extent. For *ex vivo* measurements, the aorta should be as intact as possible to best match the *in vivo* situation.

Furthermore, it was not necessary to remove the adventitia as it could be distinguished from the medial layer by location and morphology. To match these needs, the aorta was freed from surrounding fat as gently as possible and not measured parts were stored in full medium in a cell culture incubator (37 °C, 6 % CO_2).

1. Disinfect surgical instruments with 70 % technical ethanol. Fill full medium in several 35 mm cell culture dishes and pre-incubate in cell culture incubator.
2. Sacrifice mouse with CO_2 and verify that inter-toe reflex is gone (blunt forceps). Cut throat with large scissors to assure death (do not perform cervical dislocation as this might rupture the aorta). Spray fur with ethanol and open abdominal cavity completely (caudal to rostral). Cut peritoneum, open thoracic cavity at both sides until neck is reached and chest can be removed. If tissue sticks to chest piece, detach it gently by scratching. Cut oesophagus and trachea and remove lungs. Grab liver, cut below, and push liver and gastrointestinal tract aside. Grab heart (blunt forceps!) and pull it slightly upwards. Use bent scissors and cut along the spine caudal. Start at throat to get as much of parting vessels as possible and continue caudal as far as possible. Cut the aorta and transfer it to PBS.
3. From here on work under a stereo microscope with fine forceps at RT. Use fine forceps to carefully remove the thymus (the parting vessels should appear). Free the parting vessels roughly from surrounding tissue. Do not grab the vessels directly but always surrounding tissue or the heart to avoid damaging the vessel wall. Grab the heart and cut the aortic root with spring scissors. Continue with removal of surrounding tissue until all larger tissue pieces have been removed. This process should be fast (≤ 15 min) but gentle. Strike gently across the aorta once to remove blood.
4. Separate aortic arch (including the brachiocephalic artery and left common carotid artery), thoracic and abdominal part and transfer to labelled cell culture dishes with full medium (prepared in step 1). Store in a cell culture incubator (37 °C, 6 % CO_2) until measurement.

For cGMP/FRET measurements, short pieces of the aorta / parting vessels (3-4 mm in length) were opened longitudinally and pinned to a block of PDMS (luminal side facing the objective, adventitial side facing the PDMS block). The PDMS was attached to the superfusion chamber and superfused by IB during the cGMP/FRET measurement. As the luminal side faced the buffer, drug uptake from the bloodstream was simulated. The YFP fluorescence of the sensor was used to find an appropriate FOV. Measurements were performed with the 40x objective. After the measurement, the three-dimensional structure of the vessel wall could be documented at high resolution by acquisition of Z-stacks.

Instead of pixel binning, the camera gain was increased to reduce the exposure time. Laser power had to be adjusted for each individual measurement as penetration depth and structure of the tissue impacted the signal intensity. Typical settings for *ex vivo* cGMP/FRET measurements of healthy aortas were **40x objective**, **10-30 % laser power** (445 nm), **500 gain**, **200 ms exposure**, **5 sec cycle time** and **a flow rate of 2 mL/min**. A snapshot was acquired by direct excitation of YFP with **15-50 % laser power** (488 nm), **500 gain** and **200-300 ms exposure**.

To document the three-dimensional morphology and/or recombination, Z-stacks were acquired with the SPOT Pursuit camera. A **z-resolution of 0.25-2 µm** was chosen according to the required detail. **50 %-100 % laser power** (488 nm, 561 nm) and exposure times of **300-1000 ms** per image were typically applied. Z-stacks were acquired after cGMP/FRET measurements as photobleaching/toxicity was likely.

1. PDMS must be prepared at least one day in advance as it needs time for curing. Short, bent needles to pin down the aorta should also be prepared in advance.
2. The microscope is placed in a dark air-conditioned (~21 °C) room. Switch on microscope and light source. The light source should run at least 30 min before the first measurement is started. Thaw drugs on ice, pre-dilute the DEA/NO stock solution 1:1000 in 10 mM NaOH and store on ice. Connect a shot flask with IB (buffer reservoir) with the perfusion system. Flush the perfusion system with IB (1x solvent change ~10 mL) including the sample loops. Check alignment of the beam splitter using a calibration grid (Photometrics). If necessary, re-align CFP and YFP channel.
3. Assemble superfusion chamber:
    a. Add a thin layer of silicon grease to the back of the chamber and the chamber holder using a brush. Attach a square coverslip (24 x 40 mm) to the bottom of the chamber and fix it on the chamber holder.
    b. Use a surgical knife to cut a ~5 x10 mm block of PDMS. Transfer block to chamber and press down firmly on the glass coverslip. It is important that the bottom of the PDMS block and the glass coverslips are not damaged, free from dust and liquids. Otherwise, the block will detach during the measurement.
4. Isolate the aorta of a cGi500 expressing mouse as described above. Use large spring scissors to cut off a 3-4 mm long piece of the aorta or a parting vessel. Use small spring scissors to open the piece longitudinally. Add IB to the superfusion chamber until the PDMS is covered with liquid. Place chamber under a stereo microscope. Use the bent needles prepared in step 1 to pin the vessel to the PDMS with the luminal side facing away from the PDMS (towards the objective later). At the end, the vessel should be slightly stretched to block movement of the tissue during the measurement as good as possible and to keep it flat.
5. Place chamber holder onto the microscope stage and attach inlet pen (attached to superfusion) and outlet needle (attached to vacuum pump) to the chamber. Start heating of the pen and lower the objective (40x). Start superfusion and wait until buffer connects to the objective then start vacuum. Change the level of the outlet needle until a constant buffer flow is achieved. A superfusion velocity of 2 mL/min is used. Place laser safety box on the stage to protect eyes from dispersed laser light.
6. Use BF illumination with SPOT camera to bring the tissue into focus. Use the YFP fluorescence of the sensor to find an appropriate region for the cGMP/FRET measurement.
7. Switch to QuantEM camera for the actual measurement. Refocus tissue under YFP illumination and adjust the FOV. Take a snapshot of the YFP fluorescence (40x, 15-50 % laser power 488 nm, 500 gain, 200-300 ms exposure). Wait at least 1 minute and take a snapshot again. Compare both snapshots to assess the severity of the focus drift. If necessary, change the FOV to a new region which is less impacted by tissue movement.
8. Save the last snapshot and load FRET settings. Typical settings are 40x magnification, 10-30 % laser power (445 nm), 500 gain, 200 ms exposure, 5 sec cycle time. Start measurement and mark ~6 cells at different positions in the FOV.
9. Dilute drugs to their final concentrations in IB and store at RT. DEA/NO is diluted in IB directly before application as it starts to release NO at pH 7.4.
10. Record at least 30 frames before application of the first drug (baseline). Load sample loop with the first drug and apply drug via the injection valve. Note time point when drug is applied (in frames). Wash the loop 3 times with IB before loading the next drug. Use the online analysis to follow changes of the ratio trace (R ~ [cGMP]) as well as the single traces (F480/CFP and F535/YFP) to verify signals (see **2.3.5.1** for a detailed explanation). Wait until signals are back to baseline or for 50 frames if no signal is detected before applying the next drug. Due to focus drifts the baseline can change (baseline drift).
11. If the focus changes too much, a refocus is necessary during the measurement. The focus drift can be estimated by comparison of the snapshot with the actual FOV. If the morphology of

cells changed drastically or a different cell layer is in focus, start refocussing (note start and end of refocussing). Try to avoid refocus events during drug elicited cGMP/FRET signals.
The baseline should be approximately at the same level as at the start of measurement. Changes of the baseline due to photobleaching or changes of the tissue itself cannot be corrected during the measurement.

12. Record ~30 frames after the last drug application as it simplifies baseline correction during offline analysis. Stop measurement. If vessels of cGi(L2) mice are measured, switch back to SPOT camera, and acquire images of the YFP and mTomato fluorescence to assess recombination in the measured FOV.
13. If necessary, document the three-dimensional morphology of the vessel by acquisition of Z-stacks:
    a. Switch to SPOT camera. Choose appropriate magnification and focus luminal side of the vessel under YFP fluorescence (mark z-position as boundary). Focus the outermost layer of the vessel (close to adventitia) where cells are still visible and mark z-position as boundary. Set the step size (z-resolution) to the required level of detail (e.g., 0.25 µm for 40x objective). If vessels of cGi(L2) mice are measured, change to mTomato fluorescence and check if the upper or lower boundaries need to be extended.
    b. Acquire Z-stack. Typical settings for acquisition of Z-stacks are 50-100 % laser power (488 nm, 561 nm), 300-1000 ms exposure, 0.25-2 µm step size.
14. Press down PDMS with forceps and remove needles (re-use!). Discard tissue and continue from step 4 with the next part of aorta / parting vessel. It is possible to measure the aorta after several hours, but it should be noted that the quality of measurements decreases with time.

2.4.1.2 Atherosclerotic plaque

Details about the generation of atherosclerotic mice for cGMP/FRET measurements are provided in section **2.4.5.1**. The evaluation of cGMP/FRET measurements is described in sections **2.3.5.1** and **2.3.5.5**. Atherosclerotic plaques for cGMP/FRET measurements were isolated and measured as described above with some minor changes. To ease immobilisation of plaques during measurements, they were measured while still attached to the vessel wall. The following steps of the isolation process (**2.4.1.1**, **upper protocol**) were modified as follows:

3. Do not strike across the aorta to remove remaining blood as plaques might get damaged or detached.
4. When separating aortic arch (including the brachiocephalic artery and left common carotid artery), thoracic, and abdominal part, take care to not cut through plaques. Plaques can be seen from the outside by their white colour.

The vessel wall of plaque containing pieces could not be fixed on PDMS with needles as this process (handling, stretch) could lead to detachment of the plaque. Instead, the tissue was immobilised directly on the coverslip by a nylon mesh in combination with a slice hold-down with 1 mm spacing (SHD-26H/10, Warner Instruments). This did not restrict the focus drift as efficiently as pinning with needles. We used a 20x objective for these measurements (instead of 40x) to image a large portion of the plaque without losing the ability to distinguish individual cells. The following steps of the measurement protocol (**2.4.1.1**, **lower protocol**) were modified as follows:

1. Neither PDMS nor needles are used.
3. Assemble superfusion chamber:
    b. Use scissors to cut a rectangular piece of the nylon mesh, slightly larger than the inner part of the chamber.

4. Isolate the aorta of a cGi500 expressing mouse as described above. Use large spring scissors to cut off a piece of the aorta or a parting vessel containing 1-2 plaques. Use small spring scissors to open the piece longitudinally. Be careful not to cut through the plaque. Add IB to the superfusion chamber. Place chamber under a stereo microscope and carefully fix the vessel with a nylon mesh and slice hold-down. The luminal side with the plaques must face away from the chamber (towards the objective later). If the plaque is concealed by a thread, use forceps to reposition it (pull media not plaque!). Assure that the medial part is hold by as many threads (mesh / slice hold-down) as possible.
5. Place chamber holder onto the microscope stage and attach inlet pen (attached to superfusion) and outlet needle (attached to vacuum pump) to the chamber. Start heating of the pen and start superfusion. Lower the objective (2.5x) and identify plaque under brightfield illumination. Change to 20x objective and stop vacuum until buffer connects to the objective then start vacuum again. Change the level of the outlet needle until a constant buffer flow is achieved. A superfusion velocity of 2 mL/min is used. Place laser safety box on the stage to protect eyes from dispersed laser light
7. Switch to 20x QuantEM camera for the actual measurement. Refocus plaque under YFP illumination and adjust the FOV. Optimally, a well-structured part of the fibrous cap is chosen for the measurement. With this setup it is only possible to measure the top layer(s) of the fibrous cap. Take a snapshot of the YFP fluorescence (20x, 50 % laser power 488 nm, 500 gain, 200-300 ms exposure). Wait at least 1 minute and take a snapshot again. Compare both snapshots to assess the severity of the focus drift. Change the FOV to a new region which is less impacted by tissue movement if necessary.
8. Save the last snapshot and load FRET settings. Typical settings are 20x magnification, 20-30 % laser power (445 nm), 500 gain, 200 ms exposure, 5 sec cycle time. Start measurement and mark ~6 cells at different positions in the FOV.
13. Document the three-dimensional morphology of the plaque by acquisition of Z-stacks:
    b. Acquire Z-stack. Typical settings for acquisition of Z-stacks are 50 % laser power (488 nm), 300-500 ms exposure, 0.25-2 µm step size.
    c. If the plaque is too large to fit in a single FOV, several Z-stacks that overlap in x- or y-direction can be acquired and stitched later using Fiji.
14. Discard tissue and continue from step 4 with the next plaque. It is possible to measure plaques after several hours, but it should be noted that the quality of measurements decreases with time.

2.4.2 Dehydration and paraffin embedding of hearts and atherosclerotic aortae

- Embedding ring: M460-6 embedding ring (high impact polystyrene, Simport)
- Paraffin: Surgipath Paraplast X-tra (Leica), melt and keep at 56 °C
- Tissue cassette: M491-2 (Simport)
- Metal mould, magnifying lens, forceps, and cannula

Before paraffin embedding, hearts and atherosclerotic aortae were dehydrated by an increasing ethanol concentration row. Tissues were fixed before the dehydration procedure by transcardial perfusion (section **2.4.5.2** step 4) and an additional fixation step after further tissue processing (section **2.4.5.2** step 7). Fixed hearts were cut directly below the auricle with scissors before dehydration (apical part was discarded). The aorta was cut directly before the embedding procedure (see below and **Figure 9 B**).

1. Fill a 12-well plate with 60 % ethanol and place 1 aorta + heart per well. Incubate at 4 °C overnight. Replace 60 % ethanol with 70 % ethanol and incubate 1 h at RT on a shaker. Repeat procedure with increasing concentrations of ethanol (1 h 80 %, 1 h 90 %, 2x 20 min 100 %).

2. During the last ethanol incubation, prepare 2 mL reaction tubes with 100 % toluene under a fume hood. Do not continue in the well plate as toluene solves the plastic. Label tissue cassettes with a pencil and put molten paraffin on a heating plate.
3. Transfer aorta and heart to 100 % toluene and incubate for 2 min (do not exceed time as tissue becomes brittle otherwise). Transfer tissues to tissue cassette, close and drop into molten paraffin. Incubate in paraffin at 56 °C overnight.
4. Transfer tissue cassettes to new paraffin solution, stir and incubate at 56 °C overnight. Repeat this step once more (this time 2 h are sufficient but the incubation can be extended overnight).
5. Embed tissues with clean paraffin. The assembly of the paraffin embedding device (**Figure 9 A**) as well as the orientation of the aorta in the paraffin blocks (**Figure 9 B**) is schematically shown in **Figure 9**.
    a. Take out a tissue cassette and use a surgical knife to cut the aorta into 4 pieces (1x aortic arch [including branching vessels], 3x thoracic/abdominal part). Fill moulds with clean paraffin and put heart, the aortic arch, and the thoracic/abdominal parts in one mould, respectively. Cover moulds with embedding rings.
    b. Take mould and press briefly onto ice until the paraffin at the bottom starts to solidify. Take mould from ice and use injection cannula and magnifying lens to orient the tissue.
        i. Heart: cut edge should face the bottom without inclusion of air bubbles
        ii. Aortic arch: aortic root and transition to the thoracic part should face towards the bottom while the branching vessels point towards the top (see **Figure 9 B**)
        iii. Thoracic/abdominal parts: place tubes parallelly with the openings pointing towards the edge.
    c. Put mould back on ice until paraffin turns turbid then let paraffin solidify completely at -20 °C. Remove embedding ring from mould. The paraffin block should stick to the embedding ring. Store paraffin blocks at RT until sections are prepared. Sections will be cut from bottom to top.

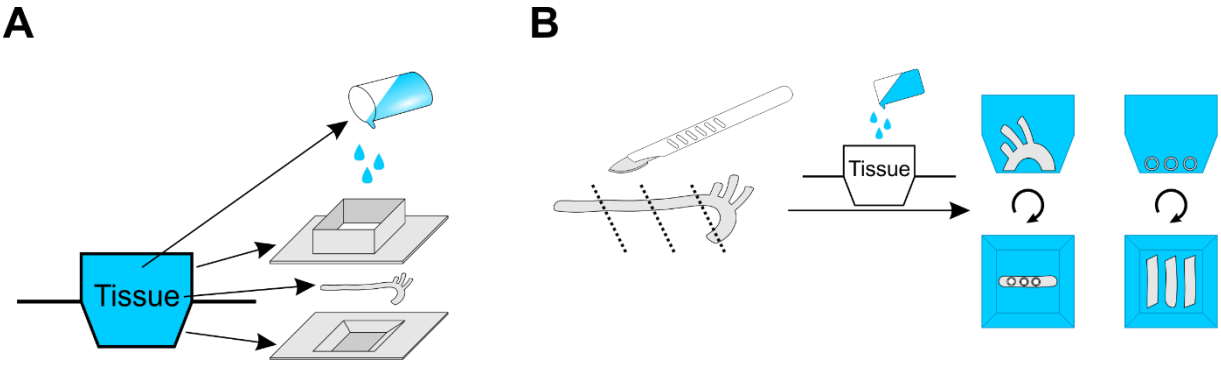

Figure 9: Embedding of aortic tissue in paraffin for preparation of histological sections. *Assembly of the paraffin embedding device (A) and schematic overview of the embedding process for aortic tissue (B).* ***A:*** *The dehydrated aorta was placed in a metal mould (bottom) and sealed by an embedding ring (top). Liquid paraffin (blue) was added from the top until the cassette has been filled completely.* ***B:*** *The dehydrated aorta was cut into 4 pieces using a surgical knife. The aortic arch was embedded with the aortic root facing the bottom of the mould. The thoracic and abdominal aortic parts were embedded next to each other with the lumen facing sidewards. The top panel shows the tissue from a side view and the bottom panel from the top. For clarity, the embedding ring that sticks to the paraffin block is omitted. Blocks were cut from bottom to top. For details see text and section* ***2.4.3****.*

2.4.3 Sectioning

- Microtome blades: Low-Profile disposable blades DB80LS (Leica)
- Polysine glass slides (Menzel)

Paraffin sections were cut with a rotary microtome (HM 335 E, Microm) from the bottom of paraffin blocks to the top. Sections were stretched in a water bath prior to mounting on adhesive Polysine glass slides. Consecutive sections were mounted on series of 5 slides (16 sections per slide). 20 sections per column were distributed across the slides of a series, then the next column was started (see **Supplementary figure IV**). Usually, 4 series were prepared per aortic arch. In total ~320 sections per tissue were collected.

1. Set angle of blade holder to 8-10° and section thickness to 10 µm. Heat water bath to 42 °C. Attach paraffin block and orient block parallel to the blade. Cut away paraffin until tissue is reached then cut ribbons of 4 sections.
2. Transfer sections to water bath and let them stretch. Transfer sections to Polysine glass slides and let dry for several minutes. Check section quality under a microscope. If sections are wrinkled, increase time in water bath, temperature of water bath or adjust cutting angle.
3. Let sections dry completely overnight and store at RT until further processing.

2.4.4 Immunohistochemistry (IHC) stainings

- **10 % methanol**: 10 mL 100 % methanol, ad 100 mL PBS, store at RT
- **30 % H_2O_2** (Roth), store at 4 °C
- **Peroxidase blocking solution**: 6.3 % H_2O_2 (300 µL 30 % H_2O_2), 0.9 % methanol (130 µL 10 % methanol), 1 mL PBS, always prepare freshly
- **Antigen retrieval solution** pH 6.0: 10 mM sodium citrate (2.94 g $Na_3C_6H_5O_7 \bullet 2\ H_2O$, Sigma-Aldrich), ad 1 L H_2O, adjust pH to 6.0 with citric acid (Roth), store at RT
- **Blocking solution**: 10 % NDS/NGS (species depends on sAb) in TBS-T
- **Nail polish**: Super Stay – Crystal Clear (Maybelline)
- **pAb solution**: pAb (see **Supplementary table IV**), 5 % NDS/NGS (species depends on sAb) in TBS-T
- **sAb solution**: biotinylated sAb (see **Supplementary table IV**), 5 % NDS/NGS (species depends on sAb) in TBS-T
- **ABC solution** (Vectastain Elite ABC Kit Peroxidase, Vector Labs): 12 µL solution A (avidin), 12 µL solution B (biotinylated horseradish peroxidase, HRP), ad 600 µL PBS, **mix and incubate 30 min at RT protected from light**, add 600 µL TBS-T directly before use
- **0.1 %** 3,3'-diaminobenzidene (**DAB**): dissolve 40 mg DAB (Sigma-Aldrich) in 40 mL PBS, store at -20 °C protected from light
- **DAB staining solution**: 0.05 % (w/v) DAB (800 µL 0.1 % DAB), 0.02 % H_2O_2 (1 µL 30 % H_2O_2), 800 µL PBS, prepare directly before use
- **Aquatex®** mounting medium (HC860590, Merck)

To investigate the expression and distribution of marker proteins (e.g., MAC-2 or αSMA) within atherosclerotic aortas, IHC was performed with paraffin sections of the aortic arch. The avidin-biotin-complex method with DAB as chromogen was used. Similar to the indirect IF method, the protein of interest was detected by a pAb which in turn was bound by a species directed biotinylated sAb. Instead of a fluorophore an enzymatic reaction was used for detection. HRP catalysed the H_2O_2-dependent oxidation of DAB, forming an insoluble brown precipitate. Biotinylated HRP formed a complex with avidin that could bind to the biotinylated sAb. Therefore, several HRP molecules were bound per sAb [306]. The brown precipitate formed by DAB had the advantage that it could be combined with X-gal stained (blue precipitate) tissue sections if the staining was not too intense. To account for unspecific

binding of sAbs and other artefacts (e.g., direct oxidation of DAB by H_2O_2), controls without pAbs were always performed in parallel. The normal serum used for blocking should match the species of the sAb.

1. Incubate slides with paraffin sections overnight at 37 °C to improve adhesion to the slide.
2. Deparaffinise sections with 100 % toluene (2x 2 min) then rehydrate with decreasing concentrations of ethanol (2x 1.5 min 100 %, 1.5 min 90 %, 1.5 min 80 %, 1.5 min 70 %, 1.5 min 60 %) under a fume hood at RT. Finally incubate sections 5 min in PBS.
3. Use PAP pen (Science Services) to separate sections that are stained with different antibodies or negative control with a hydrophobic barrier.
4. If sections of X-gal-stained tissues are used, document sections before proceeding (see next section for details).
5. Block endogenous peroxidase with peroxidase blocking solution (~500 µL/slide) 20 min at RT in a humid chamber. Wash slides 3 min at RT in PBS. Incubate slides with antigen retrieval solution 15 min at RT, then 10 min at 92 °C to unmask antigens. Let cool down for at least 10 min at RT and wash briefly in TBS-T. Block unspecific binding sites with blocking solution (~500 µL/slide) for 2 h at RT. Refresh hydrophobic barriers if necessary.
6. Remove blocking solution with a pipette and incubate with pAb solution overnight at 4 °C in a humid chamber. For negative control omit pAb.
7. Wash slides 3x 5 min in TBS-T at RT.
8. Incubate 2 h with sAb solution at RT (~500 µL/slide) in a humid chamber. Prepare ABC solution ~30 min before incubation time ends. Discard sAb solution and wash 3x 5 min in TBS-T at RT. Incubate 30 min with ABC solution (~500 µL/slide) in a humid chamber.
9. Prepare DAB staining solution and keep it protected from light until use. Discard ABC solution and wash 3x 5 min in TBS-T at RT. Incubate with DAB staining solution (~500 µL/slide) at RT until colour develops. Check colour development under a microscope. Stop staining by immersing the slides in tap water.
10. If a nuclear counterstaining is necessary, mount sections with 0.1 % Hoechst 33258 in 80 % glycerol (store horizontally in the dark at RT from now on). Otherwise, mount with Aquatex®:
    a. Cover sections with several drops of mounting medium and put a square coverslip on top. If Aquatex® is used, let dry overnight and document. If glycerol is used, fix the corners of the coverslip with a drop of transparent nail polish. Let dry briefly and seal all edges of the coverslip with nail polish, let dry overnight and document.

2.4.4.1 Documentation

IHC stainings of sections were documented in BF without phase contrast. In addition, the nuclear staining by Hoechst 33258 was documented in parallel using fluorescence settings. An upright epifluorescence microscope (Axioskop 20, ZEISS) equipped with an A-Plan 5x/0.12, an A-Plan 10x/0.5x and Plan NeoFluar 20x/0.5 objective (ZEISS) was used for documentation. An EOS 750 D (Canon) digital camera mounted with a 1.6x or 2.5x lens was used for detection. For BF illumination, a tungsten halogen lamp with condenser was used. For fluorescence illumination of Hoechst 33258 stainings, an HBO 50 mercury-vapor short-arc lamp was used with a DCLP 395 + LP 420 as excitation/emission filter. To control the camera, the EOS utility software was used.

If tissues were stained with X-gal, they were documented before and after IHC staining. Therefore, tissues were covered with TBS-T directly after rehydration and documented according to step (3). Other slides were kept in PBS during documentation.

1. Set up Koehler illumination[301] according to standard procedures [302].
2. Clean glass slide and coverslip carefully with 70 % ethanol and place slide in slide holder. Inspect staining through the eye piece to assess quality and overall appearance. Adjust brightness of the light source, exposure time and chose empty region on slide to apply white

balance. Switch to fluorescence mode and find optimal exposure time for documentation of Hoechst 33258 stained nuclei.

3. Document every section completely at 5x magnification using the 2.5x mount. Only take BF images at this magnification. Document all sections at the same day using the same settings.
4. Document interesting structures at higher magnifications (10x/20x mounted with 1.6x lens). First take BF image then document nuclei in fluorescence mode (same region).

The following table lists typical settings for exposure time and light source settings for the respective magnifications.

Table 5: Typical exposure times and light source settings for documentation of tissue sections with the Axioskop 20*. BF "x" – BF illumination (the higher "x" the higher the intensity); F: fluorescence illumination*

Magnification	Camera mount	Exposure time	Light source
5x	2.5x	1/125 second	BF "4"
10x	1.6x	1/80 second 2 seconds	BF "4" F "100 %"
20x	1.6x	1/80 second 2 seconds	BF "3" F "100 %"

2.4.5 Analysis of atherosclerosis

2.4.5.1 Generation of atherosclerotic mice

- **Atherogenic diet** (modifiziertes Altromin 1324): 20 % fat, 1.5 % cholesterol (Altromin)

Atherosclerosis was generated by a genetic approach in combination with an altered diet. Mice do not naturally develop atherosclerosis but interfering with their cholesterol/lipid metabolism leads to the development of complex atherosclerotic lesions. One of the most common genetic mouse models for atherosclerosis are ApoE-deficient mice (ApoE -/-) [244; 299]. For this work, ApoE -/- mice were used together with an atherogenic diet high in cholesterol and fat.

Atherosclerotic mice were bred for two different kinds of experiments. (1) Atherosclerotic mice expressing the cGMP biosensor cGi500 globally were bred to compare cGMP signalling in healthy and diseased vessels. (2) To assess the relevance of CNP-dependent cGMP signalling in VSMCs for plaque development, atherosclerotic mice lacking the CNP receptor GC-B selectively in SMCs were bred.

(1) cGi(L1) mice with and without GC-B LacZ as an additional transgene were bred on an ApoE-deficient background (ApoE -/- x cGi(L1) +/L1 x GC-B +/LacZ and ApoE -/- x cGi(L1) +/L1 x GC-B +/+). At the age of 25 weeks, standard chow was replaced by an atherogenic diet for 16 weeks. Afterwards, mice were subjected to cGMP/FRET measurements as described in section **2.4.1.2**.

(2) SMC-selective GC-B knockout mice (Smko mice) were bred on an ApoE-deficient background (ApoE -/- x GC-B L2/LacZ x αSMA-CreER^{T2} +/tg). As the heterozygous global ablation of GC-B by the GC-B LacZ transgene could influence plaque development, ApoE-deficient GC-B LacZ mice (LacZ-ctrl) were used as controls (ApoE -/- x GC-B L2/LacZ x αSMA-CreER^{T2} +/+). Additional control mice were ApoE-deficient mice expressing the recombinase (Cre-ctrl: ApoE -/- x GC-B L2/+ x αSMA-CreER^{T2} +/tg) or were just ApoE-deficient (Ctrl: ApoE -/- x GC-B +/L2 x αSMA-CreER^{T2} +/+). SMC-selective ablation of GC-B was induced by two sequences of intraperitoneal tamoxifen injection (5x 1 mg/mouse/day at 4 weeks and 6 weeks of age). At 8 weeks of age, standard chow was replaced by an atherogenic diet for

18 weeks. Subsequently, mice were sacrificed and analysed in several ways (**Supplementary figure VII**). Blood samples of all mice were collected at the day of experiment and parameters typically used to monitor atherosclerosis development were determined. 2 mice per genotype were used to validate the SMC-selective ablation of GC-B by western blotting and genotyping PCRs of the atherosclerotic aortas. All other mice were used for the analysis of atherosclerotic plaques. The total lesion area was assessed by Oil Red O staining of the intact aortas. The contribution of GC-B LacZ positive cells to atherosclerotic plaques was evaluated by X-gal staining of the intact aorta with subsequent quantification in histological paraffin sections. As Oil Red O and X-gal staining are compatible, both were performed on the same aortas. Finally, plaque structure was investigated by IHC stainings for the VSMC marker protein αSMA.

All three types of controls as well as the SMC-selective GC-B knockout were the result of the same breeding strategy (could be littermates). Littermates were processed at the same day. Please note that all ApoE-deficient mice (Smko, LacZ-ctrl, Cre-ctrl, Ctrl) were treated with tamoxifen to exclude effects of this partial oestrogen agonist as confounding factor.

2.4.5.2 Isolation of aortas from atherosclerotic mice

- **20 I.U./mL heparin**: dissolve 1 mg heparin (heparin sodium salt ≥180 I.U/mg, Roth) in 9 mL PBS, store at 4 °C
- 27 G cannula: 27 G 0.4 x 20 mm cannula (Sterican, B. Braun)
- 3-component narcotic: 500 mg/L Midazolam, 50 mg/L Medetomidine, 5 mg/L Fentanyl

For a reliable determination of blood parameters, it was important to starve the mice before the experiment (no chow but water ad libitum). The aorta was isolated in a similar way as described in section **2.4.1.1** but cleaned less thoroughly as this process is easier after Oil Red O staining (better contrast of tissues).

1. Starve mice overnight (no chow but water ad libitum)
2. Weigh mice, note weight, and anaesthetise mice by intraperitoneal injection of 3-component narcotic (100 µL/10 g mouse). Process two mice in parallel as anaesthesia takes several minutes. Wait until inter-toe reflex is gone. Collect ear biopsies for re-genotyping and extract DNA according to **2.2.4.1**.
3. Fill 1 mL syringe equipped with a 27 G cannula with 0.02 mL 20 I.U./mL heparin. Carefully remove skin from thorax with scissors and collect blood samples by puncturing the left ventricle of the heart with the syringe. Collect at least 500 µL and retrieve serum:
    a. Let the blood coagulate for 2 h at RT. Centrifuge 3 min at 3000 g and collect 200 µL of supernatant. Quick-freeze in liquid nitrogen and store at -80 °C until further analysis.
4. Fix heart and aorta by transcardial perfusion with Cellfix for X-gal staining. Open thorax (leave abdominal part intact) and insert 27 G cannula (connected to a roller pump perfusion system) into the left ventricle of the heart pointing towards the ascending aorta. Start perfusion with cell fix at ~0.5 mL/min. Cut vena cava inferior between heart and liver. Perfuse for 3 min at RT.
5. Isolate aorta as described in **2.4.1.1** (step 2-3) with following adaptations:
    (2) Do not remove lungs, and collect liver, spleen, and kidneys before removing the aorta. Pat tissues dry with a paper towel and note weight. Otherwise perform this step as described in **2.4.1.1**.
    (3) From here on work under a stereo microscope with fine forceps at RT. Use fine forceps to carefully remove the thymus (the parting vessels should appear). Free the parting vessels roughly from surrounding tissue. Do not grab the vessels directly but always surrounding tissue or the heart to avoid damage of the vessel wall. **Remove lungs. Grab the heart and cut the aortic root with spring scissors (approximately 1 mm of the root should remain).**

Incise heart to improve penetration with X-gal solution. Continue with removal of surrounding tissue until all larger tissue pieces and the bulk of perivascular fat have been removed.

6. Transfer aorta and heart to a 12 well plate and wash 3x 5 min with PBS on a shaker. Perform X-gal staining by replacing PBS with X-gal staining solution. Wrap plate in aluminium foil to protect from light and incubate overnight at 37 °C on a horizontal shaker (40 revolutions per minute) in the dark.
7. Stop X-gal staining by washing 3x 5 min with PBS at RT on a shaker. Finish fixation process by incubation with Cellfix for 10 min at RT. Wash 3x 5 min with PBS.
8. Remove heart, weigh, and transfer to 60 % ethanol for embedding.
9. Seal plate with parafilm and store aortas at 4 °C in PBS until Oil Red O staining is performed.

2.4.5.3 Verification of the SMC-selective GC-B knockout

The SMC-selective knockout of GC-B was exemplarily verified by western blotting and genotyping PCRs of the atherosclerotic aortas. For western blotting, the plaque rich aortic arch and abdominal part were used. To yield enough protein for western blotting, two aortas per genotype were pooled. The genotyping PCRs were performed with the thoracic part of the aorta due to its high SMC content. The SMC-selectivity was assessed by comparing the recombination in the aorta lysate with the recombination in the ear biopsy taken for re-genotyping. Due to the high sensitivity of PCR, lysates could be prepared from individual aortas.

The protocol described in section **2.4.5.2** was used with minor changes to isolate atherosclerotic aortas:

4. This step is omitted as fixation interferes with western blotting and PCR.
5. The aorta is cleaned thoroughly to remove as much non-aortic tissue as possible. Separate plaque rich parts of the aorta (aortic arch and abdominal part) from the thoracic part and collect in 1.5 mL reaction tubes. Do not pool before genotypes are confirmed by re-genotyping. Quick-freeze plaque rich parts in liquid nitrogen and store at -80 °C until western blotting is performed according to section **2.5**. Extract DNA from thoracic parts as described in section **2.2.4.1**.

The PCR for knockout verification was performed as described in **2.2.4.2**. This PCR distinguished three different versions of the GC-B allele. The wild type / GC-B LacZ allele ("+"), the floxed allele before recombination ("L2": two loxP sites present) and the inactivated allele after recombination ("L1": one loxP site present). As the loxP sites of GC-B flox mice are located surrounding exons 17 and 18 (see **Figure 19 C**) but the LacZ gene of GC-B LacZ mice is placed in exon 1, this PCR detected the GC-B LacZ allele as wild type allele.

2.4.5.4 Assessment of blood parameters

Blood serum of atherosclerotic mice was analysed to get an overview about their physiological state and to exclude confounding factors that could influence the development of atherosclerosis (e.g., ineffective elevation of plasma cholesterol). Prof. Dr. med. Andreas Peter of the "Zentrallabor des Universitätsklinikums Tübingen" kindly analysed the following blood parameters: alkaline phosphatase, cholesterol, creatine kinase, total protein, glucose, glutamic oxaloacetic transaminase, glutamate-pyruvate transaminase, high-density lipoprotein (HDL), low-density lipoprotein (LDL), urea, non-esterified fatty acids, and triglycerides.

2.4.5.5 Oil Red O staining of atherosclerotic lesions

- **78 % methanol**: 78 mL 100 % methanol, ad 100 mL H_2O, store at RT
- **1 M NaOH**: dissolve 20 g NaOH in 500 mL H_2O, store at RT
- **Oil Red O staining solution**: 35 mL Oil Red O stock, 10 mL 1 M NaOH, prepare freshly and filter solution (MN 615, Macherey-Nagel)
- **Oil Red O stock**: 0.5 % Oil Red O (0.4 g Direct Red 80, Sigma-Aldrich), 80 mL 100 % methanol, dissolve by stirring, filter solution (MN 615, Macherey-Nagel), store at RT protected from light

Oil Red O stains neutral fats and cholesteryl esters [307]. When atherosclerotic aortas are incubated with this dye, it accumulates in plaques while the remaining vessel is only slightly stained (contains mainly phospholipids). Staining with Oil Red O is a standard method to quantify lesion area in atherosclerotic aortas.

1. Isolate aortas from atherosclerotic mice as described in section **2.4.5.2**.
2. Wash aortas in 78 % methanol for 5 min at RT on a shaker. Aspirate methanol and incubate in Oil Red O solution for 90 min at RT, protected from light, on a shaker. Transfer aortas to 78 % methanol in a new 12-well plate and destain for 5 min at RT on a shaker.
3. Transfer aortas to PBS and finish cleaning process. All surrounding tissue must be removed carefully to avoid detachment of atherosclerotic lesions. Aortas can be stored in PBS at 4 °C until documentation.

2.4.5.6 Documentation and quantification of lesion area

Lesion area of Oil Red O-stained aortas was documented with an EOS 750 D (Canon) digital camera mounted with a 1.6x lens on a stereomicroscope (Stemi 2000 CS, ZEISS). Two light sources were used to illuminate the samples (KL1500 LCD, Schott). One light source illuminated the sample from below. The other light source was equipped with two gooseneck lamps, allowing for flexible illumination. Aortas were placed in a 100 mm petri dish filled with PDMS. This helped keeping the aortas in place during documentation.

1. Set light sources to 3200 K and place the PDMS coated petri dish filled with water under a stereomicroscope. Transfer an aorta to the dish and place a coverslip on top. Press the coverslip down by placing two 10 g weights at opposing corners. Check that all parts of the aorta are clearly visible, no part is twisted or folded.
2. Illuminate the aorta evenly from two opposing sites. Adjust exposure time at the camera and acquire an image (0.65x and 1x magnification). Move the aorta between images until all parts are documented. Flip aorta and document its reverse side.
3. Dehydrate documented aorta and embed in paraffin as described in section **2.4.2**.

The lesion area was determined in Fiji using the images that were acquired above. Lesions generally progress faster in the aortic arch than in the thoracic part. Therefore, lesion area in the arch and the remaining aorta was evaluated separately. Lesion area was normalised to the total area of the vessel wall (aortic arch or thoracic/abdominal aorta).

The lesion area in the aortic arch was quantified using the images acquired at 1x magnification (scale: 436.0 pixel/mm). The lesion area of the thoracic/abdominal part was quantified in the 0.65x magnification images (scale: 276.2 pixel/mm).

1. Open an image of the aortic arch in Fiji (1x magnification). Set scale to 436.0 pixel/mm. Use the polygon selection tool and mark the aortic arch within the following boundaries and save ROI as “area arch”:

a. Up to 1 mm in front of the brachiocephalic artery and up to 1 mm rear of the left subclavian artery. The brachiocephalic artery and the left subclavian artery are included up to their branching point. The left common carotid artery is included up to the length where the brachiocephalic artery branches.

2. Change selection colour and zoom into the image. Use polygon tool to mark plaques (indicated by the red colour of the Oil Red O staining) within the aortic arch and save ROIs as "plaque". If there are plaque-free regions within a plaque, mark separately and label as "hole". Select all ROIs, use "Multi measure" to quantify the area of all ROIs and export data.
3. Repeat steps 1-2 with the image of the reverse side.

The lesion area of the thoracic/abdominal aorta was quantified as described above with the following changes: Use the 0.65x magnification image and set scale to 276.2 pixel/mm. The complete aorta 1 mm rear of the left subclavian artery was analysed.

Calculation of the lesion area in percent was performed with MS Excel as follows: Import vessel and lesion area (aortic arch and thoracic/abdominal part were calculated separately) of front and reverse site into excel and calculate as follows:

$$Vessel\ area\ [mm^2] = Vessel\ area_{front} + Vessel\ area_{reverse}$$

$$Plaque\ area\ [mm^2] = \sum_{i=1}^{n} plaque\ area_{front}[i] + \sum_{i=1}^{n} plaque\ area_{reverse}[i] - \sum_{i=1}^{m} hole\ area_{front}[i] - \sum_{i=1}^{m} hole\ area_{reverse}[i]\ ; n, m: number\ of\ plaques, holes$$

$$relative\ lesion\ area\ [\%] = \frac{Plaque\ area\ [mm^2]}{Vessel\ area\ [mm^2]} \times 100\ [\%]$$

2.4.5.7 Quantification and representation of GC-B-dependent LacZ expression in atherosclerotic vessels

GC-B LacZ expression was analysed by X-gal staining. Isolation of atherosclerotic aortas and subsequent X-gal staining were performed as described in section **2.4.5.2**. For analysis, the complete paraffin-embedded aortic arch was cut into 10 µm sections (see section **2.4.2** and **2.4.3**) and the number of X-gal stained nuclei was counted across all sections. Quantification was performed without deparaffinisation. This rendered the identification of stained nuclei more difficult but had the advantage that sections could be used for further analysis by IHC. Representative sections were deparaffinised, documented, and subsequently stained by IHC.

The same set up as used for documentation of IHC stainings (**2.4.4.1**) was used for counting of X-gal-stained nuclei. All positive cells of the aortic arch (including branching vessels) were assessed for plaque and media separately. The total number of sections that could be analysed as well as the plaque burden differed from mouse to mouse. Therefore, the total number of X-gal-stained cells was normalised to the number of sections containing at least one X-gal-stained nucleus. This parameter (X-gal+ cells/positive section) indicated the average number of X-gal+ (GC-B LacZ expressing) cells in atherosclerotic plaque sections. All sections from the same aorta were documented in one run.

$$X - gal^{+} cells/positive\ section\ [rel.] = \frac{Number\ of\ X - gal^{+}\ cells\ in\ all\ sections\ of\ the\ aortic\ arch}{Number\ of\ sections\ with\ X - gal^{+}\ cells}$$

1. Set up Koehler illumination[301] according to standard procedures [302].
2. Place slide with paraffin sections in slide holder. Use 10x objective and count X-gal+ cells. Note for each section how many X-gal+ cells are counted in the media and how many are counted within plaques.
3. Transfer data to MS Excel and calculate the enrichment index (see formula above) for plaque and media separately.

As it was known in which section how many cells were X-gal+, the distribution of X-gal+ cells could be resolved spatially (first section 0 µm, next section 10 µm, etc.). By plotting the number of X-gal+ cells in a plaque section together with the position of the section, it was possible to see if X-gal+ cells were evenly distributed across all plaque sections or accumulated in specific regions. For better comparability these "plaque profiles" were aligned to each other.

4. Determine the section with the highest number of X-gal+ cells. Set this position as starting point ("0"). All sections before have a negative distance (e.g., -10 µm) and all sections after this section a positive one (e.g., +10 µm). This aligns all plaque profiles relative to the plaque section with most X-gal+ cells.
5. Calculate mean and SEM for every section of the same genotype (e.g., all sections at "10 µm") and plot the result (y-axis: mean ± SEM of X-gal+ cells per section / x-axis: distance from starting point).

2.4.5.8 Assessment of αSMA+ plaque area

In this work it was assumed that plaques are stabilised by (contractile) SMCs. These express αSMA in contrast to strongly modulated/transdifferentiated SMCs. To compare the contribution of these potentially stabilising cells, the αSMA+ area was determined in plaque sections from Smko and LacZ-ctrl mice as described below.

Sections of individual plaques of the aortic arch were stained for αSMA by IHC and documented with a 5x objective and a 2.5x lens as camera mount (see section **2.4.4**). The αSMA+ area was quantified in Fiji and normalised to the total area of the plaque. To separately analyse the αSMA+ area of the 30 µm cap region (not identical with but should comprise the fibrous cap) and the plaque core, the same analysis was performed for the respective parts. Normalisation was performed on cap or core area, respectively. The cap region was defined as the 30 µm thick layer at the luminal side of a plaque. The core was defined as the non-cap part of the plaque. As border between plaque and media the first elastic lamina below the plaque that was not disrupted was chosen in this work. The stained area was quantified semi-automatically. The parameters were determined with a random selection of images of the respective staining. Once the parameters were determined, they could be applied to all stainings of the same antigen that were performed in parallel and documented at the same day. By this approach a subjective bias of the experimenter was excluded. The following protocol describes briefly how this quantification was achieved. A detailed step by step protocol is provided in the appendix (**7.3.3**).

First, all plaques / cap regions were marked manually with ROIs:

1. Open an image of a section stained for αSMA with Fiji. Set scale to 3.36 pixel/µm (5x objective, 2.5x mount). Use "enhance contrast" function to improve visibility of the plaque structure.
2. Use a polygon selection to mark the plaque and cap region:
    a. Start at the luminal side and follow the plaque until it merges with the media. Find the elastin fibre (not stained) that is not disrupted and closest to the luminal side. Follow this fibre to mark the inner border of the plaque. Close the selection and save ROI as **"plaque"**.
    b. The cap region is defined as the 30 µm luminal layer of the plaque. Duplicate the ROI marking the plaque, change line thickness of the duplicated ROI to 60 µm and colour to blue. Check "Show all" and uncheck "Label". The inner border of the blue ROI is exactly 30 µm away from the border of the plaque (the blue ROI extends 30 µm in each direction of the yellow "plaque" ROI). Now the 30 µm cap area can be marked with a polygon selection. Save ROI as **"cap"** and delete duplicated ROI.
    c. Repeat **(a)-(b)** with all plaques of the section. Save all **"plaque"** and **"cap"** ROIs. These ROIs will be used to quantify the total plaque and cap area, respectively (step **14**).
3. Process all stainings as described above.

Second, the parameters to semi-automatically mark the αSMA+ area were determined.

4. Open 6-8 images of an αSMA staining and the negative control.
5. Place a circular ROI in a tissue free region of the first image and use the BIOP SimpleColorBalance plugin to perform a white balance of the image. Continue with the next image until all images are processed.
6. Use Fiji's "Color deconvolution" and select "H DAB". Fiji splits the image in a "haematoxylin" and a "DAB" channel. The "DAB" channel contains the IHC stained area (+ background). Repeat this step with all open images.
    a. Select "Threshold" and adjust the threshold until only αSMA positive area is visible. Note the selected threshold. And repeat this step with all deconvoluted images.
    b. Compare the threshold values from the processed images. They should be similar. Chose a value in this range and test it on all open images. If it is acceptable, verify this value with the negative control. Note the chosen threshold, e.g., "0-185".

Third, the parameters for the threshold were used to mark the αSMA+ area with ROIs. All images were processed sequentially.

7. Open an IHC staining image and perform steps **(5)-(6)**. For step **(6)** apply the threshold selected in step **(6b)**.
8. Use "Analyze Particles" with the threshold image to mark the αSMA+ area with ROIs and combine ROIs with the "OR" function. Save as **"area1"**. Invert image and use "Analyze particles" with the additional option "Exclude on edges" to mark αSMA-negative parts of the plaque that are surrounded by αSMA+ area. Combine ROIs with "OR" as **"holes 1"** and invert image again.
9. Select "holes1" and use "Analyze Particles". This marks αSMA+ area within the holes. Combine ROIs with "OR" as **"area2"**. Invert image, select "area2" and use "Analyze Particles". Combine ROIs with "OR" as **"holes2"**. Now all αSMA+ area and all αSMA-negative area should be saved as ROIs.
10. The αSMA-negative area must be excluded from the αSMA+ area. Combine "area1" and "holes1" with "XOR" as **"staining1"**. Combine "area2" and "holes2" with "XOR" as **"staining2"**.
11. Combine "staining1" and "staining2" with "OR" as **"IHC_staining"**. Discard all other ROIs and save. The "IHC_staining" ROI contains the complete αSMA+ area.
12. Repeat this procedure with all images of IHC stainings that were performed and recorded in parallel.

Fourth, the **"IHC_staining"** ROIs were used to quantify the αSMA+ area separately in plaque and cap area. The values for the plaque core were calculated from these values and the αSMA+ area was normalised to the total area of the corresponding region (plaque, cap, core).

13. Open an image and the respective ROI sets created in step **(2)** (plaque/cap area) and in step **(11)** (αSMA+ area). Set scale to 3.36 pixel/µm (5x objective, 2.5x mount). Combine the following ROIs with the "AND" function to mark the αSMA+ area in the corresponding region (keep the original ROIs!):
    a. "plaque" and "IHC_staining" as **"IHC_plaque"**.
    b. "cap" and "IHC_staining" as **"IHC_cap"**.
14. Select all ROIs ("plaque", "IHC_plaque", "cap", "IHC_cap") and use "Multi measure" to quantify the different areas and export data.
15. Import areas in MS Excel and calculate the areas for the **"core"** by subtracting cap from plaque values (the core is the non-cap area)
16. Normalise the αSMA+ area to the total area of the respective region. Below, the calculation for the αSMA+ cap area is described exemplarily. The calculations for the "complete plaque" and the "core" are performed accordingly:

$$\alpha SMA - positive\ area\ (cap\ region)[\%] = \frac{\alpha SMA^{+}\ area\ (cap\ region)[\mu m^2]}{total\ area\ (cap\ region)\ [\mu m^2]} \times 100\ [\%]$$

17. Repeat steps **(13)-(16)** with all plaques of the given section and all images of αSMA stainings.

2.5 Western blotting

Protein expression of cultured VSMCs, healthy, and atherosclerotic aortas was compared by western blotting. First, protein lysates were prepared, and their concentrations were determined. After separation of proteins by gel electrophoresis, proteins were blotted to a membrane and proteins of interest were detected immunologically.

2.5.1 Preparation of protein lysates

- **1 M NaCl**: 58.4 g NaCl, ad 1 L H_2O, store at RT
- **100 mM** phenylmethylsulfonylfluoride (**PMSF**): dissolve 174 mg PMSF (Roth) in 10 mL 100 % ethanol, store at -20 °C
- **20 %** sodium dodecyl sulphate (**SDS**): dissolve 200 g SDS at 60 °C in 800 mL H_2O, ad 1 L H_2O, store at RT

Cultured cells were serum-starved overnight before lysis. Tissues (healthy and atherosclerotic aortas) were freed from surrounding tissue as fast as possible, quick-frozen in liquid nitrogen and stored at -80 °C until lysis.

2.5.1.1 Cell culture

- Cell scraper (#70-1250, Biologix)
- **Lysis buffer C**: 21 mM Tris-Cl (21 µL 1 M Tris-Cl pH 8.0), 0.67 % SDS (33.5 µL 20 % SDS), 0.2 mM PMSF (2 µL 100 mM PMSF), ad 1 mL H_2O, always prepare freshly

Seed 1 000 000 VSMCs per 100 mm cell culture dish (see section **2.3.1** for details), let grow to ≥ 80 % confluency and serum-starve overnight.

1. Pre-heat PBS to 37 °C. Wash cells twice with PBS. Aspirate PBS as thoroughly as possible after the second wash step. Add 500 µL lysis buffer C per 100 mm cell culture dish and scratch with

the pipette until liquid gets viscous. Use cell scraper to detach remaining cells and transfer lysate to a 1.5 mL reaction tube.
2. Incubate lysates 10 min at 95 °C to disrupt protein-DNA interactions and to denature proteins. Centrifuge 5 min at 18 000 rcf at 4 °C and transfer supernatant to a new tube. Determine protein concentration according to section **2.5.2**.
3. Store lysates at -20 °C (short time) or -80 °C (long time) or use directly for western blotting.

2.5.1.2 Tissue

- FastPrep® tubes, orange caps, ¼" ceramic spheres, garnet matrix A bulk (all from MP Biomedicals)
- **Lysis buffer T**: 50 mM Tris-Cl (50 µL 1 M Tris-Cl pH 8.0), 100 mM NaCl (100 µL 1 M NaCl), 5 mM EDTA (10 µL 0.5 M EDTA), 2 % SDS (100 µL 20 % SDS), 2.5 mM PMSF (25 µL 100 mM PMSF, warm with hands until all crystals are dissolved), ad 1 mL H_2O, always prepare freshly (**do not chill on ice as SDS will precipitate!**)

A FastPrep-24 device was used to homogenise tissues. If frozen tissues were stored at -80 °C, they were transport and stored in liquid nitrogen until lysis was started.

1. Add garnet matrix A bulk (conic part should be filled), 1 ceramic sphere, and lysis buffer T (350 µL for 2 aortas) to FastPrep tubes. Take 2 aortas (2x arch + 2x abdominal part) and transfer to FastPrep tubes. Place tubes in FastPrep device and run 2x 30 sec at 6.5 M/s. **Centrifuge 1 min at 15 000 rcf at 4 °C and chill 4 min on ice between runs.**
2. Centrifuge 1 min at 15 000 rcf at 4 °C and transfer supernatant to new tube.
3. Incubate lysates 10 min at 95 °C to disrupt protein-DNA interactions and to denature proteins. Centrifuge 5 min at 18 000 rcf at 4 °C and transfer supernatant to a new tube. Determine protein concentration according to section **2.5.2**.
4. Store lysates at -20 °C (short time) or -80 °C (long time) or use directly for western blotting.

2.5.2 Protein determination by Lowry

- **BSA standard**: dissolve BSA (12.5 µg/mL, 25 µg/mL, 50 µg/mL, 100 µg/mL, 200 µg/mL) in H_2O, store at -20 °C
- Total protein kit, micro lowry, Peterson's modification (Sigma-Aldrich):
    - **Lowry reagent**: dissolve 2 g Lowry reagent in 40 mL H_2O, store at RT
    - **Folin reagent**: 18 mL Folin & Ciocalteu's phenol reagent, 90 mL H_2O, store at RT protected from light

The Peterson's modification [308] of the Lowry assay [309] was performed to determine protein concentrations in cell and tissue lysates. This colorimetric assay is based on a biuret reaction detecting the peptide bonds of proteins. Protein concentration was determined by measuring the absorbance at 660 nm and comparing the values with a standard curve which was prepared in parallel by using the BSA standard. The assay was performed in a 96-well plate format in duplicates. Absorbance at 660 nm was measured with the Multiskan EX multi-well plate reader (Thermo) and calculations were performed using MS Excel.

1. Add 95 µL H_2O to 5 µL protein lysate, lysis buffer T/C (blank for lysates), and H_2O (blank for BSA standard) in reaction tubes. Distribute 100 µL of each BSA standard to reaction tubes. Add 100 µL Lowry reagent. Mix and incubate 20 min at RT in the dark. Add 50 µL Folin reagent, mix and incubate 30 min at RT in the dark.
2. Transfer 200 µL of each reaction mix to a well of a flat-bottom 96-well plate. Use plate reader to mix samples briefly, determine absorbance at 660 nm and build mean of duplicates.

3. Establish a standard curve with the absorbance values of the BSA standard (use H_2O sample as blank). Determine function by linear regression and build inverse function. Use inverse function to estimate protein concentration in lysates (use lysis buffer as blank).

2.5.3 SDS polyacrylamide gel electrophoresis

- **20 %** ammonium persulfate (**APS**): 20 % (w/v) APS (2 g APS, Roth), 10 mL H_2O, store at -20 °C
- **Isopropanol**: 100 % (v/v) isopropanol (Sigma-Aldrich)
- **PageRuler™ prestained protein ladder** 10-180 kDa (#26616, Thermo)
- **Rotiphorese Gel 30** (Roth): 30 % (w/v) acrylamide, 0.8 % (w/v) bisacrylamide
- **10x SDS running buffer**: 0.25 M Tris (15.1 g Tris), 1.9 M glycine (72 g glycine), 0.1 % (w/v) SDS (5 g SDS), ad 500 mL H_2O, store at RT
- **5x SDS loading dye**: 0.32 M Tris-Cl (3.2 mL 1 M Tris-Cl pH 6.8), 40 % (v/v) glycerol (4 mL glycerol), 15 % (w/v) SDS (1.5 g SDS), 25 % (v/v) β-mercaptoethanol (2.5 mL β-mercaptoethanol, Roth), 0.1 % (w/v) bromophenol blue (10 mg bromophenol blue), ad 10 mL H_2O
- N,N,N',N'-Tetramethylethylendiamin (**TEMED**, Roth)
- **10 % separating gel** (1.5 mm): 10 % (w/v) acrylamide/0.3 % (w/v) bisacrylamide (3.3 mL Rotiphorese Gel 30), 1x Tris/SDS **pH 8.8** (1.25 mL 4x Tris/SDS **pH 8.8**), 4.1 mL H_2O, 0.1 % TEMED (10 µL TEMED), 0.1 % APS (50 µL 20 % APS), always prepare directly before casting the gel and add APS last as it starts the polymerisation
- **4 % stacking gel** (1.5 mm): 4 % (w/v) acrylamide/0.1 % (w/v) bisacrylamide (0.65 mL Rotiphorese Gel 30), 1x Tris/SDS **pH 6.8** (1.25 mL 4x Tris/SDS **pH 6.8**), 3.05 mL H_2O, 0.2 % TEMED (10 µL TEMED), 0.2 % APS (50 µL 20 % APS), always prepare directly before casting the gel and add APS last as it starts the polymerization
- **4x Tris/SDS pH 6.8**: 0.5 M Tris (3 g Tris), 0.4 % SDS (0.2 g), ad 50 mL H_2O, adjust pH to 6.8 with HCl, store at 4 °C
- **4x Tris/SDS pH 8.8**: 1.5 M Tris (18.2 g Tris), 0.4 % SDS (0.4 g), ad 100 mL H_2O, adjust pH to 8.8 with HCl, store at 4 °C

Proteins were separated according to their molecular weight by SDS polyacrylamide gel electrophoresis under denaturing/reducing conditions [310; 311]. For electrophoresis, the Mini-PROTEAN system (Bio-Rad) was used in combination with a Standard Power Pack P25 (Biometra) as power supply.

1. Thaw protein lysates on ice and add 20 µL 5x SDS loading dye to 80 µL of protein lysate. Store remaining lysate at -20/-80 °C. Assemble mini-protein chamber (Bio-Rad) and fill gel pouring system with H_2O to check for leakage. Remove H_2O, prepare 10 % separating gel solution and cast gel. Overlay with isopropanol to achieve an even border towards the stacking gel. Let polymerise for ~30 min. Remove isopropanol completely. Prepare 4 % stacking gel solution and cast stacking gel on top. Place combs and let polymerise for at least 30 min.
2. Denature protein lysates (+ SDS loading dye) for 5 min at 95 °C, centrifuge 1 min at 18 000 rcf at RT. Dilute samples to the same concentration (14-25 µg protein/20 µL) with 1x SDS loading dye.
3. Place SDS gels in running chamber (short plate facing inward) and fill inner and outer chamber with 1x SDS running buffer. Remove combs and rinse pockets.
4. Load 20 µL sample or 3 µL PageRuler per pocket. Fill empty pockets with 1x SDS loading dye to avoid broadening of bands. Run gel 10 min at 50 V, then ~1 h at 150 V.

2.5.4 Protein transfer and detection

- **Anode solution I**: 300 mM Tris (36.3 g Tris), 20 % (v/v) methanol (200 mL 100 % methanol), ad 1 L H_2O, adjust pH to 10.4 and store at RT
- **Anode solution II**: 25 mM Tris (3 g Tris), 20 % (v/v) methanol (200 mL 100 % methanol), ad 1 L H_2O, adjust pH to 10.4 and store at RT
- **Blocking solution**: 5 % (w/v) milk powder (5 g milk powder), ad 100 mL TBS-T, store at 4 °C for up to 3 days
- **Blotting paper**: 0.35 mm, 195 g/m^2 blotting paper (#gb46, A. Hartenstein)
- **Cathode solution**: 40 mM 6-amino hexanoic acid (5.2 g 6-amino hexanoic acid, Roth), 25 mM Tris (3 g Tris), 20 % (v/v) methanol (200 mL 100 % methanol), ad 1 L H_2O, adjust pH to 7.6 with HCl and store at RT
- **ECL reagent**: mix 1 mL WesternBright® Sirius (luminol/enhancer solution, Biozym) with 1 mL WesternBright® Peroxide (chemiluminescent detection reagent, Biozym), prepare directly before use
- **20 % NaN_3**: 20 % (w/v) NaN_3 (400 mg NaN_3, Roth), ad 2 mL H_2O, store at 4 °C
- pAb solution: pAb (see **Supplementary table IV**), 5 % (w/v) BSA (250 mg BSA), 0.05 % NaN_3 (12.5 µL 20 % NaN_3), ad 5 mL TBS-T, store at 4 °C and reuse
- Polyvinylidene fluoride (**PVDF**) **membrane**: PVDF membrane (0.2 µm pore size, **#**03010040001, Roche)
- **sAb solution**: HRP coupled sAb (see **Supplementary table IV**) in TBS-T/milk, prepare freshly
- **TBS-T/milk**: 1 % (w/v) milk powder (1 g milk powder), ad 100 mL TBS-T, store at 4 °C for up to 3 days

After separation of proteins by SDS polyacrylamide gel electrophoresis, lysates were analysed for proteins of interest by western blotting [312; 313]. Therefore, proteins were transferred from the gel to a PVDF membrane using a semi-dry blotting device (Trans-Blot® SD semi-dry transfer cell, Bio-Rad) using a discontinuous 3 buffer system developed by Kyhse-Andersen [314]. Proteins immobilised to the membrane were detected by indirect chemiluminescence. Protein specific pAbs were bound by HRP-coupled sAbs. HRP catalysed the oxidation of luminol by H_2O_2 (components of the ECL reagent) leading to the emission of light. Light was detected quantitatively with the ChemiDoc MP documentation system.

1. Disassemble gel running chamber and discard stacking gel. Prepare blotting sandwich (per sandwich): Cut 16 blotting paper and PVDF membrane slightly larger than the dimension of the gel. Soak 8 papers in cathode solution, 4 papers in anode solution I and 4 papers in anode solution II. Activate PVDF membrane in 100 % methanol for ~1 min at RT, then soak in anode solution II.
2. Assemble blotting sandwich on the western blot device. The composition is given from top (cathode) to bottom (anode). Remove air bubbles by gentle pressure after each layer:
    a. Cathode
    b. 8 blotting papers soaked with cathode solution
    c. SDS gel
    d. PVDF membrane
    e. 4 blotting papers soaked with anode solution II
    f. 4 blotting papers soaked with anode solution I
    g. Anode
3. Run western blot 1.5 h at 50 mA/gel. Disassemble blotting sandwich and block PVDF membrane in blocking solution 1 h at RT, shaking. In the meantime, label membrane and marker bands with a pen.

4. Use marker bands as orientation to cut the membrane. Every protein of interest should be located on a separate piece. Wash membrane 3x 3 min with TBS-T at RT, shaking. Incubate with pAb solution overnight at 4 °C in 50 mL falcon tubes on a roller shaker.
5. Wash membrane 3x 3 min with TBS-T/milk at RT, shaking. Incubate with sAb solution for ≥1 h at RT on a roller shaker. Wash membrane 3x 3 min with TBS-T at RT, shaking.
6. Prepare ECL reagent and assemble membrane in the original order on a tray. Wet membrane with ECL reagent.
7. Record chemiluminescence with the ChemiDoc MP at 1x1 binning with increasing exposure times (first image after 1 sec, then 30 images every 10 seconds using cumulative recording [last image is exposed for 301 seconds]).
8. Choose for every protein the image with the highest non-saturating intensity.

2.6 Software

FIJI (latest version 1.53k) was used for image analysis [315]: The update sites "ImageJ", "Fiji", "Java-8", "BIG-EPFL" and "PTBIOP" were activated to load the required plugins. The MultiStackReg plugin (latest version 1.45, http://bradbusse.net/sciencedownloads.html) created by Brad Busse was downloaded separately.

Origin Pro (latest version 9.8.5.201, OriginLab Corporation, Northampton, MA, US) and **MS Excel** (latest version 16.0.14326.20384, Microsoft Corporation, Redmond, WA, US) were used for data analysis.

CorelDRAW 2017 (latest version 19.0.0.328, Corel Corporation, Ottawa, Ontario, Canada) was used to prepare the figures.

EndNote 20 (latest build 15341, Clarivate, Boston, MA, US) was used to create the bibliography.

2.7 Statistical analysis

Statistical analysis was performed in Origin Pro. The Shapiro-Wilk test was used to test data for normal distribution. The Mann-Whitney U test was performed for pairwise comparisons of non-normally distributed data. Normally distributed data was tested for homo-/heteroscedasticity (F-test). A standard Student's t-test (homoscedastic data) or a Welch-corrected one (heteroscedastic data) was performed for pairwise comparisons. For groupwise comparisons (more than two groups) a one-way analysis of variance (ANOVA) with subsequent Bonferroni post hoc test was performed. Alternatively, multiple pairwise comparisons (Student's t-test or Mann-Whitney U test) were performed in combination with a Bonferroni correction for multiple comparisons. Statistical significance was considered for $p<.05$ and indicated in three categories (*$p<.05$, **$p<.01$, ***$p<.001$).

3 Results

3.1 cGMP signalling in cultured VSMCs

It was shown previously that VSMCs in culture [17; 102] and certain arteries [37-39] can react to NO, ANP, and CNP. Furthermore, there is some evidence that cGMP signalling can affect the VSMC phenotype. However, to our knowledge it was not analysed yet whether the exact same VSMC can respond to all three stimuli, and the exact role of cGMP in the phenotypic modulation of VSMCs is still poorly understood. To better understand cGMP signalling in VSMCs in relation to their phenotype, we directly compared cGMP generation in response to ANP and CNP within the same cell. Furthermore, we clearly characterised the phenotypic state of our cultured VSMCs and analysed how their phenotypic modulation influenced their cGMP generation.

3.1.1 Primary VSMCs show diverse cGMP response patterns

To compare their ANP- and CNP-induced cGMP generation, we isolated primary aortic VSMCs from sensor mice expressing the cGMP biosensor cGi500 globally (**Figure 10**). This FRET-based biosensor binds cGMP reversibly in the physiological range. Thus, it allows to follow cGMP concentration changes in individual cells in real time upon multiple stimulation in a non-destructive manner. Subconfluent cultures were stimulated alternatingly with increasing concentrations of ANP and CNP. At the end of each experiment, 500 nM of the NO-releasing compound DEA/NO (referred to as "NO" for reasons of simplicity) were applied to verify viability of cells that did not respond to NPs and to induce sensor-saturating cGMP concentrations. After the cGMP/FRET measurement, the phenotypic state of individual VSMCs was assessed by IF staining for αSMA and SM22α as marker proteins for contractile VSMCs. To correlate the cGMP response patterns of individual cells with their phenotype, we developed a mapping method based on gridded coverslips (see section **2.3.5.6** and **Supplementary figure III** for details). These experiments (**Figure 10**) were performed during my diploma thesis and repeated/extended in this work.

Figure 10 A shows the typical appearance of a primary VSMC culture during cGMP/FRET measurements (top left). Strong sensor fluorescence was detected in the cytosol, while the nuclei were darker, probably due to exclusion of the sensor from the nucleoplasm. A high extent of heterogeneity was observed within primary VSMC cultures with respect to morphology and sensor fluorescence intensity. The morphology ranged from thin elongated to small and large roundish cells. The former morphology was described for the contractile and the latter for the modulated phenotype. This morphological heterogeneity was also reflected by heterogeneous cGMP response patterns (**Figure 10 A,** bottom left and right panel). The right panel depicts the cGMP/FRET ratio traces of five representative individual VSMCs. These ratio traces reflect changes in intracellular cGMP concentration over time, relative to the baseline ("basal cGMP") of the corresponding cell. The red horizontal bars indicate the time span of drug application of the drug indicated below each bar. cGMP elevations started during drug application but did not decay immediately after stop of application. Especially for NP-induced cGMP signals the decay was often delayed for several minutes. The comparison of the cGMP response patterns led to the identification of 3 distinct NP-induced cGMP response patterns as indicated by three different colours: (1) Signal traces of cells that responded to ANP but not CNP (top) and cells that responded at least 1.5 times stronger to ANP than to CNP (second from top) are marked in orange. They will be referred to as "ANP-preferring cells" from here on. (2) Signal traces of cells that responded to CNP but not ANP (bottom) and cells that responded at least 1.5

times stronger to CNP than to ANP (second from bottom) are marked in cyan. They will be referred to as “CNP-preferring cells” from here on. (3) The green ratio trace (middle) represents cells without a clear preference for one of these peptides (e.g., only 1.1 times stronger cGMP response to ANP stimulation than to stimulation with CNP). They will be referred to as “ANP~CNP cells” from here on.

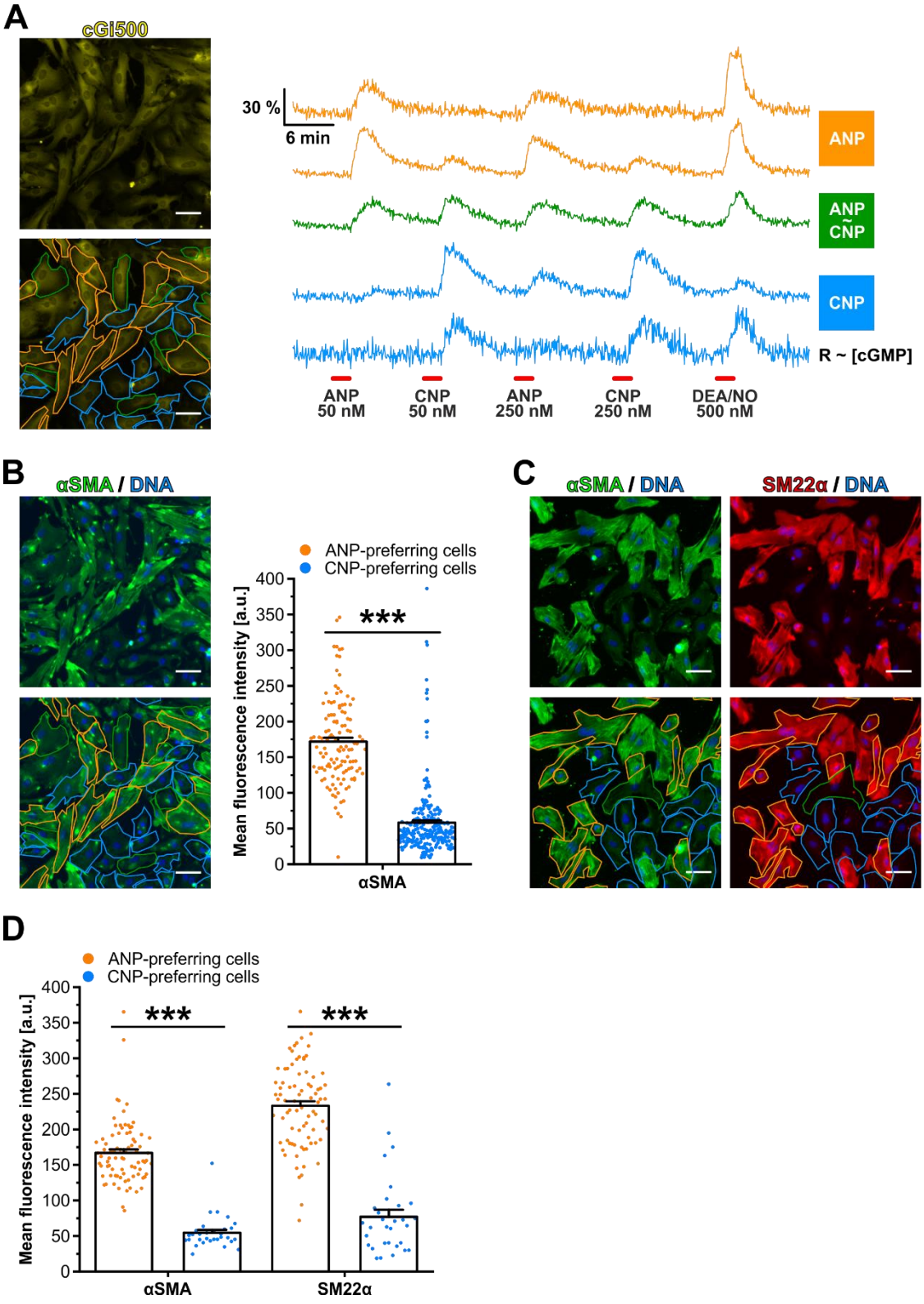

Figure 10: Phenotypic diversity of primary VSMCs is associated with distinct cGMP response patterns. *Primary aortic VSMCs from cGi(L1) mice (global sensor expression) were cultured on gridded coverslips, classified by their*

cGMP response patterns (FRET measurement) and subsequently analysed for αSMA (B) or αSMA and SM22α (C-D) expression. ***A:*** *Representative cGMP/FRET measurement of primary VSMCs after 5 days in culture. VSMCs were visualised by the YFP fluorescence (yellow) of cGi500 during the cGMP/FRET measurement (left). The cGMP response patterns of these VSMCs are highlighted in the lower left panel according to the classification shown in the right panel. The right panel shows the development of cGMP levels over time (ratio trace "R" ~ [cGMP]) of five individual VSMCs representing the different cGMP response patterns that were detected after stimulation with ANP (50 nM, 250 nM), CNP (50 nM, 250 nM), and DEA/NO (500 nM). The scale at the left indicates the percent change of the ratio trace relative to the baseline ("ΔR/R"). The ratio traces are coloured according to their classification legend at the right side. The classification was based on the analysis of 516 cells (3 individual coverslips from 5 mice). Red horizontal lines indicate drug applications.* ***B-D:*** *Analysis of contractile marker expression in ANP- and CNP-preferring cells by IF staining for αSMA (B) or αSMA and SM22α (C-D, double staining).* ***B:*** *The left two panels show the same region as depicted in A after cGMP/FRET measurement and subsequent staining for αSMA (green) and DNA (blue).* ***C:*** *Representative image section after cGMP/FRET measurement and subsequent staining for αSMA (green), SM22α (red) and DNA (blue). The NP preference of individual VSMCs is indicated by the respective colour (B, C). The expression of αSMA (B, 366 cells, 3 individual coverslips, 5 mice) or αSMA and SM22α (C, 112 cells, 2 coverslips, 4 mice) was quantified in B (right panel) and D for ANP- (orange) and CNP-preferring (cyan) cells. Each dot represents an individual VSMC. Data are represented as mean + SEM. Statistical significance is indicated by asterisks (*** p<.001). Scale bars are 50 µm. These initial experiments were performed during my diploma thesis and repeated during my doctoral thesis.*

Note that from "ANP-preferring" over "ANP~CNP" to "CNP-preferring" cells (top to bottom) cGMP responses to ANP decreased while cGMP responses to CNP increased. Variations in cGMP responses to NO were not used for classification but analysed later (see section **3.1.3**). Rarely, cells were measured under standard conditions (i.e., primary VSMCs, 12-24 h serum-starved) that did respond to NO, but neither to ANP nor CNP (not shown). The five signal traces depicted in the right panel of **Figure 10 A** illustrate all important characteristics of cells that belong to the respective group. The second stimulation with the same natriuretic peptide often elicited a weaker or similar cGMP response compared to the first stimulation despite a five times higher concentration (e.g., first, third or fifth trace), whilst the final stimulation with NO could still elicit higher (potentially sensor-limited) cGMP elevations. This indicated that the limited cGMP generation by NPs in these cases was not based on a detection limit of the cGMP biosensor cGi500, but because the NP receptors were already saturated by the lower NP concentration. However, NO did not always elicit the highest cGMP elevation as intended by the experimental setup. While this was rarely observed for ANP-preferring cells, CNP-preferring cells frequently showed weak NO-induced cGMP responses. This is exemplarily shown with the second last trace in **Figure 10 A**. Note that other cells with the same NP response pattern reacted strongly to NO. In the lower left panel of **Figure 10 A** cells are highlighted according to their cGMP response pattern. Cells that were excluded from analysis are not highlighted. Most ANP-preferring cells (orange) were elongated, while most CNP-preferring cells (cyan) were roundish. Cells belonging to the intermediate category (ANP~CNP, green) did not have a specific morphology. Further analysis will focus on ANP- and CNP-preferring cells as the heterogeneity of cells belonging to the ANP~CNP group did not allow to draw clear conclusions.

To determine the phenotypic state of every measured VSMC, the expression of proteins that are abundant in contractile VSMCs (αSMA and SM22α) was analysed by IF stainings. Initially, only the expression of αSMA was analysed by IF stainings (**Figure 10 B**). The same region as for the cGMP/FRET measurement (**Figure 10 A**) is shown. In line with the heterogenous morphologies, the expression of αSMA varied between cells. Note that the bright fluorescent dots observed in the IF staining (**Figure 10 B-C**) might be staining artefacts caused by the silicon grease that was used to seal the flow chamber during cGMP/FRET measurements. In the lower image in **Figure 10 B**, the cGMP response pattern of

each cell is indicated by the colour code introduced above. As deduced by visual inspection, cells marked in orange (ANP-preferring) showed a bright IF staining for αSMA. In contrast, cells marked in cyan (CNP-preferring) showed very weak IF staining for αSMA. To support this observation, αSMA expression was quantified computationally (**Figure 10 B**, right panel). Cells were grouped according to their NP preference and the αSMA expression of each individual cell was calculated. The mean fluorescence intensity was used as an indicator for αSMA expression. Indeed, ANP-preferring cells expressed significantly more αSMA than CNP-preferring cells (ANP: 171.8 ± 5.4 a.u. vs. CNP: 58.1 ± 3.2 a.u., **p < .001**). To further characterise the phenotype of ANP- and CNP-preferring VSMCs, the expression of SM22α was investigated in a separate series of measurements (**Figure 10 C**). Correlation of marker expression with the cGMP response patterns (**Figure 10 C,** lower panel) showed that ANP-preferring cells expressed more SM22α than CNP-preferring cells. The expression of αSMA was assessed in parallel to verify previous results and to exclude any technical issues (reference marker). Cells with strong fluorescence for SM22α showed strong fluorescence for αSMA as well, and vice versa. Computational quantification of αSMA and SM22α expression (**Figure 10 D**) verified that ANP-preferring cells expressed more αSMA and SM22α than CNP-preferring cells (αSMA – ANP: 166.9 ± 4.9 a.u. vs. CNP: 54.5 ± 4.1 a.u., **p < .001** and SM22α – ANP: 233.1 ± 6.4 a.u. vs. CNP: 76.9 ± 10.1 a.u., **p < .001**). Note that the expression levels of αSMA and SM22α cannot be directly compared based on IF staining as the mean fluorescence intensity depends on the quality of the respective antibody, the exposure time, and the fluorophore used for detection.

Together, these results indicated a connection between VSMC phenotype and NP-induced cGMP generation. This hypothesis was further investigated in the first part of this work.

3.1.2 CNP-preference indicates modulated VSMCs in culture

ANP-preferring cells were characterised by high expression of well-known SMC marker proteins. The main characteristic of CNP-preferring cells in contrast, was the lack of such. As reduced expression of SMC marker proteins is characteristic for phenotypic modulation of VSMCs in culture (see section **1.3.1** for a detailed description), we hypothesised that CNP-preferring cells developed from contractile aortic VSMCs during *in vitro* culture. To test this hypothesis, we designed a set of experiments.

First, we used SMC-selective sensor mice (lineage tracing) to test whether CNP-preferring cells were of smooth muscle origin. Like VSMC cultures with global sensor expression, VSMC cultures with SMC-selective sensor expression (SM22-Cre x cGi(L2)) showed diverse morphologies and contained ANP- and CNP-preferring cells (**Figure 11 A**, left panel). Note that only SMC-derived cells expressed the cGMP biosensor cGi500 (yellow, recombined) in these cultures. Non-recombined cells could be identified by mTomato fluorescence (not shown). The recombination rate (percent recombined cells of all cells in FOV) in our SMC-selective measurements was 91.9±1.7 %. All three NP signalling patterns that were found in VSMC cultures with global sensor expression were also found in VSMC cultures with SMC-selective sensor expression as illustrated by representative ratio traces (**Figure 11 A**, right panel). Cells that reacted strongly to ANP but not or weakly to CNP (ANP-preferring, orange), cells without clear preference (ANP~CNP, green) and cells that reacted strongly to CNP but not or weakly to ANP (CNP-preferring, cyan) were present. Analysis of contractile marker protein expression (αSMA/SM22α) showed that most CNP-preferring VSMCs expressed low levels of αSMA and SM22α (**Figure 11 B**, left) even though they (or their progenitors) expressed enough SM22α to induce recombination. ANP-preferring cells showed higher expression of both proteins with clear stress fibre formation of αSMA. These differences in contractile marker protein expression were verified by computational

quantification (**Figure 11 B**, right). ANP-preferring cells expressed significantly more αSMA than CNP-preferring cells (ANP: 1834.6 ± 120.3 a.u. vs. CNP: 1114.6 ± 86.4 a.u., **p < .001**) and SM22α (ANP: 1255.1 ± 73.5 a.u. vs. CNP: 624.0 ± 118.7 a.u., **p < .001**).

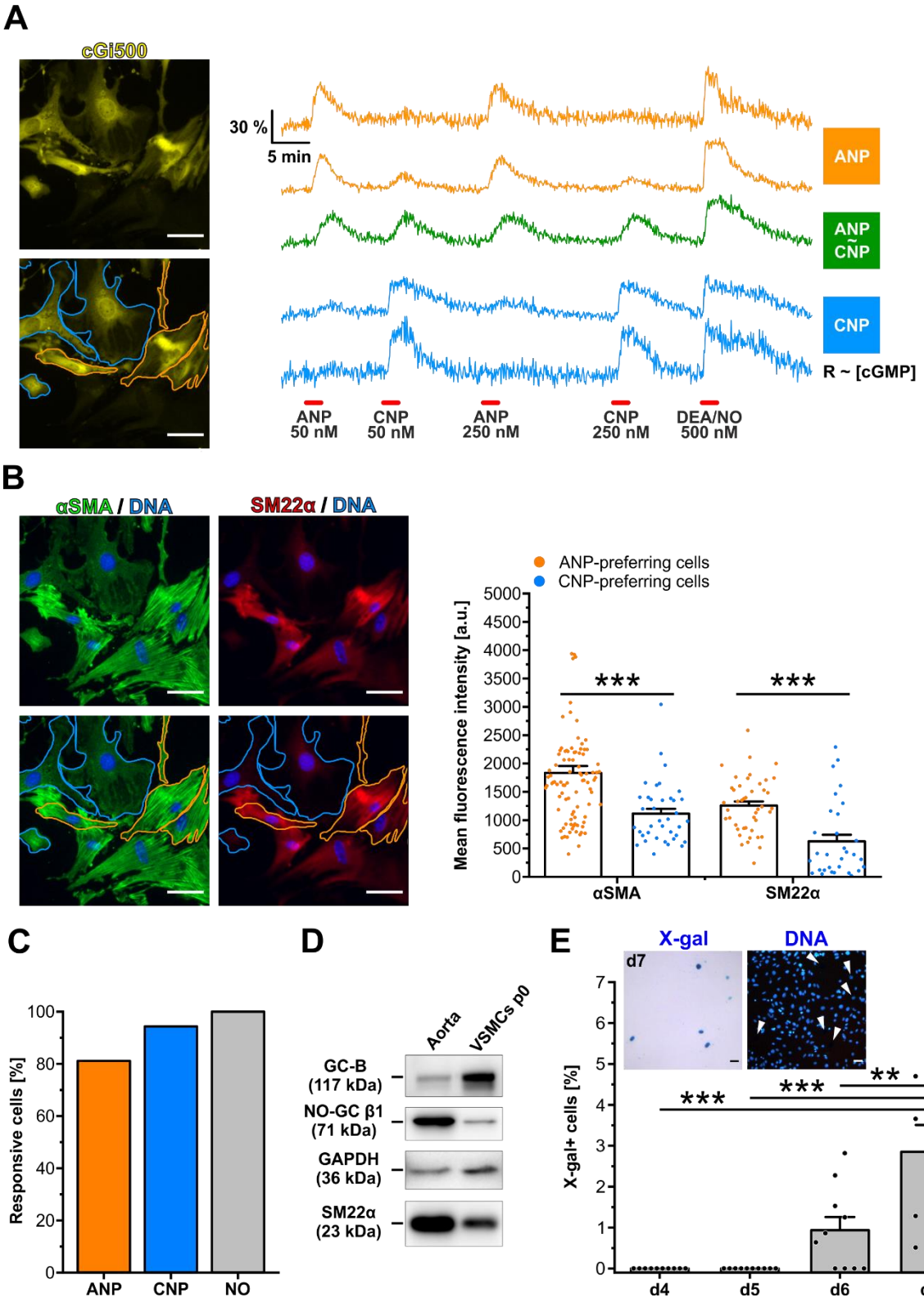

Figure 11: CNP-preferring cells are derived from SMCs (SM22α-expressing cells) and increase during culture. *Primary aortic VSMCs from SMC-selective sensor mice (SM22-Cre x cGi(L2)) were cultured on gridded coverslips (A-B) or after enzymatic adventitia removal ("adventitial-free cultures") on standard coverslips (C), classified by*

their cGMP response patterns (FRET measurement) and subsequently analysed for SM22α and/or αSMA expression (B). Primary aortic VSMCs from WT mice were cultured for 6 days, lysed, and protein expression was compared with a protein lysate from an intact aorta (litter matched females were used) by western blotting (D). Primary aortic VSMCs from GC-B reporter mice (GC-B +/LacZ) were cultured on standard coverslips for 4-7 days, stained with X-gal and the fraction of stained (X-gal+) cells was determined (E). ***A:*** *Representative cGMP/FRET measurement of primary VSMCs that expressed cGi500 under control of the SM22α promoter. Recombined cells were visualised by the YFP fluorescence (yellow) of cGi500 (left panel). The cGMP response patterns of these VSMCs were highlighted in the lower left panel according to the classification shown in the right panel. The right panel shows the development of cGMP levels over time (ratio trace "R" ~ [cGMP]) of five individual VSMCs, representing the different cGMP response patterns that were detected after stimulation with ANP (50 nM, 250 nM), CNP (50 nM, 250 nM) and DEA/NO (500 nM). The scale at the left indicates the percent change of the ratio trace relative to the baseline ("ΔR/R"). The ratio traces are coloured according to their classification legend at the right side. Red horizontal lines indicate drug applications.* ***B:*** *Analysis of contractile marker expression in ANP- and CNP-preferring cells by IF staining for SM22α and/or αSMA (double/single staining). The left two panels show the same region as depicted in A after cGMP/FRET measurement and subsequent staining for αSMA (green), SM22α (red) and DNA (blue). The NP preference of individual VSMCs is indicated by the respective colour. The expression of αSMA (132 cells, 8 individual coverslips, 2 mice) and SM22α (75 cells, 4 coverslips, 2 mice) was quantified in the right panel for ANP- (orange) and CNP-preferring (cyan) cells. Each dot represents an individual VSMC. Data are represented as mean + SEM. Statistical significance is indicated by asterisks (*** p<.001). Scale bars are 50 µm.* ***C:*** *Summary of cGMP responses to ANP, CNP and/or DEA/NO in primary "adventitia-free" VSMC cultures of SM22-Cre x cGi(L2) mice. The same order of application and concentrations as shown in A were used. Bars indicate fraction of cells (cumulated numbers, no mean) that reacted to ANP, CNP and/or NO (53 cells, 4 coverslips, 3 mice).* ***D:*** *Comparison of protein expression in lysates of intact aorta (1 mouse, 11 weeks old) and primary aortic VSMCs (6-day culture, 5 mice, 11 weeks old) by western blotting. Applied antibodies and molecular weight of the respective target protein are indicated at the left. Glyceraldehyde 3-phosphate dehydrogenase (GAPDH) was used as loading control. 5.4 µg protein was loaded per lane.* ***E:*** *Development of GC-B expression in primary aortic VSMCs over time. GC-B expressing cells (as indicated by X-gal-stained nuclei, "X-gal+" cells) after 4-7 days in culture were counted and normalized to the total amount of cells per FOV (as indicated by Hoechst 33258 staining; 10 random FOVs on 2 coverslips per condition, 5 mice). Each dot represents a FOV randomly chosen for analysis. Data are represented as mean + SEM. Statistical significance vs. day 7 is indicated by asterisks (** p<.01; *** p<.001). Inset shows a representative region of cultured VSMCs at day 7. Nuclei of GC-B expressing cells appeared blue in the brightfield image (left). The nuclei of all cells in this region were visualised by Hoechst 33258 staining (right). White arrowheads indicate the position of X-gal+ cells. Scale bars are 50 µm.*

To exclude that CNP responsive cells were derived from SM22α-expressing cells localized in the aortic adventitia rather than media, the adventitia was removed from the aorta by an additional enzymatic digest prior to VSMC culture. The fraction of cells responding to ANP, CNP or NO was quantified in VSMC cultures from these aortas (**Figure 11 C)**. Over 90 % of VSMCs in "adventitia-free" cultures that were analysed, showed a cGMP response to CNP. Around 80 % reacted to ANP and all reacted to NO. Although more cells showed a response to CNP than to ANP, more ANP-preferring than CNP- preferring cells were present (see **Supplementary figure VI**). The additional purification step was not established as standard procedure as it heavily impacted cell viability/growth (only 81 cells in 4 measurements of which 53 cells could be analysed).

In sum, our results from cGMP/FRET measurements in SMC-selective VSMC cultures in combination with contractile marker protein analysis suggested that most if not all CNP-preferring cells were derived from medial VSMCs.

Next, we tested whether CNP-preferring VSMCs developed in culture. To do so, we compared the expression of GC-B (CNP receptor) in intact aorta with cultured VSMCs by western blotting (**Figure 11 D**). Furthermore, we cultured VSMCs from GC-B LacZ reporter mice (GC-B +/LacZ) for 4-7 days and followed the development of GC-B expression over time by X-gal staining. (**Figure 11 E**). By western blotting we detected higher levels of SM22α and the β1 subunit of NO-GC in the aorta than in primary

cultured VSMCs (**Figure 11 D**). In contrast, only low levels of GC-B were detected in the aorta lysate, while the intense band for GC-B in the lysate from primary VSMCs indicated a strong upregulation after 6 days in culture (**Figure 11 D**). To investigate this upregulation in more detail, VSMCs from GC-B LacZ reporter mice were stained with X-gal after 4, 5, 6 and 7 days in culture (**Figure 11 E**). Subsequently, the amount of GC-B expressing X-gal-stained VSMCs (referred to as "X-gal+ cells" from here on) was quantified in each FOV and normalised to the total number of cells in the respective FOV as deduced from nuclear Hoechst staining. Note that nuclei showing an intense X-gal staining (dark blue, **Figure 11 E**, left inset) were not visible in the Hoechst staining (right inset). This was most likely caused by the absorbance of the X-gal-stained nuclei. Fluorescence of the Hoechst dye was excited in the range where indigo dyes (responsible for the blue colour of the X-gal staining) show strong absorbance [316]. The percentage of X-gal+ cells per FOV increased during culture from **0 %** (4 days, 5 days) over **0.9 ± 0.3 %** (6 days) to **2.9 ± 0.7 %** (7 days, **Figure 11 E**). The high variation of X-gal+ cells per FOV demonstrated that these cells were not evenly distributed within the cultures. It is worth mentioning that by this method less cells were detected than CNP-preferring cells were usually present in cultures analysed by cGMP/FRET measurements.

Together, these results indicated that GC-B is gradually upregulated in VSMCs during cell culture, potentially due to progressing phenotypic modulation.

To validate that the CNP-induced cGMP generation is mediated by its canonical receptor GC-B, we ablated GC-B genetically. VSMCs were isolated from 4-week-old GC-B knockout and litter-matched control mice that both expressed the cGMP biosensor cGi500 globally. Subconfluent cultures were analysed for their NP preference by cGMP/FRET measurements (**Figure 12**) as described above. The phenotypic state of the cells was assessed by IF stainings for αSMA and SM22α (**Supplementary figure V**). Additionally, the fraction of cells responding to ANP, CNP and NO, respectively, was quantified independent of their preference.

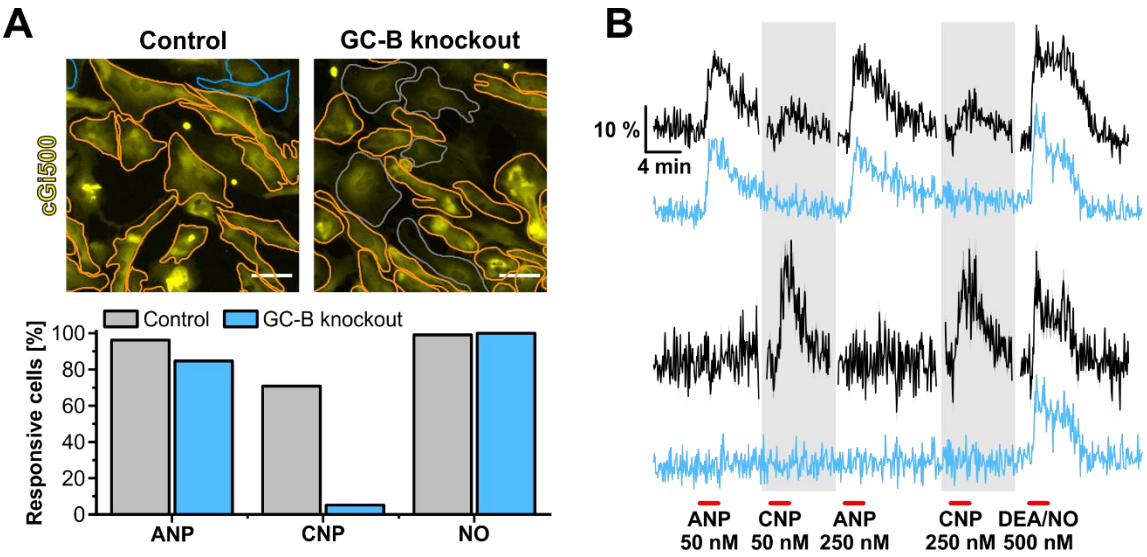

Figure 12: CNP-induced cGMP generation in primary VSMCs is mediated by GC-B. *Primary aortic VSMCs from control (cGi(L1) +/L1 x GC-B +/+) and GC-B knockout (cGi(L1) +/L1 x GC-B LacZ/LacZ) mice were cultured for 5 days and classified by their cGMP response patterns (FRET measurement).* ***A:*** *Representative cGMP/FRET measurement of primary VSMCs from control and GC-B knockout mice after 5 days in culture. VSMCs were visualised by the YFP fluorescence (yellow) of cGi500 during the cGMP/FRET measurement (top). The NP preference of individual VSMC is indicated by the respective colour (new pattern "NO-only" is indicated by a grey outline). The bottom panel depicts the percentage of cells that reacted to ANP, CNP and/or NO (grey: control, 212*

cells, 2 coverslips, 1 mouse – cyan: GC-B knockout, 215 cells, 2 coverslips, 1 mouse). For concentrations and application order see (B). ***B:*** *Comparison of cGMP response patterns that were measured in A. The ratio traces (R ~ [cGMP]) depict the development of cGMP levels over time (black: control, mean of 55 cells [top], mean of 6 cells [bottom] – cyan: GC-B knockout, mean of 68 cells [top], mean of 25 cells [bottom]). SEM is indicated as a shadow behind the corresponding ratio trace. The scale at the left indicates the percent change of the ratio trace relative to the baseline ("ΔR/R"). The upper trace (control, black) indicates how the corresponding GC-B knockout VSMCs (cyan, lower) would have reacted if they still could have responded to CNP. The top pair represents ANP-preferring and the bottom pair CNP-preferring VSMCs (this hypothesis was supported by VSMC marker analysis, see* ***Supplementary figure V****). Red horizontal lines indicate drug applications. As the control measurement lasted longer, some data points from the baseline were omitted (gaps in the black traces) to align the drug applications without distorting the time axis. The part of the ratio traces where responses to CNP were expected is highlighted in grey. Scale bars are 50 µm.*

Primary VSMC cultures from GC-B knockout as well as control mice showed heterogeneous morphologies within the same culture (**Figure 12 A**, top). While the control culture comprised ANP- (orange) and CNP-preferring (cyan) cells, no CNP-preferring cells could be detected in the GC-B knockout culture. Instead, cells reacting to NO-only (grey) were detected in the GC-B knockout culture (~15 %, **Supplementary figure V**), which were not present in the control culture. These "NO-only" cells expressed significantly less contractile marker proteins than ANP-preferring cells of the same culture (**Supplementary figure V**). The fraction of cells showing a certain cGMP signalling pattern (e.g., CNP-preferring cells) and their contractile marker protein expression is summarised in **Supplementary figure V**. To compare the cGMP responses between both genotypes, the fraction of cells that reacted to ANP, CNP or NO was quantified (**Figure 12 A**, bottom). In both control and GC-B knockout cultures, nearly all cells reacted to NO and >80 % of cells reacted to ANP with slightly less ANP-responsive cells in the GC-B knockout cultures. The fraction of cells responding to CNP with cGMP elevations dropped from 70 % in control cultures to 5 % in knockout cultures. These 5 % of CNP-responding cells were based on minor elevations of the ratio trace by CNP application, meaning that the cGMP transients might have been caused by cross activation of the ANP receptor GC-A.

To validate whether the loss of CNP responses could explain the cGMP response patterns observed in the GC-B knockout cultures, we compared the cGMP response patterns (ratio traces) between GC-B knockout and control cultures (**Figure 12 B**). Indeed, for all cGMP response patterns of GC-B knockout VSMCs (cyan traces), we identified a matching cGMP response pattern in the control culture (black traces) that differed only by the presence of CNP-induced cGMP signals. The only exception were the 5 % of GC-B knockout VSMCs with a weak cGMP transient in response to CNP application (not shown).

Taken together, our results indicate that CNP-preferring cells are of smooth muscle origin and that their potential to respond to CNP develops or increases in culture over time by functional expression of GC-B.

3.1.3 CNP-preferring cells are characterised by expression of fibroblast markers and react weaker to NO than to CNP

After demonstrating that CNP-preferring cells in our experiments were derived from SM22α-expressing cells and that CNP responsiveness developed/increased in culture, we aimed to characterise these CNP-preferring cells in more detail. So far, the hallmark of CNP preferring cells – besides strong CNP-induced cGMP responses – was low expression of the SMC marker proteins αSMA and SM22α. Therefore, we searched for proteins that were expressed higher in CNP-preferring cells than in ANP-preferring ones. In addition, we analysed NO-dependent cGMP signalling in primary

VSMCs in more detail as our previous experiments indicated that CNP-preferring cells tended to show weak NO-induced cGMP responses.

SMCs were isolated from cGi(L1) mice, expressing the cGMP biosensor cGi500 globally. Subconfluent cultures were analysed for their NP preference by cGMP/FRET measurements and differences in protein expression were assessed by subsequent IF stainings. We analysed the expression of αSMA and FSP 1 (**Figure 13 A**), and PDGFRα (**Figure 13 B**). In line with previous experiments, high αSMA expression was detected in rather elongated ANP-preferring cells (**Figure 13 A**; ANP: 2508.1 ± 122.9 a.u. vs. CNP: 703.7 ± 61.5 a.u., **p < .001**). Large roundish CNP-preferring VSMCs expressed low levels of αSMA. Inversely, FSP 1 expression was moderately but significantly increased in CNP-preferring cells in comparison to ANP-preferring cells (**Figure 13 A**; ANP: 1393.2 ± 113.6 a.u. vs. CNP: 2103.7 ± 125.9 a.u., **p < .001**).

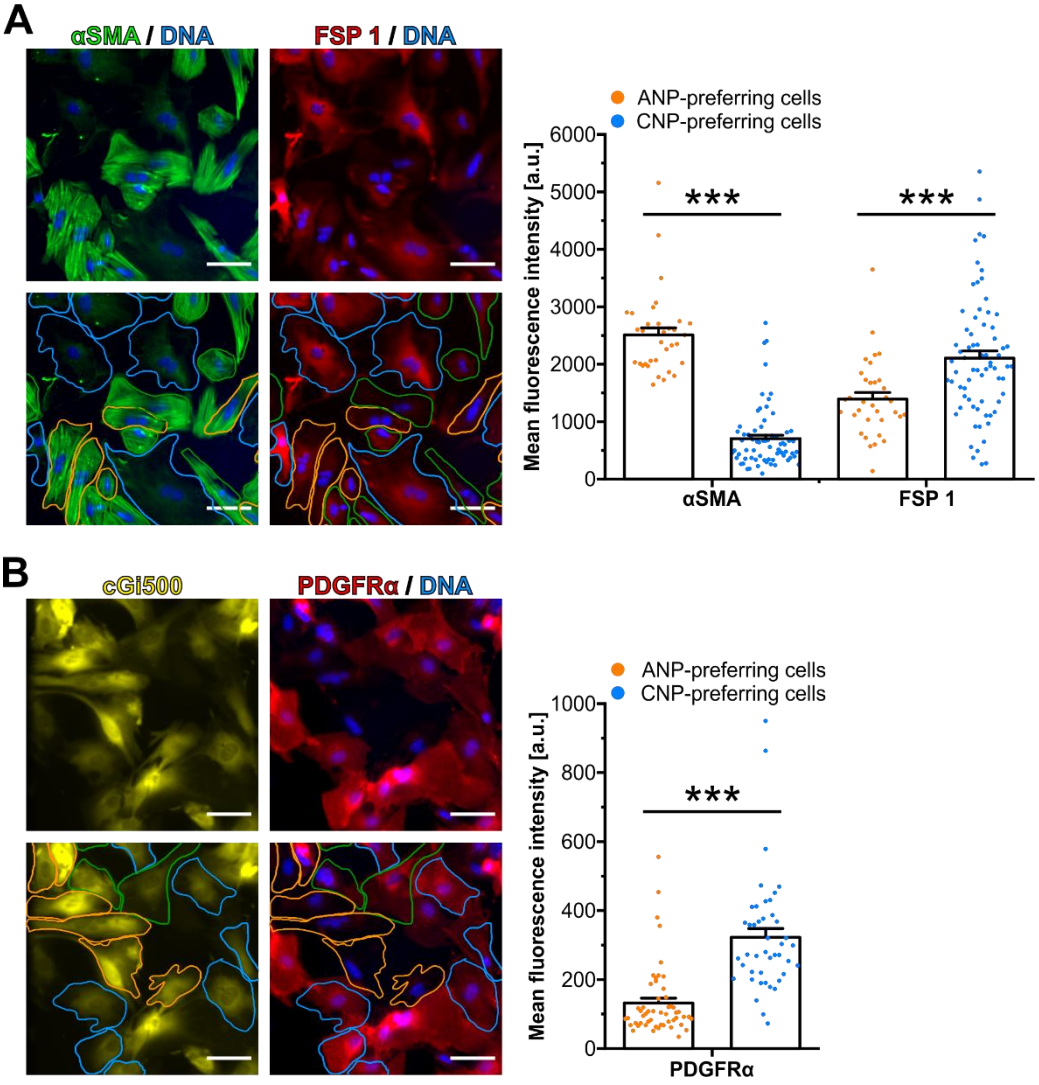

Figure 13: CNP-preferring VSMCs express fibroblast markers. *Primary aortic VSMCs from cGi(L1) mice were cultured for 5 days on gridded coverslips, classified by their cGMP response patterns (FRET measurement) and subsequently analysed for αSMA and FSP 1 (A) or PDGFRα (B) expression.* ***A:*** *Analysis of αSMA and FSP 1 expression in ANP- and CNP-preferring cells by IF staining (double staining). Left: Representative image section after cGMP/FRET measurement and subsequent staining for αSMA (green), FSP 1 (red), and DNA (blue). The NP preference of individual VSMCs is indicated by the respective colour (bottom). The expression of αSMA and FSP 1 (105 cells, 4 coverslips, 3 mice) for ANP- (orange) and CNP-preferring (cyan) cells was quantified in the right panel.*

B: *Analysis of PDGFRα expression in ANP- and CNP-preferring cells by IF staining. Left: Representative image section during cGMP/FRET measurement and after subsequent staining for PDGFRα (red) and DNA (blue). During the measurement cells were visualised by the YFP fluorescence (yellow) of cGi500. The NP preference of individual VSMCs is indicated by the respective colour (bottom). The expression of PDGFRα (97 cells, 5 coverslips, 2 mice) for ANP- (orange) and CNP-preferring (cyan) cells was quantified in the right panel. Each dot represents an individual VSMC. Data are represented as mean + SEM. Statistical significance is indicated by asterisks (*** p<.001). NP preference was assessed by stimulation with ANP, CNP, and DEA/NO as shown in* ***Figure 10 A****. Scale bars are 50 µm.*

Since an initial experiment showed impaired staining quality for PDGFRα when performed as double staining with αSMA (data not shown), the IF staining for PDGFRα was performed as single staining (**Figure 13 B**). The membrane localisation of PDGFRα got apparent by comparison with the cytosolic YFP fluorescence of cGi500 in the same cells (**Figure 13 B**). ANP-preferring cells exhibited no/low expression of PDGFRα, and CNP-preferring cells showed varying but significantly increased expression of PDGFRα (**Figure 13 B**; ANP: 131.7 ± 14.1 a.u. vs. CNP: 322.8 ± 25.3 a.u., **p < .001**). Despite the low fluorescence intensity of this staining in general, the quantification of PDGFRα expression allowed for a clear discrimination of the ANP- and the CNP-preferring VSMC population.

Based on these results, CNP-preferring cells appear to lose SMC lineage markers like αSMA and SM22α and gain markers often used to describe fibroblasts (FSP 1, PDGFRα). Together with the results from our lineage tracing (**Figure 11 A-B**) and adventitia-free VSMC culture (**Figure 11 C**) experiments and the increased expression of GC-B in VSMC cultures over several days (**Figure 11 E**), it seemed likely that primary VSMCs showed similarities with fibroblasts due to phenotypic modulation in cell culture rather than being real fibroblasts themselves.

Next, we compared NO-induced cGMP increases between ANP- and CNP-preferring cells. To do so, we compared the expression of the NO-GC β1 subunit (which is shared between NO-GC 1 and NO-GC 2) between ANP- and CNP-preferring primary VSMCs (**Figure 14 A**). Furthermore, the NO-induced cGMP response was normalised to the highest NP-induced cGMP response for each individual cell. With this, we aimed to compare the relative potency of NO to induce cGMP generation between ANP- and CNP-preferring cells (**Figure 14 B**). Finally, the fraction of cells responding to ANP, CNP, and/or NO was quantified (**Figure 14 C**).

Both αSMA and NO-GC β1 were strongly expressed in ANP-preferring cells, whereas CNP-preferring cells showed lower expression levels (**Figure 14 A**; αSMA – ANP: 1414.7 ± 56.5 a.u. vs. CNP: 646.1 ± 49.8 a.u., **p < .001**, NO-GC β1 – ANP: 522.4 ± 30.7 a.u. vs. CNP: 231.2 ± 33.5 a.u., **p < .001**) with few exceptions (see arrowheads). Relative quantification of the NO-induced cGMP responses (**Figure 14 B**) matched the results shown by the NO-GC β1 expression as detected by IF staining. Most ANP-preferring cells responded strongest to NO (**Figure 14 B**). Most CNP-preferring cells, however, reacted stronger to CNP than to NO. This reduction was statistically significant (ANP: 106.5 ± 3.3 % vs. CNP: 69.9 ± 4.8 % NO- over NP-induced cGMP generation, **p < .001**). Still, most cells reacted to NO as shown in **Figure 14 C**. Around 80 % of cells reacted to ANP and nearly all to CNP. Recent single-cell RNA sequencing of primary VSMC cultures in our laboratory confirmed a reduced NO-GC expression in modulated VSMCs (data not shown).

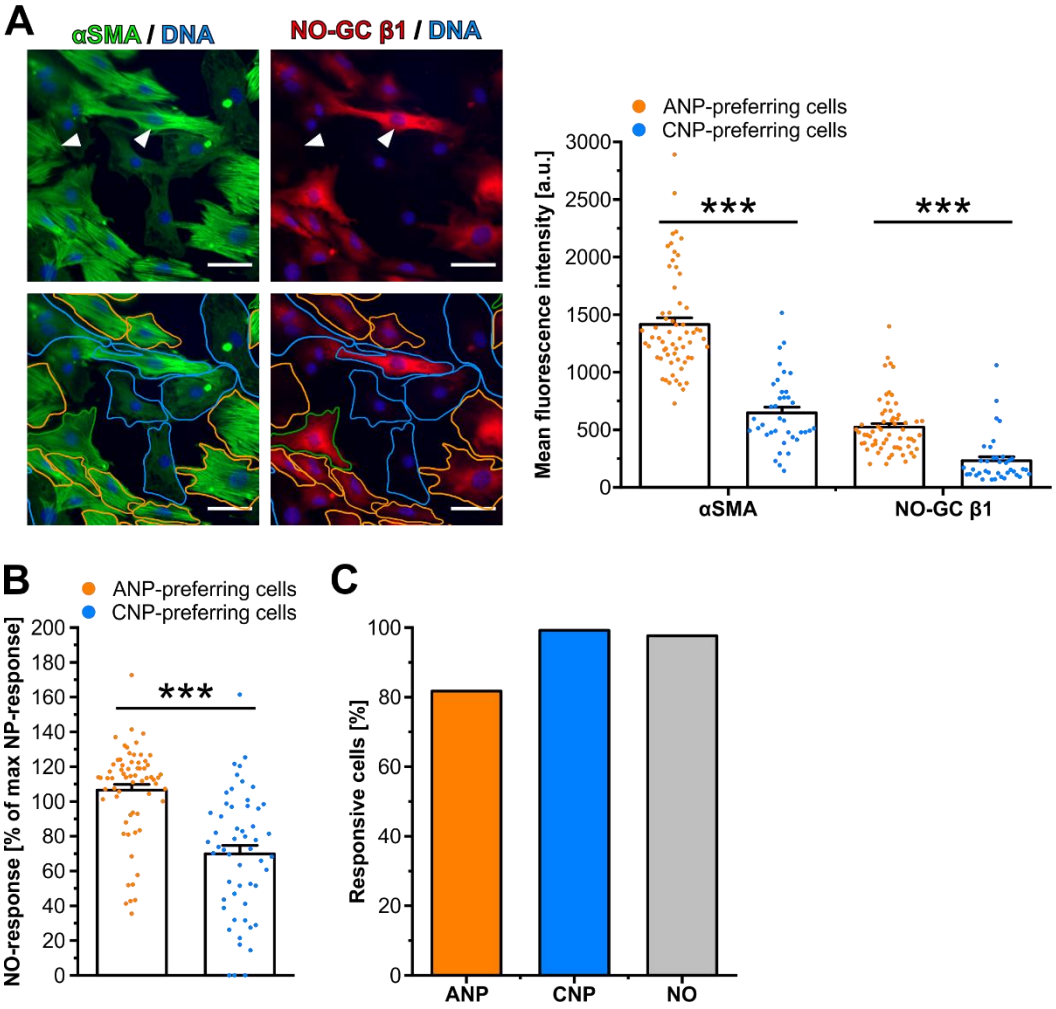

Figure 14: CNP-preferring VSMCs show weaker cGMP responses to NO than to CNP. *Primary aortic VSMCs from cGi(L1) mice were cultured for 7 days on gridded coverslips, classified by their cGMP response patterns (FRET measurement) and subsequently analysed for αSMA and NO-GC β1 expression (A). Additionally, the relative strength of the NO-induced cGMP response (B) and the fraction of cells that responded to ANP, CNP, or NO (C) were quantified.* ***A:*** *Analysis of αSMA and NO-GC β1 expression in ANP- and CNP-preferring cells by IF staining (double staining). Left: Representative image section after cGMP/FRET measurement and subsequent staining for αSMA (green), NO-GC β1 (red), and DNA (blue). White arrowheads mark cells mentioned in the main text. The NP preference of individual VSMCs is indicated by the respective colour (bottom). The expression of αSMA and NO-GC β1 (100 cells, 4 coverslips, 2 mice) for ANP- (orange) and CNP-preferring (cyan) cells was quantified in the right panel. The same concentrations and drug application order as shown in* ***Figure 10 A*** *were used for classification of the NP preference* ***B:*** *Quantification of the NO-induced cGMP response (normalised to the highest NP-induced cGMP response of each individual VSMC) for the cells measured in A (119 cells, 4 coverslips, 2 mice). Each dot represents an individual VSMC. Data are represented as mean + SEM. Statistical significance is indicated by asterisks (*** p<.001). Scale bars are 50 µm.* ***C:*** *Percentage of cells (cumulated numbers, no mean) measured in A that reacted to ANP, CNP, and/or NO (136 cells, 4 coverslips, 2 mice).*

Together, these results indicated that contractile VSMCs, characterised by high expression of αSMA and SM22α, generated cGMP primarily upon stimulation with ANP and NO. Cell culture modulated these VSMCs towards a fibroblast-like phenotype, as characterised by high expression of PDGFRα and FSP 1. These modulated VSMCs responded mainly to CNP.

3.1.4 NP preference is susceptible to phenotypic modulation and age

The results described in the sections above indicated that the phenotype of VSMCs in culture correlated with their NP preference. Next, we investigated this connection in more detail by analysing

the NP preference of VSMCs after application of manoeuvres that influence phenotypic modulation of VSMCs. Specifically, we tested the effect of serum concentration (soluble factors), fibronectin-coated surfaces (ECM) and passaging (**Figure 15**).

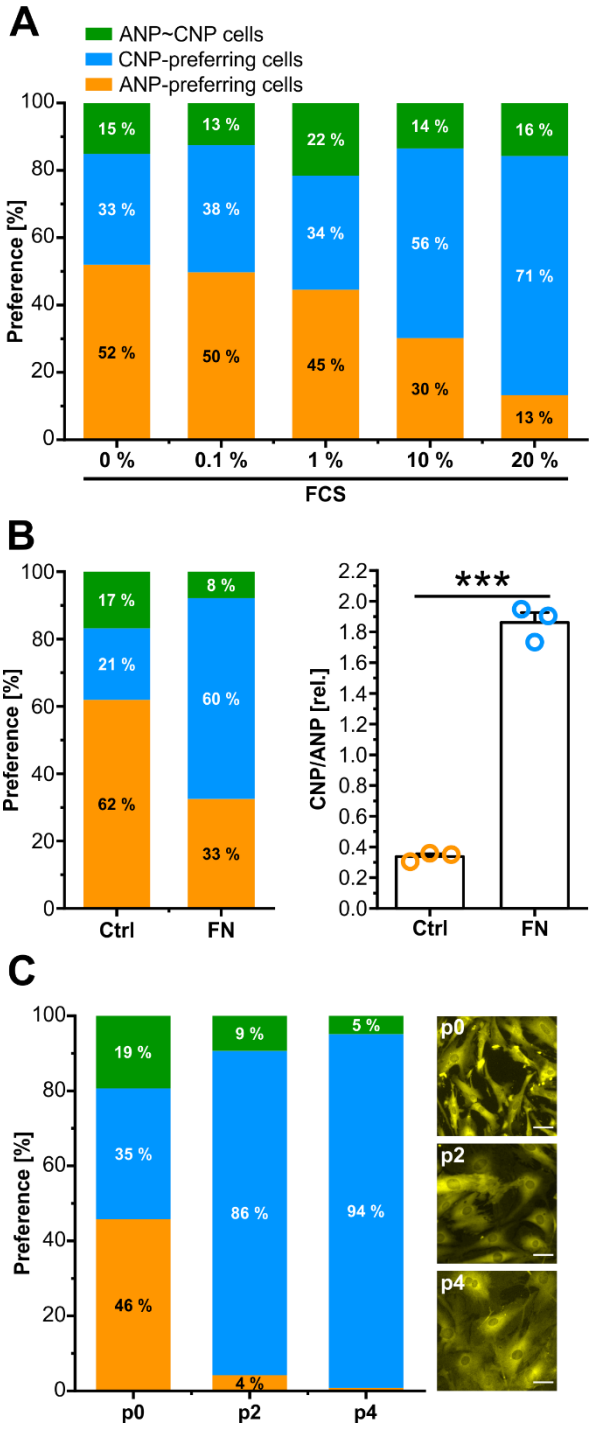

Figure 15: Promotion of a modulated VSMC phenotype shifts NP-dependent cGMP signalling towards CNP preference. *Aortic VSMCs from cGi(L1) mice were cultured on glass coverslips under various conditions known to influence the phenotype of VSMCs and classified by their cGMP response patterns (FRET measurement). The percentage of cells in each category was calculated and compared between the different conditions. Drugs were applied as shown in* ***Figure 10 A****.* ***A:*** *Effect of serum concentration on NP preference. Cell culture medium was supplemented with* ***0 % - 20 % FCS*** *(high serum concentrations promote the modulated VSMC phenotype) for 48 h before cGMP/FRET measurements. Bars indicate the fraction of cells in each category under each condition (cumulated numbers, no mean). 0 % (179 cells, 3 coverslips) – 0.1 % (167 cells, 3 coverslips) – 1 % (74 cells, 2 coverslips) – 10 % (96 cells, 2 coverslips) – 20 % (121 cells, 2 coverslips).* ***B:*** *Effect of fibronectin coating on NP preference. VSMCs were cultured in 10 % FCS on uncoated (control) or fibronectin-coated (FN, promotes modulated VSMC phenotype) glass coverslips for cGMP/FRET measurements. Left: Bars indicate the fraction of cells in each category under each condition (cumulated numbers, no mean). Right: Ratio of CNP- and ANP-preferring cells per measurement. Each circle represents an individual coverslip. Data are represented as mean + SEM. Statistical significance is indicated by asterisks (*** p<.001). Ctrl (155 cells, 3 coverslips) – FN (292 cells, 3 coverslips). Collaboration with Hyazinth Dobrowinski* ***C:*** *Effect of passaging on NP preference. Aortic VSMCs were seeded on glass coverslips for cGMP/FRET measurements or in cell culture dishes for passaging (promotes modulated VSMC phenotype) and grown in 10 % FCS. Primary VSMCs (p0), VSMCs of passage 2 (p2) and VSMCs of passage 4 (p4) were measured. Left: Bars indicate the fraction of cells in each category under each condition (cumulated numbers, no mean). Right: Representative image section of a cGMP/FRET measurement for primary, passage 2 and passage 4 VSMCs. VSMCs were visualised by the YFP fluorescence (yellow) of cGi500. Scale bars are 50 µm. p0 (284 cells, 5 coverslips, 20 mice) – p2 (214 cells, 6 coverslips, 20 mice) – p4 (123 cells, 5 coverslips, 20 mice).*

Serum starvation was reported to promote the contractile VSMC phenotype [196-198]. VSMCs in our experiments were cultured with 10 % FCS as supplement to allow efficient growth but were normally serum-starved for 12-24 h before cGMP/FRET measurements. To investigate the effect of serum concentration on NP preference, VSMCs were cultured as usual (e.g., with 10 % FCS), but instead of serum starvation for 12-24 h, the serum concentration of the medium was changed to 0-20 % FCS for **48 h** before cGMP/FRET measurements. For cGMP/FRET measurements, representative regions based

on cell morphology were chosen and the fraction of ANP/CNP-preferring, and ANP~CNP cells was quantified. Under low serum conditions (e.g., 0, 0.1, 1 % FCS), ANP-preferring cells were more prevalent (45-52 %) than CNP-preferring cells (33-38 %) (**Figure 15 A**). Under high serum conditions (10, 20 % FCS) cultures contained more CNP-preferring (56-71 %) than ANP-preferring (13-30 %) cells, indicating a more modulated VSMC culture than under low serum conditions. While there was a clear effect between low and high serum conditions, the differences within the low serum conditions (0, 0.1, 1 % FCS) were subtle.

In contrast to serum starvation, growth on fibronectin-coated surfaces was reported to induce modulation away from the contractile phenotype [152]. To test whether this promoted CNP preference as well, VSMCs were cultured either on uncoated (Ctrl) or on fibronectin-coated (FN) glass coverslips. Representative regions of subconfluent cultures were chosen based on cell morphology and analysed for their NP preference by cGMP/FRET measurements (**Figure 15 B**). In this experiment, growth on fibronectin decreased the fraction of ANP-preferring VSMCs as compared to control conditions (Ctrl: 62 % vs. FN: 33 %) (**Figure 15 B**, left). This shift from a mainly ANP-preferring towards predominantly CNP-preferring VSMC culture by growth on fibronectin was validated statistically (**Figure 15 B**, right, CNP/ANP ratio: Ctrl 0.34 ± 0.02 rel. vs. FN 1.86 ± 0.07 rel., **p<.001**) and in line with a more modulated VSMC culture upon growth on fibronectin-coated surfaces.

Passaging (also known as subculturing) was also described as an efficient way to promote the modulated VSMC phenotype [148; 190]. VSMCs were isolated from cGi(L1) mice, expressing the cGMP biosensor cGi500 globally and either cultured on glass coverslips for cGMP/FRET measurement or subjected to passaging. Primary VSMCs (p0), VSMCs that were passaged twice (p2) and VSMCs that were passaged four times (p4) were analysed for their NP preference (**Figure 15 C**). Representative regions of subconfluent cultures were chosen based on cell morphology. In primary VSMC cultures (p0), all three NP-induced cGMP response patterns were frequently observed, consistent with our observations in other primary VSMC cultures (e.g., **Figure 15 A-B**, control conditions). 46 % of primary cells preferred ANP (46 %), around 35 % of the cells preferred CNP and 19 % showed no clear preference (ANP~CNP cells). Already in p2 nearly all cells preferred CNP (86 %). Only 4 % of cells preferred ANP and 9 % had no clear preference. In p4, only a single cell out of 123 cells measured showed ANP preference. 94 % of cells preferred CNP, and the ANP~CNP group was reduced to 5 %. This shift towards CNP-preferring cells was accompanied by a more modulated (rounded) morphology of VSMCs (**Figure 15 C**, right). As indicated in the figure legend, the number of cells per measurement decreased with each passage.

Together these results showed that promotion of the modulated VSMC phenotype by various methods led to more CNP-preferring cells.

Modulated VSMCs are known to be involved in cardiovascular disease development and the prevalence of cardiovascular diseases increases with age [317]. Therefore, we asked if VSMCs from old mice were more likely to give rise to CNP-preferring (modulated) VSMCs. We compared NP preference between primary VSMC cultures of young (≤ 8 weeks), middle-aged (9-16 weeks), and old mice (≥ 17 weeks). Representative regions of subconfluent cultures were chosen based on cell morphology for cGMP/FRET measurements. The fraction of ANP-/CNP-preferring cells and ANP~CNP cells was quantified and compared as a function of age (**Figure 16**). The fraction of CNP-preferring cells increased with age from 17 % (young) over 42 % (middle-aged) to 68 % (old) (**Figure 16 A**). Inversely, the fraction of ANP-preferring cells decreased with age from 65 % (young), over 30 % (middle-aged) to 11 % (old).

The shift from ANP- to CNP-preferring cells with increasing age of the mice was reflected by the morphology of measured VSMCs. While most cells in VSMC cultures from young and middle-aged mice were elongated, mainly rounded cells were found in cultures from old mice.

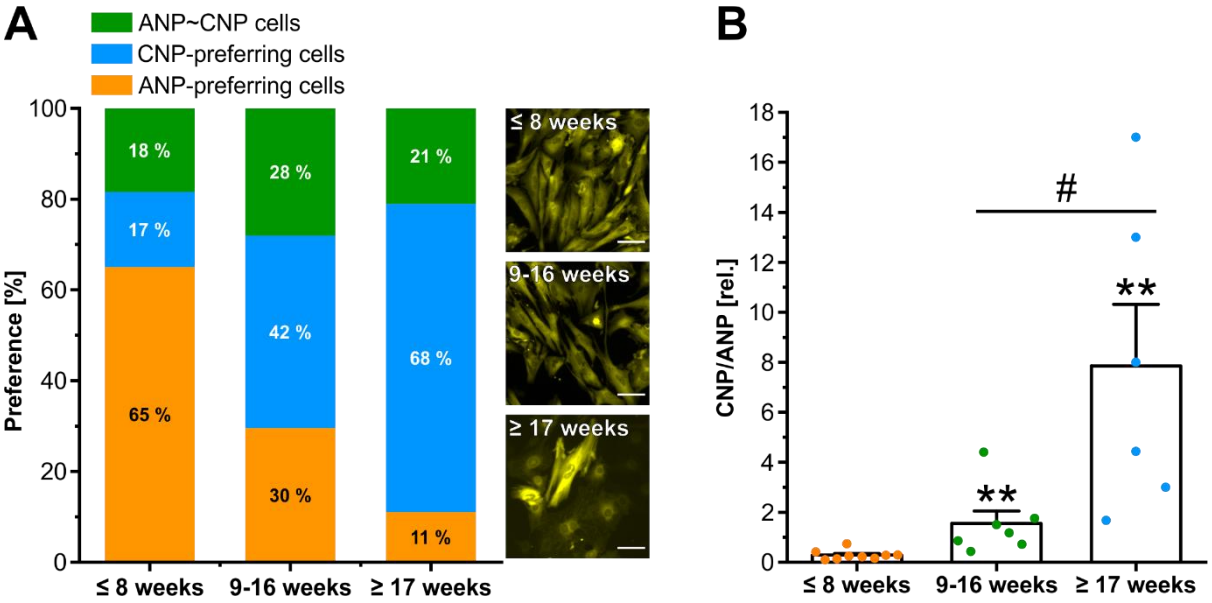

Figure 16: Aging shifts NP-dependent cGMP signalling in VSMCs towards CNP preference. *Primary aortic VSMCs from sensor expressing young, middle-aged, and old mice were cultured on glass coverslips and classified by their cGMP response patterns (FRET measurement). The percentage of cells in each category was calculated and compared between the 3 age groups (≤ 8 weeks: "young" – 9-16 weeks: "middle-aged" – ≥ 17 weeks: "old"). Drugs were applied as shown in* ***Figure 10 A****.* ***A-B:*** *Effect of age on NP preference.* ***A:*** *Bars indicate the fraction of cells in each category under each condition (cumulated numbers, no mean, left). Right: Representative image section of a cGMP/FRET measurement for primary aortic VSMCs from young, middle-aged, and old mice. VSMCs were visualised by the YFP fluorescence (yellow) of cGi500. Scale bars are 50 µm.* ***B:*** *Ratio of CNP- and ANP-preferring cells per measurement. Each dot represents an individual coverslip. Data are represented as mean + SEM. Statistical significance vs "≤ 8 weeks" is indicated by asterisks (** p<.01). Statistical significance between groups indicated by the horizontal line is indicated by hashes (# p<.05). Young (≤ 8 weeks, 412 cells, 9 coverslips, 3 mice) – middle-aged (9-16 weeks, 196 cells, 7 coverslips, 2 mice) – old (≥ 17 weeks, 171 cells, 6 coverslips, 3 mice).*

To directly compare the amount of CNP- and ANP-preferring cells prepared from mice of different age, the ratio of these two groups was calculated (**Figure 16 B**). In all cultures of young mice, more ANP- than CNP-preferring cells were present (CNP/ANP ratios: 0.1-0.7 rel.). Some cultures of middle-aged mice contained more ANP- than CNP-preferring cells and some vice versa (CNP/ANP ratios: 0.4-4.4 rel.). In all cultures of old mice, more CNP- than ANP-preferring cells were present (CNP/ANP ratios: 1.7-17). The shift from ANP- to CNP-preferring cells with age was significant between all age groups. Considering the tight connection between NP preference and VSMC phenotype demonstrated by the experiments shown in **Figure 15**, it is likely that VSMCs in/from older mice are more susceptible to phenotypic modulation. Note that there was a high variation of the CNP/ANP ratio within each age group.

In summary, we could gain new insights concerning cGMP signalling in VSMCs by using a cell culture approach. We carefully analysed cGMP signalling in VSMC cultures grown under various conditions at the single-cell level with a combination of cGMP/FRET imaging, IF stainings and genetic approaches. This allowed us to identify a close connection between phenotype and cGMP signalling in VSMCs on a single-cell level: While contractile VSMCs in culture preferred ANP, modulated fibroblast-like VSMCs

preferred CNP. In addition, the NO-induced cGMP responses of modulated VSMCs were often reduced (in relation to their CNP-induced cGMP response). All conditions that favoured the modulated VSMC phenotype also favoured CNP preference. Importantly, age was identified as a new factor that promoted CNP-dependent cGMP signalling in cultured VSMCs.

3.2 cGMP signalling in healthy and diseased aortas

After having identified a connection between NP-induced cGMP signalling and VSMC phenotype in culture, we investigated whether a similar connection exists in intact arteries. The culture model has the advantage that it is simple and can be analysed in various ways. It is especially suited to investigate phenotypic modulation of VSMCs as the phenotype can be modulated during the cultivation process. At the same time the simplicity of this model is its downside. Even when surfaces are coated with ECM components it is hard to mimic the complexity of the ECM, naturally surrounding VSMCs in an intact vessel. Furthermore, VSMCs in intact vessels are exposed to mechanical forces which are not present in cell culture experiments. Both factors are known to influence VSMC phenotype and/or behaviour [152; 318]. The accessibility of drugs can also be very different as the physical barrier provided by the endothelium is missing in cultured cells. Therefore, it is important to support findings of cell culture experiments with data generated in the respective tissue *ex vivo* or if possible *in vivo*.

Our cell culture experiments suggested that contractile VSMCs prefer ANP over CNP, whereas modulated VSMCs prefer CNP over ANP. Therefore, we compared cGMP signalling in healthy aortas (comprised of contractile VSMCs) with cGMP signalling in atherosclerotic plaques (thought to contain also modulated VSMCs).

3.2.1 CNP-induced cGMP signals in healthy arteries are hardly detectable

We measured cGMP/FRET in isolated aortas of cGi(L1) mice (including the branching arteries) *ex vivo* under close-to-native conditions (**Figure 17**). Pieces of isolated aortas or smaller arteries (carotid arteries, brachiocephalic artery) were opened longitudinally and measured from the luminal side with a confocal spinning disk microscope. In contrast to the cell culture experiments described in **Figure 10 A**, the pGC ligands CNP (250 nM) and ANP (250 nM), and the NO-releasing compound DEA/NO (1 µM) were applied only in “high” concentrations to assure tissue penetration.

As a confocal microscope was used, the medial layer of arteries could be focussed for measurements (**Figure 17 A**). The characteristic morphology of the media as visualised by confocal imaging (max. intensity projection of a Z-stack recording) of an aorta isolated from a SMC-selective sensor mouse is shown at the right. Elongated VSMCs were aligned next to each other and rows of VSMCs were separated by dark, non-fluorescent areas. This distinct morphology was used to identify the medial layer in aortas of cGi(L1) mice that were used for most cGMP/FRET measurements. The max. intensity projection was used to depict structures with considerable expansion in the z-direction in a single image (“as if the tissue was pressed flat into a single plane”). Note, that during a cGMP/FRET measurement no Z-stack was acquired. Therefore, only the part of cells that was located within the focal plane could be visualised.

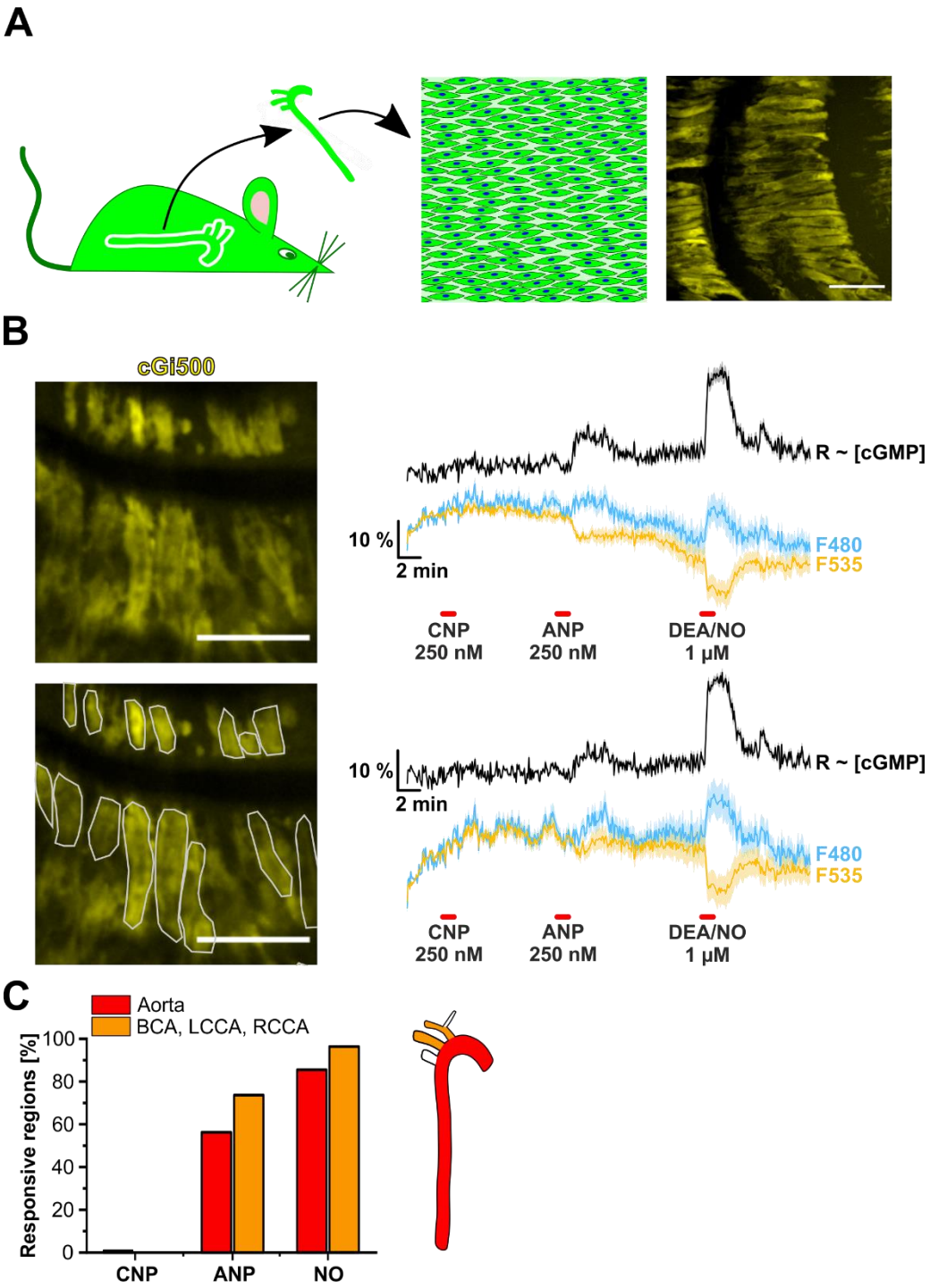

Figure 17: CNP-induced cGMP signals are hardly detectable in healthy arteries, while ANP and NO trigger robust cGMP elevations. *Aortas were isolated from cGi(L1) mice, opened longitudinally and cGMP/FRET measurements were performed with the luminal side facing the objective. cGMP responses to ANP, CNP and DEA/NO in the medial layer (as identified by morphology) of individual pieces were recorded. The entire aorta (arch, thoracic and abdominal part; A-B) as well as smaller arteries parting from the aorta (left and right carotid arteries, brachiocephalic artery; C) were analysed.* ***A****: Schematic representation (left) and image section of a max intensity projection (right) showing the medial layer of a sensor expressing aorta. VSMCs were visualised by the YFP fluorescence (yellow) of cGi500. The green colour represents sensor fluorescence in the scheme at the left.* ***B:*** *Representative cGMP/FRET measurement of a healthy aorta (medial layer). Sensor expressing cells were visualised by the YFP fluorescence (yellow) of cGi500 during the cGMP/FRET measurement (left; image section). Potential cells used for the analysis of cGMP responses are indicated at the lower left. The right panel shows the development of cGMP levels over time. Two response patterns that were typically detected after stimulation of*

healthy aortas with CNP (250 nM), ANP (250 nM) and DEA/NO (1 µM) are shown. Top: Regions that reacted to ANP and DEA/NO but not CNP (mean of 14 regions). Bottom: Regions that reacted to DEA/NO but neither to ANP nor CNP (mean of 32 regions). The "potential" response to ANP in the ratio trace (bottom) could not be verified by clear antiparallel separation of the single traces. Black: ratio traces (R ~ [cGMP]), cyan: CFP fluorescence, yellow: YFP fluorescence. The single traces (cyan/yellow) were applied to distinguish "real" cGMP/FRET signals from signals "feigned" by focus drift or tissue movement. SEM is indicated as a shadow behind the corresponding trace. The scale at the left indicates the percent change of the ratio trace and the single traces relative to their baseline ("ΔR/R" and "ΔF/F", respectively). Red horizontal lines indicate drug applications. Scale bars are 20 µm. ***C:*** *Summary of cGMP responses to CNP (250 nM), ANP (250 nM), and/or DEA/NO (250 nM) in healthy aortas and smaller arteries of cGi(L1) mice. Bars indicate fraction of regions (cumulated numbers, no mean) that reacted to CNP, ANP, and/or DEA/NO. Red: aorta (414 regions, 23 measurements, 19 mice). Orange: smaller arteries (110 regions, 8 measurements, 7 mice). BCA: brachiocephalic artery, LCCA: left common carotid artery, RCCA: right common carotid artery. A scheme depicting the vessels used for analysis is shown at the right side.*

Individual VSMCs could be identified by their morphology in all cGMP/FRET measurements of healthy arteries (e.g., **Figure 17 B**, the outlines of individual VSMCs are indicated in the lower panel). In areas of weak fluorescence or low contrast it was not possible to reliably identify cells. In these areas, circular ROIs were used to analyse cGMP signalling. By doing so, signals of dim cells were still caught. Furthermore, due to tissue movement it was possible that one cell moved out of its ROI while another cell moved into this ROI. In consequence, this ROI would contain the signal of two cells. To account for ROIs that detected more than one cell, we will use the term "region" instead of "cells" for *ex vivo* measurements, albeit most cGMP/FRET signals were derived from single cells. As *ex vivo* measurements were prone to artefacts due to tissue movement and deformation (resulting in a focus drift), it was essential to verify signals by the antiparallel development of CFP and YFP fluorescence. Therefore, in addition to the ratio trace (R ~ [cGMP], black), the single traces of CFP (F480, cyan) and YFP (F535, yellow) fluorescence are shown for *ex vivo* measurements (**Figure 17 B**, **Figure 18 C-D**). Only elevations of the ratio trace that were supported by clear trace separation (antiparallel development) were accepted as real cGMP signals.

cGMP/FRET measurements in healthy aortas revealed heterogeneous cGMP response patterns (**Figure 17 B**). Two different cGMP response patterns that were identified in most cGMP/FRET measurements are depicted (**Figure 17 B**, right). These two response patterns represent 80 % of all responses that were measured in healthy arteries (without regions that were excluded from analysis, **Supplementary table VII**). Like ANP-preferring VSMCs (contractile phenotype) in culture, healthy arteries showed clear cGMP responses to ANP and NO (**Figure 17 B**, top). In response to both drugs, the single traces showed a clear antiparallel development (CFP fluorescence increased while YFP fluorescence decreased). In contrast to ANP-preferring VSMCs in culture, no elevation of cGMP levels after CNP application was detected in regions of healthy arteries that reacted to ANP and NO (**Figure 17 B**, top).

In several regions, a robust cGMP response was only elicited by NO (**Figure 17 B**, bottom). No change of the ratio trace after CNP application was detected. After ANP application, an elevation of the ratio trace was visible as well, but no clear antiparallel development of the single traces was detected. It seemed that the separation of the single traces was caused by the different extent of decrease and increase while moving in parallel. These potentially "false" cGMP signals were excluded from analysis (**Figure 17 B**, bottom). Note that before signals were grouped by their response patterns, they were verified in every individual region (e.g., not with the mean traces). Due to this conservative approach, it is possible that some ANP-induced cGMP signals were excluded from analysis. However, CNP-induced cGMP signals were clearly absent in most measurements.

Quantification of regions with (verified) cGMP responses to ANP, CNP and NO, respectively, demonstrated that cGMP in healthy aortas and branching vessels was almost exclusively generated in response to ANP (**Figure 17 C**; 56 % in aortas and 74 % in smaller arteries) and/or NO (86 % in aortas and 96 % in smaller arteries). cGMP generation upon application of CNP was hardly ever detectable (0.7 % in aortas [= 3 out of 414 regions] and 0 % in smaller arteries).

Together, clear cGMP responses to ANP and/or NO but almost no responses to CNP were detected in healthy aortas. These cGMP response patterns reflected the main characteristic of contractile VSMCs in culture, namely their responses to ANP and NO, but not or only weakly to CNP (**Figure 10**).

3.2.2 Plaques in atherosclerotic arteries show strong CNP-induced cGMP signals

By our cGMP/FRET measurements in healthy arteries, we could not identify a signalling pattern that matched the CNP-preferring (modulated) VSMCs in culture. We hypothesised that *in vivo*, phenotypic modulation of VSMCs as it occurs during the progression of atherosclerotic disease might lead to development of CNP-responding VSMCs. Therefore, we analysed cGMP signalling in atherosclerotic aortas. Additionally, we compared cGMP signalling in plaques from GC-B reporter (GC-B +/LacZ = heterozygous GC-B knockout) and control (GC-B +/+) mice to assess whether heterozygous ablation of GC-B affects cGMP signalling in atherosclerotic plaques.

To analyse cGMP signalling in potentially modulated plaque VSMCs under close-to-native conditions, cGMP/FRET measurements were performed *ex vivo* with atherosclerotic plaques from cGi(L1) mice expressing the cGMP biosensor cGi500 globally (**Figure 18**). Pieces of isolated aortas or branching vessels (carotid arteries, brachiocephalic artery) were opened longitudinally and plaques were measured from the luminal side (still attached to the vessel wall) with a confocal spinning disk microscope.

The time course of experiments is described in **Figure 18 A**. 25 weeks after birth, plaque development of ApoE-deficient mice was accelerated by feeding of an atherogenic diet for 16 weeks (see section **1.3.2.3** for a description of this atherosclerosis model). Subsequently, mice were sacrificed, and their aortas were subjected to cGMP/FRET measurements. **Figure 18 B** illustrates schematically how plaques would theoretically appear under a confocal microscope (e.g., during cGMP/FRET measurements). Plaques (red patches), mainly from the aortic arch, the brachiocephalic artery and abdominal part but also from the thoracic part were used for cGMP/FRET measurements (left). As a confocal microscope was used for cGMP/FRET measurements, it was not possible to measure the entire plaque, but only a thin layer of it (**Figure 18 B**, optical sections, 1-5). By measuring these “optical sections”, we intended to compare cGMP signalling of fibrous cap VSMCs (spindle shaped) with cells of the plaque core (rhomboid), but the described setup only enabled analysis of potential fibrous cap cells (see panel D, right image).

Representative cGMP/FRET measurements of an atherosclerotic plaque from control (**Figure 18 C**) and GC-B reporter mice (**Figure 18 D**) are shown. The top-down view of plaques provided by the max. intensity projections (left images) demonstrated a heterogeneous morphology within and between plaques. This heterogeneity did not depend on the heterozygous GC-B knockout but was generally observed between individual plaques. In general, it was hard to distinguish individual cells due to poor signal-to-noise ratio in several plaques (e.g., **Figure 18 C**).

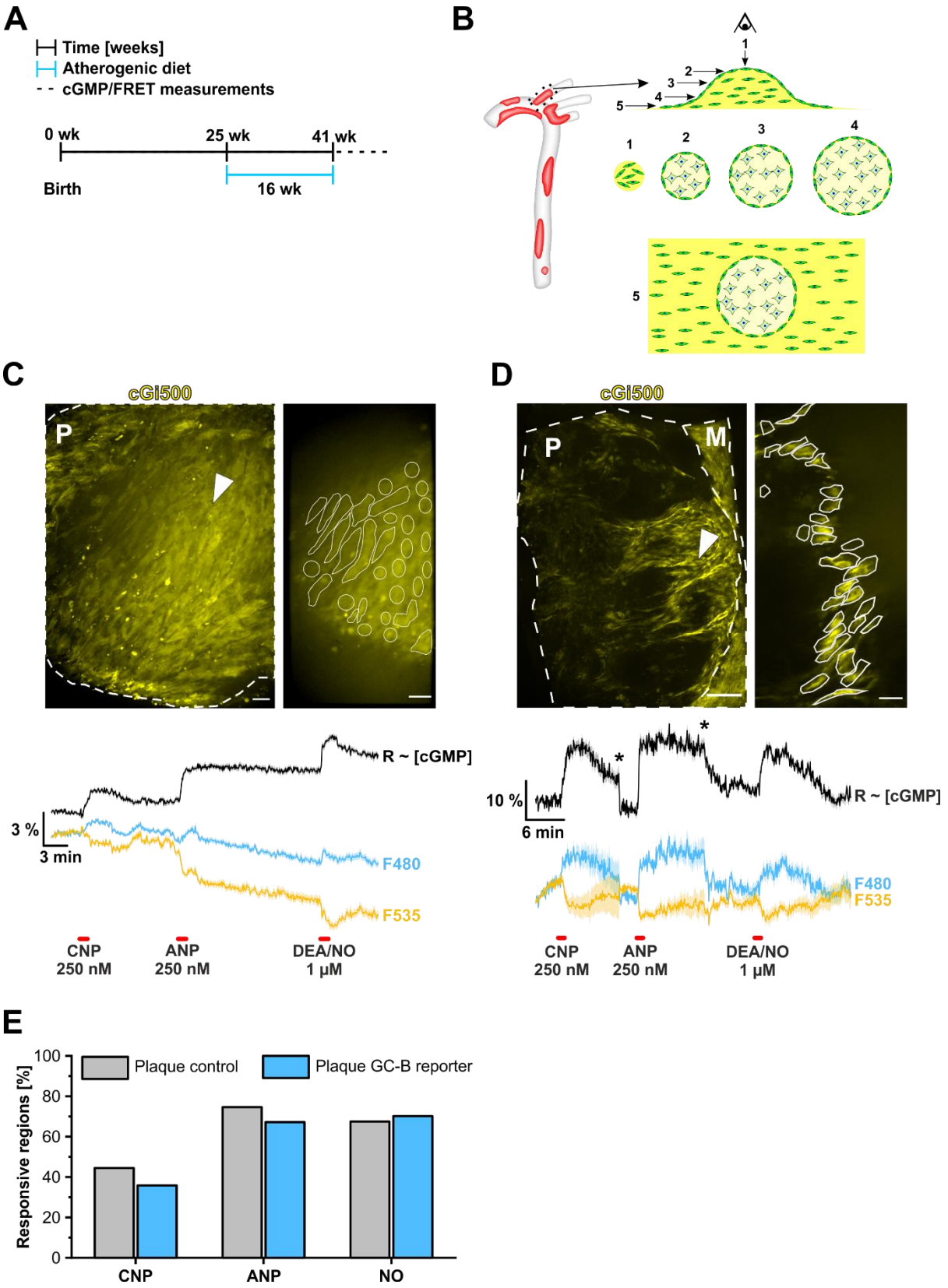

Figure 18: Atherosclerotic plaques show strong CNP-induced cGMP responses. *Atherosclerotic aortas were isolated from control (ApoE -/- x cGi(L1) +/L1 x GC-B +/+) and GC-B reporter (ApoE -/- x cGi(L1) +/L1 x GC-B +/LacZ) mice, opened longitudinally and cGMP/FRET measurements were performed with the plaque facing the objective. cGMP responses to ANP, CNP, and DEA/NO in individual plaques (presumably the fibrous cap) that were still attached to the medial layer were recorded. Plaques located in the entire aorta including the smaller arteries*

*parting from the aorta were analysed. **A**: Overview of the experimental procedure for cGMP/FRET measurements in atherosclerotic plaques. 25 weeks after birth, ApoE-deficient mice were fed an atherogenic diet for 16 weeks. Afterwards, mice were euthanised and the aorta was isolated for cGMP/FRET measurements. **B:** Schematic representation of atherosclerotic aortas / plaque structure. Left: Typical distribution of plaques within atherosclerotic aortas. Right: Schematic illustration of a plaque from a cGi500 expressing sensor mouse. The top part shows a plaque from the side. Arrows indicate the imaging planes that are shown below. 1-5: expected appearance of a plaque during a confocal cGMP/FRET measurement. Due to the high expansion of plaques along the z-axis only a "section" of a plaque could be measured. Spindle shaped cells indicate medial and fibrous cap VSMCs. Rhomboid shaped cells indicate core VSMCs. Extracellular matrix is shown in yellow. cGi500 expression is shown in green. **C-D:** Representative cGMP/FRET measurements of an atherosclerotic plaque from control (C) and GC-B reporter (D) mice. Top: Maximum intensity projection of the plaques that were measured (left) and image of the plaque during cGMP/FRET measurement (right). Sensor expressing cells were visualised by the YFP fluorescence (yellow) of cGi500. Dashed lines outline plaque (P) and media (M). The arrowhead indicates the region that was measured. Regions used for the analysis of cGMP responses were highlighted in the right images. Scale bars (C and D right image) are 25 µm. The scale bar in the left image (D) is 100 µm. Bottom: Development of cGMP levels over time in atherosclerotic plaques. An exemplary response pattern of regions that reacted to ANP, CNP, and DEA/NO is shown for control (C, mean of 14 regions) and GC-B LacZ reporter (D, mean of 7 regions) mice. Note that only ~22 % of regions that were analysed reacted to all three stimuli. Black: ratio traces (R ~ [cGMP]), cyan: CFP fluorescence, yellow: YFP fluorescence. The single traces (cyan/yellow) were applied to distinguish "real" cGMP/FRET signals from signals "feigned" by focus drift / tissue movement. SEM is indicated as a shadow behind the corresponding trace. The scale at the left indicates the percent change of the ratio trace and the single traces relative to their baseline ("ΔR/R" and "ΔF/F", respectively). Red horizontal lines indicate drug applications. **E:** Summary of cGMP responses to CNP (250 nM), ANP (250 nM), and/or DEA/NO (1 µM) in atherosclerotic plaques of control and GC-B reporter mice. Bars indicate fraction of cells (cumulated numbers, no mean) that reacted to ANP, CNP, and/or DEA/NO. Grey: control (126 regions, 9 measurements, 3 mice). Cyan: GC-B reporter (67 regions, 5 measurements, 3 mice).*

Plaques with a shallow curvature (**Figure 18 C**) allowed to measure a large part of the potential fibrous cap. Individual cells with various morphologies could be analysed in atherosclerotic plaques as indicated by non-circular ROIs (e.g. elongated cells [**Figure 18 C**], elongated and rounded cells [**Figure 18 D**]). Similar to measurements in healthy arteries, circular ROIs were placed in regions where individual cells could not be identified (e.g., circular ROIs in **Figure 18 C**). Some plaques showed no single elevation, but several hills and valleys (**Figure 18 D**). cGMP/FRET measurements of such plaques (**Figure 18 D**) could be performed at a deeper optical section. In general, only the outer cell layers (potential fibrous cap) but not the inside of atherosclerotic plaques (**Figure 18 C-D**, right images) could be detected with sufficient intensity to evaluate cGMP signalling.

cGMP signalling in the potential fibrous cap cells of atherosclerotic plaques was strikingly different from cGMP signalling in VSMCs of healthy arteries. In contrast to healthy arteries, robust cGMP responses were not only observed after application of ANP and/or NO, but also CNP potently increased cGMP in atherosclerotic plaques. While the cGMP response patterns were heterogeneous in general, regions with robust cGMP responses to all three stimuli (CNP, ANP and NO) were detected in plaques from both control (**Figure 18 C**; 14 out of 26 regions in this measurement) and GC-B reporter (**Figure 18 D**; 7 out of 18 regions in this measurement) mice. Around 22 % of all regions that could be analysed across all measurements responded to CNP, ANP and NO (**Supplementary table VII**). In general, focus drifts were more severe in measurements of atherosclerotic plaques than of healthy arteries. Therefore, we refer to regions instead of cells in these measurements as well. Focus drifts can affect cGMP/FRET signals (e.g., baseline drift of the cGMP ratio trace [**Figure 18 C**], return to baseline only after focus adjustment [**Figure 18 D**, asterisks]). Focus drifts can usually be identified by the lack of antiparallel trace separation of the CFP (F480) and YFP (F535) traces (e.g., between CNP and ANP application [**Figure 18 C**]) which is characteristic for cGMP-induced signals.

As already mentioned, no differences between plaques from control and GC-B reporter mice were detected that could not be explained by plaque heterogeneity or region placement. Furthermore, we detected no clear differences in cGMP response patterns between plaques that were based on the vessel part (e.g., aortic arch vs brachiocephalic artery) they originated from but the n-number of plaques per vessel region was low. Most regions showed responses to ANP (75 % [Ctrl] and 67 % [GC-B reporter]) and/or NO (67 % [Ctrl] and 70 % [GC-B reporter]). More than one third of all regions that could be analysed showed CNP-induced cGMP signals (44 % [Ctrl] and 36 % [GC-B reporter]). This considerable amount of CNP-induced cGMP responses in atherosclerotic plaques was strikingly different from cGMP generation in healthy arteries, which was almost exclusively generated by ANP and NO. The CNP-responsive regions reflected the behaviour of ANP~CNP cells and CNP-preferring cells in culture that showed strong responses to CNP. Due to movement artefacts the baseline could shift so strong that signal height could not be assessed reliably (see effect of focus adjustment in **Figure 18 D**). Therefore, it was not tried to distinguish ANP~CNP and CNP-preferring cells in plaques. Nonetheless, around 8 % of measured regions reacted to CNP but not to ANP (**Supplementary table VII**), reminding of cells with strong CNP preference.

Together, the experiments so far demonstrated that the findings with the cell culture model correlated with the *ex vivo* analysis of arteries under close-to-native conditions. Furthermore, NP-dependent cGMP signalling showed a previously unknown plasticity. While cGMP in contractile VSMCs was generated by ANP and/or NO, potential phenotypic modulation of VSMCs made these cells susceptible to CNP as also demonstrated *ex vivo* in the context of atherosclerosis.

3.3 Influence of GC-B-dependent cGMP signalling on atherosclerosis

Comparison of healthy and atherosclerotic vessels by cGMP/FRET measurements demonstrated that CNP-induced cGMP responses *ex vivo* were a unique feature of atherosclerotic plaques. Therefore, we sought to decipher the function of GC-B-dependent cGMP signalling in SMCs in atherosclerosis development. To do so, we used a genetic mouse model where functional GC-B expression could be ablated selectively in SMCs in a time-controlled manner. To allow identification of cells that express GC-B in these mice, we bred them with GC-B LacZ reporter mice (the same reporter as used in **Figure 11E**). Note that the resulting heterozygous knockin of the LacZ reporter into the GC-B gene locus did not affect cGMP signalling in atherosclerotic plaques in the previous experiments as shown by cGMP imaging (**Figure 18 D**).

SMC-selective GC-B knockout mice (Smko) and litter-matched controls (LacZ-ctrl, Cre-ctrl, Ctrl) were bred on an ApoE-deficient background. After development of atherosclerotic plaques, blood samples and other physiological parameters of the experimental mice were analysed to exclude indirect effects of GC-B ablation on atherosclerosis. The further experimental steps are illustrated in **Supplementary figure VII**.

3.3.1 SMC-selective deletion of GC-B successfully ablates GC-B in atherosclerotic aortas

SMC-selective ablation of GC-B in experimental mice was achieved with the Cre/loxP system (see section 1.5 for an explanation of Cre/loxP-dependent gene knockout) using αSMA-CreER^{T2}. The inducible CreER^{T2} allowed for time-controlled recombination. Herein, recombination in SMCs was induced via intraperitoneal injection of tamoxifen at 6 and 8 weeks of age (**Figure 19 A**, left). All experimental mice (including the controls) were treated with tamoxifen to exclude effects of this partial oestrogen agonist as confounding factor. From 8 weeks of age on, mice were fed an atherogenic

diet for 18 weeks to accelerate the development of atherosclerotic plaques. At the age of 26 weeks, mice were sacrificed, physiological parameters were assessed, and atherosclerotic aortas were subjected to further analysis (see **Supplementary figure VII** for a schematic overview). The short name and complete genotype of the SMC-selective knockout and the three different types of control animals are listed in **Figure 19 A** (right).

Smko and LacZ-ctrl mice expressed β-galactosidase under control of the GC-B promoter. Hence, cells of these mice that expressed GC-B (LacZ-ctrl mice) or would have expressed GC-B (Smko mice) could be identified by their blue-coloured nuclei (X-gal+ cells) after X-gal staining. We will use the term "potentially CNP-responsive cells" when referring to the function of X-gal+ cells detected in Smko or LacZ-ctrl mice.

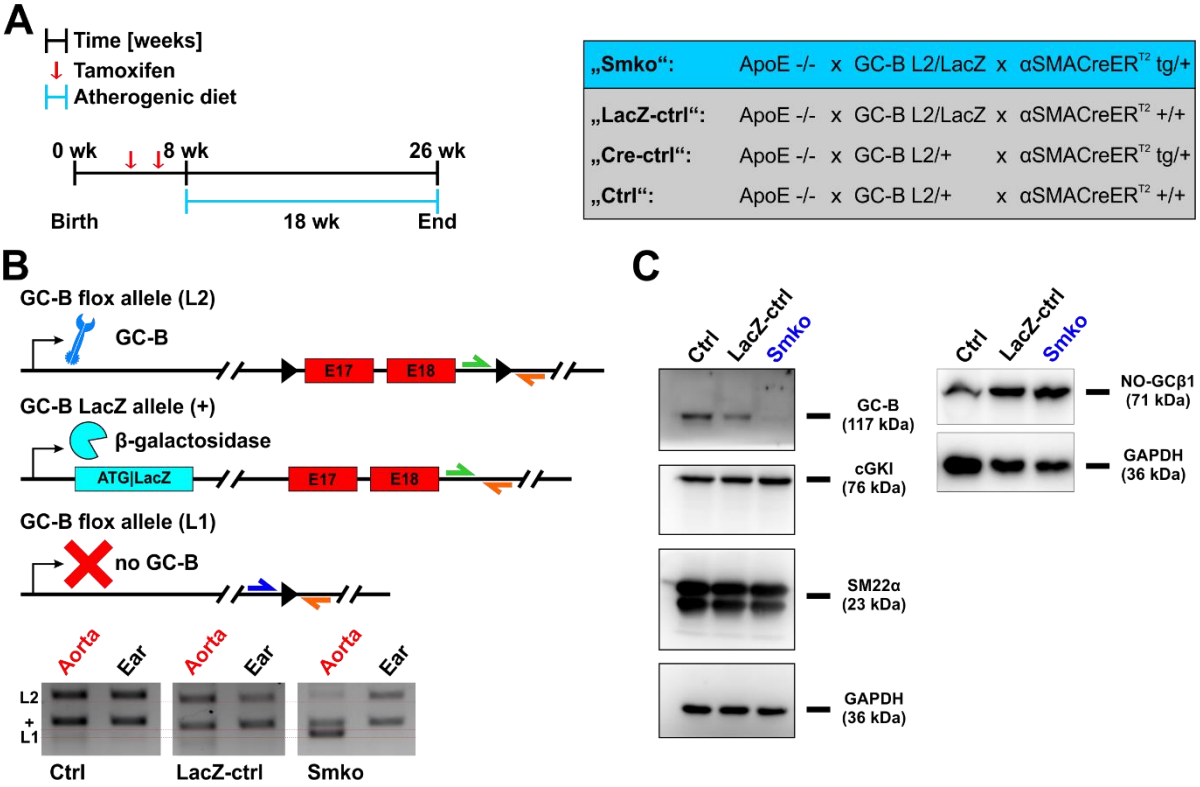

Figure 19: GC-B is expressed in atherosclerotic aorta and efficiently deleted by a SMC-selective knockout. *SMC-selective GC-B knockout and control mice were bred on an ApoE-deficient background to assess the effect of GC-B dependent cGMP signalling in VSMCs on atherosclerosis development. After induction of atherosclerosis by an atherogenic diet, the SMC-selective knockout was verified by PCR (B) and western blotting (C).* ***A****: Overview of the experimental procedure to generate atherosclerotic, SMC-selective knockout mice (left) and genotype of knockout (cyan) and control (grey) mice (right). Tamoxifen was injected for five consecutive days at 4 and 6 weeks of age. 8 weeks after birth, ApoE-deficient mice were fed an atherogenic diet for 18 weeks. Afterwards, mice were euthanised and the aorta was isolated for further analysis.* ***B:*** *Verification of SMC-selective GC-B ablation by PCR. Aortas and ears were taken at the day of experiment (tamoxifen induced, atherosclerotic). Two mice per genotype were used (only one PCR per genotype is shown) Top: Schematic representation of the different GC-B alleles of experimental mice before (top, "L2") and after Cre-dependent recombination (bottom, "L1"). The LacZ reporter gene replaces the first exon of the GC-B gene. Exons 17 and 18 of GC-B flox mice are flanked by loxP sites (triangle). Primer binding sites responsible for the L1, +, and L2 band in the PCR shown below are indicated by blue, orange, and green arrows. The expected gene product is indicated above. This PCR could distinguish WT (+), non-recombined (L2) and recombined (L1 = knockout) alleles. Please note that the GC-B LacZ transgene (= knockout) was detected as WT (+) allele in this PCR. Bottom: PCR used for detection of the recombined GC-B flox allele. The identity of bands is indicated at the left, the genotype at the bottom (see A for complete genotype) and the lysates at the top. The red line is located below the expected position of the indicated band. Ear lysates served as control*

*to exclude off-target recombination **C:** Verification of GC-B ablation in aortas/atherosclerotic plaques by western blotting. Lesion rich parts of atherosclerotic aortas were used to prepare protein lysates. Two aortas per genotype were pooled to increase protein concentration Applied antibodies and expected molecular weight of the respective target protein are indicated at the right. GAPDH was used as loading control. 14 µg protein (left) and 25 µg protein (right) were loaded per lane.*

First, the SMC-selective knockout of GC-B was verified at the genomic and protein level. Smko mice carried a GC-B LacZ allele and a GC-B flox (L2) allele. As no functional GC-B can be transcribed from the GC-B LacZ allele, a SMC-selective knockout of GC-B could be achieved by Cre-dependent recombination (= inactivation) of the GC-B flox allele in SMCs (see **Figure 7 A** for a detailed explanation). Therefore, we analysed the recombination state of the GC-B flox allele in Smko and control mice by a specialised genotyping PCR (**Figure 19 B**, top). This PCR allowed to distinguish if no loxP site (wild type / GC-B LacZ allele), one loxP site (excision of exons 17 and 18 = inactivation of GC-B) or two loxP sites (no recombination) were present at the DNA level. To verify tissue selectivity of recombination, we simultaneously analysed DNA of atherosclerotic aortas (high SMC content) and of ear biopsies (low SMC content) that were taken at the day of experiment (**Figure 19 B**, bottom). Neither aorta nor ear lysates of LacZ-ctrl and Ctrl mice, both of which lack the αSMA-CreER^{T2} transgene, showed recombination of the GC-B flox allele. This showed that there was no recombination in the absence of αSMA-CreER^{T2}. In contrast, the aorta lysate of the Smko mouse clearly showed recombination of the GC-B flox allele (L1, 448 base pairs, “bp”) and a DNA fragment derived from the GC-B LacZ allele (+, 506 bp). The ear lysate, in contrast, showed no recombination, and its band pattern matched the one from LacZ-ctrl lysates, confirming that the GC-B flox allele was not globally recombined. In addition to the recombined L1 band, the aorta lysate from Smko mice showed a weak band for the non-recombined GC-B flox allele (L2, 684 bp). As aorta also contains other cells like endothelial cells, no complete recombination was expected. In sum, the PCR results indicated a successful SMC-selective knockout of the GC-B gene in Smko mice at the DNA level.

We continued to use western blotting to assess whether GC-B was also absent at the protein level in plaque-rich lysates from Smko mice (**Figure 19 C**). Expression of GC-B was clearly detected in lysates of atherosclerotic aortas from Ctrl and LacZ-ctrl mice, but undetectable in lysates from Smko mice. cGKI and the NO-GC β1 subunit were similarly expressed in aortic lysates of all three groups. The presence of SMCs in these lysates was verified by detection of SM22α, which was detected as a double band. Note that no biological replicates of these western blots were possible due to limitations of available mice. Therefore, conclusions based on differences in band intensities should be drawn carefully.

Several physiological parameters that could influence the development of atherosclerosis were analysed to check whether these were affected by the SMC-selective ablation of GC-B (**Table 6**). Parameters from the three control groups were pooled. None of the analysed parameters were significantly different between Smko and control mice of the same sex. Sex in contrast had an impact on several of these parameters. Plasma cholesterol and LDL in female mice was significantly lower than in male mice of the same group. Also, the heart-to-body weight ratio of female control mice was significantly lower than of male control mice.

Table 6: Physiological parameters of 26-week-old atherosclerotic Smko and control mice after 18 weeks atherogenic diet. *Mice were starved overnight, anesthetised, weight, and blood samples were drawn. Controls: values from Cre-ctrl, LacZ-ctrl, and Ctrl mice were pooled. Data are represented as mean ± SEM. Statistical significance vs sex is indicated by hashes (# p<.05; ## p<.01; ### p<.001). There were no statistically significant differences between genotypes. HDL: high-density lipoprotein, LDL: low-density lipoprotein. Blood samples were analysed by Prof. Dr. med. Andreas Peter in the "Zentrallabor des Universitätsklinikums Tübingen".*

	Male		Female	
Parameter	**Controls**	**Smko**	**Controls**	**Smko**
	(n = 9)	*(n = 4)*	*(n = 16)*	*(n = 5)*
Total cholesterol [mg/dL]	1263 ± 91	1269 ± 38	778 ± 64$^{###}$	842 ± 75$^{##}$
Triglyceride [mg/dL]	79 ± 10	95 ± 25	84 ± 9	85 ± 24
HDL [mg/dL]	10 ± 1	13 ± 1	9 ± 1	9 ± 2
LDL [mg/dL]	291 ± 40	289 ± 16	155 ± 16$^{##}$	143 ± 23$^{##}$
	(n = 9)	*(n = 4)*	*(n = 16)*	*(n = 6)*
Body weight [g]	35.5 ± 1.5	34.5 ± 0.9	26.3 ± 0.7$^{###}$	23.4 ± 0.8$^{###}$
Heart-to-body weight [mg/g]	7.9 ± 0.2	6.9 ± 0.6	6.8 ± 0.2$^{#}$	7.0 ± 0.3
Kidney-to-body weight [mg/g]	16.2 ± 0.8	17.4 ± 1.1	15.1 ± 0.5	14.3 ± 1.3

Together, these results demonstrated that in Smko mice GC-B was successfully ablated in atherosclerotic tissue without affecting physiological parameters relevant in atherosclerosis.

3.3.2 Total lesion area after 18 weeks atherogenic diet is not affected by SMC-selective ablation of GC-B

To assess whether SMC-selective ablation of GC-B influenced the progression of atherosclerosis, we compared the lesion area of atherosclerotic aortas from Smko and control mice (**Figure 20**). Aortas were stained with Oil Red O to visualise atherosclerotic plaques along the vessel wall and documented from both sides. The lesion area was quantified computationally and normalised to the total vessel area. Lesion area in atheroprone regions (i.e., aortic arch) was quantified separately from the remaining aorta (thoracic/abdominal part) to account for potential differences in plaque development.

As physiological parameters of female and male mice showed significant differences (**Table 6**), lesion area was also evaluated as a function of sex. After Oil Red O staining, plaques could be clearly distinguished from the lesion-free vessel wall by their intense red colour (**Figure 20 A**). Light orange / yellow staining was not included in the analysis of lesion area (e.g., some patches in the bottom part of the female control aorta). No striking differences in lesion area were apparent in these sample images. Large parts of the aortic arch were covered by few but extended plaques. Around 50-55 % of the aortic arch was covered by plaques on average (**Figure 20 B**, top panel, male Controls: 49.7 ± 4.1 %, male Smko: 54.1 ± 2.4 %, female Controls: 54.6 ± 1.9 %, female Smko: 54.5 ± 2.3 %). No statistically significant differences were detected between any of the 4 groups. In the thoracic/abdominal aorta more, but smaller plaques were found which were often located at and protruding into branching vessels (**Figure 20 A**). In total, a smaller fraction of the vessel wall (around 11-16 %) of the thoracic/abdominal aorta was covered by plaques (**Figure 20 B**, bottom panel, male Controls: 13.0 ± 2.4 %, male Smko: 11.8 ± 3.6 %, female Controls: 15.7 ± 2.2 %, female Smko: 11.4 ± 6.7 %), much less than in the aortic arch. Again, no statistically significant differences in the relative lesion area were detected.

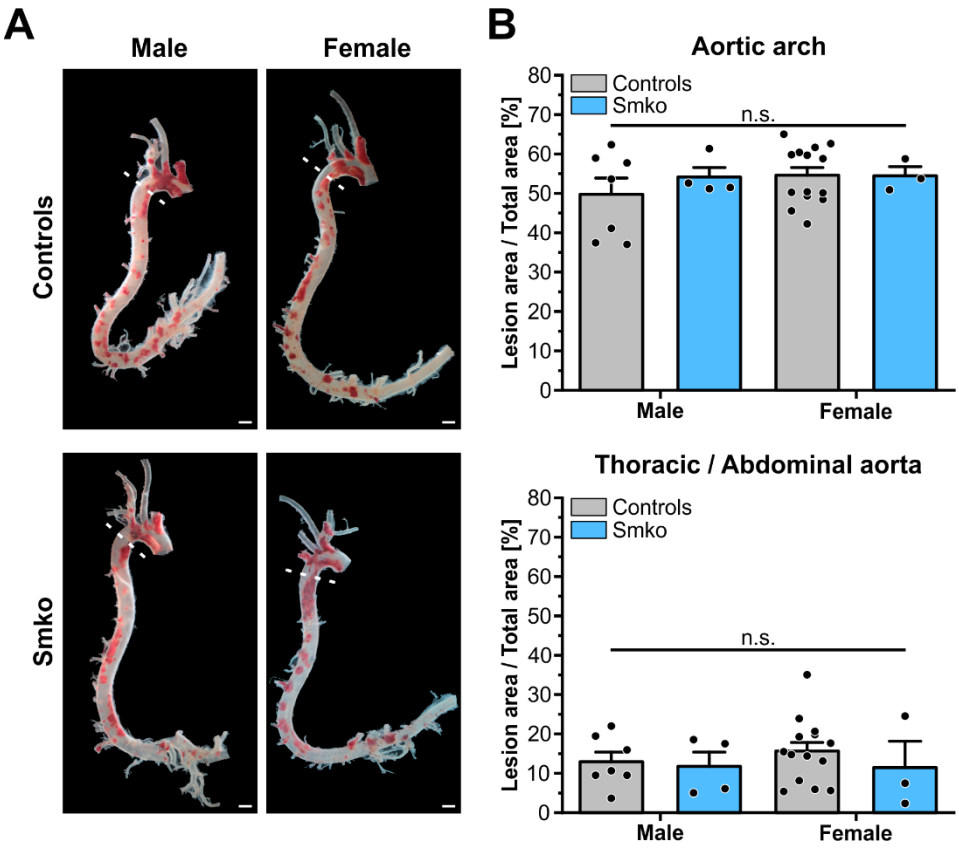

Figure 20: Lesion area after 18 weeks atherogenic diet is not different between Smko and control mice. *SMC-selective GC-B knockout (Smko) and control (LacZ-ctrl, Cre-ctrl, Ctrl) mice were bred on an ApoE-deficient background to assess the effect of GC-B-dependent cGMP signalling in VSMCs on lesion area. After SMC-selective GC-B ablation by tamoxifen injection, mice were fed an atherogenic diet for 18 weeks and lesion area was assessed by Oil Red O staining.* ***A:*** *Representative images of atherosclerotic aortas of Smko and control mice after Oil Red O staining. Sex is indicated at the top, the genotype at the left. Atherosclerotic lesions appeared red. Dashed lines indicate the transition from arch to thoracic/abdominal aorta. Scale bars are 1 mm.* ***B:*** *Relative lesion area of the aortic arch (top) or thoracic/abdominal aorta (bottom) from Smko and control mice (data from LacZ-ctrl, Cre-ctrl and Ctrl mice were pooled). Lesion area was determined from both sides of the aorta, summed, and normalised to the total area of the aorta. Each dot represents an aorta. Data are represented as mean + SEM. No statistically significant differences (sex or genotype) were found. n.s.: not significant. Controls male: 7 mice; Smko male: 4 mice; Controls female: 14 mice; Smko female: 3 mice.*

Overall, the Oil Red O staining showed the typical atherosclerotic plaque development in ApoE-deficient mice (**Figure 6**) which accumulate plaques mainly in the aortic arch and at branching points. Neither genotype-dependent (Smko vs. controls) nor sex-dependent (male vs. female) differences in lesion area were found in the aortic arch and thoracic/abdominal aorta.

3.3.3 Composition of atherosclerotic plaques is altered in SMC-selective GC-B-deficient mice

After analysing atherosclerosis progression in terms of lesion area, we took a closer look at the composition of plaques in the aortic arch (and branching vessels). First, we compared the distribution of GC-B LacZ reporter (X-gal+) cells between Smko and LacZ-ctrl mice. The other control groups (Cre-ctrl and Ctrl, see **Figure 19 A** for exact genotype) were not included in these evaluations as they did not have the reporter transgene GC-B LacZ. Therefore, we pooled data of male and female mice to allow for higher n-numbers and meaningful statistical evaluation. It is likely that X-gal+ cells in atherosclerotic aortas of these mice were modulated VSMCs (see section **4.3** for a detailed explanation).

Paraffin sections of the aortic arch (and branching vessels) were prepared and X-gal+ cells were separately quantified in plaque and media of all sections (**Figure 21**). X-gal+ cells were found in sections from Smko and LacZ-ctrl mice (**Figure 21 A**). Plaques from mice with different genotypes (e.g., **Figure 21 A**, bottom left and top right) were sometimes more similar than plaques of the same group (see sample images of Smko mice). A trend for plaques with an increased number of X-gal+ cells was observed in Smko as compared to LacZ-ctrl mice.

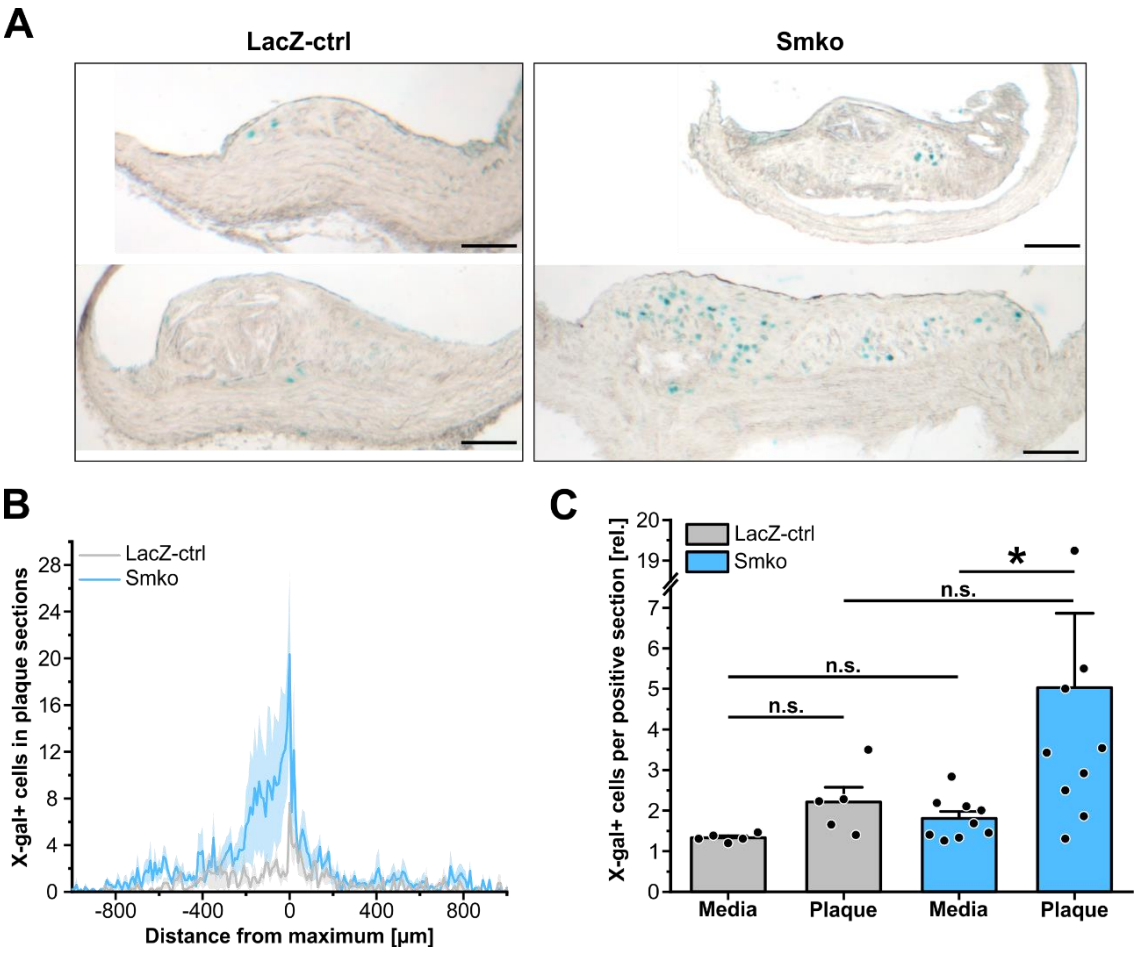

Figure 21: Atherosclerotic plaques of Smko mice show an increased number of X-gal+ cells. *SMC-selective GC-B knockout (Smko) and control (LacZ-ctrl) mice were bred on an ApoE-deficient background to assess the effect of GC-B-dependent cGMP signalling in VSMCs on abundance of (potentially) CNP-responsive cells. After SMC-selective GC-B ablation by tamoxifen injection, mice were fed an atherogenic diet for 18 weeks and GC-B LacZ reporter positive (X-gal+) cells were visualised via X-gal staining. X-gal+ cells within plaque or media (counted separately) were quantified per section (10 µm) of the aortic arch.* ***A:*** *Representative images of sections from atherosclerotic plaques in the aortic arch of Smko and control mice after X-gal staining. Genotype is indicated at the top. Two images per genotype are shown to emphasize the heterogeneous distribution of X-gal+ cells between sections. X-gal+ cells appeared as blue dots (nuclear staining). Scale bars are 100 µm.* ***B:*** *Distribution of X-gal+ cells in plaques of the aortic arch ("plaque profile"). The X-gal+ cells in the plaque area were counted in consecutive sections of the aortic arch. The section with most X-gal+ cells was chosen as reference (0 position) and the number of X-gal+ cells in every section was plotted according to the distance from the reference section (e.g., -200 µm means the section that is located 200 µm in front of the reference section). The line indicates the mean profile of the corresponding genotype. SEM is represented by a shadow of the same colour.* ***C:*** *Enrichment of X-gal+ cells in media and plaques of Smko and LacZ-ctrl mice. The total number of X-gal+ cells in plaque and media across all sections of the aortic arch was determined and divided by the number of sections that contained at least one X-gal+ cell. Each dot represents an aortic arch. Data are represented as mean + SEM. Statistical significance is indicated by asterisks (* p<.05). n.s.: not significant. Smko: 9 mice; LacZ-ctrl: 5 mice. 136-404 sections per mouse were analysed.*

Interestingly, most X-gal+ cells accumulated in the plaque core and only few were found in the cap region (e.g., left cell in upper control or cells at the right in lower Smko plaque). Furthermore, although cells were sometimes distributed across the complete plaque section (lower plaques), they often appeared as clusters (e.g., **Figure 21 A**, top right plaque). In general, there was a huge heterogeneity concerning the number of X-gal+ cells in individual plaque sections. This heterogeneity was not only observed between sections of LacZ-ctrl and Smko mice but also between sections of the same genotype or even mouse (**Figure 21 A**).

To analyse this distribution of X-gal+ cells in more detail, plaque profiles were created. Therefore, the number of X-gal+ cells within plaques was documented along with their position in the aortic arch (and branching vessels). For better comparability, all profiles were aligned to the plaque section with most X-gal+ cells, so that for every mouse the most enriched plaque section was at the same position (± 0 µm). These plaque profiles confirmed that X-gal+ cells strongly accumulated in one specific region (most cells were found between -400 µm and +200 µm relative to the section with the maximal number of X-gal+ cells, **Figure 21 B**). As already indicated with the sample images (**Figure 21 A**), there was a trend for more X-gal+ cells in plaques from Smko mice. The large SEM of these curves reflects the strong variation that was found between mice of the same genotype. Outside of the 600 µm range mentioned above, only few X-gal+ cells were found in sections of control mice. The profile of Smko mice, in contrast, showed an additional elevation between -800 µm and -400 µm. All in all, there was a trend for more X-gal+ cells which were distributed across a wider range in plaques from Smko mice as compared to LacZ-ctrl mice (**Figure 21 B**).

To confirm this trend (more X-gal+ cells in plaques from Smko mice), the number of X-gal+ cells in plaque and media sections was determined and normalised to the number of sections (**Figure 21 C**). Only sections with at least one X-gal+ cell were included in these calculations (see section **2.4.5.7** for details). Note, that X-gal+ cells were summed up across all plaques of a given section and the media of the complete vessel wall. As already indicated by the plaque profiles, plaques of Smko mice showed a strong trend for more X-gal+ cells compared to plaques of LacZ-ctrl mice (Smko plaque: 5.0 ± 1.8 vs. LacZ-ctrl plaque: 2.2 ± 0.4 X-gal+ cells/positive section, not significant, **Figure 21 C**). Interestingly, within Smko mice, plaques contained significantly more X-gal+ cells (modulated VSMCs) than the media. The same trend was also present in LacZ-ctrl mice but did not reach statistical significance. In general, the number of X-gal+ cells per positive section varied stronger between plaques of Smko mice than between plaques of the LacZ-ctrl group (**Figure 21 C**). Both groups contained plaques with few X-gal+ cells whereas a high number of X-gal+ cells was only detected in plaques of Smko mice. Note that plaques with a low number of X-gal+ cells on average could contain individual sections that were rich in X-gal+ cells. Nonetheless, the number of potentially CNP-responsive cells (X-gal+) in plaque sections of either group was lower than the 36 % of regions with CNP-induced cGMP responses that we detected in our cGMP/FRET measurements of atherosclerotic plaques from GC-B LacZ reporter mice (see section **3.2.2** and **Figure 18 E**). This finding matched the results of our cell culture measurements, where the fraction of X-gal+ cells in culture was lower than the fraction of CNP-preferring cells usually detected in primary VSMC cultures (see **Figure 11 E** and **Supplementary figure VI B**).

Based on these experiments, it appears that SMC-selective ablation of GC-B promoted the enrichment of plaques with potentially CNP-responsive cells (= modulated/transdifferentiated VSMCs), pointing towards an inhibitory effect of GC-B-dependent cGMP signalling on phenotypic modulation/ transdifferentiation of VSMCs during plaque development.

Next, we analysed how the SMC-selective ablation of GC-B affected the expression of αSMA as a marker for VSMCs of the fibrous cap, and therefore plaque stability of atherosclerotic lesions (**Figure 22**). Smooth muscle-rich fibrous caps were shown to stabilise atherosclerotic plaques [207; 234; 319].

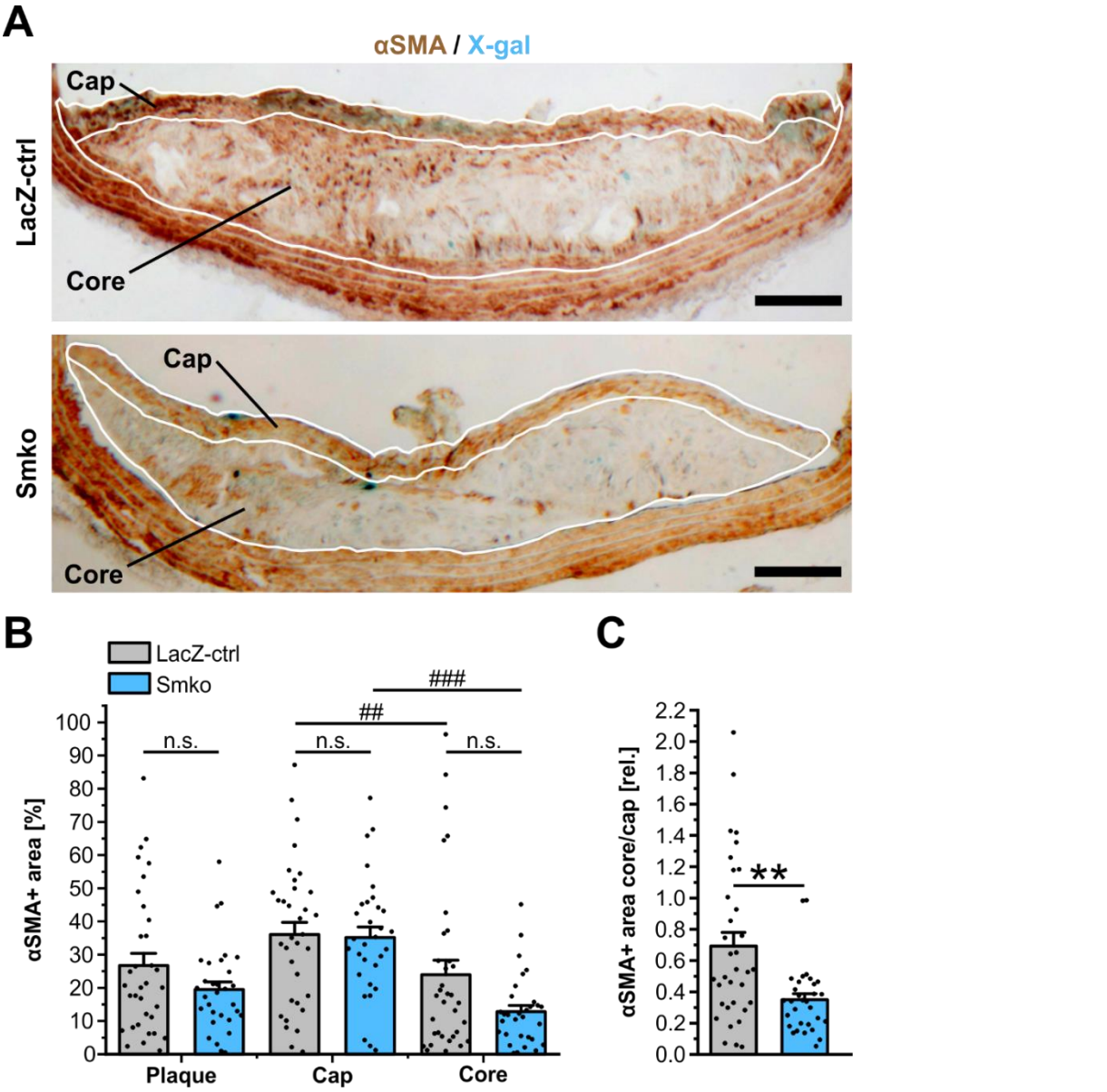

Figure 22: Atherosclerotic plaques of Smko mice exhibit an altered distribution of αSMA. *SMC-selective knockout (Smko) and control (LacZ-ctrl) mice were bred on an ApoE-deficient background to assess the effect of GC-B-dependent cGMP signalling in VSMCs on αSMA expression in atherosclerotic plaques. After SMC-selective GC-B ablation by tamoxifen injection, mice were fed an atherogenic diet for 18 weeks and sections of the aortic arch were prepared. Consecutive sections were stained for αSMA (contractile SMC marker), and the stained area was quantified.* ***A:*** *Exemplary images of IHC stainings for αSMA in plaque sections from LacZ-ctrl and Smko mice. Genotype is indicated at the left. 30 µm cap area and core (non-cap region of the plaque) are outlined by a white line. αSMA+ area appeared brown. Blue staining indicated nuclei of GC-B LacZ reporter (X-gal+) cells. Scale bars are 100 µm.* ***B:*** *Quantification of αSMA+ area (% of total area) of the plaque ("Plaque"), the cap ("Cap") and the core ("Core") region of plaques from control (LacZ-ctrl) and Smko mice.* ***C:*** *Core-to-cap distribution of αSMA in plaques from control (LacZ-ctrl) and Smko mice. Distribution was calculated as αSMA+ area in the core [%] divided by αSMA+ area in the cap [%]. Each dot represents an individual plaque. Data is represented as mean + SEM. Statistical significance vs genotype is indicated by asterisks (** p<.01, n.s.: not significant). Statistical significance between regions is indicated by hashes (## p<.01, ### p<.001). Smko: 31 plaques from 6 mice; LacZ-ctrl: 34 plaques from 6 mice.*

As suggested by Shankman et al. in 2015 [239], the 30 µm luminal part of a plaque was used as "cap region" for analysis purposes. A reduction of αSMA+ area in the cap region of a plaque can indicate plaque destabilisation. In addition, less αSMA+ area in atherosclerotic plaques could indicate an enrichment of plaques with strongly modulated/transdifferentiated VSMCs (CNP-responsive, αSMA low). Therefore, we quantified the αSMA+ area in atherosclerotic plaques and compared its distribution between the 30 µm cap region and the core region. The 30 µm cap region often covered the complete αSMA+ area at the luminal side (e.g., **Figure 22 A**, lower image). For reasons of comparability, the same groups as in **Figure 21** (LacZ-ctrl and Smko mice) were analysed for αSMA expression in plaque sections of the aortic arch (and branching vessels). Several plaques of each mouse were included in the analysis.

Overall, the αSMA staining of plaques from LacZ-ctrl and Smko mice showed the expected characteristics for atherosclerotic plaques (**Figure 22 A**). Most plaques were covered by an αSMA-rich fibrous cap, while less αSMA was found in the core region (**Figure 22 A**). In general, we observed a strong heterogeneity in αSMA staining between plaques of the same group (see **Figure 22 B**). Still, the atherosclerotic plaques that are depicted in **Figure 22 A** showed several characteristics frequently (but not exclusively) found in each group. For orientation, the plaque border and the cap area were indicated in each image. αSMA was highly expressed in the media, at the border between plaque and media (see section **2.4.5.8** for definition) and at the luminal side of the plaques (fibrous cap). As mentioned above, the 30 µm cap area was often (lower image) but not always (upper image) a good approximation. As shown in the control image (LacZ-ctrl), in some plaques the αSMA+ layer that is characteristic for the fibrous cap, extended further into the plaque. The plaque core could also contain patches of αSMA+ cells. The accumulation of αSMA in the cap and exclusion from the core was more prominent in Smko than in LacZ-ctrl plaques. These observations were verified by computational quantification of the αSMA+ area (**Figure 22 B-C**). αSMA+ cells contributed more to the cap region than to the core of plaques in LacZ-ctrl (36 ± 4 % [cap] vs. 24 ± 4 % [core], $p<.01$) and Smko (35 ± 3 % [cap] vs. 13 ± 2 % [core], $p<.001$, **Figure 22 B**) mice. No statistically significant differences in the αSMA+ area of the entire plaque, cap, or core region between LacZ-ctrl and Smko mice were detected. Nonetheless, there was an interesting trend towards less αSMA+ area in plaques from Smko mice (27 ± 4 % [LacZ-ctrl] vs. 19 ± 2 % [Smko], $p>.34$). This trend for less αSMA+ area was also visible specifically in the core region of plaques from Smko mice (24 ± 4 % [LacZ-ctrl] vs. 13 ± 2 % [Smko], $p>.11$). The reduced αSMA content in the core region was significant, when normalised to the αSMA content in the cap region of each individual plaque section (**Figure 22 C**, 0.69 ± 0.09 rel. [LacZ-ctrl] vs. 0.34 ± 0.04 rel. [Smko], $p<.01$). The observation, that less αSMA was present in the core of Smko plaques, could indicate more modulated/transdifferentiated VSMCs (αSMA low) in these plaques.

While SMC-selective ablation of GC-B did not impact the progression of atherosclerosis in terms of total lesion area, cGMP signalling via GC-B in VSMCs seemed to modulate the structure of plaques. We could identify a trend in plaques from Smko mice to accumulate more X-gal+ cells than plaques from control mice, with significantly more X-gal+ cells in the plaque as compared to the media (**Figure 21 C**). Hence, silencing CNP signalling in VSMCs by ablation of its receptor led to an increased fraction of potentially modulated/transdifferentiated VSMCs in the plaque core. Indeed, this was accompanied by a decreased αSMA+ area in the core of Smko plaques as compared to control plaques.

4 Discussion

4.1 cGMP signalling in cultured VSMCs

VSMC plasticity describes the ability of VSMCs to adapt to different situations by changes of their phenotype. In their contractile phenotype, VSMCs regulate blood flow by contraction and relaxation. In their modulated phenotype, they participate in vascular development, repair and disease-associated vascular remodelling [144; 320]. While this phenotypic plasticity of VSMCs is beneficial for physiological processes, it is also involved in the development of vascular diseases like atherosclerosis and restenosis (see section **1.3.2**). Many studies investigated how the phenotypic modulation of VSMCs could be controlled as this would allow to influence the outcome of these deadly vascular diseases [54; 321]. A suitable model that reflects several aspects of phenotypic modulation as observed *in vivo*, are SMC cultures. Already in primary culture VSMCs gradually change from a contractile, "healthy" phenotype to a modulated, disease-associated phenotype, a process where cGMP signalling might be involved [54].

4.1.1 VSMC cultures show phenotype-dependent heterogeneity of cGMP signalling pathways

Primary and passaged VSMCs generate cGMP upon stimulation with ANP, CNP, and/or NO [17; 102]. To our knowledge, all studies so far investigated cGMP generation upon application of ANP, CNP, or NO in VSMC cultures at the population and not at the single-cell level. Therefore, it remained unclear whether the same VSMC could respond to different stimuli or diverse VSMCs responded to just one of these stimuli. To clarify this issue, we compared for the first time the potential of VSMCs to generate cGMP upon stimulation with ANP, CNP, and NO within the same cell in a phenotype-specific context. Thereby, we discovered an unprecedented heterogeneity of cGMP signalling pathways in primary VSMCs. One type of VSMCs reacted primarily to **ANP** and NO, whereas another type of VSMCs reacted primarily to **CNP** and NO. By analysis of marker protein expression and lineage tracing, we could identify the former type of VSMCs as contractile VSMCs and the latter as modulated VSMCs (see below). In addition, we identified VSMCs that showed robust responses to ANP, CNP, and NO, potentially belonging to cells with an intermediate phenotype (neither fully contractile, nor fully modulated).

The in-cell comparison of the responsiveness to different cGMP-stimulating agents required a technique that allowed to measure cGMP repetitively in a non-destructive way at single-cell resolution. Furthermore, it had to be possible to subsequently identify the phenotype of measured cells (e.g., by detection of marker proteins). Therefore, we combined FRET-based cGMP measurements with subsequent IF stainings (to our knowledge for the first time). An important question was about the appropriate concentrations of ANP, CNP, and DEA/NO (fast NO-releasing compound). There are several studies addressing the question of physiological ANP/CNP concentrations in blood and tissues [72; 98]. There are various sources of CNP and different processes that affect its synthesis (e.g., inflammation, shear stress) [72] which make it difficult to determine the exact concentration present at SMCs within the vessel wall at a given time. Therefore, we decided to compare the potential of VSMCs to generate cGMP by applying receptor-saturating concentrations (50 nM) of ANP and CNP. To verify receptor saturation and to test the robustness of NP preference, we additionally applied a five-times higher concentration of both peptides (250 nM). To distinguish receptor from sensor saturation, we applied 500 nM DEA/NO which was expected to generate sensor-saturating concentrations of cGMP. Indeed, the chosen NP concentrations seemed to be receptor-saturating in many cases. This could be deduced from comparison of NO- and NP-induced cGMP signals within the same cell (**Figure 10 A**, **Figure 11 A**).

In cells where DEA/NO generated higher cGMP levels than the NPs, whilst stimulation with increasing concentrations of the same NP (e.g., 50 nM ANP vs. 250 nM ANP) did not lead to higher cGMP levels, the NP concentration was receptor-saturating. Interestingly, the second stimulus (high concentration) with the same NP frequently elicited a weaker, instead of a similar, cGMP response (**Figure 10 A**, **Figure 11 A**). The reduced second responses upon NP stimulation were probably the result of two independent negative feedback mechanisms. Upon stimulation with their respective ligand, the activity of GC-A and GC-B can be downregulated by dephosphorylation of the receptors [90; 91]. Furthermore, elevated cGMP levels increase the activity of PDE 5 [16], the main cGMP-degrading PDE in VSMCs [17].

In culture, phenotypic modulation of primary VSMCs from a contractile to a modulated phenotype gets apparent in less than a week [148; 189]. To compare cGMP signals in phenotypically diverse VSMCs, we decided to investigate cultures between days 5 and 7, when both, contractile and modulated VSMCs were expected to be present. The morphology of cultured VSMCs could provide a first indication about their phenotype [151]. In culture, an elongated, spindle-shaped morphology was reported for contractile VSMCs and a less elongated, more roundish one ("rhomboid") for modulated VSMCs [148; 151; 191]. As expected, we found both morphologies in our VSMC cultures (e.g., **Figure 10**, **Figure 11**, **Figure 13**). The different morphologies of VSMCs correlated with diverse cGMP response patterns. Rather elongated VSMCs reacted strongly to ANP and NO but only weakly, if at all, to CNP. The contractile phenotype of these ANP-preferring cells was verified by the high expression of αSMA and SM22α. Rather rounded cells reacted strongly to CNP and NO but only weakly, if at all, to ANP. The morphology of these CNP-preferring cells in combination with the low expression of contractile marker proteins indicated a modulated phenotype. A third group of cells reacted to ANP, CNP, and NO, but without a clear preference for ANP or CNP (ANP~CNP). It is unclear whether cells of this category started but not finished phenotypic modulation towards the modulated phenotype (transition state between ANP and CNP preference), or whether these cells represented an own subtype of VSMCs. Across all cultures from cGi(L1) mice that were grown under standard conditions (e.g., primary VSMCs, 12-24 h serum starvation) we found that **42 %** of analysed cells were ANP-preferring/contractile VSMCs, **37 %** CNP-preferring/modulated VSMCs, and **21 %** ANP~CNP VSMCs (**Supplementary figure VI**). Some cells did neither respond to ANP, nor to CNP, nor to NO. As it was unclear whether these cells lacked any GCs, were dead or the low signal -to-noise ratio concealed cGMP signals, they were excluded from analysis. These findings were obtained with cultures from sensor mice that expressed the cGMP biosensor cGi500 globally and reproduced in cultures with SMC-selective sensor expression (**Figure 11**).

Besides the strong phenotype-dependent changes in NP-dependent cGMP signalling, we observed minor changes in NO-dependent cGMP signalling as well (**Figure 14**). On average, NO induced weaker cGMP signals than CNP in CNP-preferring cells. In ANP-preferring cells, in contrast, NO was the most potent cGMP elevating stimulus. This statistically significant higher potential of NO to induce cGMP signals in ANP-preferring cells (**Figure 14 B**) was associated with increased levels of NO-GC β1-subunit in these cells, compared to CNP-preferring cells (**Figure 14 A**). With our approach we could not distinguish between general and isoform-specific downregulation of NO-GC. Therefore, the reduced expression of the β1-subunit in CNP-preferring cells might reflect the loss/downregulation of a single isoform or reflect a general downregulation of NO-GC [6]. Whether the reduced expression of NO-GC in modulated/CNP-preferring VSMCs in comparison to ANP-preferring VSMCs has a functional

relevance (e.g., increased threshold concentration for NO to elicit functionally relevant cGMP signals in modulated VSMCs), remains to be elucidated.

The phenotype dependent heterogeneity of cGMP signalling pathways that we discovered in primary VSMCs implicated that analysis of cGMP signalling in cultured VSMCs at the population level is a risky oversimplification. Depending on the cGMP-elevating agent that would be used in an experiment, the observed effect would be based on another subpopulation of VSMCs. While ANP would elevate cGMP in the contractile VSMC subpopulation, CNP would elevate cGMP in the modulated subpopulation. NO would affect contractile and modulated VSMC subpopulations with a potentially stronger effect in contractile VSMCs.

We further characterised CNP-preferring cells by identifying proteins which were upregulated in these cells. As modulated VSMCs resemble fibroblasts, we included FSP 1 and PDGFRα in our search. FSP 1 is a rather unspecific fibroblast marker [171; 175]. PDGFRα expression has been detected in fibroblast populations from various organs [175] and recently it was even detected in the adventitia and media of healthy aortas [182]. Expression of both, FSP 1 [176; 177] as well as PDGFRα [183], in potentially modulated VSMCs has been reported. Analysis of primary VSMC cultures demonstrated that FSP 1 expression was moderately but significantly increased in CNP-preferring cells, whereas αSMA expression was significantly decreased in these cells (**Figure 13 A**). Like FSP 1, the expression of PDGFRα was higher in CNP- than ANP-preferring cells as well (**Figure 13 B**). This indicated that the modulated CNP-preferring VSMCs had adopted a fibroblast-like state in culture. The fibroblast-like state of CNP-preferring VSMCs is especially interesting in the context of atherosclerosis. It was previously demonstrated that under appropriate conditions the VSMC culture model could be used to mimic transdifferentiation processes which occur during atherosclerosis [179; 199; 322]. For instance, incubation of cultured VSMC-derived cells, isolated from atherosclerotic arteries, with connective tissue growth factor induced a fibroblast-like phenotype (e.g., high expression of collagen1a1, FSP 1) [179]. Recently, it was shown by combination of lineage tracing with single-cell RNA sequencing that VSMCs could transdifferentiate to fibroblast-like cells (called “fibromyocytes”) during atherosclerosis as indicated by expression of fibroblast markers like lumican or collagen1a1 [187]. These studies, and the fibroblast-like state of CNP-preferring cells, might point to a certain degree of transdifferentiation in our cultures that was linked to increased CNP-dependent cGMP signalling.

4.1.2 CNP/GC-B-dependent cGMP signalling is a new marker for phenotypic modulation of VSMCs in culture

To test whether strong CNP/GC-B-dependent cGMP signalling is a new marker for modulated/ transdifferentiated VSMCs, we designed two sets of experiments: (1) We used SMC-selective reporter mice in combination with enzymatic dissociation of the vascular adventitia to check whether CNP-preferring cells were of smooth muscle origin (**Figure 11 A-C**). (2) We genetically ablated GC-B to test whether CNP/cGMP signals were generated via GC-B and analysed whether expression of GC-B increased in culture using western blotting and GC-B LacZ reporter mice (**Figure 12**, **Figure 11 D-E**).

SMC-selective expression of our FRET-based cGMP biosensor was achieved with SM22-Cre mice (SM22-Cre x cGi(L2)). We used the constitutively active SM22-Cre as it was known for its high recombination efficiency in VSMCs. We assessed the fraction of recombined cells in our primary VSMC cultures from SMC-selective sensor mice to estimate the contribution of non-SMCs to these cultures. SMC-selective Cre expression led to a recombination of 91.9±1.7 % in our primary VSMC cultures,

indicating that less than 10 % of cultured cells might be of non-SMC origin. Most likely, the bulk of these non-recombined cells originated from remnants of the adventitial layer. Indeed, when the adventitia was completely removed by an enzymatic dissociation step, before VSMCs were cultured from SMC-selective sensor mice, the recombination was close to 100 %.

To exclude that CNP-preferring cells in our cultures were derived from non-SMCs like endothelial or adventitial cells, we compared cGMP signalling between VSMC cultures from mice with global and SMC-selective sensor expression with (**Figure 10**, **Figure 11 A-B**), and without (**Figure 11 C**) potential adventitial contamination (**Supplementary figure VI**). We found a similar heterogeneity of cGMP signalling pathways (ANP-, CNP-preferring, and ANP~CNP cells) in all three types of VSMC cultures (**Supplementary figure VI B**). Like in VSMC cultures from global sensor mice, ANP-preferring cells of VSMC cultures from SMC-selective sensor mice expressed high levels of αSMA and SM22α, whereas CNP-preferring cells expressed low levels (**Figure 11 B**). For some CNP-preferring cells the fluorescence detected in the SM22α staining was as low that they might be SM22α negative (**Figure 11 B**). As these cells were initially recombined using the SM22-Cre transgene, the latter finding could be considered a further indication for strong downregulation of contractile marker proteins in VSMCs by phenotypic modulation during *in vitro* growth. Still, the SM22-Cre mice used in this work were created by random integration and not by knockin of the recombinase into the SM22α locus [37]. Hence, the Cre expression profile could be different from the original SM22α expression [283]. Together, these experiments indicated that most CNP-preferring cells were SMC-derived modulated VSMCs.

Next, we addressed the question whether CNP-preferring cells developed due to phenotypic modulation in culture or pre-existed in the aortic media. First, we ablated GC-B globally in cGi500-expressing mice and compared cGMP signalling in VSMC cultures from these mice with cultures from GC-B-expressing control mice (**Figure 12**). Analysis of the cGMP responses clearly demonstrated that CNP responses in culture were mediated by GC-B. In control cultures all cGMP signalling phenotypes (ANP-, CNP-preferring, and ANP~CNP cells) were found, while in GC-B knockout cultures no CNP-preferring cells nor ANP~CNP cells were detected (**Supplementary figure V**). Around 15 % of VSMCs in GC-B knockout cultures reacted only to NO, a signalling pattern that was not detected in cultures from the control group. The NO-only cells in the knockout were probably “CNP-preferring cells” that could not respond to CNP. Their cGMP signalling pattern resembled the one of control VSMCs that reacted to CNP and NO but not ANP (just without response to CNP, **Figure 12 B**). Furthermore, like CNP-preferring cells of the control group, NO-only cells expressed significantly less αSMA and SM22α than ANP-preferring cells, indicating that NO-only cells were modulated VSMCs (**Supplementary figure V A-B**). Despite global ablation of GC-B, slight cGMP elevations due to CNP stimulation were detected in 5 % of the knockout cells, whereas 70 % of VSMCs in control cultures reacted to CNP (**Figure 12 A**). The 5 % CNP responses in knockout cultures were based on small elevations of the ratio trace (supported by single trace separation, hence real signals, data not shown). It is known that GC-A can be stimulated by high concentrations of CNP [11; 12]. As all of these “CNP-responsive knockout cells” showed clear cGMP responses to ANP stimulation, cross-activation of GC-A by a relatively high CNP concentration was probably the reason for CNP-dependent cGMP signals in knockout cultures. The small fraction of GC-B knockout cells where potential cross-activation of GC-A was detected (5 % GC-B knockout vs. 70 % control, **Figure 12 A**) was neglectable for our results, especially as the classification itself should not have been affected.

After demonstrating that GC-B was functionally expressed in VSMC cultures and that it mediated the CNP-dependent cGMP signals in these cultures, we tested whether GC-B expression increased in culture over time. Thus, whether GC-B could serve as a marker for progressing phenotypic modulation of VSMCs. The CNP receptor GC-B was strongly upregulated in primary VSMCs after 6 days in culture in comparison to whole aorta (litter-matched mice, 11-week-old) as demonstrated by western blotting (**Figure 11 D**). This correlated with reduced levels of the contractile marker SM22α in lysates of the 6 days culture (**Figure 11 D**), indicating an increased expression of GC-B due to phenotypic modulation of VSMCs in culture. Following GC-B expression in culture over 4-7 days using GC-B LacZ reporter mice supported this notion (**Figure 11 E**). The fraction of reporter-positive cells (X-gal-stained nuclei = X-gal+ cells) in VSMC cultures significantly increased with the time VSMCs were kept in culture. The first indications for GC-B expression by this method were found at day 6. The number of X-gal+ cells significantly increased further at day 7. Interestingly, no X-gal+ cells were detected at day 5 (or before) where most cGMP/FRET measurements were performed. Even after 7 days in culture the fraction of X-gal+ cells was far below the fraction of CNP-preferring cells usually found in measurements (~3 % vs. >30 %) and even further below the fraction of CNP-responsive cells (>70 %). As we verified that CNP responses were mediated via GC-B, this stressed the superior sensitivity of cGMP/FRET measurements over the enzyme-based GC-B LacZ reporter approach. Considering the cGMP response patterns of ANP-preferring (no/weak CNP response), ANP~CNP (moderate/strong CNP response), and CNP-preferring (strong CNP response) cells, one could speculate that phenotypic modulation of VSMCs gradually increased expression of GC-B. Only cells that underwent extensive phenotypic modulation would express sufficient levels of GC-B to surpass the detection level of the enzyme-based LacZ reporter approach. This would explain the late increase (day 6) and the small fraction of X-gal+ cells (~3 %) that were detected in VSMC cultures from GC-B LacZ reporter mice.

Together, our cGMP/FRET measurements in combination with IF-based marker protein analysis and reporter- / western blot-based expression analysis of GC-B led to the following hypothesis: Contractile VSMCs generate cGMP upon stimulation with ANP and NO. Phenotypic modulation of VSMCs towards a modulated/fibroblast-like phenotype in culture decreases/abolishes the sensitivity towards ANP/NO and renders VSMCs susceptible to CNP by increased expression of GC-B. Therefore, CNP/GC-B-dependent cGMP signalling could be used as a marker to identify modulated VSMCs in culture. It could even be possible to assess the degree of phenotypic modulation by this new marker.

Generation of cGMP by ANP/NO in contractile VSMCs and a shift from GC-A to GC-B expression in culture is also supported by the literature and by recent single-cell sequencing data of our laboratory (data not shown): It was shown that VSMCs of murine vessels (contractile) from various vascular beds relaxed upon stimulation with ANP or NO via GC-A- or NO-GC-dependent signalling, respectively [37; 39]. Furthermore, high levels of GC-A mRNA and low levels of GC-B mRNA were found in intact rat aortas by northern blotting [250]. In primary/passaged VSMCs, the authors detected a strong increase of GC-B mRNA [250]. Interestingly, in this study already in primary VSMCs no mRNA encoding for GC-A was detected. This seemingly contrasts with the strong ANP-induced cGMP responses we detected in primary cultured and even in passaged VSMCs. In contrast to the mRNA-based study, we analysed GC-A expression at the functional level. Even if the expression of GC-A at the mRNA level was rapidly lost due to phenotypic modulation of VSMCs in our culture model, VSMCs would stay responsive to ANP until GC-A was removed from the membrane.

4.1.3 Heterogeneity of cGMP signalling pathways in VSMC cultures can change based on culture conditions

Phenotypic modulation of VSMCs in culture is known to be an ongoing process [148] that can be influenced by cell culture conditions [152]. To test whether NP preference was tightly connected with VSMC phenotype, we shifted the phenotypic balance of cultured VSMCs by various cell culture conditions. Thereby, we demonstrated that the NP preference paralleled expected phenotypic changes (e.g., more ANP-preferring cells under conditions that favour contractile VSMCs). Low serum conditions were reported to favour contractile VSMC cultures [196-198]. As expected, under **low serum** conditions (0 % - 1 % FCS) **more** and under **high serum** conditions (10 % - 20 % FCS) **less** ANP- than CNP-preferring cells were detected (**Figure 15 A**). It is still unknown whether the promotion of contractile VSMC cultures by low serum conditions is based directly on phenotypic modulation of VSMCs or impaired proliferation, selectively of modulated VSMCs [195-198]. Our results could be explained by either mechanism. The different serum conditions were applied for 48 h before cGMP/FRET measurements. This period was enough for 1-2 cell doublings (proliferation dependent shift of preference) but also for profound changes of the proteome (phenotypic modulation dependent shift of preference). The ECM component fibronectin and passaging are known to shift VSMCs towards the modulated phenotype [148; 190; 192]. In line with an increased fraction of modulated VSMCs, we found more CNP- than ANP-preferring cells on fibronectin-coated surfaces (**Figure 15 B**) or in passaged VSMC cultures (**Figure 15 C**) than under control conditions. Of all tested cell culture conditions, passaging had the most striking impact on NP preference. Already from the second passage onwards almost no ANP-preferring cells could be detected (**Figure 15 C**). Despite this tremendous shift in NP preference, most cells still showed responses to ANP in passage 2, and even in passage 4 ANP-induced cGMP responses were detected. This strong effect of passaging on NP preference could be explained, at least in part, by the long culture time. We demonstrated before that the GC-B expression / fraction in/of GC-B-positive cells increased in culture over time (**Figure 11 E**). The higher the passage the longer VSMCs have grown in culture.

Beside the well-known factors for phenotypic modulation described above, we identified increased age to favour the formation of CNP-preferring VSMCs in culture. The fraction of CNP-preferring cells in primary VSMC cultures increased together with the age of mice they were isolated from, whereas the fraction of ANP-preferring cells decreased concomitantly (**Figure 16**). The exact ratio of CNP-/ANP-preferring cells varied strongly within each age group. To achieve sufficiently high n-numbers for meaningful interpretation, we had to pool data from experiments performed at different days. Considering the high susceptibility of phenotypic modulation to environmental factors it was not surprising that cultures showed some variation concerning the fraction of ANP-/CNP-preferring cells, from preparation to preparation. Furthermore, no litter-matched mice could be used for the respective experiments, introducing additional heterogeneity. A connection between increased age and an increased susceptibility of contractile VSMCs for phenotypic modulation towards CNP-preferring/ modulated VSMCs would be interesting as the modulated phenotype is associated with development of cardiovascular diseases [144] and the prevalence of these diseases increases with age [317].

Together, these results not only demonstrated a strong link between VSMC phenotype and NP-dependent cGMP signalling, but also a high susceptibility of both to environmental factors. A major limitation of our phenotypic cell culture modulation approach was that we could not distinguish selection of a certain phenotype due to cell culture conditions from phenotypic modulation. This would

require measuring the same cells at different days thereby following their phenotypic modulation over time.

4.1.4 Possible impact of cGMP signalling heterogeneity in VSMC cultures on the interpretation of experimental results

A plethora of studies investigated cGMP signalling in cultured VSMCs and the impact of its manipulation on phenotypic modulation and proliferation [54]. These studies proofed that cultured VSMCs can generate cGMP upon stimulation with ANP, CNP, and/or NO. Concerning phenotypic modulation of VSMCs by cGMP, some studies came to the conclusion that cGMP promotes phenotypic modulation/growth of VSMCs while others reported that cGMP inhibits these processes [54]. These studies had in common that they treated their cultures like a phenotypically homogenous cell assembly in respect to cGMP signalling. Here, we demonstrated for the first time that primary as well as passaged VSMC cultures are highly heterogenous in regard to the cGMP signalling pathways in individual cells (**Figure 15 C**, **Supplementary figure VI B**) and that this heterogeneity is based on different VSMC phenotypes present in these cultures. Besides ANP-preferring/contractile and CNP-preferring/ modulated VSMCs, we identified a third cGMP signalling phenotype. Cells that reacted to ANP, CNP, and NO, but showed no preference for ANP over CNP or vice versa (ANP~CNP cells, **Figure 10 A**).

This cGMP signalling heterogeneity in VSMC cultures must be considered in studies that investigate the effect of cGMP-elevating drugs on VSMCs. For instance, stimulation of primary VSMC cultures with CNP should primarily affect modulated/CNP-preferring VSMCs, whereas stimulation with ANP should primarily affect contractile/ANP-preferring VSMCs. Hence, different effects of cGMP-elevating drugs might not be based on activation of different downstream signalling within the same cell (e.g., due to compartmentalised cGMP pools), but based on different effects of cGMP in different cells (e.g., modulated vs. contractile VSMCs). Compartmentation of cGMP signalling is a concept that is used to explain why different cGMP-elevating agents can induce differential effects in a putative homogeneous cell population [24]. How such compartmentation is achieved in detail remains elusive. One possibility is the local containment of cGMP signals via PDEs. Two recent studies performed with primary [17] or passaged [102] VSMC cultures point towards such a mechanism. A FRET-based life cell imaging approach was used in these studies to compare the effects of various PDE inhibitors on ANP-, CNP-, and NO-induced cGMP responses. In these studies, cGMP generated by these stimuli was affected by different PDE inhibitors. Therefore, the authors of the latter study concluded that cGMP pools in VSMCs were compartmentalised by different PDEs [102]. A major limitation of both studies was that they investigated cGMP generation by ANP, CNP, or NO in separate cultures but not within the same cell. The heterogeneity concerning cGMP signalling in VSMC cultures, as demonstrated in the present work, provides another possible explanation why ANP-, CNP-, and NO-induced cGMP signals were affected by different PDE inhibitors. For instance, it was recently published that cGMP/cAMP-degrading PDE 10A was strongly upregulated in modulated rat aortic SMCs (passage 10-15) in comparison to contractile ones [131]. Inhibition of PDE 10A in the modulated rat aortic SMCs led to growth arrest in a GC-B dependent manner. GC-A was only weakly expressed in the modulated SMCs, at least at the mRNA level. As we demonstrated that modulated VSMCs in culture show only weak ANP-induced cGMP signals, one would expect a strong impact of PDE 10A inhibition on CNP-induced but not ANP-induced cGMP levels in a purely modulated VSMC culture. ANP-induced cGMP levels in contractile VSMCs would not/mildly be affected by PDE 10A inhibition due to the weak expression of PDE 10A in contractile VSMCs. Consequently, when investigating the effect of PDE 10A inhibition on

ANP-/CNP-induced cGMP levels in a heterogeneous VSMC culture, one would detect no/mild effect of PDE 10A inhibition on ANP-induced cGMP and a strong effect on CNP-induced cGMP. When assuming that VSMC cultures are homogenous, one would wrongly conclude that PDE 10A compartmentalised CNP-induced cGMP without affecting ANP-induced cGMP. To distinguish whether differential effects of cGMP-elevating agents (ANP, CNP, or NO) are based on compartmentalised cGMP pools within a given cell or based on differences of cGMP pathways between cells of a heterogeneous cell culture, it would be necessary to investigate the effects of PDE inhibition on ANP-, CNP, and NO-induced cGMP elevations within the same cells. A recently published review provides an in-depth discussion on this topic as well as a hypothetical experiment to solve this important question [24].

In this work, we did not only identify heterogeneous cGMP signalling pathways in VSMC cultures. We could also influence the cGMP signalling phenotype of VSMCs by various experimental conditions (**Figure 15**, **Figure 16**). For instance, the age of mice from which VSMCs were isolated, or the concentration of FCS in the cell culture medium, notably changed the fraction of ANP-preferring/ contractile and CNP-preferring/modulated VSMCs that were present in primary VSMC cultures. Thus, not only the cGMP signalling heterogeneity of VSMC cultures but also the influence of experimental conditions on this heterogeneity might decide the outcome of experiments where the effect of cGMP-elevating drugs on VSMCs is investigated. For instance, the same drug might have different effects in two independent VSMC cultures if the ratio of ANP-/CNP-preferring cells is different between the cultures. Taking the example from above, an inhibitory GC-B dependent effect of PDE10 A inhibition on VSMC growth might not be visible in primary VSMC cultures from 3/4-week-old mice, as these cultures contain only a small fraction of CNP-preferring/modulated VSMCs (< 10 % CNP-preferring cells, **Supplementary figure V C**).

Besides the experimental difficulties arising from heterogeneous cGMP pathways in VSMC cultures, this heterogeneity could proof useful regarding treatment of cardiovascular diseases. In atherosclerosis, for instance, modulated/disease-associated VSMCs of atherosclerotic plaques are found next to contractile/healthy VSMCs of the vessel wall. When VSMCs are targeted by drugs to treat atherosclerosis, both types of VSMCs (contractile/modulated) could be affected, but potentially with different outcome. The presence of ANP-preferring/contractile and CNP-preferring/modulated VSMCs within the same culture allows to directly compare the effect of cGMP-elevating agents on both phenotypes. This might help to screen for drugs that target VSMCs of atherosclerotic plaques without negatively impacting the healthy vasculature, or vice versa. Nonetheless, observations made in VSMC cultures can only be a first indication that would need confirmation *in vivo*. Considering, that a similar heterogeneity of cGMP pathways as observed in culture, was demonstrated between healthy and atherosclerotic arteries (**Figure 17**, **Figure 18**), the cell culture model appears to be a promising model for atherosclerosis research.

4.2 cGMP signalling in healthy and diseased aortas

After linking VSMC phenotypes with differential cGMP signalling patterns in cell culture, we transferred our findings to the *ex vivo* situation as the cell culture model cannot simulate the complex environment of VSMCs in a native artery (e.g., ECM composition). Therefore, we compared cGMP signals in healthy and atherosclerotic aortas by confocal FRET microscopy. We used healthy arteries to investigate cGMP signalling in contractile VSMCs. For investigation of phenotypically modulated VSMCs, we decided to use atherosclerotic arteries as cGMP/cGKI-dependent signalling in VSMCs was demonstrated to be

important during atherosclerosis development [124]. Moreover, in atherosclerosis not only phenotypic modulation but also transdifferentiation takes place (see sections **1.3.1** and **1.3.2.2**) [153]. Like in cell culture measurements, we aimed to investigate cGMP signalling in VSMCs of various phenotypes, from mildly modulated VSMCs of the fibrous cap (still expressing considerable amounts of contractile markers [203; 214]) to modulated/transdifferentiated VSMCs of the plaque core (lacking contractile markers [214]) simultaneously by optical sectioning via confocal FRET microscopy (**Figure 18 B**). According to our hypothesis based on cell culture experiments, we expected that mild phenotypic modulation would lead to increased CNP and decreased ANP responses, whereas strong phenotypic modulation/transdifferentiation would lead to complete loss of ANP-induced cGMP signals. However, we had to realise only cells of the fibrous cap but not of the plaque core could be analysed with our imaging setup (**Figure 18 D**). The problem to detect cells of the plaque core was probably the result of limited tissue penetration in combination with strong background fluorescence of the fat-rich plaque core (potentially by strong light scattering).

Most measurements in healthy arteries and all measurements in atherosclerotic blood vessels were performed with mice expressing the FRET-based cGMP sensor cGi500 globally. Therefore, we used the characteristic morphology of the vascular media to select appropriate regions for our measurements in healthy aortas. Where possible, individual cells were marked by ROIs for analysis (**Figure 17 B**). Focus drift was the major limitation for analysis of cGMP signalling in our *ex vivo* set up. Besides tissue movement due to buffer flow or convection (heated buffer, non-heated objectives), tissue swelling due to differences in osmolarity of buffer and tissue might have contributed to focus drift during *ex vivo* measurements. Furthermore, we measured aortas, a tissue known for contraction and relaxation. At least for ANP and NO, it was reported that they relax murine aortas [37; 39; 323]. Therefore, the drug applications had the potential to directly induce focus drifts, leading to “loss of cells and signals” as cells moved out of focus. Another problem with focus drifts was that it did not necessarily affect CFP and YFP fluorescence the same way. This could lead to elevations of the ratio trace (false signals) that were not based on changes in cGMP concentration (e.g., **Figure 18 D** second refocus event). Based on the working principle of our sensor, cGMP elevations should lead to an increase in CFP and simultaneous decrease in YFP fluorescence (antiparallel movement). So, we accepted only signals where this behaviour was clearly visible as “real” cGMP-dependent FRET signals. By this conservative approach we assured that only real cGMP responses were included in our analysis. On the other hand, one must be aware that focus drift could potentially obfuscate proper trace separation, leading to the exclusion of real signals. Thus, the percentage of regions that responded to a certain stimulus should be considered as the minimum of responding regions. cGMP/FRET measurements in atherosclerotic aortas were even more challenging than measurements in healthy aortas. The stronger focus drift and often mediocre contrast in measurements of atherosclerotic plaques, compared to healthy aortas, made it hard (**Figure 18 C**) but not impossible (**Figure 18 D**) to reach cellular resolution. Due to these technical limitations of *ex vivo* cGMP/FRET measurements in healthy and atherosclerotic aortas, we decided to refer to “regions” instead of “cells” even though many of the signals analysed, at least in healthy aortas, were derived from individual cells.

Despite these technical limitations we managed to measure cGMP/FRET signals in healthy and atherosclerotic aortas in real time with (close to) single-cell resolution. We could reliably demonstrate that cells of healthy arteries (aorta and branching vessels alike) could respond to ANP (56-74 %) and NO (86-96 %) while cGMP elevations upon CNP stimulation were the exception in the healthy vessel wall (< 1 %) (**Figure 17 B-C**). These results were in line with studies demonstrating that SMC-selective

genetic ablation of GC-A [37] or the NO-GC β1-subunit [39] impaired the relaxation of aortas by ANP or NO, respectively. These two studies could demonstrate functional NO/ANP-dependent cGMP signalling in aortic VSMCs but not whether the same VSMCs could respond to both stimuli. Here, we demonstrated for the first time that in healthy aortas the same VSMC/region could show robust cGMP responses to ANP and NO (**Figure 17 B**, upper panel). In addition, we identified regions that showed robust cGMP responses either to NO or ANP but not both (**Figure 17 B**, lower panel, response only to NO). It was recently demonstrated by single-cell RNA sequencing that already in healthy aortas several subpopulations of VSMCs existed [141]. The heterogeneous cGMP signalling we detected in the healthy aortic media might correlate to different subpopulations which remains to be shown. It should be noted that some ANP-induced cGMP signals of cells that reacted only to NO (and vice versa) were probably excluded from analysis due to our conservative approach (see above). In this work, we focussed on cGMP signalling in large conduit arteries like the aorta, brachiocephalic artery, and carotid arteries. It is likely that VSMCs from other vessels show different cGMP signalling patterns. For instance, it was reported that SMC-selective genetic ablation of GC-B impaired CNP-dependent relaxation of mesenteric arteries [38]. This could indicate an important role of GC-B-dependent cGMP signalling in mesenteric artery VSMCs that we did not observe in VSMCs of the healthy aorta. In pathologically remodelled arteries, robust cGMP elevations upon CNP application (> 30 % of all analysed regions, **Figure 18 E**) were detected in the potential fibrous cap of atherosclerotic plaques (contains modulated VSMCs). This was a tremendous difference to the healthy aorta where less than 1 % of all regions showed robust CNP-induced cGMP responses. In around 8 % of analysed plaque regions, CNP- but not ANP-induced cGMP signals could be reliably detected (**Supplementary table VII**). According to our hypothesis based on cGMP/FRET measurements in cell culture, the plaque cells of these regions reflected strongly modulated CNP-preferring cells. Around one fifth of all analysed regions reacted to ANP and NO, in addition to CNP. It was unclear whether these regions reflected the behaviour of ANP~CNP or CNP-preferring VSMCs as the strong impact of focus drifts on signal heights (e.g., refocus events in **Figure 18 D**) did not allow to reliably quantify the strength of individual cGMP signals.

Our *ex vivo* experiments confirmed the suitability of our cell culture model to investigate cGMP signalling in healthy and diseased arteries, but also demonstrated some differences between cultured and native VSMCs. VSMCs in healthy aorta preparations responded strongly to ANP and NO, like contractile VSMCs in cell culture. In contrast to contractile VSMCs in culture which frequently showed an additional weak CNP-induced cGMP response, CNP responses were hardly detected in the healthy aorta (< 1 %). This might be an indication that already after 5 days in culture, when we performed the cGMP/FRET measurements, most contractile VSMCs were slightly phenotypically modulated. Strong CNP-induced cGMP responses, like those observed in modulated VSMCs in culture, were only detected in potentially modulated VSMCs of atherosclerotic plaques.

Still, the cGMP response patterns of atherosclerotic plaque cells *ex vivo* did only partially reflect the extreme changes observed by phenotypic modulation of cultured VSMCs. While some regions of the atherosclerotic arteries showed robust cGMP responses to CNP but not to ANP, many regions reacted to CNP, ANP, and NO (resembling ANP~CNP cells). Some of these potential ANP~CNP regions could certainly be attributed to the problem in reaching real/reliable single-cell resolution in our *ex vivo* cGMP/FRET measurements. Detection of CNP- and ANP-preferring cells within the same ROI (= region) would lead to an ANP~CNP signalling pattern. More importantly, the low number of regions with clear CNP preference in relation to potential ANP~CNP regions might indicate a less severe phenotypic modulation in most regions of the fibrous cap than the one experienced in cell culture. Indeed, fibrous

cap VSMCs still express considerable levels of contractile markers like αSMA [203; 228] (see also **Figure 22 A**), while CNP-preferring cells in culture showed only residual expression of contractile marker proteins but expressed fibroblast markers (**Figure 13**). Loss of SMC lineage markers with concomitant expression of markers for other cell lineages is known for phenotypically modulated/ transdifferentiated VSMC-derived cells of the plaque core [153]. These VSMC-derived cells of the plaque core include fibroblast-like cells that were identified by the expression of fibroblast markers [187]. Thus, it is tempting to speculate that these fibroblast-like cells of atherosclerotic plaques might represent our CNP-preferring cells in culture which we would consequently expect in the core of atherosclerotic plaques, where we could not measure any cells with our imaging setup. Admittedly, in the aforementioned study also considerable amounts of such transdifferentiated cells were detected in the fibrous cap. This might explain the regions reacting to CNP but not ANP in our cGMP/FRET measurements of the fibrous cap.

According to our hypothesis, contractile VSMCs attenuate their responsiveness to ANP and simultaneously increase their responsiveness to CNP during phenotypic modulation. Thus, they change from ANP-preferring (healthy vessel wall) over ANP~CNP (fibrous cap) to CNP-preferring cells (fibrous cap / plaque core). While our observations from cGMP/FRET measurements in healthy and atherosclerotic diseased arteries are in line with this hypothesis, it would require further experiments to provide definitive proof. It would be mandatory to analyse cGMP signalling in VSMC-derived cells of the plaque core. Optimally one would measure VSMC-derived cells of the fibrous cap in parallel. To achieve this, one could use multiphoton microscopy for better plaque penetration (also less scattering due to longer wavelengths) in combination with red-shifted cGMP indicators that are selectively expressed in SMC-derived cells.

To assure the validity of our morphological VSMC identification in healthy arteries, we verified that VSMCs could respond to ANP and/or NO with SMC-selective sensor mice (data not shown). All measurements of atherosclerotic plaques, in contrast, were performed with global sensor mice (cGi(L1)). Hence, the conclusions that we measured cGMP signalling of VSMCs in atherosclerotic plaques were based on the following assumptions: The fibrous cap where we potentially measured cGMP is mainly comprised by VSMCs with a thin endothelial layer on top. It is unlikely that the CNP-dependent cGMP signals were derived from the endothelium as genetic ablation of GC-B in αSMA-expressing cells reduced GC-B below detection limits in lysates of atherosclerotic aortas (**Figure 19 C**). Thus, the CNP-induced cGMP signals detected in our measurements using globally expressing sensor mice were most likely generated by αSMA-expressing cells which excluded the endothelium. Finally, the cGMP response patterns detected in atherosclerotic plaques in combination with the ones from healthy arteries reflected the changes in cGMP signalling we observed in VSMC cultures.

The emergence of CNP-dependent cGMP signalling in atherosclerotic arteries, in contrast to its absence in healthy ones, strongly suggested CNP-dependent cGMP signalling as a new reliable marker for phenotypic modulation of VSMCs not only in cell culture but also in intact arteries *ex vivo*. Moreover, CNP-dependent cGMP signalling could potentially be used as an indicator for atherosclerosis development *in vivo*. Indeed, radioactively labelled CNP as a marker for atherosclerotic plaques was already tested several years ago [324]. Liu and colleagues identified accumulation of radioactively labelled CNP in plaque-like lesions of rabbit femoral arteries by positron emission tomography. They attributed this accumulation to binding of CNP to the clearance receptor Npr-C but whether GC-B was involved in this process was not tested.

4.3 Influence of GC-B-dependent cGMP signalling on atherosclerosis

Our *ex vivo* cGMP/FRET measurements in combination with our cell culture experiments indicated that during atherosclerosis cGMP signalling in VSMCs shifted from a mainly ANP/NO-based signalling towards a CNP-based signalling. This shift was most likely based on phenotypic modulation/ transdifferentiation of VSMCs during disease development. To investigate the functional importance of this process, we ablated the CNP receptor GC-B selectively in SMCs (Smko mice) and compared atherosclerosis development between Smko and control mice still expressing GC-B after 18 weeks atherogenic diet. In total, we have analysed three parameters. Lesion area was quantified to estimate atherosclerosis progression. Potentially CNP-responsive cells (X-gal+ reporter cells for expression of the GC-B locus) and αSMA+ areas were quantified in plaques to determine changes in plaque composition. As a reminder: in our system X-gal+ cells indicated that the GC-B locus was transcribed in these cells. In LacZ-ctrl mice (express GC-B LacZ) this should lead to functional expression of GC-B. In Smko mice, no functional GC-B should be expressed in SMCs but X-gal+ cells would express GC-B under "normal" circumstances (potentially CNP-responsive/modulated VSMCs).

Our inducible SMC-selective (αSMA-CreER^{T2}-dependent) knockout approach efficiently deleted GC-B in atherosclerotic aortas (**Figure 19 B-C**) as verified at the genomic (by PCR) and protein (by western blotting) level. The band pattern of the PCR demonstrated that recombination was restricted to SMC-rich tissue of Smko mice (**Figure 19 B**). Importantly, GC-B expression on the protein level was reduced below detection limit in atherosclerotic aortas of Smko mice, whereas GC-B was clearly detected in lysates of control mice (**Figure 19C**). This indicated that in atherosclerotic tissue GC-B was mainly expressed in cells of smooth muscle origin. Consequently, we assumed that most X-gal+ cells that we detected in atherosclerotic aortas of our GC-B LacZ reporter mice (LacZ-ctrl and Smko, **Figure 21**) were SMC-derived. Considering, that we detected CNP-dependent cGMP signalling only in atherosclerotic aortas (presence of modulated/transdifferentiated VSMCs), it is likely that these X-gal+ cells were modulated/transdifferentiated VSMCs.

Before we compared the lesion area of atherosclerotic aortas between Smko and control mice, we verified that SMC-selective ablation of GC-B had no significant influence on important physiological parameters for atherosclerosis development like total cholesterol, HDL, or LDL (**Table 6**). Analysis of atherosclerotic lesions by Oil Red O staining revealed the expected characteristics for lesion development in mice (**Figure 20 A**). Atherosclerotic plaques had preferentially developed in the aortic arch and branching vessels of Smko and control mice (**Figure 20**). While approximately half the aortic arch and branching vessels were covered by lesions, the rest of the aorta was only covered to ~15 % (**Figure 20 B**). Neither lesion area of the aortic arch or thoracic/abdominal aortas nor the sites of lesion formation were different between Smko and control mice (**Figure 20**). Therefore, we could exclude that CNP-dependent cGMP signalling via GC-B in SMCs had an influence on atherosclerotic plaque burden (see section **1.3.2.2** for a definition). That GC-B in SMCs had no influence on lesion area was interesting as endothelium-derived CNP was shown to affect murine atherosclerosis progression in terms of lesion area [83]. Moyes and colleagues reported that endothelium-selective ablation of CNP increased lesion area in ApoE-deficient mice. In the same study they observed anti-inflammatory actions of endothelial CNP. As inflammation is an important factor for atherosclerosis development [325], increased inflammation after endothelium-selective ablation of CNP might explain the increased lesion area in their experiments. In this study they did not identify the receptor that was responsible for the anti-atherogenic effects of CNP. It is unlikely that GC-B in VSMCs was responsible for this anti-

atherogenic effect as we did observe no effect on lesion area after SMC-selective ablation of GC-B. Whether GC-B in non-SMCs or possibly Npr-C mediated signalling can exert atheroprotective actions, remains to be shown.

For the cGMP downstream effector, cGKI, a SMC-dependent atherosclerosis promoting effect was reported by Wolfsgruber and colleagues [124]. SMC-selective ablation of cGKI impaired contribution of VSMCs to atherosclerotic plaque development which led to a reduced lesion area in knockout mice of this study. Based on additional cell culture experiments, Wolfsgruber and colleagues proposed NO-dependent cGMP signalling to be involved in this process. This assumption was later supported by another group, demonstrating that global ablation of NO-GC 1 attenuated lesion development as well [55]. Our data demonstrated that GC-B-dependent cGMP signalling in VSMCs was not involved in the atherosclerosis promoting actions of cGKI. In contrast to SMC-selective ablation of cGKI [124], SMC-selective ablation of GC-B did not affect lesion area and increased the contribution of potentially modulated X-gal+ VSMCs to plaque development (**Figure 21**). That CNP/GC-B-dependent and cGKI-dependent cGMP signalling in SMCs had different effects on atherosclerosis development, might be related to the phenotypic plasticity of VSMCs. We demonstrated that CNP, in contrast to NO, could not induce cGMP responses in contractile VSMCs of healthy aortas (**Figure 17 C**). Hence, CNP could act only on VSMCs that already started phenotypic modulation (e.g., cells of the fibrous cap, **Figure 18 E**), whereas NO/cGKI could already act on medial VSMCs prior to plaque development. This phenotype-dependent cGMP signalling could lead to opposing effects in VSMCs as was demonstrated in cell culture by Weinmeister and colleagues [123]. They investigated the effect of membrane-permeable cGMP analogues on VSMC growth in culture. The cGKI-dependent growth-promoting effect of 8-Br-cGMP on primary VSMCs (large fraction of contractile VSMCs) was converted to a mild cGKI-dependent growth-inhibiting effect of 8-Br-cGMP in subcultured VSMCs of higher passages (modulated VSMCs). As we demonstrated that already in passage 4, most subcultured VSMCs were of the CNP-preferring/ modulated phenotype, growth inhibition by CNP via GC-B/cGKI would be plausible. Indeed, that CNP can exert growth-inhibiting effects on passaged VSMCs was demonstrated by several groups. Depending on the study they attributed the growth inhibition to cGMP-dependent signalling via GC-B [131; 263] or to cGMP-independent signalling via Npr-C [103]. An anti-proliferative effect of GC-B-dependent cGMP signalling could also explain why we found more potentially modulated VSMCs (X-gal+ cells) in atherosclerotic plaques from Smko mice than in plaques from LacZ-ctrl mice (**Figure 21 C**, trend). Nonetheless, a proliferation-based mechanism would raise the question why lesion area was not affected (**Figure 20**) by the increase of potentially modulated VSMCs in plaques of Smko mice (**Figure 21**).

We detected X-gal+ cells throughout lesions of the aortic arch (and branching vessels) from Smko and LacZ-ctrl mice. They frequently accumulated in the core region of plaques but were also found in the cap of lesions (**Figure 21 A**). Interestingly, X-gal+ cells were not evenly distributed across all plaques of Smko and LacZ-ctrl mice, but mainly accumulated in plaque sections within few hundred micrometres (**Figure 21 B**). The accumulation of X-gal+ cells within a few or even individual plaques could indicate that strong phenotypic modulation/transdifferentiation of VSMCs is not a continuous process in atherosclerosis but rather restricted to a certain stage of plaque development. It should be noted that the exact region of the aorta where plaques with a high number of X-gal+ cells were located did differ between mice. In general, the small quantity of X-gal+ cells found in plaques (**Figure 21 C**) stood in contrast to the large fraction of CNP-responsive regions in our cGMP/FRET measurements of atherosclerotic plaques (**Figure 18 E**). A similar discrepancy between the detection of phenotypically

modulated VSMCs via cGMP/FRET measurements and via X-gal staining of cells from GC-B LacZ reporter mice was already observed in our cell culture experiments (**Figure 11 E**, see also section **4.1.2**). We concluded that only after extensive phenotypic modulation sufficient GC-B was expressed to be detectable via X-gal staining, whereas our highly sensitive cGMP/FRET measurements were capable to already detect functional GC-B expression in less severely modulated VSMCs. Thus, we hypothesized that the X-gal+ cells only indicated the most extensively modulated/transdifferentiated VSMCs and that atherosclerotic plaques of LacZ-ctrl and Smko mice were more enriched in CNP-responsive modulated VSMCs than was apparent by our GC-B LacZ reporter approach. To quantify the contribution of modulated VSMCs to atherosclerotic plaques of Smko and LacZ-ctrl mice, we calculated the average number of X-gal+ cells per plaque section. As we already detected X-gal+ cells in the media of the aortic arch, we quantified the X-gal+ cells within the media as well (**Figure 21 C**). Plaques of LacZ-ctrl mice contained slightly more X-gal+ modulated VSMCs than the media. Plaques from Smko mice, in contrast, showed a strong and statistically significant increase of X-gal+ modulated VSMCs, compared to the media. In general, it appeared that SMC-selective ablation of GC-B increased the contribution of modulated (X-gal+) VSMCs to plaque formation. Therefore, we concluded that GC-B-dependent cGMP signalling in VSMCs negatively regulated the contribution of modulated/transdifferentiated VSMCs to plaque development. As mentioned above, a possible mechanism how GC-B-dependent cGMP signalling could impair the contribution of modulated VSMCs to plaque development would be an anti-proliferative effect of CNP on growth of modulated/transdifferentiated VSMCs. Another possibility would be an autoregulatory inhibition of phenotypic modulation by GC-B. In LacZ-ctrl mice, functional GC-B/cGMP signalling in modulated VSMCs would slow down further phenotypic modulation or potentially transdifferentiation. In Smko mice, no such inhibition would be present, allowing extensive phenotypic modulation of VSMCs, as indicated by the strong enrichment of atherosclerotic plaques with X-gal+ cells. It should be noted that already the media of Smko mice appeared to be more enriched with X-gal+ cells than the media of LacZ-ctrl mice (trend only). Nonetheless, such an autoinhibitory mechanism could not be based on CNP-dependent cGMP signalling alone. We demonstrated that potential fibrous cap cells could respond to CNP. If CNP alone would be sufficient to limit phenotypic modulation, then the fibrous cap of Smko mice should be rich in X-gal+ cells and show other signs of increased phenotypic modulation. Determination of the αSMA+ area (contractile marker) in the 30 µm cap region by IHC staining (**Figure 22 B**) did not show differences between LacZ-ctrl and Smko mice. Analysis of the αSMA+ area of entire plaques (cap and core region) showed a trend for less αSMA+ area in plaques of Smko mice than in plaques of LacZ-ctrl mice. As the X-gal+ cells mainly accumulated in the core region of plaques of Smko and LacZ-ctrl mice, we compared the distribution of αSMA between the 30 µm cap and core region by forming the ratio for each plaque (**Figure 22 C**). Indeed, there was significantly less αSMA in the core of Smko plaques in relation to the cap area than in LacZ-ctrl mice. This observation was in line with the high number of X-gal+ modulated VSMCs in plaques from Smko mice that were frequently found to express no/low αSMA (**Supplementary figure VIII B**). Still, it should be noted that the fibrous cap is not identical with the 30 µm cap region used for analysis. Therefore, it is possible that αSMA from a fibrous cap that extended further into the plaque than 30 µm was quantified as αSMA in the core region.

In addition to αSMA, we analysed the expression of MAC-2 (also known as galectin-3) in atherosclerotic plaques of Smko and LacZ-ctrl mice (**Supplementary figure VIII A**). Expression of MAC-2 in VSMC-derived cells of atherosclerotic plaques has been demonstrated to be a marker for transdifferentiation of VSMCs to macrophage-like cells [155; 237]. While this new concept of VSMC-to-macrophage-like

cell transdifferentiation was questioned in the beginning [238], it is now widely accepted that VSMCs in atherosclerotic lesions cannot only give rise to modulated VSMCs and macrophage-like cells but also to other cell types like (myo-)fibroblast-like or osteochondrocyte-like cells [153]. Interestingly, we found several X-gal+ cells in MAC-2+ regions of atherosclerotic plaques from Smko and LacZ-ctrl mice, in addition to some αSMA+ (modulated) X-gal+ cells (**Supplementary figure VIII**). This indicated that GC-B is not only a marker for modulated VSMCs in cell culture and atherosclerotic plaques but could also be a marker for VSMCs that transdifferentiated to macrophage-like cells. Considering the various VSMC-derived cell types that can be found in atherosclerotic plaques, it would be interesting to investigate whether CNP-dependent cGMP signalling might be a common marker connecting all modulated/transdifferentiated VSMC-derived cells. Further IHC stainings of atherosclerotic plaques from our GC-B LacZ reporter mice for marker proteins of the various VSMC-derived cell types could help to solve this question. As we identified a fibroblast-like cell type in our cultured modulated VSMCs (**Figure 13**), IHC stainings for FSP 1 would be a good starting point.

Altogether, our findings indicated that functional CNP/GC-B-dependent cGMP signalling in modulated VSMCs attenuated the development of strongly modulated/transdifferentiated VSMCs with low/absent αSMA expression in atherosclerotic plaques by a yet unknown mechanism. Whether this function of CNP signalling is beneficial for the outcome of atherosclerosis, remains to be shown.

5 Summary and outlook

In summary, we successfully applied cGMP/FRET imaging to analyse cGMP signalling in real time with single-cell resolution in cultured VSMCs, and to demonstrate how cGMP signalling of VSMCs changes upon pathophysiological processes during atherosclerosis. Thereby, we identified a previously unknown heterogeneity of NP-induced cGMP generation in primary VSMC cultures and linked it with phenotypic plasticity (**Figure 23 A**).

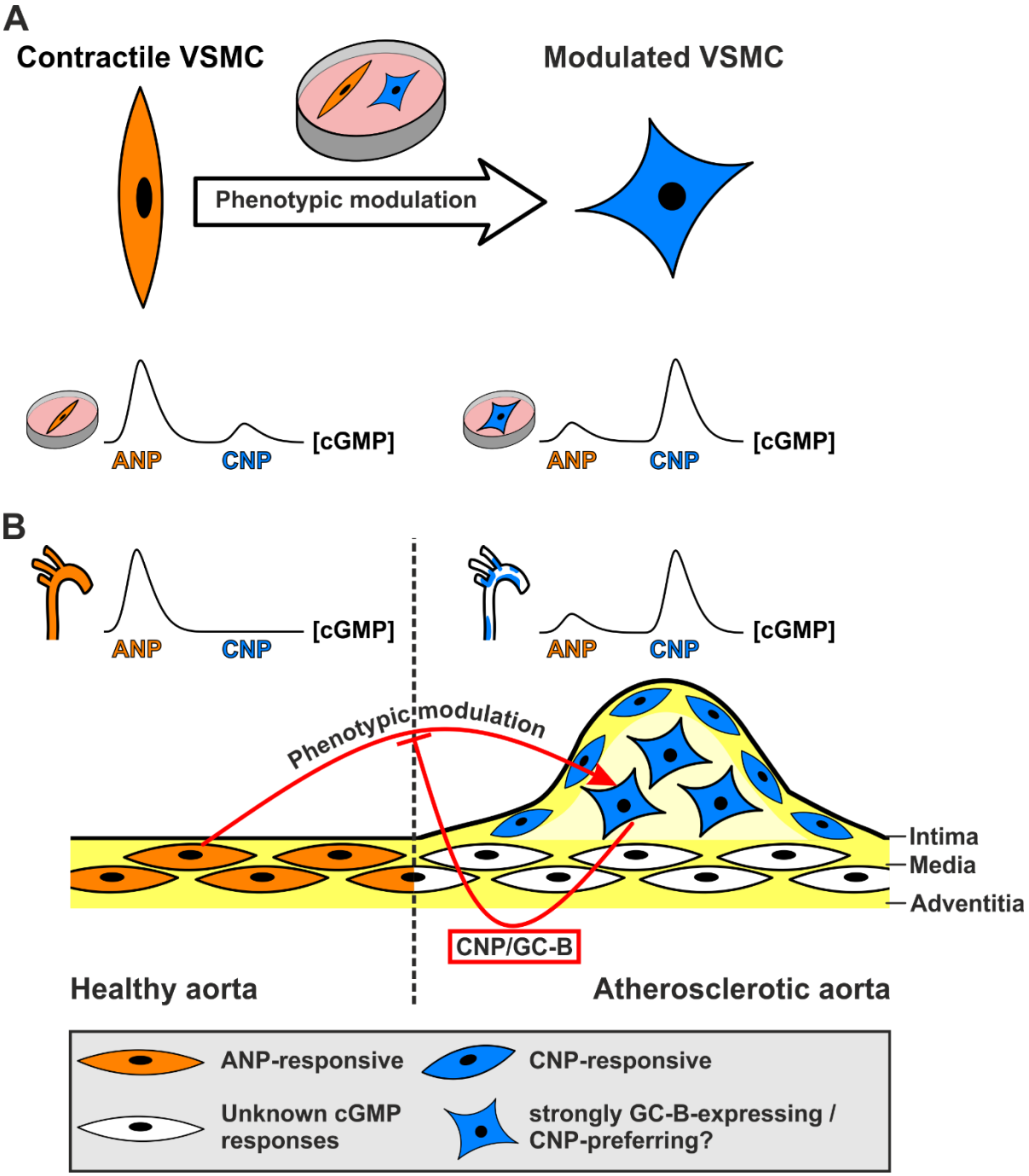

Figure 23: Summary of cGMP signalling pathways in cultured VSMCs and VSMCs of healthy and atherosclerotic arteries. *Generation of cGMP by ANP and CNP changes depending on the phenotypic state of VSMCs.* ***A:*** *In culture, contractile VSMCs prefer ANP over CNP (orange), whereas modulated VSMCs prefer CNP over ANP (cyan).* ***B:*** *As predicted by the cell culture model, pathological remodelling of arteries shifts ANP-dependent to CNP-dependent*

cGMP signalling. CNP/GC-B-dependent cGMP signalling in VSMCs impairs the contribution of strongly GC-B-expressing modulated/transdifferentiated VSMCs to atherosclerotic plaque development. ANP: atrial natriuretic peptide, cGMP: 3',5'-cyclic guanosine monophosphate, CNP: C-type natriuretic peptide, GC-B: guanylyl cyclase-B, VSMC: vascular smooth muscle cell. For details see text.

Contractile VSMCs (αSMA/SM22α high) mainly generated cGMP in response to ANP and NO but showed no or only weak responses to CNP. Modulated VSMCs (αSMA/SM22α low) mainly generated cGMP in response to CNP, could have attenuated cGMP responses to NO, and showed weak or no responses to ANP. These modulated VSMCs adopted a fibroblast-like state, marked by increased expression of FSP 1 and PDGFRα. Cell culture conditions known to modulate VSMC phenotype concomitantly modulated the NP preference, emphasising the connection between VSMC phenotype and NP preference. Our cell culture model also predicted the changes in NP-dependent cGMP signalling between healthy (contractile VSMCs) and atherosclerotic (modulated/transdifferentiated VSMCs) arteries (**Figure 23 B**). While cGMP signalling in healthy arteries was dominated by ANP and/or NO, atherosclerotic vessels exhibited considerable CNP-dependent cGMP responses. Again, in healthy as well as pathologically remodelled vessels cGMP generation showed some heterogeneity instead of a homogeneous single cGMP signalling pattern. Finally, we demonstrated that expression of the CNP receptor GC-B in VSMCs influenced the structure of plaques but not total lesion area. It appeared that GC-B expression limited the contribution of strongly GC-B-expressing VSMCs to plaque development.

Despite the new insights about phenotype-dependent cGMP signalling in VSMCs during health and disease given in this work, much remains to be done. For instance, (1) the western blot analysis of GC-B expression in healthy aorta and cultured VSMCs should be repeated and include passaged VSMCs, atherosclerotic aortas and aortas from mice of various ages. (2) Experiments need to be designed to analyse cGMP signalling in the core of atherosclerotic plaques. A possible approach could be based on multiphoton microscopy in combination with SMC-selective sensor mice. (3) So far, the X-gal+ cells in our atherosclerosis model as well as the plaques of Smko and LacZ-ctrl mice are poorly characterised. Further characterisation of these, especially with respect to a potentially beneficial/detrimental function, needs to be done. We already performed single-cell RNA sequencing with cells from atherosclerotic aortas of Smko and LacZ-ctrl mice for detailed characterisation. (5) Most importantly, the mechanism how GC-B expression in VSMCs impairs the contribution of VSMCs to atherosclerotic plaques needs to be elucidated in the future.

Based on our experiments, we suggest CNP/GC-B-dependent cGMP signalling as a new marker for phenotypic modulation in culture and *in vivo*. Furthermore, we hypothesise that phenotypic modulation/transdifferentiation of VSMCs shifts the NP preference from ANP to CNP via downregulation of GC-A and upregulation of GC-B. During plaque development this renders VSMCs susceptible to CNP. CNP-dependent cGMP signalling then limits further modulation towards the modulated phenotype or even transdifferentiation, in particular in the plaque core where these processes are most extreme. This hypothesis suggests that systematic manipulation of CNP-induced cGMP signalling in plaque-associated VSMCs could be a new therapeutical approach to treat atherosclerotic disease. With the CNP analogue vosoritide, a drug that was recently approved for application in humans [35], a potential medication is at hand.

6 References

1. Kuhn, M. (2016). Molecular physiology of membrane guanylyl cyclase receptors. *Physiol Rev, 96*(2), 751-804. doi:10.1152/physrev.00022.2015

2. Hofmann, F. (2020). The cGMP system: Components and function. *Biol Chem, 401*(4), 447-469. doi:10.1515/hsz-2019-0386

3. Minorsky, P. V. (2003). The hot and the classic. *Plant Physiol, 131*(4), 1578-1579. doi:10.1104/pp.900069

4. Thoonen, R., Sips, P. Y., Bloch, K. D., & Buys, E. S. (2013). Pathophysiology of hypertension in the absence of nitric oxide/cyclic GMP signaling. *Curr Hypertens Rep, 15*(1), 47-58. doi:10.1007/s11906-012-0320-5

5. Kemp-Harper, B., & Feil, R. (2008). Meeting report: cGMP matters. *Sci Signal, 1*(9), pe12. doi:10.1126/stke.19pe12

6. Friebe, A., & Koesling, D. (2009). The function of NO-sensitive guanylyl cyclase: What we can learn from genetic mouse models. *Nitric Oxide, 21*(3-4), 149-156. doi:10.1016/j.niox.2009.07.004

7. Gerzer, R., Hofmann, F., & Schultz, G. (1981). Purification of a soluble, sodium-nitroprusside-stimulated guanylate cyclase from bovine lung. *Eur J Biochem, 116*(3), 479-486. doi:10.1111/j.1432-1033.1981.tb05361.x

8. Stone, J. R., & Marletta, M. A. (1994). Soluble guanylate cyclase from bovine lung: Activation with nitric oxide and carbon monoxide and spectral characterization of the ferrous and ferric states. *Biochemistry, 33*(18), 5636-5640. doi:10.1021/bi00184a036

9. Friebe, A., & Koesling, D. (2003). Regulation of nitric oxide-sensitive guanylyl cyclase. *Circ Res, 93*(2), 96-105. doi:10.1161/01.RES.0000082524.34487.31

10. Forstermann, U., & Sessa, W. C. (2012). Nitric oxide synthases: Regulation and function. *Eur Heart J, 33*(7), 829-837, 837a-837d. doi:10.1093/eurheartj/ehr304

11. Koller, K. J., & Goeddel, D. V. (1992). Molecular biology of the natriuretic peptides and their receptors. *Circulation, 86*(4), 1081-1088. doi:10.1161/01.cir.86.4.1081

12. Suga, S., Nakao, K., Hosoda, K., Mukoyama, M., Ogawa, Y., Shirakami, G., … Imura, H. (1992). Receptor selectivity of natriuretic peptide family, atrial natriuretic peptide, brain natriuretic peptide, and C-type natriuretic peptide. *Endocrinology, 130*(1), 229-239. doi:10.1210/endo.130.1.1309330

13. Biel, M., & Michalakis, S. (2009). Cyclic nucleotide-gated channels. *Handb Exp Pharmacol*(191), 111-136. doi:10.1007/978-3-540-68964-5_7

14. Hofmann, F., Feil, R., Kleppisch, T., & Schlossmann, J. (2006). Function of cGMP-dependent protein kinases as revealed by gene deletion. *Physiol Rev, 86*(1), 1-23. doi:10.1152/physrev.00015.2005

15. Bender, A. T., & Beavo, J. A. (2006). Cyclic nucleotide phosphodiesterases: Molecular regulation to clinical use. *Pharmacol Rev, 58*(3), 488-520. doi:10.1124/pr.58.3.5

16. Francis, S. H., Blount, M. A., & Corbin, J. D. (2011). Mammalian cyclic nucleotide phosphodiesterases: Molecular mechanisms and physiological functions. *Physiol Rev, 91*(2), 651-690. doi:10.1152/physrev.00030.2010

17. Krawutschke, C., Koesling, D., & Russwurm, M. (2015). Cyclic GMP in vascular relaxation: Export is of similar importance as degradation. *Arterioscler Thromb Vasc Biol, 35*(9), 2011-2019. doi:10.1161/ATVBAHA.115.306133

18. Dazert, P., Meissner, K., Vogelgesang, S., Heydrich, B., Eckel, L., Bohm, M., … Kroemer, H. K. (2003). Expression and localization of the multidrug resistance protein 5 (MRP5/ABCC5), a cellular export pump for cyclic nucleotides, in human heart. *Am J Pathol, 163*(4), 1567-1577. doi:10.1016/S0002-9440(10)63513-4

19. Sinha, C., Ren, A., Arora, K., Moon, C. S., Yarlagadda, S., Zhang, W., … Naren, A. P. (2013). Multi-drug resistance protein 4 (MRP4)-mediated regulation of fibroblast cell migration reflects a dichotomous role of intracellular cyclic nucleotides. *J Biol Chem, 288*(6), 3786-3794. doi:10.1074/jbc.M112.435925

20. Friebe, A., Sandner, P., & Schmidtko, A. (2017). Meeting report of the 8(th) international conference on cGMP "cGMP: Generators, effectors, and therapeutic implications" at Bamberg, Germany, from june 23 to 25, 2017. *Naunyn Schmiedebergs Arch Pharmacol, 390*(12), 1177-1188. doi:10.1007/s00210-017-1429-5

21. Bentzon, J. F., & Falk, E. (2010). Atherosclerotic lesions in mouse and man: Is it the same disease? *Curr Opin Lipidol, 21*(5), 434-440. doi:10.1097/MOL.0b013e32833ded6a

22. Antl, M., von Bruhl, M. L., Eiglsperger, C., Werner, M., Konrad, I., Kocher, T., … Schlossmann, J. (2007). IRAG mediates NO/cGMP-dependent inhibition of platelet aggregation and thrombus formation. *Blood, 109*(2), 552-559. doi:10.1182/blood-2005-10-026294

23. Young, J. M., Waters, H., Dong, C., Fulle, H. J., & Liman, E. R. (2007). Degeneration of the olfactory guanylyl cyclase D gene during primate evolution. *PLoS One, 2*(9), e884. doi:10.1371/journal.pone.0000884

24. Feil, R., Lehners, M., Stehle, D., & Feil, S. (2021). Visualising and understanding cGMP signals in the cardiovascular system. *Br J Pharmacol*doi:10.1111/bph.15500

25. Murrell, W. (1879). Nitro-glycerine as a remedy for angina pectoris. *The Lancet, 113*(2890), 80-81. doi:10.1016/S0140-6736(02)46032-1

26. Shamloul, R., & Ghanem, H. (2013). Erectile dysfunction. *Lancet, 381*(9861), 153-165. doi:10.1016/S0140-6736(12)60520-0

27. Friebe, A., Sandner, P., & Schmidtko, A. (2020). cGMP: A unique 2nd messenger molecule - recent developments in cGMP research and development. *Naunyn Schmiedebergs Arch Pharmacol, 393*(2), 287-302. doi:10.1007/s00210-019-01779-z

28. Sandner, P. (2018). From molecules to patients: Exploring the therapeutic role of soluble guanylate cyclase stimulators. *Biol Chem, 399*(7), 679-690. doi:10.1515/hsz-2018-0155

29. Ghofrani, H. A., Galie, N., Grimminger, F., Grunig, E., Humbert, M., Jing, Z. C., … Group, P.-S. (2013). Riociguat for the treatment of pulmonary arterial hypertension. *N Engl J Med, 369*(4), 330-340. doi:10.1056/NEJMoa1209655

30. EMA (2015). Entresto. Available from https://www.ema.europa.eu/en/medicines/human/EPAR/entresto (accessed 2021/05/07 2021)

31. McMurray, J. J., Packer, M., Desai, A. S., Gong, J., Lefkowitz, M. P., Rizkala, A. R., … Committees. (2014). Angiotensin-neprilysin inhibition versus enalapril in heart failure. *N Engl J Med, 371*(11), 993-1004. doi:10.1056/NEJMoa1409077

32. Feygina, E. E., Katrukha, A. G., & Semenov, A. G. (2019). Neutral endopeptidase (neprilysin) in therapy and diagnostics: Yin and yang. *Biochemistry (Mosc), 84*(11), 1346-1358. doi:10.1134/S0006297919110105

33. Savarirayan, R., Irving, M., Bacino, C. A., Bostwick, B., Charrow, J., Cormier-Daire, V., … Hoover-Fong, J. (2019). C-type natriuretic peptide analogue therapy in children with achondroplasia. *N Engl J Med, 381*(1), 25-35. doi:10.1056/NEJMoa1813446

34. Savarirayan, R., Tofts, L., Irving, M., Wilcox, W., Bacino, C. A., Hoover-Fong, J., … Day, J. (2020). Once-daily, subcutaneous vosoritide therapy in children with achondroplasia: A randomised, double-blind, phase 3, placebo-controlled, multicentre trial. *Lancet, 396*(10252), 684-692. doi:10.1016/S0140-6736(20)31541-5

35. Duggan, S. (2021). Vosoritide: First approval. *Drugs, 81*(17), 2057-2062. doi:10.1007/s40265-021-01623-w

36. Baillie, G. S., Tejeda, G. S., & Kelly, M. P. (2019). Therapeutic targeting of 3',5'-cyclic nucleotide phosphodiesterases: Inhibition and beyond. *Nat Rev Drug Discov, 18*(10), 770-796. doi:10.1038/s41573-019-0033-4

37. Holtwick, R., Gotthardt, M., Skryabin, B., Steinmetz, M., Potthast, R., Zetsche, B., … Kuhn, M. (2002). Smooth muscle-selective deletion of guanylyl cyclase-A prevents the acute but not chronic effects of ANP on blood pressure. *Proc Natl Acad Sci U S A, 99*(10), 7142-7147. doi:10.1073/pnas.102650499

38. Nakao, K., Kuwahara, K., Nishikimi, T., Nakagawa, Y., Kinoshita, H., Minami, T., … Nakao, K. (2017). Endothelium-derived C-type natriuretic peptide contributes to blood pressure regulation by maintaining endothelial integrity. *Hypertension, 69*(2), 286-296. doi:10.1161/HYPERTENSIONAHA.116.08219

39. Groneberg, D., Konig, P., Wirth, A., Offermanns, S., Koesling, D., & Friebe, A. (2010). Smooth muscle-specific deletion of nitric oxide-sensitive guanylyl cyclase is sufficient to induce hypertension in mice. *Circulation, 121*(3), 401-409. doi:10.1161/CIRCULATIONAHA.109.890962

40. Weber, S., Bernhard, D., Lukowski, R., Weinmeister, P., Worner, R., Wegener, J. W., … Feil, R. (2007). Rescue of cGMP kinase I knockout mice by smooth muscle specific expression of either isozyme. *Circ Res, 101*(11), 1096-1103. doi:10.1161/CIRCRESAHA.107.154351

41. Tao, H., Zhang, L. M., Castresana, M. R., Shillcutt, S. D., & Newman, W. H. (1995). C-natriuretic peptide but not atrial natriuretic peptide increases cyclic GMP in cerebral arterial smooth muscle cells. *Life Sci, 56*(26), 2357-2365. doi:10.1016/0024-3205(95)00229-y

42. Hall, C. N., & Garthwaite, J. (2009). What is the real physiological NO concentration in vivo? *Nitric Oxide, 21*(2), 92-103. doi:10.1016/j.niox.2009.07.002

43. Costa, E. D., Rezende, B. A., Cortes, S. F., & Lemos, V. S. (2016). Neuronal nitric oxide synthase in vascular physiology and diseases. *Front Physiol, 7*, 206. doi:10.3389/fphys.2016.00206

44. Pautz, A., Art, J., Hahn, S., Nowag, S., Voss, C., & Kleinert, H. (2010). Regulation of the expression of inducible nitric oxide synthase. *Nitric Oxide, 23*(2), 75-93. doi:10.1016/j.niox.2010.04.007

45. Geller, D. A., & Billiar, T. R. (1998). Molecular biology of nitric oxide synthases. *Cancer Metastasis Rev, 17*(1), 7-23. doi:10.1023/a:1005940202801

46. Stuehr, D. J., Santolini, J., Wang, Z. Q., Wei, C. C., & Adak, S. (2004). Update on mechanism and catalytic regulation in the NO synthases. *J Biol Chem, 279*(35), 36167-36170. doi:10.1074/jbc.R400017200

47. Budworth, J., Meillerais, S., Charles, I., & Powell, K. (1999). Tissue distribution of the human soluble guanylate cyclases. *Biochem Biophys Res Commun, 263*(3), 696-701. doi:10.1006/bbrc.1999.1444

48. Koesling, D., Mergia, E., & Russwurm, M. (2016). Physiological functions of NO-sensitive guanylyl cyclase isoforms. *Curr Med Chem, 23*(24), 2653-2665. doi:10.2174/0929867323666160812145050

49. Harteneck, C., Wedel, B., Koesling, D., Malkewitz, J., Bohme, E., & Schultz, G. (1991). Molecular cloning and expression of a new alpha-subunit of soluble guanylyl cyclase. Interchangeability of the alpha-subunits of the enzyme. *FEBS Lett, 292*(1-2), 217-222. doi:10.1016/0014-5793(91)80871-y

50. Russwurm, M., Behrends, S., Harteneck, C., & Koesling, D. (1998). Functional properties of a naturally occurring isoform of soluble guanylyl cyclase. *Biochem J, 335 (Pt 1)*, 125-130. doi:10.1042/bj3350125

51. Mergia, E., Friebe, A., Dangel, O., Russwurm, M., & Koesling, D. (2006). Spare guanylyl cyclase NO receptors ensure high NO sensitivity in the vascular system. *J Clin Invest, 116*(6), 1731-1737. doi:10.1172/JCI27657

52. Wen, L., Feil, S., Wolters, M., Thunemann, M., Regler, F., Schmidt, K., … Feil, R. (2018). A shear-dependent NO-cGMP-cGKI cascade in platelets acts as an auto-regulatory brake of thrombosis. *Nat Commun, 9*(1), 4301. doi:10.1038/s41467-018-06638-8

53. Friebe, A., Mergia, E., Dangel, O., Lange, A., & Koesling, D. (2007). Fatal gastrointestinal obstruction and hypertension in mice lacking nitric oxide-sensitive guanylyl cyclase. *Proc Natl Acad Sci U S A, 104*(18), 7699-7704. doi:10.1073/pnas.0609778104

54. Lehners, M., Dobrowinski, H., Feil, S., & Feil, R. (2018). cGMP signaling and vascular smooth muscle cell plasticity. *J Cardiovasc Dev Dis, 5*(2), 20. doi:10.3390/jcdd5020020

55. Segura-Puimedon, M., Mergia, E., Al-Hasani, J., Aherrahrou, R., Stoelting, S., Kremer, F., … Aherrahrou, Z. (2016). Proatherosclerotic effect of the alpha1-subunit of soluble guanylyl cyclase by promoting smooth muscle phenotypic switching. *Am J Pathol, 186*(8), 2220-2231. doi:10.1016/j.ajpath.2016.04.010

56. Kuhlencordt, P. J., Gyurko, R., Han, F., Scherrer-Crosbie, M., Aretz, T. H., Hajjar, R., … Huang, P. L. (2001). Accelerated atherosclerosis, aortic aneurysm formation, and ischemic heart disease in apolipoprotein E/endothelial nitric oxide synthase double-knockout mice. *Circulation, 104*(4), 448-454. doi:10.1161/hc2901.091399

57. Moroi, M., Zhang, L., Yasuda, T., Virmani, R., Gold, H. K., Fishman, M. C., & Huang, P. L. (1998). Interaction of genetic deficiency of endothelial nitric oxide, gender, and pregnancy in vascular response to injury in mice. *J Clin Invest, 101*(6), 1225-1232. doi:10.1172/JCI1293

58. Yogo, K., Shimokawa, H., Funakoshi, H., Kandabashi, T., Miyata, K., Okamoto, S., … Takeshita, A. (2000). Different vasculoprotective roles of NO synthase isoforms in vascular lesion formation in mice. *Arterioscler Thromb Vasc Biol, 20*(11), E96-E100. doi:10.1161/01.atv.20.11.e96

59. Kuhlencordt, P. J., Hotten, S., Schodel, J., Rutzel, S., Hu, K., Widder, J., … Ertl, G. (2006). Atheroprotective effects of neuronal nitric oxide synthase in apolipoprotein e knockout mice. *Arterioscler Thromb Vasc Biol, 26*(7), 1539-1544. doi:10.1161/01.ATV.0000223143.88128.19

60. Morishita, T., Tsutsui, M., Shimokawa, H., Horiuchi, M., Tanimoto, A., Suda, O., … Nakashima, Y. (2002). Vasculoprotective roles of neuronal nitric oxide synthase. *FASEB J, 16*(14), 1994-1996. doi:10.1096/fj.02-0155fje

61. Detmers, P. A., Hernandez, M., Mudgett, J., Hassing, H., Burton, C., Mundt, S., … Pure, E. (2000). Deficiency in inducible nitric oxide synthase results in reduced atherosclerosis in apolipoprotein E-deficient mice. *J Immunol, 165*(6), 3430-3435. doi:10.4049/jimmunol.165.6.3430

62. Vermeersch, P., Buys, E., Sips, P., Pokreisz, P., Marsboom, G., Gillijns, H., … Janssens, S. (2009). Gender-specific modulation of the response to arterial injury by soluble guanylate cyclase alpha1. *Open Cardiovasc Med J, 3*, 98-104. doi:10.2174/1874192400903010098

63. Fernando, V., Zheng, X., Walia, Y., Sharma, V., Letson, J., & Furuta, S. (2019). S-nitrosylation: An emerging paradigm of redox signaling. *Antioxidants (Basel), 8*(9). doi:10.3390/antiox8090404

64. Nishikimi, T., Kuwahara, K., & Nakao, K. (2011). Current biochemistry, molecular biology, and clinical relevance of natriuretic peptides. *J Cardiol, 57*(2), 131-140. doi:10.1016/j.jjcc.2011.01.002

65. Wu, C., Wu, F., Pan, J., Morser, J., & Wu, Q. (2003). Furin-mediated processing of pro-C-type natriuretic peptide. *J Biol Chem, 278*(28), 25847-25852. doi:10.1074/jbc.M301223200

66. Potter, L. R., Yoder, A. R., Flora, D. R., Antos, L. K., & Dickey, D. M. (2009). Natriuretic peptides: Their structures, receptors, physiologic functions and therapeutic applications. *Handb Exp Pharmacol*(191), 341-366. doi:10.1007/978-3-540-68964-5_15

67. Steinhelper, M. E. (1993). Structure, expression, and genomic mapping of the mouse natriuretic peptide type-B gene. *Circ Res, 72*(5), 984-992. doi:10.1161/01.res.72.5.984

68. Yeung, V. T., Ho, S. K., Nicholls, M. G., & Cockram, C. S. (1996). Binding of CNP-22 and CNP-53 to cultured mouse astrocytes and effects on cyclic GMP. *Peptides, 17*(1), 101-106. doi:10.1016/0196-9781(95)02099-3

69. Goetze, J. P., Bruneau, B. G., Ramos, H. R., Ogawa, T., de Bold, M. K., & de Bold, A. J. (2020). Cardiac natriuretic peptides. *Nat Rev Cardiol, 17*(11), 698-717. doi:10.1038/s41569-020-0381-0

70. Ogawa, T., & de Bold, A. J. (2014). The heart as an endocrine organ. *Endocr Connect, 3*(2), R31-44. doi:10.1530/EC-14-0012

71. Moyes, A. J., & Hobbs, A. J. (2019). C-type natriuretic peptide: A multifaceted paracrine regulator in the heart and vasculature. *Int J Mol Sci, 20*(9). doi:10.3390/ijms20092281

72. Prickett, T. C., & E, A. E. (2020). Circulating products of C-type natriuretic peptide and links with organ function in health and disease. *Peptides, 132*, 170363. doi:10.1016/j.peptides.2020.170363

73. Sellitti, D. F., Koles, N., & Mendonca, M. C. (2011). Regulation of C-type natriuretic peptide expression. *Peptides, 32*(9), 1964-1971. doi:10.1016/j.peptides.2011.07.013

74. Zhang, Z., Xiao, Z., & Diamond, S. L. (1999). Shear stress induction of C-type natriuretic peptide (CNP) in endothelial cells is independent of NO autocrine signaling. *Ann Biomed Eng, 27*(4), 419-426. doi:10.1114/1.203

75. Chun, T. H., Itoh, H., Ogawa, Y., Tamura, N., Takaya, K., Igaki, T., … Nakao, K. (1997). Shear stress augments expression of C-type natriuretic peptide and adrenomedullin. *Hypertension, 29*(6), 1296-1302. doi:10.1161/01.hyp.29.6.1296

76. Suga, S., Itoh, H., Komatsu, Y., Ogawa, Y., Hama, N., Yoshimasa, T., & Nakao, K. (1993). Cytokine-induced C-type natriuretic peptide (CNP) secretion from vascular endothelial cells--evidence for CNP as a novel autocrine/paracrine regulator from endothelial cells. *Endocrinology, 133*(6), 3038-3041. doi:10.1210/endo.133.6.8243333

77. Stingo, A. J., Clavell, A. L., Heublein, D. M., Wei, C. M., Pittelkow, M. R., & Burnett, J. C., Jr. (1992). Presence of C-type natriuretic peptide in cultured human endothelial cells and plasma. *Am J Physiol, 263*(4 Pt 2), H1318-1321. doi:10.1152/ajpheart.1992.263.4.H1318

78. Horio, T., Tokudome, T., Maki, T., Yoshihara, F., Suga, S., Nishikimi, T., … Kangawa, K. (2003). Gene expression, secretion, and autocrine action of C-type natriuretic peptide in cultured adult rat cardiac fibroblasts. *Endocrinology, 144*(6), 2279-2284. doi:10.1210/en.2003-0128

79. Kelsall, C. J., Chester, A. H., Sarathchandra, P., & Singer, D. R. (2006). Expression and localization of C-type natriuretic peptide in human vascular smooth muscle cells. *Vascul Pharmacol, 45*(6), 368-373. doi:10.1016/j.vph.2006.06.011

80. Mendonca, M. C., Koles, N., Doi, S. Q., & Sellitti, D. F. (2010). Transforming growth factor-beta1 regulation of C-type natriuretic peptide expression in human vascular smooth muscle cells: Dependence on TSC22D1. *Am J Physiol Heart Circ Physiol, 299*(6), H2018-2027. doi:10.1152/ajpheart.00656.2010

81. Woodard, G. E., Rosado, J. A., & Brown, J. (2002). Expression and control of C-type natriuretic peptide in rat vascular smooth muscle cells. *Am J Physiol Regul Integr Comp Physiol, 282*(1), R156-165. doi:10.1152/ajpregu.2002.282.1.R156

82. Moyes, A. J., Chu, S. M., Aubdool, A. A., Dukinfield, M. S., Margulies, K. B., Bedi, K. C., … Hobbs, A. J. (2020). C-type natriuretic peptide co-ordinates cardiac structure and function. *Eur Heart J, 41*(9), 1006-1020. doi:10.1093/eurheartj/ehz093

83. Moyes, A. J., Khambata, R. S., Villar, I., Bubb, K. J., Baliga, R. S., Lumsden, N. G., … Hobbs, A. J. (2014). Endothelial C-type natriuretic peptide maintains vascular homeostasis. *J Clin Invest, 124*(9), 4039-4051. doi:10.1172/JCI74281

84. Nussenzveig, D. R., Lewicki, J. A., & Maack, T. (1990). Cellular mechanisms of the clearance function of type C receptors of atrial natriuretic factor. *J Biol Chem, 265*(34), 20952-20958. doi:10.1016/S0021-9258(17)45309-9

85. Matsukawa, N., Grzesik, W. J., Takahashi, N., Pandey, K. N., Pang, S., Yamauchi, M., & Smithies, O. (1999). The natriuretic peptide clearance receptor locally modulates the physiological effects of the natriuretic peptide system. *Proc Natl Acad Sci U S A, 96*(13), 7403-7408. doi:10.1073/pnas.96.13.7403

86. Anand-Srivastava, M. B. (2005). Natriuretic peptide receptor-C signaling and regulation. *Peptides, 26*(6), 1044-1059. doi:10.1016/j.peptides.2004.09.023

87. Murthy, K. S., & Makhlouf, G. M. (1999). Identification of the G protein-activating domain of the natriuretic peptide clearance receptor (NPR-C). *J Biol Chem, 274*(25), 17587-17592. doi:10.1074/jbc.274.25.17587

88. Bennett, B. D., Bennett, G. L., Vitangcol, R. V., Jewett, J. R., Burnier, J., Henzel, W., & Lowe, D. G. (1991). Extracellular domain-IgG fusion proteins for three human natriuretic peptide receptors. Hormone pharmacology and application to solid phase screening of synthetic peptide antisera. *J Biol Chem, 266*(34), 23060-23067. doi:10.1016/S0021-9258(18)54463-X

89. Potter, L. R., & Hunter, T. (1998). Phosphorylation of the kinase homology domain is essential for activation of the A-type natriuretic peptide receptor. *Mol Cell Biol, 18*(4), 2164-2172. doi:10.1128/MCB.18.4.2164

90. Potter, L. R. (1998). Phosphorylation-dependent regulation of the guanylyl cyclase-linked natriuretic peptide receptor B: Dephosphorylation is a mechanism of desensitization. *Biochemistry, 37*(8), 2422-2429. doi:10.1021/bi972303k

91. Potter, L. R., & Garbers, D. L. (1992). Dephosphorylation of the guanylyl cyclase-A receptor causes desensitization. *J Biol Chem, 267*(21), 14531-14534. doi:10.1016/S0021-9258(18)42069-8

92. Potter, L. R., & Hunter, T. (1998). Identification and characterization of the major phosphorylation sites of the B-type natriuretic peptide receptor. *J Biol Chem, 273*(25), 15533-15539. doi:10.1074/jbc.273.25.15533

93. Shuhaibar, L. C., Egbert, J. R., Edmund, A. B., Uliasz, T. F., Dickey, D. M., Yee, S. P., … Jaffe, L. A. (2016). Dephosphorylation of juxtamembrane serines and threonines of the NPR2 guanylyl cyclase is required for rapid resumption of oocyte meiosis in response to luteinizing hormone. *Dev Biol, 409*(1), 194-201. doi:10.1016/j.ydbio.2015.10.025

94. Wagner, B. M., Robinson, J. W., Lin, Y. W., Lee, Y. C., Kaci, N., Legeai-Mallet, L., & Potter, L. R. (2021). Prevention of guanylyl cyclase-B dephosphorylation rescues achondroplastic dwarfism. *JCI Insight, 6*(9). doi:10.1172/jci.insight.147832

95. Sabrane, K., Kruse, M. N., Fabritz, L., Zetsche, B., Mitko, D., Skryabin, B. V., … Kuhn, M. (2005). Vascular endothelium is critically involved in the hypotensive and hypovolemic actions of atrial natriuretic peptide. *J Clin Invest, 115*(6), 1666-1674. doi:10.1172/JCI23360

96. Nakao, K., Osawa, K., Yasoda, A., Yamanaka, S., Fujii, T., Kondo, E., … Nakao, K. (2015). The local CNP/GC-B system in growth plate is responsible for physiological endochondral bone growth. *Sci Rep, 5*, 10554. doi:10.1038/srep10554

97. Tamura, N., Doolittle, L. K., Hammer, R. E., Shelton, J. M., Richardson, J. A., & Garbers, D. L. (2004). Critical roles of the guanylyl cyclase B receptor in endochondral ossification and development of female reproductive organs. *Proc Natl Acad Sci U S A, 101*(49), 17300-17305. doi:10.1073/pnas.0407894101

98. Potter, L. R., Abbey-Hosch, S., & Dickey, D. M. (2006). Natriuretic peptides, their receptors, and cyclic guanosine monophosphate-dependent signaling functions. *Endocr Rev, 27*(1), 47-72. doi:10.1210/er.2005-0014

99. Spiranec, K., Chen, W., Werner, F., Nikolaev, V. O., Naruke, T., Koch, F., … Kuhn, M. (2018). Endothelial C-type natriuretic peptide acts on pericytes to regulate microcirculatory flow and blood pressure. *Circulation, 138*(5), 494-508. doi:10.1161/CIRCULATIONAHA.117.033383

100. Villar, I. C., Panayiotou, C. M., Sheraz, A., Madhani, M., Scotland, R. S., Nobles, M., … Hobbs, A. J. (2007). Definitive role for natriuretic peptide receptor-C in mediating the vasorelaxant activity of C-type natriuretic peptide and endothelium-derived hyperpolarising factor. *Cardiovasc Res, 74*(3), 515-525. doi:10.1016/j.cardiores.2007.02.032

101. Madhani, M., Scotland, R. S., MacAllister, R. J., & Hobbs, A. J. (2003). Vascular natriuretic peptide receptor-linked particulate guanylate cyclases are modulated by nitric oxide-cyclic GMP signalling. *Br J Pharmacol, 139*(7), 1289-1296. doi:10.1038/sj.bjp.0705365

102. Zhang, L., Bouadjel, K., Manoury, B., Vandecasteele, G., Fischmeister, R., & Leblais, V. (2019). Cyclic nucleotide signalling compartmentation by PDEs in cultured vascular smooth muscle cells. *Br J Pharmacol, 176*(11), 1780-1792. doi:10.1111/bph.14651

103. Khambata, R. S., Panayiotou, C. M., & Hobbs, A. J. (2011). Natriuretic peptide receptor-3 underpins the disparate regulation of endothelial and vascular smooth muscle cell proliferation by C-type natriuretic peptide. *Br J Pharmacol, 164*(2b), 584-597. doi:10.1111/j.1476-5381.2011.01400.x

104. Lopez, M. J., Wong, S. K., Kishimoto, I., Dubois, S., Mach, V., Friesen, J., … Beuve, A. (1995). Salt-resistant hypertension in mice lacking the guanylyl cyclase-A receptor for atrial natriuretic peptide. *Nature, 378*(6552), 65-68. doi:10.1038/378065a0

105. Angelis, E., Tse, M. Y., & Pang, S. C. (2005). Interactions between atrial natriuretic peptide and the renin-angiotensin system during salt-sensitivity exhibited by the proanp gene-disrupted mouse. *Mol Cell Biochem, 276*(1-2), 121-131. doi:10.1007/s11010-005-3672-1

106. Chusho, H., Tamura, N., Ogawa, Y., Yasoda, A., Suda, M., Miyazawa, T., … Nakao, K. (2001). Dwarfism and early death in mice lacking C-type natriuretic peptide. *Proc Natl Acad Sci U S A, 98*(7), 4016-4021. doi:10.1073/pnas.071389098

107. Bubb, K. J., Aubdool, A. A., Moyes, A. J., Lewis, S., Drayton, J. P., Tang, O., … Hobbs, A. J. (2019). Endothelial C-type natriuretic peptide is a critical regulator of angiogenesis and vascular remodeling. *Circulation, 139*(13), 1612-1628. doi:10.1161/CIRCULATIONAHA.118.036344

108. Steinmetz, M., Potthast, R., Sabrane, K., & Kuhn, M. (2004). Diverging vasorelaxing effects of C-type natriuretic peptide in renal resistance arteries and aortas of GC-A-deficient mice. *Regul Pept, 119*(1-2), 31-37. doi:10.1016/j.regpep.2003.12.005

109. Leung, Y. K., Du, J., Huang, Y., & Yao, X. (2010). Cyclic nucleotide-gated channels contribute to thromboxane a2-induced contraction of rat small mesenteric arteries. *PLoS One, 5*(6), e11098. doi:10.1371/journal.pone.0011098

110. Yao, X., Leung, P. S., Kwan, H. Y., Wong, T. P., & Fong, M. W. (1999). Rod-type cyclic nucleotide-gated cation channel is expressed in vascular endothelium and vascular smooth muscle cells. *Cardiovasc Res, 41*(1), 282-290. doi:10.1016/s0008-6363(98)00158-8

111. Vaandrager, A. B., Hogema, B. M., & de Jonge, H. R. (2005). Molecular properties and biological functions of cGMP-dependent protein kinase II. *Front Biosci, 10*, 2150-2164. doi:10.2741/1687

112. Wernet, W., Flockerzi, V., & Hofmann, F. (1989). The cDNA of the two isoforms of bovine cGMP-dependent protein kinase. *FEBS Lett, 251*(1-2), 191-196. doi:10.1016/0014-5793(89)81453-x

113. Sandberg, M., Natarajan, V., Ronander, I., Kalderon, D., Walter, U., Lohmann, S. M., & Jahnsen, T. (1989). Molecular cloning and predicted full-length amino acid sequence of the type I beta isozyme of cGMP-dependent protein kinase from human placenta. Tissue distribution and developmental changes in rat. *FEBS Lett, 255*(2), 321-329. doi:10.1016/0014-5793(89)81114-7

114. Richie-Jannetta, R., Francis, S. H., & Corbin, J. D. (2003). Dimerization of cGMP-dependent protein kinase Ibeta is mediated by an extensive amino-terminal leucine zipper motif, and dimerization modulates enzyme function. *J Biol Chem, 278*(50), 50070-50079. doi:10.1074/jbc.M306796200

115. Ammendola, A., Geiselhoringer, A., Hofmann, F., & Schlossmann, J. (2001). Molecular determinants of the interaction between the inositol 1,4,5-trisphosphate receptor-associated cGMP kinase substrate (IRAG) and cGMP kinase Ibeta. *J Biol Chem, 276*(26), 24153-24159. doi:10.1074/jbc.M101530200

116. Surks, H. K., Mochizuki, N., Kasai, Y., Georgescu, S. P., Tang, K. M., Ito, M., … Mendelsohn, M. E. (1999). Regulation of myosin phosphatase by a specific interaction with cGMP- dependent protein kinase Ialpha. *Science, 286*(5444), 1583-1587. doi:10.1126/science.286.5444.1583

117. Ruth, P., Landgraf, W., Keilbach, A., May, B., Egleme, C., & Hofmann, F. (1991). The activation of expressed cGMP-dependent protein kinase isozymes I alpha and I beta is determined by the different amino-termini. *Eur J Biochem, 202*(3), 1339-1344. doi:10.1111/j.1432-1033.1991.tb16509.x

118. Ruth, P., Pfeifer, A., Kamm, S., Klatt, P., Dostmann, W. R., & Hofmann, F. (1997). Identification of the amino acid sequences responsible for high affinity activation of cGMP kinase Ialpha. *J Biol Chem, 272*(16), 10522-10528. doi:10.1074/jbc.272.16.10522

119. Geiselhoringer, A., Gaisa, M., Hofmann, F., & Schlossmann, J. (2004). Distribution of IRAG and cGKI-isoforms in murine tissues. *FEBS Lett, 575*(1-3), 19-22. doi:10.1016/j.febslet.2004.08.030

120. Surks, H. K. (2007). cGMP-dependent protein kinase I and smooth muscle relaxation: A tale of two isoforms. *Circ Res, 101*(11), 1078-1080. doi:10.1161/CIRCRESAHA.107.165779

121. Morgado, M., Cairrao, E., Santos-Silva, A. J., & Verde, I. (2012). Cyclic nucleotide-dependent relaxation pathways in vascular smooth muscle. *Cell Mol Life Sci, 69*(2), 247-266. doi:10.1007/s00018-011-0815-2

122. Webb, R. C. (2003). Smooth muscle contraction and relaxation. *Adv Physiol Educ, 27*(1-4), 201-206. doi:10.1152/advan.00025.2003

123. Weinmeister, P., Lukowski, R., Linder, S., Traidl-Hoffmann, C., Hengst, L., Hofmann, F., & Feil, R. (2008). Cyclic guanosine monophosphate-dependent protein kinase I promotes adhesion of primary vascular smooth muscle cells. *Mol Biol Cell, 19*(10), 4434-4441. doi:10.1091/mbc.E08-04-0370

124. Wolfsgruber, W., Feil, S., Brummer, S., Kuppinger, O., Hofmann, F., & Feil, R. (2003). A proatherogenic role for cGMP-dependent protein kinase in vascular smooth muscle cells. *Proc Natl Acad Sci U S A, 100*(23), 13519-13524. doi:10.1073/pnas.1936024100

125. Koeppen, M., Feil, R., Siegl, D., Feil, S., Hofmann, F., Pohl, U., & de Wit, C. (2004). cGMP-dependent protein kinase mediates NO- but not acetylcholine-induced dilations in resistance vessels in vivo. *Hypertension, 44*(6), 952-955. doi:10.1161/01.HYP.0000147661.80059.ca

126. Pfeifer, A., Klatt, P., Massberg, S., Ny, L., Sausbier, M., Hirneiss, C., … Hofmann, F. (1998). Defective smooth muscle regulation in cGMP kinase I-deficient mice. *EMBO J, 17*(11), 3045-3051. doi:10.1093/emboj/17.11.3045

127. Sausbier, M., Schubert, R., Voigt, V., Hirneiss, C., Pfeifer, A., Korth, M., … Hofmann, F. (2000). Mechanisms of NO/cGMP-dependent vasorelaxation. *Circ Res, 87*(9), 825-830. doi:10.1161/01.res.87.9.825

128. Yamahara, K., Itoh, H., Chun, T. H., Ogawa, Y., Yamashita, J., Sawada, N., … Nakao, K. (2003). Significance and therapeutic potential of the natriuretic peptides/cGMP/cGMP-dependent protein kinase pathway in vascular regeneration. *Proc Natl Acad Sci U S A, 100*(6), 3404-3409. doi:10.1073/pnas.0538059100

129. Aicher, A., Heeschen, C., Feil, S., Hofmann, F., Mendelsohn, M. E., Feil, R., & Dimmeler, S. (2009). cGMP-dependent protein kinase I is crucial for angiogenesis and postnatal vasculogenesis. *PLoS One, 4*(3), e4879. doi:10.1371/journal.pone.0004879

130. Lukowski, R., Weinmeister, P., Bernhard, D., Feil, S., Gotthardt, M., Herz, J., … Feil, R. (2008). Role of smooth muscle cGMP/cGKI signaling in murine vascular restenosis. *Arterioscler Thromb Vasc Biol, 28*(7), 1244-1250. doi:10.1161/ATVBAHA.108.166405

131. Luo, L., Zhang, Y., Hsu, C., Korshunov, V. A., Long, X., Knight, P. A., … Yan, C. (2021). Role of PDE10A in vascular smooth muscle cell hyperplasia and pathological vascular remodeling. *Cardiovasc Res.* doi:10.1093/cvr/cvab304

132. Aizawa, T., Wei, H., Miano, J. M., Abe, J., Berk, B. C., & Yan, C. (2003). Role of phosphodiesterase 3 in NO/cGMP-mediated antiinflammatory effects in vascular smooth muscle cells. *Circ Res, 93*(5), 406-413. doi:10.1161/01.RES.0000091074.33584.F0

133. Menges, L., Krawutschke, C., Fuchtbauer, E. M., Fuchtbauer, A., Sandner, P., Koesling, D., & Russwurm, M. (2019). Mind the gap (junction): cGMP induced by nitric oxide in cardiac myocytes originates from cardiac fibroblasts. *Br J Pharmacol, 176*(24), 4696-4707. doi:10.1111/bph.14835

134. Shuhaibar, L. C., Egbert, J. R., Norris, R. P., Lampe, P. D., Nikolaev, V. O., Thunemann, M., … Jaffe, L. A. (2015). Intercellular signaling via cyclic GMP diffusion through gap junctions restarts meiosis in mouse ovarian follicles. *Proc Natl Acad Sci U S A, 112*(17), 5527-5532. doi:10.1073/pnas.1423598112

135. Graham, D. (2019). Vascular physiology. In R. M. Touyz & C. Delles (Eds.), *Textbook of vascular medicine*, (pp. 13-22). Cham: Springer International Publishing.

136. Pugsley, M. K., & Tabrizchi, R. (2000). The vascular system. An overview of structure and function. *J Pharmacol Toxicol Methods, 44*(2), 333-340. doi:10.1016/s1056-8719(00)00125-8

137. Wagenseil, J. E., & Mecham, R. P. (2009). Vascular extracellular matrix and arterial mechanics. *Physiol Rev, 89*(3), 957-989. doi:10.1152/physrev.00041.2008

138. Stenmark, K. R., Yeager, M. E., El Kasmi, K. C., Nozik-Grayck, E., Gerasimovskaya, E. V., Li, M., … Frid, M. G. (2013). The adventitia: Essential regulator of vascular wall structure and function. *Annu Rev Physiol, 75*, 23-47. doi:10.1146/annurev-physiol-030212-183802

139. Mazurek, R., Dave, J. M., Chandran, R. R., Misra, A., Sheikh, A. Q., & Greif, D. M. (2017). Vascular cells in blood vessel wall development and disease. *Adv Pharmacol, 78*, 323-350. doi:10.1016/bs.apha.2016.08.001

140. Majesky, M. W. (2007). Developmental basis of vascular smooth muscle diversity. *Arterioscler Thromb Vasc Biol, 27*(6), 1248-1258. doi:10.1161/ATVBAHA.107.141069

141. Dobnikar, L., Taylor, A. L., Chappell, J., Oldach, P., Harman, J. L., Oerton, E., … Jorgensen, H. F. (2018). Disease-relevant transcriptional signatures identified in individual smooth muscle cells from healthy mouse vessels. *Nat Commun, 9*(1), 4567. doi:10.1038/s41467-018-06891-x

142. Stary, H. C., Blankenhorn, D. H., Chandler, A. B., Glagov, S., Insull, W., Jr., Richardson, M., … et al. (1992). A definition of the intima of human arteries and of its atherosclerosis-prone regions. A report from the committee on vascular lesions of the council on arteriosclerosis, american heart association. *Arterioscler Thromb, 12*(1), 120-134. doi:10.1161/01.atv.12.1.120

143. Nakashima, Y., Wight, T. N., & Sueishi, K. (2008). Early atherosclerosis in humans: Role of diffuse intimal thickening and extracellular matrix proteoglycans. *Cardiovasc Res, 79*(1), 14-23. doi:10.1093/cvr/cvn099

144. Owens, G. K., Kumar, M. S., & Wamhoff, B. R. (2004). Molecular regulation of vascular smooth muscle cell differentiation in development and disease. *Physiol Rev, 84*(3), 767-801. doi:10.1152/physrev.00041.2003

145. Carmeliet, P. (2000). Mechanisms of angiogenesis and arteriogenesis. *Nat Med, 6*(4), 389-395. doi:10.1038/74651

146. Bentzon, J. F., & Majesky, M. W. (2018). Lineage tracking of origin and fate of smooth muscle cells in atherosclerosis. *Cardiovasc Res, 114*(4), 492-500. doi:10.1093/cvr/cvx251

147. Marx, S. O., Totary-Jain, H., & Marks, A. R. (2011). Vascular smooth muscle cell proliferation in restenosis. *Circ Cardiovasc Interv, 4*(1), 104-111. doi:10.1161/CIRCINTERVENTIONS.110.957332

148. Chamley-Campbell, J., Campbell, G. R., & Ross, R. (1979). The smooth muscle cell in culture. *Physiol Rev, 59*(1), 1-61. doi:10.1152/physrev.1979.59.1.1

149. Poole, J. C., Cromwell, S. B., & Benditt, E. P. (1971). Behavior of smooth muscle cells and formation of extracellular structures in the reaction of arterial walls to injury. *Am J Pathol, 62*(3), 391-414.

150. Campbell, J. H., & Campbell, G. R. (2012). Smooth muscle phenotypic modulation--a personal experience. *Arterioscler Thromb Vasc Biol, 32*(8), 1784-1789. doi:10.1161/ATVBAHA.111.243212

151. Rensen, S. S., Doevendans, P. A., & van Eys, G. J. (2007). Regulation and characteristics of vascular smooth muscle cell phenotypic diversity. *Neth Heart J, 15*(3), 100-108. doi:10.1007/BF03085963

152. Beamish, J. A., He, P., Kottke-Marchant, K., & Marchant, R. E. (2010). Molecular regulation of contractile smooth muscle cell phenotype: Implications for vascular tissue engineering. *Tissue Eng Part B Rev, 16*(5), 467-491. doi:10.1089/ten.TEB.2009.0630

153. Grootaert, M. O. J., & Bennett, M. R. (2021). Vascular smooth muscle cells in atherosclerosis:Time for a reassessment. *Cardiovasc Res.* doi:10.1093/cvr/cvab046

154. Durham, A. L., Speer, M. Y., Scatena, M., Giachelli, C. M., & Shanahan, C. M. (2018). Role of smooth muscle cells in vascular calcification: Implications in atherosclerosis and arterial stiffness. *Cardiovasc Res, 114*(4), 590-600. doi:10.1093/cvr/cvy010

155. Feil, S., Fehrenbacher, B., Lukowski, R., Essmann, F., Schulze-Osthoff, K., Schaller, M., & Feil, R. (2014). Transdifferentiation of vascular smooth muscle cells to macrophage-like cells during atherogenesis. *Circ Res, 115*(7), 662-667. doi:10.1161/CIRCRESAHA.115.304634

156. Sweeney, H. L., & Hammers, D. W. (2018). Muscle contraction. *Cold Spring Harb Perspect Biol, 10*(2). doi:10.1101/cshperspect.a023200

157. Morgan, K. G., & Gangopadhyay, S. S. (2001). Invited review: Cross-bridge regulation by thin filament-associated proteins. *J Appl Physiol (1985), 91*(2), 953-962. doi:10.1152/jappl.2001.91.2.953

158. Babu, G. J., Warshaw, D. M., & Periasamy, M. (2000). Smooth muscle myosin heavy chain isoforms and their role in muscle physiology. *Microsc Res Tech, 50*(6), 532-540. doi:10.1002/1097-0029(20000915)50:6<532::AID-JEMT10>3.0.CO;2-E

159. van Eys, G. J., Niessen, P. M., & Rensen, S. S. (2007). Smoothelin in vascular smooth muscle cells. *Trends Cardiovasc Med, 17*(1), 26-30. doi:10.1016/j.tcm.2006.11.001

160. Owens, G. K. (1995). Regulation of differentiation of vascular smooth muscle cells. *Physiol Rev, 75*(3), 487-517. doi:10.1152/physrev.1995.75.3.487

161. Liu, R., & Jin, J. P. (2016). Calponin isoforms CNN1, CNN2 and CNN3: Regulators for actin cytoskeleton functions in smooth muscle and non-muscle cells. *Gene, 585*(1), 143-153. doi:10.1016/j.gene.2016.02.040

162. Frid, M. G., Printesva, O. Y., Chiavegato, A., Faggin, E., Scatena, M., Koteliansky, V. E., … Sartore, S. (1993). Myosin heavy-chain isoform composition and distribution in developing and adult human aortic smooth muscle. *J Vasc Res, 30*(5), 279-292. doi:10.1159/000159007

163. Kuro-o, M., Nagai, R., Nakahara, K., Katoh, H., Tsai, R. C., Tsuchimochi, H., … Takaku, F. (1991). cDNA cloning of a myosin heavy chain isoform in embryonic smooth muscle and its expression during vascular development and in arteriosclerosis. *J Biol Chem, 266*(6), 3768-3773. doi:10.1016/S0021-9258(19)67861-0

164. Neuville, P., Geinoz, A., Benzonana, G., Redard, M., Gabbiani, F., Ropraz, P., & Gabbiani, G. (1997). Cellular retinol-binding protein-1 is expressed by distinct subsets of rat arterial smooth muscle cells in vitro and in vivo. *Am J Pathol, 150*(2), 509-521.

165. Kocher, O., & Gabbiani, G. (1986). Cytoskeletal features of normal and atheromatous human arterial smooth muscle cells. *Hum Pathol, 17*(9), 875-880. doi:10.1016/s0046-8177(86)80637-2

166. Kocher, O., Gabbiani, F., Gabbiani, G., Reidy, M. A., Cokay, M. S., Peters, H., & Huttner, I. (1991). Phenotypic features of smooth muscle cells during the evolution of experimental carotid artery intimal thickening. Biochemical and morphologic studies. *Lab Invest, 65*(4), 459-470.

167. Asada, H., Paszkowiak, J., Teso, D., Alvi, K., Thorisson, A., Frattini, J. C., … Dardik, A. (2005). Sustained orbital shear stress stimulates smooth muscle cell proliferation via the extracellular signal-regulated protein kinase 1/2 pathway. *J Vasc Surg, 42*(4), 772-780. doi:10.1016/j.jvs.2005.05.046

168. Worth, N. F., Rolfe, B. E., Song, J., & Campbell, G. R. (2001). Vascular smooth muscle cell phenotypic modulation in culture is associated with reorganisation of contractile and cytoskeletal proteins. *Cell Motil Cytoskeleton, 49*(3), 130-145. doi:10.1002/cm.1027

169. Ma, X., & Adelstein, R. S. (2014). The role of vertebrate nonmuscle myosin II in development and human disease. *Bioarchitecture, 4*(3), 88-102. doi:10.4161/bioa.29766

170. Eriksson, U., Das, K., Busch, C., Nordlinder, H., Rask, L., Sundelin, J., … Peterson, P. A. (1984). Cellular retinol-binding protein. Quantitation and distribution. *J Biol Chem, 259*(21), 13464-13470.

171. Tarbit, E., Singh, I., Peart, J. N., & Rose'Meyer, R. B. (2019). Biomarkers for the identification of cardiac fibroblast and myofibroblast cells. *Heart Fail Rev, 24*(1), 1-15. doi:10.1007/s10741-018-9720-1

172. Skalli, O., Bloom, W. S., Ropraz, P., Azzarone, B., & Gabbiani, G. (1986). Cytoskeletal remodeling of rat aortic smooth muscle cells in vitro: Relationships to culture conditions and analogies to in vivo situations. *J Submicrosc Cytol, 18*(3), 481-493.

173. Acampora, K. B., Nagatomi, J., Langan, E. M., 3rd, & LaBerge, M. (2010). Increased synthetic phenotype behavior of smooth muscle cells in response to in vitro balloon angioplasty injury model. *Ann Vasc Surg, 24*(1), 116-126. doi:10.1016/j.avsg.2009.07.019

174. Zhou, W., Dasgupta, C., Negash, S., & Raj, J. U. (2007). Modulation of pulmonary vascular smooth muscle cell phenotype in hypoxia: Role of cGMP-dependent protein kinase. *Am J Physiol Lung Cell Mol Physiol, 292*(6), L1459-1466. doi:10.1152/ajplung.00143.2006

175. Kuwabara, J. T., & Tallquist, M. D. (2017). Tracking adventitial fibroblast contribution to disease: A review of current methods to identify resident fibroblasts. *Arterioscler Thromb Vasc Biol, 37*(9), 1598-1607. doi:10.1161/ATVBAHA.117.308199

176. Brisset, A. C., Hao, H., Camenzind, E., Bacchetta, M., Geinoz, A., Sanchez, J. C., … Bochaton-Piallat, M. L. (2007). Intimal smooth muscle cells of porcine and human coronary artery express s100a4, a marker of the rhomboid phenotype in vitro. *Circ Res, 100*(7), 1055-1062. doi:10.1161/01.RES.0000262654.84810.6c

177. Martinez-Gonzalez, J., Berrozpe, M., Varela, O., & Badimon, L. (2001). Heterogeneity of smooth muscle cells in advanced human atherosclerotic plaques: Intimal smooth muscle cells expressing a fibroblast surface protein are highly activated by platelet-released products. *Eur J Clin Invest, 31*(11), 939-949. doi:10.1046/j.1365-2362.2001.00920.x

178. Allahverdian, S., Chaabane, C., Boukais, K., Francis, G. A., & Bochaton-Piallat, M. L. (2018). Smooth muscle cell fate and plasticity in atherosclerosis. *Cardiovasc Res, 114*(4), 540-550. doi:10.1093/cvr/cvy022

179. Pan, H., Xue, C., Auerbach, B. J., Fan, J., Bashore, A. C., Cui, J., … Reilly, M. P. (2020). Single-cell genomics reveals a novel cell state during smooth muscle cell phenotypic switching and potential therapeutic targets for atherosclerosis in mouse and human. *Circulation, 142*(21), 2060-2075. doi:10.1161/CIRCULATIONAHA.120.048378

180. Morikawa, S., Mabuchi, Y., Kubota, Y., Nagai, Y., Niibe, K., Hiratsu, E., … Matsuzaki, Y. (2009). Prospective identification, isolation, and systemic transplantation of multipotent mesenchymal stem cells in murine bone marrow. *J Exp Med, 206*(11), 2483-2496. doi:10.1084/jem.20091046

181. Diaz-Lezama, N., Wolf, A., Koch, S., Pfaller, A. M., Biber, J., Guillonneau, X., … Grosche, A. (2021). PDGF receptor alpha signaling is key for muller cell homeostasis functions. *Int J Mol Sci, 22*(3). doi:10.3390/ijms22031174

182. Kimura, K., Ramirez, K., Nguyen, T. A. V., Yamashiro, Y., Sada, A., & Yanagisawa, H. (2021). Contribution of PDGFRalpha-positive cells in maintenance and injury responses in mouse large vessels. *Sci Rep, 11*(1), 8683. doi:10.1038/s41598-021-88126-6

183. Li, L., Blumenthal, D. K., Terry, C. M., He, Y., Carlson, M. L., & Cheung, A. K. (2011). PDGF-induced proliferation in human arterial and venous smooth muscle cells: Molecular basis for differential effects of PDGF isoforms. *J Cell Biochem, 112*(1), 289-298. doi:10.1002/jcb.22924

184. Liu, M., & Gomez, D. (2019). Smooth muscle cell phenotypic diversity. *Arterioscler Thromb Vasc Biol, 39*(9), 1715-1723. doi:10.1161/ATVBAHA.119.312131

185. Albarran-Juarez, J., Kaur, H., Grimm, M., Offermanns, S., & Wettschureck, N. (2016). Lineage tracing of cells involved in atherosclerosis. *Atherosclerosis, 251*, 445-453. doi:10.1016/j.atherosclerosis.2016.06.012

186. Newman, A. A. C., Serbulea, V., Baylis, R. A., Shankman, L. S., Bradley, X., Alencar, G. F., … Owens, G. K. (2021). Multiple cell types contribute to the atherosclerotic lesion fibrous cap by PDGFRbeta and bioenergetic mechanisms. *Nat Metab, 3*(2), 166-181. doi:10.1038/s42255-020-00338-8

187. Wirka, R. C., Wagh, D., Paik, D. T., Pjanic, M., Nguyen, T., Miller, C. L., … Quertermous, T. (2019). Atheroprotective roles of smooth muscle cell phenotypic modulation and the TCF21 disease gene as revealed by single-cell analysis. *Nat Med, 25*(8), 1280-1289. doi:10.1038/s41591-019-0512-5

188. Kim, J. B., Zhao, Q., Nguyen, T., Pjanic, M., Cheng, P., Wirka, R., … Quertermous, T. (2020). Environment-sensing aryl hydrocarbon receptor inhibits the chondrogenic fate of modulated smooth muscle cells in atherosclerotic lesions. *Circulation, 142*(6), 575-590. doi:10.1161/CIRCULATIONAHA.120.045981

189. Thyberg, J., Palmberg, L., Nilsson, J., Ksiazek, T., & Sjolund, M. (1983). Phenotype modulation in primary cultures of arterial smooth muscle cells. On the role of platelet-derived growth factor. *Differentiation, 25*(2), 156-167. doi:10.1111/j.1432-0436.1984.tb01351.x

190. Chamley, J. H., Campbell, G. R., McConnell, J. D., & Groschel-Stewart, U. (1977). Comparison of vascular smooth muscle cells from adult human, monkey and rabbit in primary culture and in subculture. *Cell Tissue Res, 177*(4), 503-522. doi:10.1007/BF00220611

191. Hao, H., Ropraz, P., Verin, V., Camenzind, E., Geinoz, A., Pepper, M. S., … Bochaton-Piallat, M. L. (2002). Heterogeneity of smooth muscle cell populations cultured from pig coronary artery. *Arterioscler Thromb Vasc Biol, 22*(7), 1093-1099. doi:10.1161/01.atv.0000022407.91111.e4

192. Hedin, U., & Thyberg, J. (1987). Plasma fibronectin promotes modulation of arterial smooth-muscle cells from contractile to synthetic phenotype. *Differentiation, 33*(3), 239-246. doi:10.1111/j.1432-0436.1987.tb01563.x

193. Bjorkerud, S. (1991). Effects of transforming growth factor-beta 1 on human arterial smooth muscle cells in vitro. *Arterioscler Thromb, 11*(4), 892-902.

194. Karnik, S. K., Brooke, B. S., Bayes-Genis, A., Sorensen, L., Wythe, J. D., Schwartz, R. S., … Li, D. Y. (2003). A critical role for elastin signaling in vascular morphogenesis and disease. *Development, 130*(2), 411-423. doi:10.1242/dev.00223

195. Chamley-Campbell, J. H., Campbell, G. R., & Ross, R. (1981). Phenotype-dependent response of cultured aortic smooth muscle to serum mitogens. *J Cell Biol, 89*(2), 379-383. doi:10.1083/jcb.89.2.379

196. Poliseno, L., Cecchettini, A., Mariani, L., Evangelista, M., Ricci, F., Giorgi, F., … Rainaldi, G. (2006). Resting smooth muscle cells as a model for studying vascular cell activation. *Tissue Cell, 38*(2), 111-120. doi:10.1016/j.tice.2005.12.004

197. Han, M., Wen, J. K., Zheng, B., Cheng, Y., & Zhang, C. (2006). Serum deprivation results in redifferentiation of human umbilical vascular smooth muscle cells. *Am J Physiol Cell Physiol, 291*(1), C50-58. doi:10.1152/ajpcell.00524.2005

198. Kato, M., & Kyogoku, M. (1990). Competence growth factors evoke the phenotypic transition of arterial smooth muscle cells. *Ann N Y Acad Sci, 598*, 232-237. doi:10.1111/j.1749-6632.1990.tb42295.x

199. Rong, J. X., Shapiro, M., Trogan, E., & Fisher, E. A. (2003). Transdifferentiation of mouse aortic smooth muscle cells to a macrophage-like state after cholesterol loading. *Proc Natl Acad Sci U S A, 100*(23), 13531-13536. doi:10.1073/pnas.1735526100

200. Hui, D. Y. (2008). Intimal hyperplasia in murine models. *Curr Drug Targets, 9*(3), 251-260. doi:10.2174/138945008783755601

201. Emini Veseli, B., Perrotta, P., De Meyer, G. R. A., Roth, L., Van der Donckt, C., Martinet, W., & De Meyer, G. R. Y. (2017). Animal models of atherosclerosis. *Eur J Pharmacol, 816*, 3-13. doi:10.1016/j.ejphar.2017.05.010

202. Chakraborty, R., Chatterjee, P., Dave, J. M., Ostriker, A. C., Greif, D. M., Rzucidlo, E. M., & Martin, K. A. (2021). Targeting smooth muscle cell phenotypic switching in vascular disease. *JVS Vasc Sci, 2*, 79-94. doi:10.1016/j.jvssci.2021.04.001

203. Chappell, J., Harman, J. L., Narasimhan, V. M., Yu, H., Foote, K., Simons, B. D., … Jorgensen, H. F. (2016). Extensive proliferation of a subset of differentiated, yet plastic, medial vascular smooth muscle cells contributes to neointimal formation in mouse injury and atherosclerosis models. *Circ Res, 119*(12), 1313-1323. doi:10.1161/CIRCRESAHA.116.309799

204. Regan, C. P., Adam, P. J., Madsen, C. S., & Owens, G. K. (2000). Molecular mechanisms of decreased smooth muscle differentiation marker expression after vascular injury. *J Clin Invest, 106*(9), 1139-1147. doi:10.1172/JCI10522

205. Ross, R. (1999). Atherosclerosis--an inflammatory disease. *N Engl J Med, 340*(2), 115-126. doi:10.1056/NEJM199901143400207

206. WHO (2020). The top 10 causes of death. Available from https://www.who.int/news-room/fact-sheets/detail/the-top-10-causes-of-death (accessed 2021/07/21 2021)

207. Basatemur, G. L., Jorgensen, H. F., Clarke, M. C. H., Bennett, M. R., & Mallat, Z. (2019). Vascular smooth muscle cells in atherosclerosis. *Nat Rev Cardiol, 16*(12), 727-744. doi:10.1038/s41569-019-0227-9

208. Tabas, I., Williams, K. J., & Boren, J. (2007). Subendothelial lipoprotein retention as the initiating process in atherosclerosis: Update and therapeutic implications. *Circulation, 116*(16), 1832-1844. doi:10.1161/CIRCULATIONAHA.106.676890

209. Nakashima, Y., Fujii, H., Sumiyoshi, S., Wight, T. N., & Sueishi, K. (2007). Early human atherosclerosis: Accumulation of lipid and proteoglycans in intimal thickenings followed by macrophage infiltration. *Arterioscler Thromb Vasc Biol, 27*(5), 1159-1165. doi:10.1161/ATVBAHA.106.134080

210. Skalen, K., Gustafsson, M., Rydberg, E. K., Hulten, L. M., Wiklund, O., Innerarity, T. L., & Boren, J. (2002). Subendothelial retention of atherogenic lipoproteins in early atherosclerosis. *Nature, 417*(6890), 750-754. doi:10.1038/nature00804

211. Gimbrone, M. A., Jr., & Garcia-Cardena, G. (2016). Endothelial cell dysfunction and the pathobiology of atherosclerosis. *Circ Res, 118*(4), 620-636. doi:10.1161/CIRCRESAHA.115.306301

212. Libby, P. (2021). The changing landscape of atherosclerosis. *Nature, 592*(7855), 524-533. doi:10.1038/s41586-021-03392-8

213. Zmyslowski, A., & Szterk, A. (2017). Current knowledge on the mechanism of atherosclerosis and pro-atherosclerotic properties of oxysterols. *Lipids Health Dis, 16*(1), 188. doi:10.1186/s12944-017-0579-2

214. Jacobsen, K., Lund, M. B., Shim, J., Gunnersen, S., Fuchtbauer, E. M., Kjolby, M., … Bentzon, J. F. (2017). Diverse cellular architecture of atherosclerotic plaque derives from clonal expansion of a few medial SMCs. *JCI Insight, 2*(19). doi:10.1172/jci.insight.95890

215. Llorente-Cortes, V., Martinez-Gonzalez, J., & Badimon, L. (1998). Esterified cholesterol accumulation induced by aggregated LDL uptake in human vascular smooth muscle cells is reduced by HMG-CoA reductase inhibitors. *Arterioscler Thromb Vasc Biol, 18*(5), 738-746. doi:10.1161/01.atv.18.5.738

216. Chaabane, C., Coen, M., & Bochaton-Piallat, M. L. (2014). Smooth muscle cell phenotypic switch: Implications for foam cell formation. *Curr Opin Lipidol, 25*(5), 374-379. doi:10.1097/MOL.0000000000000113

217. Klouche, M., Rose-John, S., Schmiedt, W., & Bhakdi, S. (2000). Enzymatically degraded, nonoxidized LDL induces human vascular smooth muscle cell activation, foam cell transformation, and proliferation. *Circulation, 101*(15), 1799-1805. doi:10.1161/01.cir.101.15.1799

218. Naito, M., Nomura, H., Esaki, T., & Iguchi, A. (1997). Characteristics of macrophage-derived foam cells isolated from atherosclerotic lesions of rabbits. *Atherosclerosis, 135*(2), 241-247. doi:10.1016/s0021-9150(97)00177-9

219. Campbell, J. H., Reardon, M. F., Campbell, G. R., & Nestel, P. J. (1985). Metabolism of atherogenic lipoproteins by smooth muscle cells of different phenotype in culture. *Arteriosclerosis, 5*(4), 318-328. doi:10.1161/01.atv.5.4.318

220. Choi, H. Y., Rahmani, M., Wong, B. W., Allahverdian, S., McManus, B. M., Pickering, J. G., … Francis, G. A. (2009). ATP-binding cassette transporter A1 expression and apolipoprotein A-I binding are impaired in intima-type arterial smooth muscle cells. *Circulation, 119*(25), 3223-3231. doi:10.1161/CIRCULATIONAHA.108.841130

221. Bentzon, J. F., Otsuka, F., Virmani, R., & Falk, E. (2014). Mechanisms of plaque formation and rupture. *Circ Res, 114*(12), 1852-1866. doi:10.1161/CIRCRESAHA.114.302721

222. Schrijvers, D. M., De Meyer, G. R., Kockx, M. M., Herman, A. G., & Martinet, W. (2005). Phagocytosis of apoptotic cells by macrophages is impaired in atherosclerosis. *Arterioscler Thromb Vasc Biol, 25*(6), 1256-1261. doi:10.1161/01.ATV.0000166517.18801.a7

223. Martinet, W., Schrijvers, D. M., & De Meyer, G. R. (2011). Necrotic cell death in atherosclerosis. *Basic Res Cardiol, 106*(5), 749-760. doi:10.1007/s00395-011-0192-x

224. New, S. E., Goettsch, C., Aikawa, M., Marchini, J. F., Shibasaki, M., Yabusaki, K., … Aikawa, E. (2013). Macrophage-derived matrix vesicles: An alternative novel mechanism for microcalcification in atherosclerotic plaques. *Circ Res, 113*(1), 72-77. doi:10.1161/CIRCRESAHA.113.301036

225. Lin, M. E., Chen, T. M., Wallingford, M. C., Nguyen, N. B., Yamada, S., Sawangmake, C., … Giachelli, C. M. (2016). Runx2 deletion in smooth muscle cells inhibits vascular osteochondrogenesis and calcification but not atherosclerotic lesion formation. *Cardiovasc Res, 112*(2), 606-616. doi:10.1093/cvr/cvw205

226. Harman, J. L., & Jorgensen, H. F. (2019). The role of smooth muscle cells in plaque stability: Therapeutic targeting potential. *Br J Pharmacol, 176*(19), 3741-3753. doi:10.1111/bph.14779

227. Nakashima, Y., Plump, A. S., Raines, E. W., Breslow, J. L., & Ross, R. (1994). ApoE-deficient mice develop lesions of all phases of atherosclerosis throughout the arterial tree. *Arterioscler Thromb, 14*(1), 133-140. doi:10.1161/01.atv.14.1.133

228. Aikawa, M., Sivam, P. N., Kuro-o, M., Kimura, K., Nakahara, K., Takewaki, S., … et al. (1993). Human smooth muscle myosin heavy chain isoforms as molecular markers for vascular development and atherosclerosis. *Circ Res, 73*(6), 1000-1012. doi:10.1161/01.res.73.6.1000

229. Ross, R., Wight, T. N., Strandness, E., & Thiele, B. (1984). Human atherosclerosis. I. Cell constitution and characteristics of advanced lesions of the superficial femoral artery. *Am J Pathol, 114*(1), 79-93.

230. Raines, E. W. (2000). The extracellular matrix can regulate vascular cell migration, proliferation, and survival: Relationships to vascular disease. *Int J Exp Pathol, 81*(3), 173-182. doi:10.1046/j.1365-2613.2000.00155.x

231. Allahverdian, S., Ortega, C., & Francis, G. A. (2022). Smooth muscle cell-proteoglycan-lipoprotein interactions as drivers of atherosclerosis. *Handb Exp Pharmacol, 270*, 335-358. doi:10.1007/164_2020_364

232. Bennett, M. R., Sinha, S., & Owens, G. K. (2016). Vascular smooth muscle cells in atherosclerosis. *Circ Res, 118*(4), 692-702. doi:10.1161/CIRCRESAHA.115.306361

233. Libby, P., Pasterkamp, G., Crea, F., & Jang, I. K. (2019). Reassessing the mechanisms of acute coronary syndromes. *Circ Res, 124*(1), 150-160. doi:10.1161/CIRCRESAHA.118.311098

234. Kolodgie, F. D., Burke, A. P., Farb, A., Gold, H. K., Yuan, J., Narula, J., … Virmani, R. (2001). The thin-cap fibroatheroma: A type of vulnerable plaque: The major precursor lesion to acute coronary syndromes. *Curr Opin Cardiol, 16*(5), 285-292. doi:10.1097/00001573-200109000-00006

235. Toschi, V., Gallo, R., Lettino, M., Fallon, J. T., Gertz, S. D., Fernandez-Ortiz, A., … Badimon, J. J. (1997). Tissue factor modulates the thrombogenicity of human atherosclerotic plaques. *Circulation, 95*(3), 594-599. doi:10.1161/01.cir.95.3.594

236. Falk, E., Nakano, M., Bentzon, J. F., Finn, A. V., & Virmani, R. (2013). Update on acute coronary syndromes: The pathologists' view. *Eur Heart J, 34*(10), 719-728. doi:10.1093/eurheartj/ehs411

237. Feil, S., Hofmann, F., & Feil, R. (2004). SM22alpha modulates vascular smooth muscle cell phenotype during atherogenesis. *Circ Res, 94*(7), 863-865. doi:10.1161/01.RES.0000126417.38728.F6

238. Swirski, F. K., & Nahrendorf, M. (2014). Do vascular smooth muscle cells differentiate to macrophages in atherosclerotic lesions? *Circ Res, 115*(7), 605-606. doi:10.1161/CIRCRESAHA.114.304925

239. Shankman, L. S., Gomez, D., Cherepanova, O. A., Salmon, M., Alencar, G. F., Haskins, R. M., … Owens, G. K. (2015). Klf4-dependent phenotypic modulation of smooth muscle cells has a key role in atherosclerotic plaque pathogenesis. *Nat Med, 21*(6), 628-637. doi:10.1038/nm.3866

240. Wang, Y., Dubland, J. A., Allahverdian, S., Asonye, E., Sahin, B., Jaw, J. E., … Francis, G. A. (2019). Smooth muscle cells contribute the majority of foam cells in ApoE (apolipoprotein E)-deficient mouse atherosclerosis. *Arterioscler Thromb Vasc Biol, 39*(5), 876-887. doi:10.1161/ATVBAHA.119.312434

241. Naik, V., Leaf, E. M., Hu, J. H., Yang, H. Y., Nguyen, N. B., Giachelli, C. M., & Speer, M. Y. (2012). Sources of cells that contribute to atherosclerotic intimal calcification: An in vivo genetic fate mapping study. *Cardiovasc Res, 94*(3), 545-554. doi:10.1093/cvr/cvs126

242. Bentzon, J. F., Weile, C., Sondergaard, C. S., Hindkjaer, J., Kassem, M., & Falk, E. (2006). Smooth muscle cells in atherosclerosis originate from the local vessel wall and not circulating progenitor cells in ApoE knockout mice. *Arterioscler Thromb Vasc Biol, 26*(12), 2696-2702. doi:10.1161/01.ATV.0000247243.48542.9d

243. Rosenfeld, M. E., Averill, M. M., Bennett, B. J., & Schwartz, S. M. (2008). Progression and disruption of advanced atherosclerotic plaques in murine models. *Curr Drug Targets, 9*(3), 210-216. doi:10.2174/138945008783755575

244. Daugherty, A., Tall, A. R., Daemen, M., Falk, E., Fisher, E. A., Garcia-Cardena, G., … Council on Basic Cardiovascular, S. (2017). Recommendation on design, execution, and reporting of animal atherosclerosis studies: A scientific statement from the american heart association. *Circ Res, 121*(6), e53-e79. doi:10.1161/RES.0000000000000169

245. Meir, K. S., & Leitersdorf, E. (2004). Atherosclerosis in the apolipoprotein-E-deficient mouse: A decade of progress. *Arterioscler Thromb Vasc Biol, 24*(6), 1006-1014. doi:10.1161/01.ATV.0000128849.12617.f4

246. Plump, A. S., Smith, J. D., Hayek, T., Aalto-Setala, K., Walsh, A., Verstuyft, J. G., … Breslow, J. L. (1992). Severe hypercholesterolemia and atherosclerosis in apolipoprotein E-deficient mice created by homologous recombination in es cells. *Cell, 71*(2), 343-353. doi:10.1016/0092-8674(92)90362-g

247. Feingold, K. R. (2000). Introduction to lipids and lipoproteins. In K. R. Feingold, B. Anawalt, A. Boyce, et al. (Eds.), *Endotext*. South Dartmouth (MA).

248. Getz, G. S., & Reardon, C. A. (2009). Apoprotein E as a lipid transport and signaling protein in the blood, liver, and artery wall. *J Lipid Res, 50 Suppl*, S156-161. doi:10.1194/jlr.R800058-JLR200

249. Doran, A. C., Meller, N., & McNamara, C. A. (2008). Role of smooth muscle cells in the initiation and early progression of atherosclerosis. *Arterioscler Thromb Vasc Biol, 28*(5), 812-819. doi:10.1161/ATVBAHA.107.159327

250. Suga, S., Nakao, K., Kishimoto, I., Hosoda, K., Mukoyama, M., Arai, H., … et al. (1992). Phenotype-related alteration in expression of natriuretic peptide receptors in aortic smooth muscle cells. *Circ Res, 71*(1), 34-39. doi:10.1161/01.res.71.1.34

251. Cornwell, T. L., & Lincoln, T. M. (1989). Regulation of intracellular Ca2+ levels in cultured vascular smooth muscle cells. Reduction of Ca2+ by atriopeptin and 8-bromo-cyclic GMP is mediated by cyclic GMP-dependent protein kinase. *J Biol Chem, 264*(2), 1146-1155.

252. Browner, N. C., Dey, N. B., Bloch, K. D., & Lincoln, T. M. (2004). Regulation of cGMP-dependent protein kinase expression by soluble guanylyl cyclase in vascular smooth muscle cells. *J Biol Chem, 279*(45), 46631-46636. doi:10.1074/jbc.M408518200

253. Garg, U. C., & Hassid, A. (1989). Nitric oxide-generating vasodilators and 8-bromo-cyclic guanosine monophosphate inhibit mitogenesis and proliferation of cultured rat vascular smooth muscle cells. *J Clin Invest, 83*(5), 1774-1777. doi:10.1172/JCI114081

254. Tulis, D. A., Bohl Masters, K. S., Lipke, E. A., Schiesser, R. L., Evans, A. J., Peyton, K. J., … Schafer, A. I. (2002). YC-1-mediated vascular protection through inhibition of smooth muscle cell proliferation and platelet function. *Biochem Biophys Res Commun, 291*(4), 1014-1021. doi:10.1006/bbrc.2002.6552

255. Chiche, J. D., Schlutsmeyer, S. M., Bloch, D. B., de la Monte, S. M., Roberts, J. D., Jr., Filippov, G., … Bloch, K. D. (1998). Adenovirus-mediated gene transfer of cGMP-dependent protein kinase increases the sensitivity of cultured vascular smooth muscle cells to the antiproliferative and pro-apoptotic effects of nitric oxide/cGMP. *J Biol Chem, 273*(51), 34263-34271. doi:10.1074/jbc.273.51.34263

256. Dey, N. B., Foley, K. F., Lincoln, T. M., & Dostmann, W. R. (2005). Inhibition of cGMP-dependent protein kinase reverses phenotypic modulation of vascular smooth muscle cells. *J Cardiovasc Pharmacol, 45*(5), 404-413. doi:10.1097/01.fjc.0000157455.38068.12

257. Choi, C., Sellak, H., Brown, F. M., & Lincoln, T. M. (2010). cGMP-dependent protein kinase and the regulation of vascular smooth muscle cell gene expression: Possible involvement of Elk-1 sumoylation. *Am J Physiol Heart Circ Physiol, 299*(5), H1660-1670. doi:10.1152/ajpheart.00677.2010

258. Hassid, A., Arabshahi, H., Bourcier, T., Dhaunsi, G. S., & Matthews, C. (1994). Nitric oxide selectively amplifies FGF-2-induced mitogenesis in primary rat aortic smooth muscle cells. *Am J Physiol, 267*(3 Pt 2), H1040-1048. doi:10.1152/ajpheart.1994.267.3.H1040

259. Dobrowinski, H. (2021). Influence of cGMP signaling on VSMC growth and its dependence on fibronectin in cultured VSMCs and development of atherosclerosis. *Doctoral thesis, University of Tübingen*. Retrieved from http://hdl.handle.net/10900/91054

260. Komalavilas, P., Shah, P. K., Jo, H., & Lincoln, T. M. (1999). Activation of mitogen-activated protein kinase pathways by cyclic GMP and cyclic GMP-dependent protein kinase in contractile vascular smooth muscle cells. *J Biol Chem, 274*(48), 34301-34309. doi:10.1074/jbc.274.48.34301

261. Furuya, M., Yoshida, M., Hayashi, Y., Ohnuma, N., Minamino, N., Kangawa, K., & Matsuo, H. (1991). C-type natriuretic peptide is a growth inhibitor of rat vascular smooth muscle cells. *Biochem Biophys Res Commun, 177*(3), 927-931. doi:10.1016/0006-291x(91)90627-j

262. Cahill, P. A., & Hassid, A. (1993). Differential antimitogenic effectiveness of atrial natriuretic peptides in primary versus subcultured rat aortic smooth muscle cells: Relationship to expression of ANF-C receptors. *J Cell Physiol, 154*(1), 28-38. doi:10.1002/jcp.1041540105

263. Hutchinson, H. G., Trindade, P. T., Cunanan, D. B., Wu, C. F., & Pratt, R. E. (1997). Mechanisms of natriuretic-peptide-induced growth inhibition of vascular smooth muscle cells. *Cardiovasc Res, 35*(1), 158-167. doi:10.1016/s0008-6363(97)00086-2

264. Rudic, R. D., Shesely, E. G., Maeda, N., Smithies, O., Segal, S. S., & Sessa, W. C. (1998). Direct evidence for the importance of endothelium-derived nitric oxide in vascular remodeling. *J Clin Invest, 101*(4), 731-736. doi:10.1172/JCI1699

265. Chyu, K. Y., Dimayuga, P., Zhu, J., Nilsson, J., Kaul, S., Shah, P. K., & Cercek, B. (1999). Decreased neointimal thickening after arterial wall injury in inducible nitric oxide synthase knockout mice. *Circ Res, 85*(12), 1192-1198. doi:10.1161/01.res.85.12.1192

266. Wu, C. H., Chang, W. C., Chang, G. Y., Kuo, S. C., & Teng, C. M. (2004). The inhibitory mechanism of YC-1, a benzyl indazole, on smooth muscle cell proliferation: An in vitro and in vivo study. *J Pharmacol Sci, 94*(3), 252-260. doi:10.1254/jphs.94.252

267. Tulis, D. A., Durante, W., Peyton, K. J., Chapman, G. B., Evans, A. J., & Schafer, A. I. (2000). YC-1, a benzyl indazole derivative, stimulates vascular cGMP and inhibits neointima formation. *Biochem Biophys Res Commun, 279*(2), 646-652. doi:10.1006/bbrc.2000.3942

268. Hirschberg, K., Tarcea, V., Pali, S., Barnucz, E., Gwanmesia, P. N., Korkmaz, S., … Szabo, G. (2013). Cinaciguat prevents neointima formation after arterial injury by decreasing vascular smooth muscle cell migration and proliferation. *Int J Cardiol, 167*(2), 470-477. doi:10.1016/j.ijcard.2012.01.032

269. Barber, M. N., Gaspari, T. A., Kairuz, E. M., Dusting, G. J., & Woods, R. L. (2005). Atrial natriuretic peptide preserves endothelial function during intimal hyperplasia. *J Vasc Res, 42*(2), 101-110. doi:10.1159/000083429

270. Furuya, M., Aisaka, K., Miyazaki, T., Honbou, N., Kawashima, K., Ohno, T., … Matsuo, H. (1993). C-type natriuretic peptide inhibits intimal thickening after vascular injury. *Biochem Biophys Res Commun, 193*(1), 248-253. doi:10.1006/bbrc.1993.1616

271. Pelisek, J., Fuchs, A. T., Kuehnl, A., Tian, W., Kuhlmann, M. T., Rolland, P. H., … Nikol, S. (2006). C-type natriuretic peptide for reduction of restenosis: Gene transfer is superior over single peptide administration. *J Gene Med, 8*(7), 835-844. doi:10.1002/jgm.905

272. Ahluwalia, A., Foster, P., Scotland, R. S., McLean, P. G., Mathur, A., Perretti, M., … Hobbs, A. J. (2004). Antiinflammatory activity of soluble guanylate cyclase: cGMP-dependent down-regulation of P-selectin expression and leukocyte recruitment. *Proc Natl Acad Sci U S A, 101*(5), 1386-1391. doi:10.1073/pnas.0304264101

273. Nguyen, T. H., Axell, A., Turek, I., Wright, B., Meehan-Andrews, T., & Irving, H. R. (2022). Modulation of inflammatory cytokine production in human monocytes by cGMP and IRAK3. *Int J Mol Sci, 23*(5). doi:10.3390/ijms23052552

274. Huang, P. L., Huang, Z., Mashimo, H., Bloch, K. D., Moskowitz, M. A., Bevan, J. A., & Fishman, M. C. (1995). Hypertension in mice lacking the gene for endothelial nitric oxide synthase. *Nature, 377*(6546), 239-242. doi:10.1038/377239a0

275. Tsou, C. Y., Chen, C. Y., Zhao, J. F., Su, K. H., Lee, H. T., Lin, S. J., … Lee, T. S. (2014). Activation of soluble guanylyl cyclase prevents foam cell formation and atherosclerosis. *Acta Physiol (Oxf), 210*(4), 799-810. doi:10.1111/apha.12210

276. Alexander, M. R., Knowles, J. W., Nishikimi, T., & Maeda, N. (2003). Increased atherosclerosis and smooth muscle cell hypertrophy in natriuretic peptide receptor A-/-apolipoprotein E-/- mice. *Arterioscler Thromb Vasc Biol, 23*(6), 1077-1082. doi:10.1161/01.ATV.0000071702.45741.2E

277. Tawa, M., Nakano, K., Yamashita, Y., He, Q., Masuoka, T., Okamura, T., & Ishibashi, T. (2021). Alteration of the soluble guanylate cyclase system in coronary arteries of high cholesterol diet-fed rabbits. *Pharmacol Res Perspect, 9*(4), e00838. doi:10.1002/prp2.838

278. Priksz, D., Bombicz, M., Varga, B., Kurucz, A., Gesztelyi, R., Balla, J., … Juhasz, B. (2018). Upregulation of myocardial and vascular phosphodiesterase 9a in a model of atherosclerotic cardiovascular disease. *Int J Mol Sci, 19*(10)doi:10.3390/ijms19102882

279. Feil, R. (2007). Conditional somatic mutagenesis in the mouse using site-specific recombinases. *Handb Exp Pharmacol*(178), 3-28. doi:10.1007/978-3-540-35109-2_1

280. Feil, R., Wagner, J., Metzger, D., & Chambon, P. (1997). Regulation of Cre recombinase activity by mutated estrogen receptor ligand-binding domains. *Biochem Biophys Res Commun, 237*(3), 752-757. doi:10.1006/bbrc.1997.7124

281. MacNab, M. W., Tallarida, R. J., & Joseph, R. (1984). An evaluation of tamoxifen as a partial agonist by classical receptor theory--an explanation of the dual action of tamoxifen. *Eur J Pharmacol, 103*(3-4), 321-326. doi:10.1016/0014-2999(84)90493-x

282. Fontaine, C., Abot, A., Billon-Gales, A., Flouriot, G., Berges, H., Grunenwald, E., … Arnal, J. F. (2013). Tamoxifen elicits atheroprotection through estrogen receptor alpha AF-1 but does not accelerate reendothelialization. *Am J Pathol, 183*(1), 304-312. doi:10.1016/j.ajpath.2013.03.010

283. Chakraborty, R., Saddouk, F. Z., Carrao, A. C., Krause, D. S., Greif, D. M., & Martin, K. A. (2019). Promoters to study vascular smooth muscle. *Arterioscler Thromb Vasc Biol, 39*(4), 603-612. doi:10.1161/ATVBAHA.119.312449

284. Zhang, J., Zhong, W., Cui, T., Yang, M., Hu, X., Xu, K., … Chen, Y. E. (2006). Generation of an adult smooth muscle cell-targeted Cre recombinase mouse model. *Arterioscler Thromb Vasc Biol, 26*(3), e23-24. doi:10.1161/01.ATV.0000202661.61837.93

285. Kuhbandner, S., Brummer, S., Metzger, D., Chambon, P., Hofmann, F., & Feil, R. (2000). Temporally controlled somatic mutagenesis in smooth muscle. *Genesis, 28*(1), 15-22. doi:10.1002/1526-968x(200009)28:1<15::aid-gene20>3.0.co;2-c

286. Wirth, A., Benyo, Z., Lukasova, M., Leutgeb, B., Wettschureck, N., Gorbey, S., … Offermanns, S. (2008). G12-G13-LARG-mediated signaling in vascular smooth muscle is required for salt-induced hypertension. *Nat Med, 14*(1), 64-68. doi:10.1038/nm1666

287. Wendling, O., Bornert, J. M., Chambon, P., & Metzger, D. (2009). Efficient temporally-controlled targeted mutagenesis in smooth muscle cells of the adult mouse. *Genesis, 47*(1), 14-18. doi:10.1002/dvg.20448

288. Murgai, M., Ju, W., Eason, M., Kline, J., Beury, D. W., Kaczanowska, S., … Kaplan, R. N. (2017). Klf4-dependent perivascular cell plasticity mediates pre-metastatic niche formation and metastasis. *Nat Med, 23*(10), 1176-1190. doi:10.1038/nm.4400

289. Fu, X., Khalil, H., Kanisicak, O., Boyer, J. G., Vagnozzi, R. J., Maliken, B. D., … Molkentin, J. D. (2018). Specialized fibroblast differentiated states underlie scar formation in the infarcted mouse heart. *J Clin Invest, 128*(5), 2127-2143. doi:10.1172/JCI98215

290. Shen, Z., Li, C., Frieler, R. A., Gerasimova, A. S., Lee, S. J., Wu, J., … Mortensen, R. M. (2012). Smooth muscle protein 22 alpha-Cre is expressed in myeloid cells in mice. *Biochem Biophys Res Commun, 422*(4), 639-642. doi:10.1016/j.bbrc.2012.05.041

291. Faggin, E., Puato, M., Zardo, L., Franch, R., Millino, C., Sarinella, F., … Chiavegato, A. (1999). Smooth muscle-specific SM22 protein is expressed in the adventitial cells of balloon-injured rabbit carotid artery. *Arterioscler Thromb Vasc Biol, 19*(6), 1393-1404. doi:10.1161/01.atv.19.6.1393

292. Li, L., Miano, J. M., Cserjesi, P., & Olson, E. N. (1996). SM22 alpha, a marker of adult smooth muscle, is expressed in multiple myogenic lineages during embryogenesis. *Circ Res, 78*(2), 188-195. doi:10.1161/01.res.78.2.188

293. Bajar, B. T., Wang, E. S., Zhang, S., Lin, M. Z., & Chu, J. (2016). A guide to fluorescent protein FRET pairs. *Sensors (Basel), 16*(9). doi:10.3390/s16091488

294. Russwurm, M., Mullershausen, F., Friebe, A., Jager, R., Russwurm, C., & Koesling, D. (2007). Design of fluorescence resonance energy transfer (FRET)-based cGMP indicators: A systematic approach. *Biochem J, 407*(1), 69-77. doi:10.1042/BJ20070348

295. Thunemann, M., Wen, L., Hillenbrand, M., Vachaviolos, A., Feil, S., Ott, T., … Feil, R. (2013). Transgenic mice for cGMP imaging. *Circ Res, 113*(4), 365-371. doi:10.1161/CIRCRESAHA.113.301063

296. Thunemann, M., Schmidt, K., de Wit, C., Han, X., Jain, R. K., Fukumura, D., & Feil, R. (2014). Correlative intravital imaging of cGMP signals and vasodilation in mice. *Front Physiol, 5*, 394. doi:10.3389/fphys.2014.00394

297. Ter-Avetisyan, G., Rathjen, F. G., & Schmidt, H. (2014). Bifurcation of axons from cranial sensory neurons is disabled in the absence of Npr2-induced cGMP signaling. *J Neurosci, 34*(3), 737-747. doi:10.1523/JNEUROSCI.4183-13.2014

298. Troster, P., Haseleu, J., Petersen, J., Drees, O., Schmidtko, A., Schwaller, F., … Schmidt, H. (2018). The absence of sensory axon bifurcation affects nociception and termination fields of afferents in the spinal cord. *Front Mol Neurosci, 11*, 19. doi:10.3389/fnmol.2018.00019

299. Piedrahita, J. A., Zhang, S. H., Hagaman, J. R., Oliver, P. M., & Maeda, N. (1992). Generation of mice carrying a mutant apolipoprotein E gene inactivated by gene targeting in embryonic stem cells. *Proc Natl Acad Sci U S A, 89*(10), 4471-4475. doi:10.1073/pnas.89.10.4471

300. Thunemann, M., Fomin, N., Krawutschke, C., Russwurm, M., & Feil, R. (2013). Visualization of cGMP with cGi biosensors. *Methods Mol Biol, 1020*, 89-120. doi:10.1007/978-1-62703-459-3_6

301. Koehler, A. (1893). Ein neues Beleuchtungsverfahren für mikrophotographische Zwecke. *Z Wiss Mikrosk, 10*(4), 433-440.

302. Wilson, M. (2017). Koehler illumination: A brief history and a practical set up in five easy steps. Available from https://www.leica-microsystems.com/science-lab/koehler-illumination-a-brief-history-and-a-practical-set-up-in-five-easy-steps/ (accessed 2021/02/19

303. Fellers, T. J., & Davidson, M. W. CCD noise sources and signal-to-noise ratio. Available from https://www.olympus-lifescience.com/de/microscope-resource/primer/digitalimaging/concepts/ccdsnr/ (accessed 2021/03/03 2021)

304. Fellers, T. J., Vogt, K. M., & Davidson, M. W. CCD signal-to-noise ratio. Available from https://www.microscopyu.com/tutorials/ccd-signal-to-noise-ratio (accessed 03/03/2021 2021)

305. Maragos, C. M., Morley, D., Wink, D. A., Dunams, T. M., Saavedra, J. E., Hoffman, A., … Keefer, L. K. (1991). Complexes of .NO with nucleophiles as agents for the controlled biological release of nitric oxide. Vasorelaxant effects. *J Med Chem, 34*(11), 3242-3247. doi:10.1021/jm00115a013

306. Strept(avidin)–biotin complex method for IHC detection. Available from https://www.thermofisher.com/de/de/home/life-science/protein-biology/protein-biology-learning-center/protein-biology-resource-library/pierce-protein-methods/avidin-biotin-complex-method-ihc-detection.html (accessed 2021/02/19)

307. Ramirez-Zacarias, J. L., Castro-Munozledo, F., & Kuri-Harcuch, W. (1992). Quantitation of adipose conversion and triglycerides by staining intracytoplasmic lipids with oil red o. *Histochemistry, 97*(6), 493-497. doi:10.1007/BF00316069

308. Peterson, G. L. (1977). A simplification of the protein assay method of lowry et al. Which is more generally applicable. *Anal Biochem, 83*(2), 346-356. doi:10.1016/0003-2697(77)90043-4

309. Lowry, O. H., Rosebrough, N. J., Farr, A. L., & Randall, R. J. (1951). Protein measurement with the folin phenol reagent. *J Biol Chem, 193*(1), 265-275.

310. Laemmli, U. K. (1970). Cleavage of structural proteins during the assembly of the head of bacteriophage t4. *Nature, 227*(5259), 680-685. doi:10.1038/227680a0

311. Lottspeich, F., & Engels, J. W. (2018). *Bioanalytics : Analytical methods and concepts in biochemistry and molecular biology*. Newark, GERMANY: John Wiley & Sons, Incorporated.

312. Towbin, H., Staehelin, T., & Gordon, J. (1979). Electrophoretic transfer of proteins from polyacrylamide gels to nitrocellulose sheets: Procedure and some applications. *Proc Natl Acad Sci U S A, 76*(9), 4350-4354. doi:10.1073/pnas.76.9.4350

313. Renart, J., Reiser, J., & Stark, G. R. (1979). Transfer of proteins from gels to diazobenzyloxymethyl-paper and detection with antisera: A method for studying antibody specificity and antigen structure. *Proc Natl Acad Sci U S A, 76*(7), 3116-3120. doi:10.1073/pnas.76.7.3116

314. Kyhse-Andersen, J. (1984). Electroblotting of multiple gels: A simple apparatus without buffer tank for rapid transfer of proteins from polyacrylamide to nitrocellulose. *J Biochem Biophys Methods, 10*(3-4), 203-209. doi:10.1016/0165-022x(84)90040-x

315. Schindelin, J., Arganda-Carreras, I., Frise, E., Kaynig, V., Longair, M., Pietzsch, T., … Cardona, A. (2012). Fiji: An open-source platform for biological-image analysis. *Nat Methods, 9*(7), 676-682. doi:10.1038/nmeth.2019

316. Smith, G. D., Chen, V. J., Holden, A., Keefe, M. H., & Lieb, S. G. (2019). Analytical characterization of 5,5 '-dibromoindigo and its first discovery in a museum textile. *Heritage Science, 7*(1). doi:10.1186/s40494-019-0305-7

317. Yazdanyar, A., & Newman, A. B. (2009). The burden of cardiovascular disease in the elderly: Morbidity, mortality, and costs. *Clin Geriatr Med, 25*(4), 563-577, vii. doi:10.1016/j.cger.2009.07.007

318. Humphrey, J. D., Schwartz, M. A., Tellides, G., & Milewicz, D. M. (2015). Role of mechanotransduction in vascular biology: Focus on thoracic aortic aneurysms and dissections. *Circ Res, 116*(8), 1448-1461. doi:10.1161/CIRCRESAHA.114.304936

319. Davies, M. J., Richardson, P. D., Woolf, N., Katz, D. R., & Mann, J. (1993). Risk of thrombosis in human atherosclerotic plaques: Role of extracellular lipid, macrophage, and smooth muscle cell content. *Br Heart J, 69*(5), 377-381. doi:10.1136/hrt.69.5.377

320. Roostalu, U., & Wong, J. K. (2018). Arterial smooth muscle dynamics in development and repair. *Dev Biol, 435*(2), 109-121. doi:10.1016/j.ydbio.2018.01.018

321. Lincoln, T. M., Wu, X., Sellak, H., Dey, N., & Choi, C. S. (2006). Regulation of vascular smooth muscle cell phenotype by cyclic GMP and cyclic GMP-dependent protein kinase. *Front Biosci, 11*, 356-367. doi:10.2741/1803

322. Vengrenyuk, Y., Nishi, H., Long, X., Ouimet, M., Savji, N., Martinez, F. O., … Fisher, E. A. (2015). Cholesterol loading reprograms the microRNA-143/145-myocardin axis to convert aortic smooth muscle cells to a dysfunctional macrophage-like phenotype. *Arterioscler Thromb Vasc Biol, 35*(3), 535-546. doi:10.1161/ATVBAHA.114.304029

323. Drewett, J. G., Fendly, B. M., Garbers, D. L., & Lowe, D. G. (1995). Natriuretic peptide receptor-B (guanylyl cyclase-B) mediates C-type natriuretic peptide relaxation of precontracted rat aorta. *J Biol Chem, 270*(9), 4668-4674. doi:10.1074/jbc.270.9.4668

324. Liu, Y., Abendschein, D., Woodard, G. E., Rossin, R., McCommis, K., Zheng, J., … Woodard, P. K. (2010). Molecular imaging of atherosclerotic plaque with (64)Cu-labeled natriuretic peptide and pet. *J Nucl Med, 51*(1), 85-91. doi:10.2967/jnumed.109.066977

325. Soehnlein, O., & Libby, P. (2021). Targeting inflammation in atherosclerosis - from experimental insights to the clinic. *Nat Rev Drug Discov, 20*(8), 589-610. doi:10.1038/s41573-021-00198-1

326. Shahoud, J. S., Miao, J. H., & Bolla, S. R. (2021). Anatomy, thorax, heart aorta. In *Statpearls*. Treasure Island (FL).

327. Cook, M. J. (1965). *The anatomy of the laboratory mouse*: Academic Press.

7 Appendix

7.1 Supplementary figures

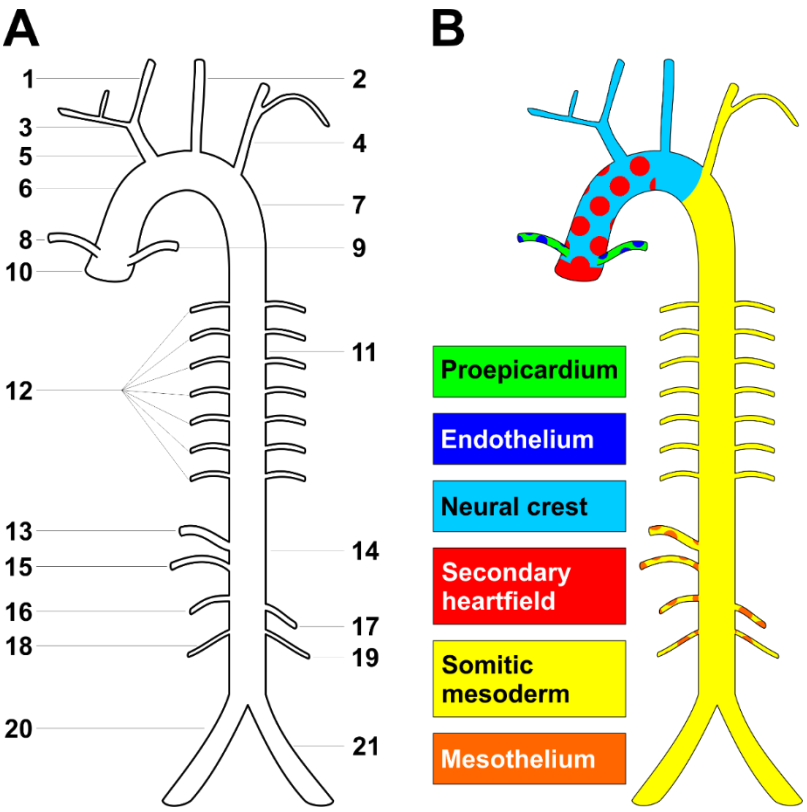

Supplementary figure I: Structure of the murine aorta and developmental origin of medial VSMCs. *Schematic representation of the murine aorta and branching vessels (A) and a colour coded version indicating the developmental origin of medial VSMCs (B).* ***A:*** *The aorta consists of three regions, the aortic arch (6: ascending and 7: descending), the descending thoracic aorta (11) and the abdominal aorta (14). It is attached to the heart via the aortic root (10). Several branching vessels depart from the aortic arch. The right (8) and left (9) coronary arteries, the brachiocephalic artery (5), the left common carotid artery (2) and the left subclavian artery (4). The brachiocephalic artery (5) branches into the right common carotid artery (1) and the right subclavian artery (3). The intercostal arteries (12) part from the descending thoracic aorta (11). The coeliac artery (13), superior mesenteric artery (15), right (16) and left (17) renal arteries and right (18) and left (19) gonadal arteries part from the abdominal (14) part of the aorta which later splits into the right (20) and left (21) iliac arteries and the middle caudal artery (not shown).* ***B:*** *The murine aorta is composed of VSMCs from at least 6 different developmental origins as indicated by the respective colours. Patches indicate a mixed origin. The developmental origin corresponding to each colour is denoted at the left. This figure is adapted from [320; 326; 327].*

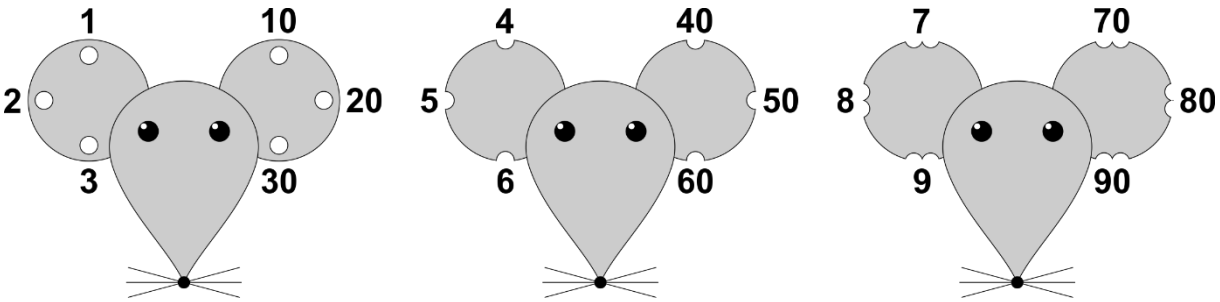

Supplementary figure II: *System for mouse numbering. Ears of mice were marked by punches as indicated in the figure. The numbers 1-99 were built by combination of one right ear (unit position) and one left ear (decade) mark (left ear + right ear = number). Complete punch (1-3/10-30, left), half punch (4-6/40-60, middle), double half punch (7-9/70-90, right).*

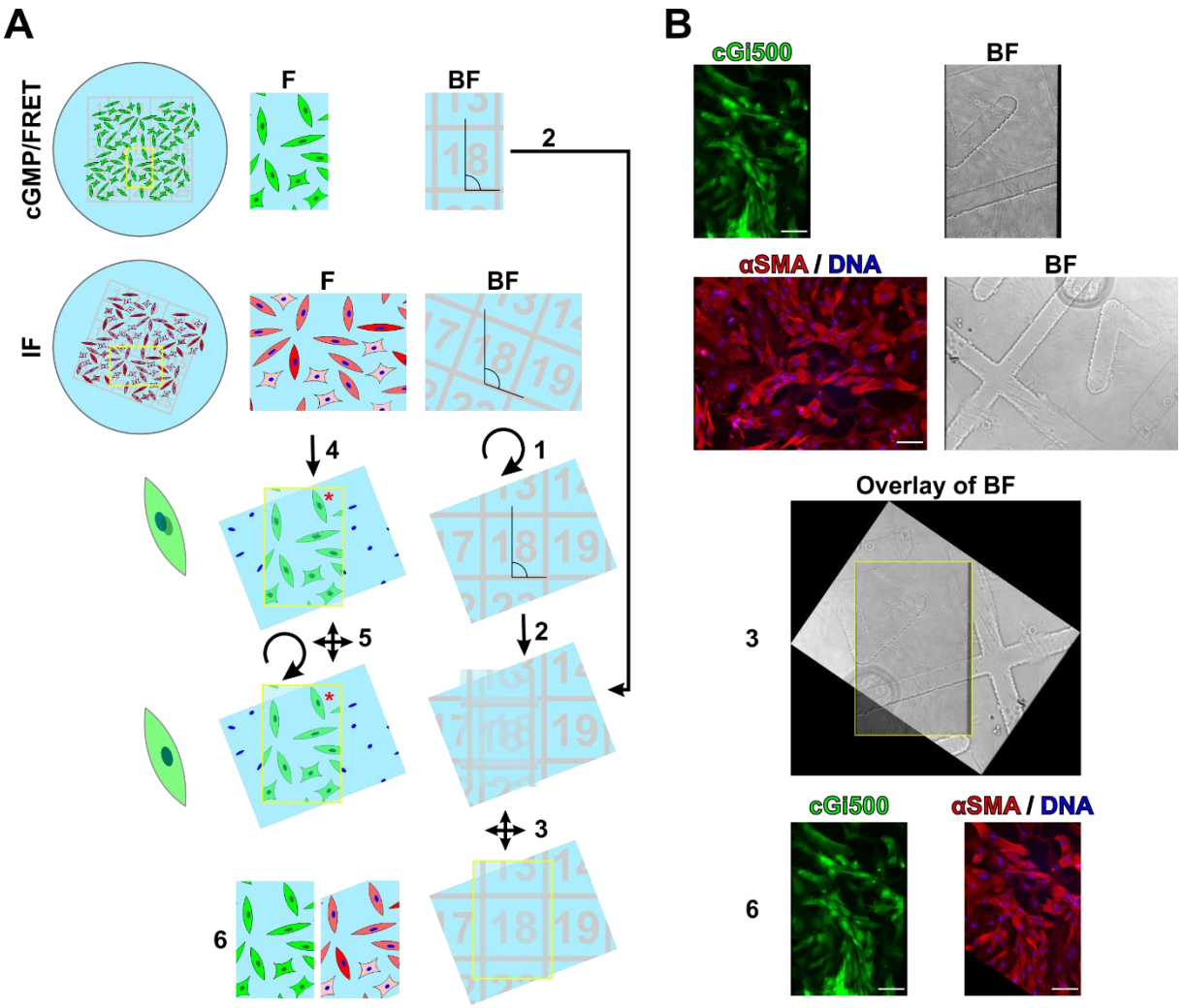

Supplementary figure III: Technical steps to correlate cells measured in cGMP/FRET measurements with the associated IF staining. *Schematic step by step explanation of the steps that were performed to identify cells that have been measured in cGMP/FRET measurements in the subsequent IF staining (A). Representation of Important steps with images from a cGMP/FRET measurement and subsequent IF staining (B). Steps 1-6 were performed after the cGMP/FRET measurements and documentation of the IF staining using FIJI.* ***A:*** *Before starting a cGMP/FRET measurement, cells were documented by their sensor fluorescence (F, snapshot) and their position on the coverslip was assessed with a brightfield (BF) image of the grid (top). After IF staining the same region was identified via the coordinates of the grid and an BF image of the grid as well as fluorescence images of the staining were acquired. (1) The angle of one grid line was determined in both BF images and the BF of the IF staining was*

rotated to match the angles. (2) A transparent overlay of both BF images was created and (3) the image of the cGMP/FRET measurement was moved until both grids matched (sharp non-blurry overlay). (4) The fluorescence image of the nuclear staining was rotated by the angle determined in 1 and the snapshot was pasted as a transparent overlay at the position determined in 3. The red asterisk marks the cell shown at the left as nucleus/snapshot overlay. (5) The coarse alignment performed in 1-3 was refined by small rotations of the fluorescence image and translation of the snapshot until the nuclear staining and the snapshot overlayed as good as possible. (6) The refined rotation angle was applied to the fluorescence images of all fluorophores (including the nuclear staining) and the images were cropped at the refined snapshot position. Now all cells of the IF staining were at the exact same position as the cells during the cGMP/FRET measurement. BF: brightfield, cGMP: 3',5'-cyclic guanosine monophosphate, F: fluorescence, FRET: Förster resonance energy transfer, IF: immunofluorescence. ***B:*** *Fluorescence and BF image of a cGMP/FRET measurement (YFP fluorescence of cGi500 is shown in green) with subsequent IF staining for αSMA (red) and DNA (blue) (top). Overlay of both BF images at the end of step 3 (middle). At the end of step 6 the positions of cells during the cGMP/FRET measurement matched the positions of the cells after IF staining (bottom). Scale bars are 100 µm. αSMA: α-smooth muscle actin, BF: brightfield, cGi500: cGMP indicator with an apparent EC_{50} of 500 nM, DNA: 2'-deoxyribonucleic acid.*

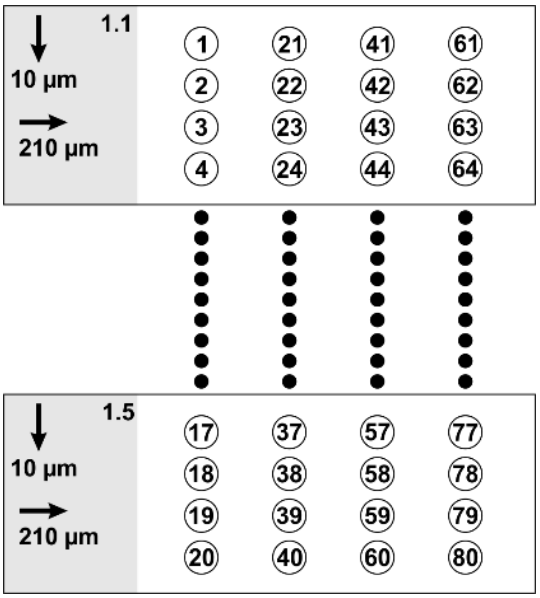

Supplementary figure IV: Order of paraffin sections in slide series. *Consecutive paraffin sections (10 µm thickness) were distributed across all slides of a series in columns. Each circle represents a section, the number indicates the cutting order. "1.1" indicates the first slide of series 1 and "1.5" the fifth slide of series 1. The distance between sections on each slide (20 sections per column, 5 slides per series) is indicated by arrows at the left.*

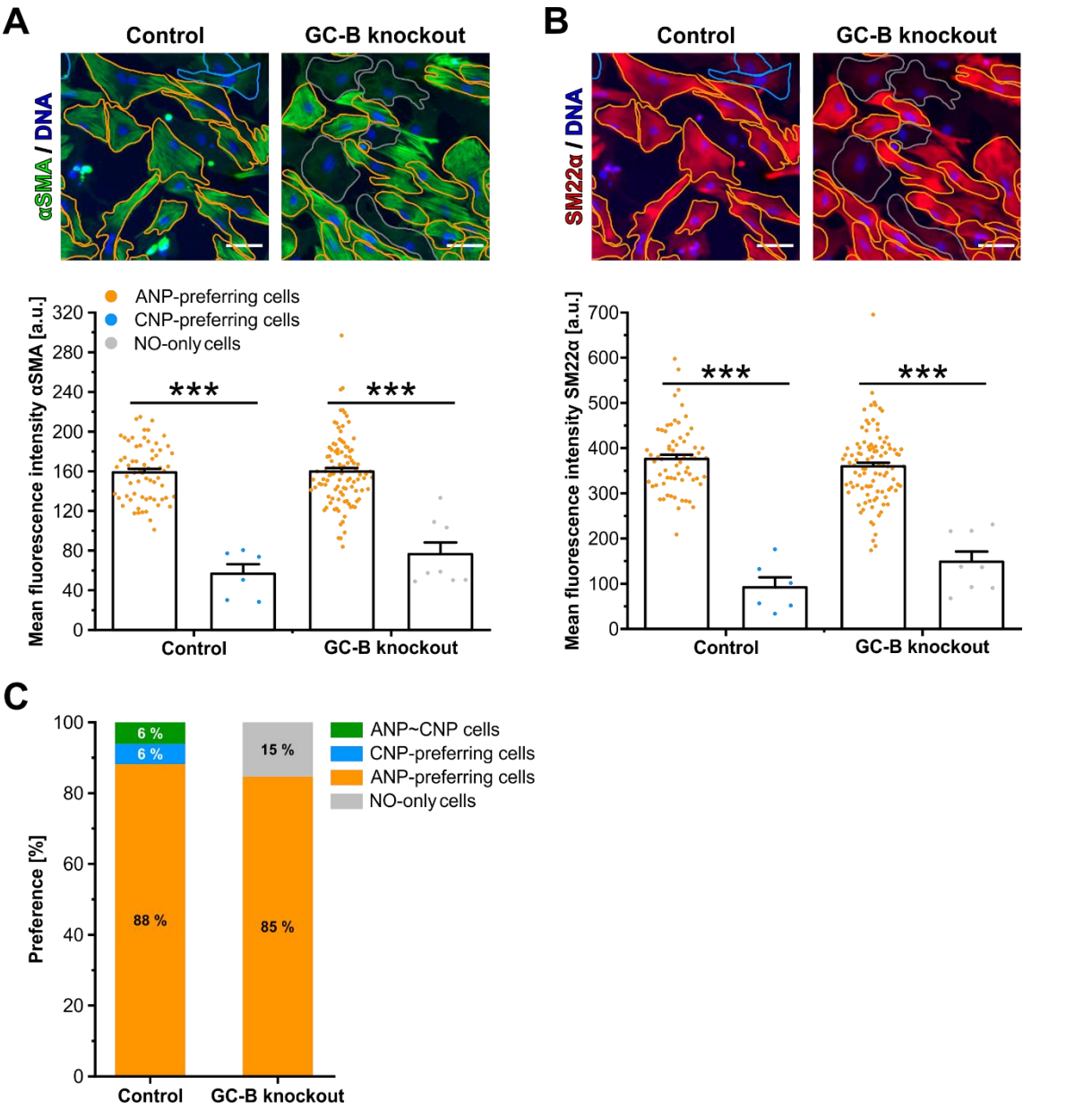

Supplementary figure V: NO-only cells from GC-B knockout mice resemble CNP-preferring cells from control mice. *Primary aortic VSMCs from control (cGi(L1) +/L1 x GC-B LacZ +/+) and GC-B knockout (cGi(L1) +/L1 x GC-B LacZ/LacZ) mice were cultured on gridded coverslips for 5 days, classified by their cGMP response patterns (FRET measurement) and subsequently analysed for αSMA (A) and SM22α (B) expression. The percentage of cells in each category was calculated and compared between control and GC-B knockout cultures (C).* ***A-B****: Analysis of αSMA (A) and SM22α (B) expression in ANP-preferring, CNP-preferring and NO-only cells from control and GC-B knockout mice by IF staining (double staining). Top: Representative image section after cGMP/FRET measurement and subsequent staining for αSMA (green), SM22α (red) and DNA (blue). The cGMP response patterns are indicated by the respective colour. Bottom: The expression of αSMA and SM22α (control: 71 cells, 1 coverslip, 1 mouse; GC-B knockout: 108 cells, 1 coverslip, 1 mouse) for ANP-preferring (orange), CNP-preferring (cyan) and NO-only (grey) cells is quantified. Each dot represents an individual VSMC. Data are represented as mean + SEM. Statistical significance is indicated by asterisks (*** p<.001). Scale bars are 50 µm.* ***C:*** *Bars indicate the fraction of cells in each category under each condition (cumulated numbers, no mean). Control (212 cells, 2 coverslips, 1 mouse), GC-B knockout (215 cells, 2 coverslips, 1 mouse).*

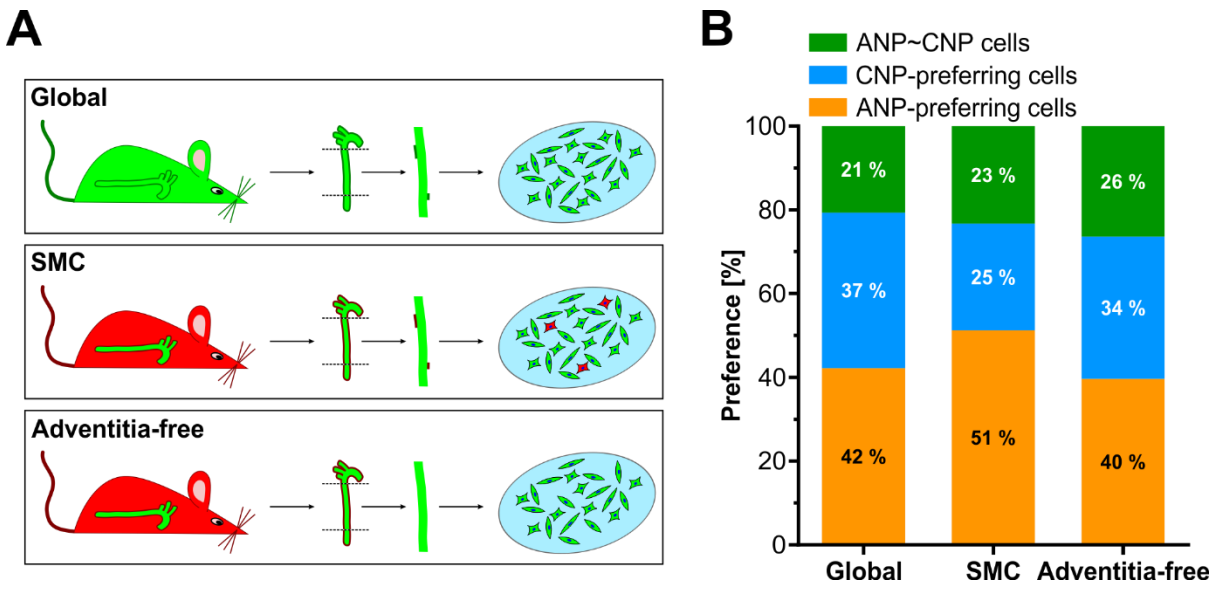

Supplementary figure VI: Overview of cGMP signalling patterns in primary aortic VSMCs. *Mouse models expressing the cGi500 biosensor under different conditions were used to ascertain that the cGMP signalling heterogeneity detected in VSMC cultures is not based on a heterogeneous cell origin. Primary aortic VSMCs from these mice (≤ 18 weeks) were cultured on glass coverslips and classified by their cGMP response patterns (FRET measurement). This figure summarises the results obtained in all experiments under "standard" conditions (e.g., primary VSMCs, 12-24 h serum starvation).* ***A:*** *Schematic representation of cell culture models shown in (B). Global: mice expressing cGi500 in all cells/tissues – SMC: mice expressing cGi500 in SMCs under the control of a constitutively active Cre (SM22-Cre) – Adventitia-free: mice expressing cGi500 in SMCs under the control of a constitutively active Cre (SM22-Cre). Enzymatic adventitia removal was applied before VSMCs were isolated from the aorta. Left: Expression of cGi500 in mice. The aorta is highlighted. Red indicates mTomato expression in non-recombined cells/tissues; green indicates expression of cGi500 in recombined cells/tissues. Middle: Expression of cGi500 in the intact aorta (left) and the cleaned part used for VSMC cultures (right). Dashed lines indicate the part that is used for isolation of VSMCs; solid lines surrounding the aorta indicate the adventitia; Right: Expression of cGi500 in primary cultured VSMCs directly before cGMP/FRET measurements. Spindle-shaped cells indicate contractile VSMCs; Cobblestone-shaped cells indicate modulated VSMCs or adventitia-derived cells; blue dots represent the nucleus; cyan circle represents the coverslip.* ***B:*** *Comparison of NP preference in primary aortic VSMC cultures described in (A). Bars indicate the fraction of cells in each category (cumulated numbers, no mean). Global (2440 cells, 45 coverslips, 43 mice) – SMC (373 cells, 17 coverslips, 10 mice) – Adventitia-free (53 cells, 4 coverslips, 3 mice).*

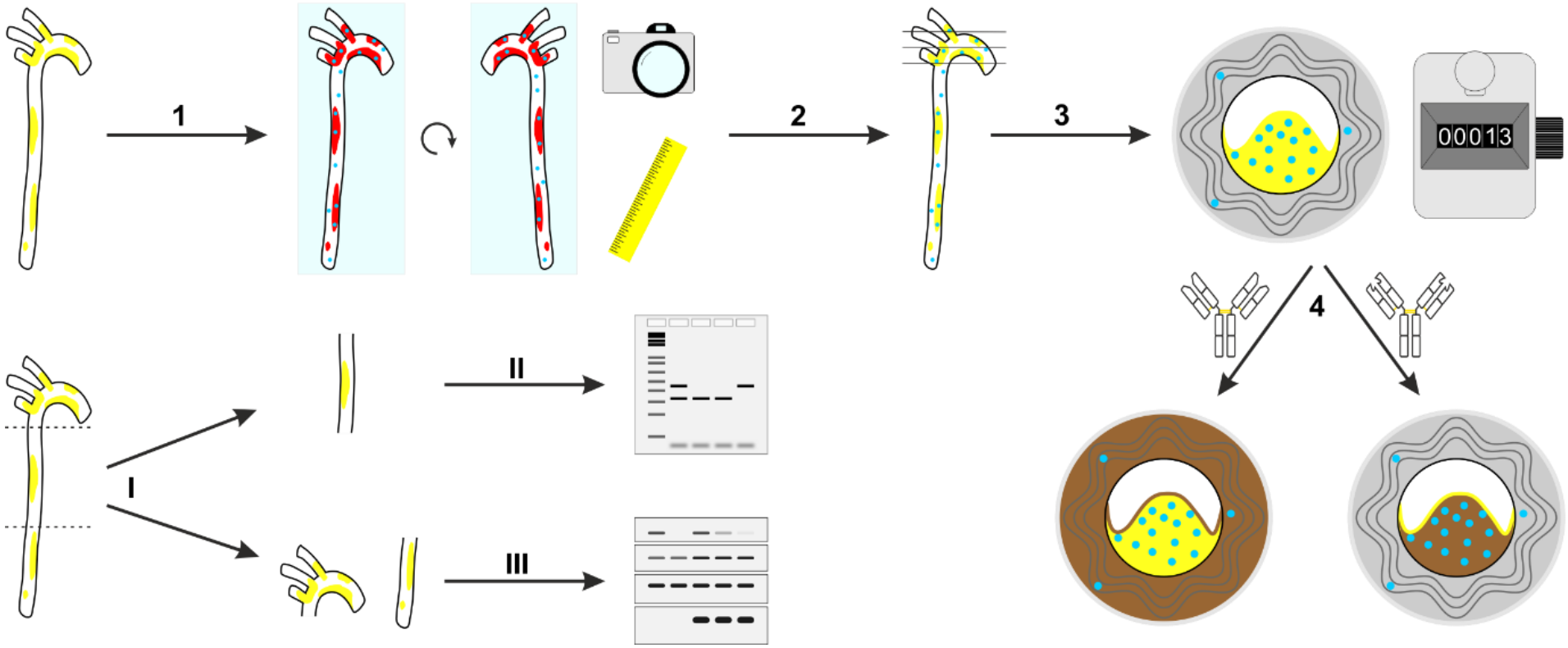

Supplementary figure VII: Experimental design to analyse the role of GC-B expression in VSMCs for atherosclerosis. *SMC-selective GC-B knockout and control mice were bred on an ApoE-deficient background to assess the effect of GC-B-dependent cGMP signalling in VSMCs on atherosclerosis development. After induction of atherosclerosis by an atherogenic diet, plaque size (1) was determined in whole mounts. Paraffin sections of the aortic arch were prepared (2) and the enrichment with GC-B LacZ reporter cells (3) was assessed. Plaque structure was analysed by IHC stainings (4). For some aortas the plaque rich parts were separated from the less enriched parts (I). The SMC-selective knockout was verified by PCR (II) and western blotting (III). Yellow: unstained plaques – red: Oil Red O-stained plaques – brown: IHC-stained area – blue: X-gal-stained nuclei – light blue: glass slide for immobilisation – white/grey: non-plaque tissue – thin grey lines: sections – y-shaped symbol: antibodies.*

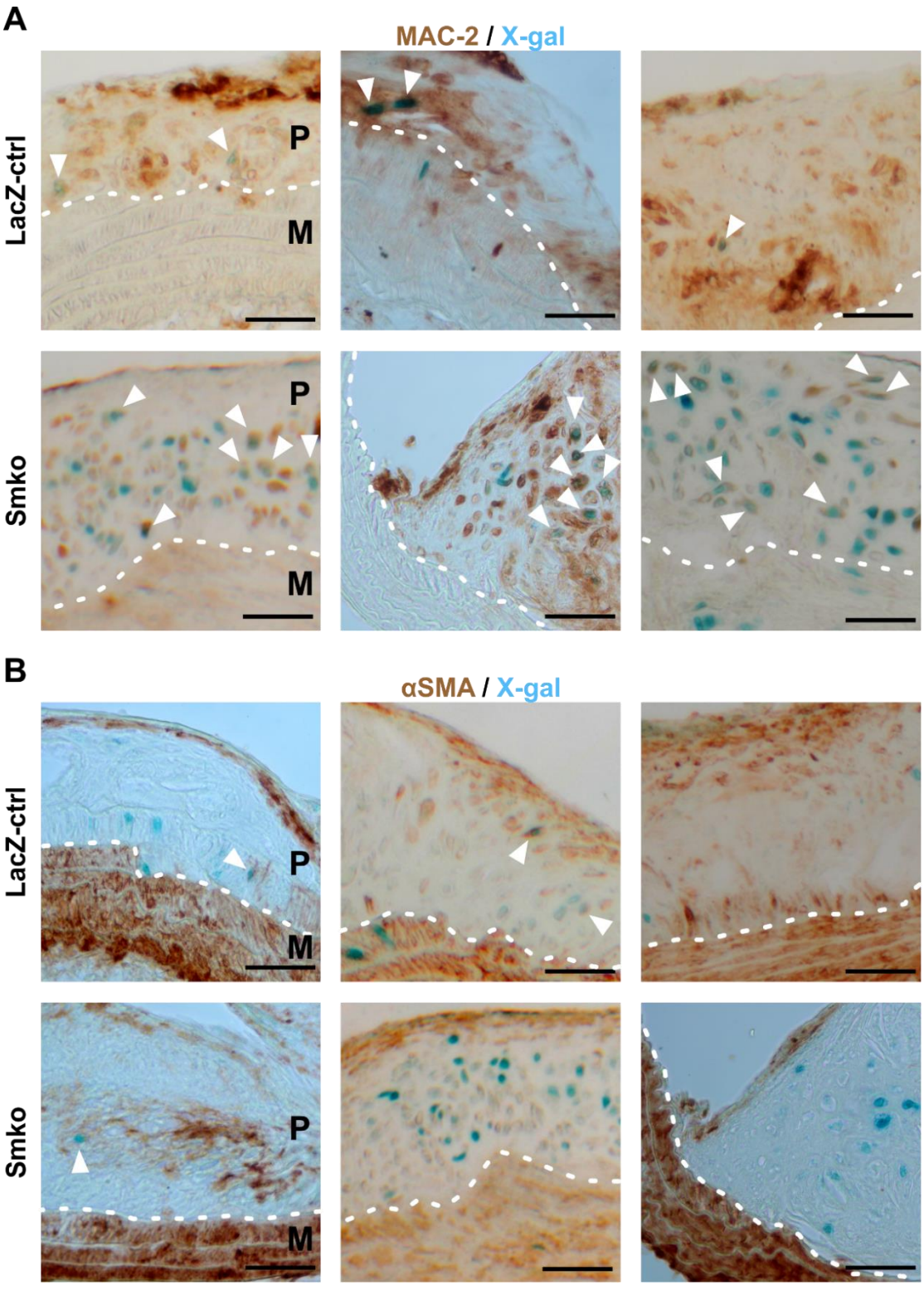

Supplementary figure VIII: X-gal+ cells in atherosclerotic plaques of GC-B LacZ reporter mice (LacZ-ctrl, Smko) were frequently positive for MAC-2 but rarely for αSMA as indicated by IHC stainings. *To characterise potentially modulated/transdifferentiated GC-B-expressing VSMC-derived cells in atherosclerotic plaques, GC-B LacZ reporter mice (Smko, LacZ-ctrl) mice were bred on an ApoE-deficient background. After SMC-selective GC-B ablation by tamoxifen injection, mice were fed an atherogenic diet for 18 weeks to develop atherosclerotic plaques and GC-B LacZ reporter positive (X-gal+) cells were visualised via X-gal staining. Sections of the atherosclerotic aortic arch were stained for MAC-2 (marker for macrophage-like cells, A) and αSMA (marker for contractile and fibrous cap VSMCs, B) by IHC.* ***A-B:*** *Exemplary images of IHC stainings for MAC-2 (**A**) and αSMA*

*(**B**) in plaque sections from LacZ-ctrl (top) and Smko (bottom) mice. Genotype is indicated at the left. The border between plaque and media is indicated by a dashed white line. All images are oriented with the plaque facing top and the media facing bottom. MAC-2+ area appeared brown. Blue staining indicated nuclei of GC-B LacZ reporter (X-gal+) cells. White arrowheads indicate MAC-2/X-gal (A) and αSMA/X-gal (B) double positive cells, respectively. P: plaque, M: media. Scale bars are 50 µm. Plaque sections from 3 Smko and 2 LacZ-ctrl mice are shown.*

7.2 Supplementary tables

Supplementary table I: Common reagents and their brand.

Reagent	Company	Reagent	Company
Acetic acid	Sigma-Aldrich	$K_4Fe(CN)_6$	Roth
Bromophenol blue	Roth	KH_2PO_4	Roth
$CaCl_2$	Roth	Methanol	Sigma-Aldrich
D-glucose	Fisher	$MgCl_2$•6 H_2O	Roth
Dimethyl sulfoxide	Roth	NaCl	Roth
EDTA•2 H_2O	Roth	Na_2HPO_4•2 H_2O	Roth
Ethanol	Sigma-Aldrich	Na L-glutamate•H_2O	Merck
Glutardialdehyde (25 %)	Roth	NaOH (pellets)	Roth
Glycerol	Roth	SDS	Roth
HCl (37 %)	Roth	Toluene	Roth
HEPES	Roth	Tris (Trizma base)	Sigma-Aldrich
Hoechst No. 33258	Sigma-Aldrich	Tween-20	Roth
KCl	Sigma-Aldrich	Xylene cyanol	Roth
$K_3Fe(CN)_6$	Merck		

Supplementary table II: Common compounds and their brand. *The catalogue (#) and/or Lot number are indicated in parentheses.*

Compound	Company	Compound	Company
ANP (1-28, #1912)	Tocris	Milk powder (#T145.2)	Roth
BSA (#8076.4)	Roth	NDS (#S30-100ML)	Millipore
CNP (1-22, #3520)	Tocris	NGS (#S26-100ML)	Millipore
DEA/NO (#ALX-430-034-M010)	Axxora	Tamoxifen (#T5648-1G)	Sigma-Aldrich
FCS (#10270106, Lot-41G6601K)	Gibco	X-gal (#15520018)	Invitrogen

Supplementary table III: Brand names and the companies they belong to.

Brand name	Company
A. Hartenstein	A. Hartenstein GmbH, Würzburg, Germany
Abcam	Abcam plc, Cambridge, MA, USA
AHF	AHF analysentechnik AG, Tübingen, Germany
Allied Vision	Allied Vision Technologies GmbH, Stadtroda, Germany
Altromin	Altromin Spezialfutter GmbH & Co. KG, Lage, Germany
Avantor	VWR International GmbH, Darmstadt, Germany
Axxora	Enzo Biochem Inc., Farmingdale, NY, USA
B. Braun	B. Braun Melsungen AG, Melsungen, Germany
Bio-Rad	Bio-Rad Laboratories Inc., Hercules, CA, USA
Biologix	Biologix Group Ltd., Jinan, Shandong, China
Biometra	Analytik Jena AG, Jena, Germany
Bioron	Bioron GmbH, Römerberg, Germany
Biozym	Biozym Scientific GmbH, Hessisch Oldendorf, Germany
Canon	Canon Deutschland GmbH, Krefeld, Germany
Cedarlane	Cedarlane, Burlington, ON, Canada
Cell Signaling	Cell Signaing Technology Inc., Danvers, MA, USA
ChemSolute	Th. Geyer GmbH & Co. KG, Renningen, Germany
Chroma	Chroma Technology Corp., Bellows Falls, VT, USA
Dianova	Biozol Diagnostica Vertrieb GmbH, Eching, Germany
Dow	Dow Europe GmbH, Wiesbaden, Germany
Dunnlab	Dunn Labortechnik GmbH, Asbach, Germany
Entosphinx	Ento sphinx s.r.o., Pardubice, Czech Republic
F•S•T	Fine Science Tools Inc., Foster City, CA, USA
Fisher	Thermo Fisher Scientific Inc., Waltham, MA, USA
GE Healthcare	General Electric Corp., Chicago, IL, USA
Genaxxon	Genaxxon bioscience GmbH, Ulm, Germany
Gibco	Thermo Fisher Scientific Inc., Waltham, MA, USA
Invitrogen	Thermo Fisher Scientific Inc., Waltham, MA, USA
KNF Neuberger	KNF Neuberger GmbH, Freiburg im Breisgau, Germany
Leica	Leica Biosystems GmbH, Wetzlar, Germany
Life Technologies	Thermo Fisher Scientific Inc., Waltham, MA, USA
Obermeier	Kurt Obermeier GmbH & Co. KG, Bad-Berleburg, Germany
Macherey-Nagel	Macherey-Nagel GmbH & Co. KG, Düren, Germany
Maybelline	L'Oréal S.A., Clichy, France
Menzel	Thermo Fisher Scientific Inc., Waltham, MA, USA
Merck	Merck KGaA, Darmstadt, Germany

Brand name	Company
Microm	PHC Holding Corp., Dreieich, Germany
Millipore	Merck KGaA, Darmstadt, Germany
MP Biomedicals	MP Biomedicals LLC, Santa Ana, CA, USA
Nippon Genetics	Nippon Genetics Co. Ltd., Bunkyo-ku, Tokyo, Japan
Photometrics	Teledyne Photometrics Inc., Tucson, AZ, USA
QImaging	QImaging Corp., Surrey, BC, Canada
Roche	F. Hoffmann-La Roche AG, Basel, Switzerland
Roth	Carl Roth GmbH & Co. KG, Karlsruhe, Germany
Saint-Gobain	Compagnie de Saint-Gobain, Courbevoie, France
Schott	Schott AG, Mainz, Germany
Sigma-Aldrich	Merck KGaA, Darmstadt, Germany
Science Services	Science Services GmbH, München, Germany
Simport	Simport Scientific Inc., Bernard-Pilon Beloeil, QC, Canada
SPOT Imaging	Diagnostic Instruments Inc., Sterling Heights, MI, USA
ssniff	ssniff Spezialdiäten GmbH, Soest, Germany
Thermo	Thermo Fisher Scientific Inc., Waltham, MA, USA
Thomy	Nestlé S.A., Vevey, Switzerland
TILL Photonics	TILL Photonics GmbH, Gräfeling, Germany
Tocris	Bio-Techne Corp., Minneapolis, MN, USA
Ushio	Ushio Europe B.V., BD Oude Meer, The Netherlands
Vector Labs	Vector Laboratories Inc., Burlingame, CA, USA
Visitron	Visitron Systems GmbH, Puchheim, Germany
Warner Instruments	Harvard Bioscience Inc., Hamden, CT, USA
Yokogawa	Yokogawa Electric Corp., Musashino, Tokyo, Japan
ZEISS	Carl Zeiss AG, Oberkochen, Germany

Supplementary table IV: Common antibodies and their dilutions. *WB: Western blot; IHC: Immunohistochemistry; IF: Immunofluorescence.*

Antibody	Company	Dilution	Source
αSMA	A2547 Sigma-Aldrich	1:500 IF	Mouse
αSMA	ab124964 Abcam	1:2000 IHC	Rabbit
cGKI (DH)	AG Feil	1:5000 WB	Rabbit
FSP 1	07-2274 Millipore	1:300 IF	Rabbit
GAPDH	2118 Cell Signaling	1:1000 WB	Rabbit
GC-B	Donation Hannes Schmidt	1:5000 WB	Guinea pig
Mac-2	Cl8942 Cedarlane	1:200 IHC	Rat
NO-GC β1 1A	Donation Andreas Friebe	1:800 IF	Rabbit
NO-GC β1 2A	Donation Andreas Friebe	1:10 000 WB	Rabbit
PDGFRα	3174 Cell Signaling	1:500 IF	Rabbit
SM22α	ab14106 Abcam	1:1000 WB 1:500 IF	Rabbit
α-mouse Alx488	A11029 Life Technologies	1:500 IF	Goat
α-mouse Alx555	A21424 Life Technologies	1:500 IF	Goat
α-rabbit Alx488	A11008 Life Technologies	1:500 IF	Goat
α-rabbit Alx555	A21428 Life Technologies	1:500 IF	Goat
α-guinea pig HRP	706-035-148 Dianova	1:10 000 WB	Donkey
α-rabbit HRP	70749 Cell Signaling	1:5000 WB	Goat
α-rabbit biotinylated	BA-1000 Vector Labs	1:250 IHC	Goat
α-rat biotinylated	BA-4001 Vector Labs	1:250 IHC	Rabbit

Supplementary table V: PCR primer

Primer	Sequence (5' → 3')
Cre800	GCTGCCACGACCAAGTGACAGCAATG
Cre1200	GTAGTTATTCGGATCATCAGCTACAC
BB01	CTCTGCTGCCTCCTGGCTTCT
BB02	CGAGGCGGATCACAAGCAATA
BB03	TCAATGGGCGGGGGTCGTT
BB22	TGCCACCCTATCCTTAGTCC
BB23	GTGTTCTGGCAGCACCAC
BB24	TCGCTATTACGCCAGCTG
BB27	GCCACTTTTGCACCCGGATG
BB29	CCTGCTTTGATGCCATTATCG
BB30	CTGCAACAACCAAAGCTCAG
RF115	GCCTAGCCGAGGGAGAGCCG
RF117	GCCGCCCCGACTGCATCT
RF151	AGTTCTTGTGTGACTTGGGAG

Supplementary table VI: PCR programs

Mouse line	Primer (volume)		Product size		PCR program		
SM22-Cre αSMA-CreER^{T2}	Cre800 Cre1200	(0.25 µL) (0.25 µL)	tg +	402 bp none	95 °C 95 °C 58 °C 72 °C 72 °C	5 min 10 sec 30 sec 30 sec 5 min	 35x
cGi(L1) cGi(L2)	BB01 BB02 BB03	(0.3 µL) (0.3 µL) (0.3 µL)	+ L1 L2	330 bp 250 bp 250 bp	95 °C 95 °C 61 °C 72 °C 72 °C	5 min 10 sec 30 sec 30 sec 5 min	 35x
GC-B LacZ	BB22 BB23 BB24	(0.25 µL) (0.25 µL) (0.25 µL)	LacZ +	398 bp 348 bp	94 °C 94 °C 57 °C 72 °C 72 °C	3 min 30 sec 30 sec 30 sec 10 min	 35x
GC-B flox	BB27 BB29 BB30	(0.3 µL) (0.3 µL) (0.3 µL)	L2 + L1	684 bp 506 bp 448 bp	94 °C 94 °C 59 °C 72 °C 72 °C	3 min 30 sec 30 sec 45 sec 5 min	 35x
ApoE	RF115 RF117 RF151	(0.3 µL) (0.075 µL) (0.3 µL)	- +	245 bp 163 bp	95 °C 95 °C 65 °C 72 °C 72 °C	5 min 10 sec 30 sec 30 sec 5 min	 35x

Supplementary table VII: *Summary of cGMP signalling patterns from all ex vivo cGMP/FRET measurements. All cGMP signalling patterns that were measured in healthy arteries (pooled from aorta and branching vessels, see* ***Figure 17 B*** *for a representative measurement) and atherosclerotic plaques (pooled from control and GC-B LacZ reporter mice, see* ***Figure 18 B*** *and* ***C*** *for representative measurements, respectively) are summarised. The cGMP signalling patterns indicate to which stimuli (CNP, ANP, NO) a cGMP/FRET response was detected within the same region/cell. Only cGMP/FRET signals that were verified by clear antiparallel development of CFP (F480) and YFP (F535) fluorescence were included. For instance, the cGMP signalling pattern "ANP – NO" includes regions/cells that reacted as shown in* ***Figure 17 B (top)*** *and "NO" includes regions/cells that reacted as shown in* ***Figure 17 B (bottom)****. If a region/cell reacted to at least one of the three stimuli (e.g., ANP) but it was unclear whether or not it reacted to the other stimuli (e.g., CNP or NO), it was defined as "unclear response pattern".*

cGMP signalling pattern	**Healthy arteries [% of analysed regions]**	**Atherosclerotic plaques [% of analysed regions]**
CNP	0.0 %	**4.1 %**
CNP – ANP	0.0 %	**7.8 %**
CNP – ANP – NO	0.0 %	**21.8 %**
CNP – NO	**0.4 %**	**4.1 %**
ANP	**10.5 %**	**15 %**
ANP – NO	**48.5 %**	**16.1 %**
NO	**31.7 %**	**11.9 %**
Unclear response pattern	**8.9 %**	**19.2 %**
Total regions analysed	515	193

7.3 Extended methods

7.3.1 Calculation of cGMP/FRET ratios

1. Correct fluorescence signals of cells for background artefacts (excitation light, environment light, etc.).

$$\bar{F}_{480_t} corrected = \bar{F}_{480}(ROI)_t - \bar{F}_{480}(background)_t$$
$$\bar{F}_{535_t} corrected = \bar{F}_{535}(ROI)_t - \bar{F}_{535}(background)_t$$

2. Calculate the $\bar{F}_{480}/\bar{F}_{535}$ ratio as an indicator for [cGMP].

$$\bar{R}_t = \frac{\bar{F}_{480_t} corrected}{\bar{F}_{535_t} corrected}$$

3. Normalise ratio and single traces to baseline (signal before first drug application).

$$\bar{R}_{baseline} = \sum_{t=0}^{t1} \bar{R}_t$$
$$R\ (\sim[cGMP]) = \frac{\bar{R}_t - \bar{R}_{baseline}}{\bar{R}_{baseline}} \times 100\ [\%] = \frac{\Delta \bar{R}_t}{\bar{R}_{baseline}} \times 100\ [\%]$$

t: time point within the measurement (each image represents one time point)
$\bar{F}_{480/535_t}$**:** mean fluorescence intensity in the CFP (480) or YFP (535) channel at the indicated time point
$\bar{R}$**:** ratio of CFP/YFP fluorescence (inverse of FRET)
$\bar{R}_{baseline}$**:** mean ratio of the baseline
t1: last time point of the baseline (usually the first 30 images = 150 s of a measurement are taken)

7.3.2 Semi-automatic quantification of cGMP/FRET responses with Origin Pro

1. Plot cGMP/FRET ratio traces together with drug applications into separate graphs (Script: PlotRatios.ogs) using Origin. Choose traces of cells that reacted to all stimuli and set up baseline correction with "Peak Analyzer". Choose an exponential function for baseline correction. Place two anchor points at the beginning and end of the trace and one anchor point between each signal. Choose "snap to spectrum" to place anchor points to actual data points of the ratio trace. This is necessary for batch processing of all traces. Use the preview function to verify that the baseline is corrected properly. Select to overwrite the original data. Safe settings and test with 2-3 further traces (adjust settings if necessary). Perform baseline correction by batch processing with all signals. If no exponential function can be used for baseline correction, choose "Interpolation". In this case the baseline correction is performed without batch processing.
   Inspect all corrected traces (ignore "na" cells) to verify that baseline correction worked properly. If it did not work for single cells, replace the trace by the original one and adjust parameters for this cell individually.
2. Smooth ratio traces using a custom script (Script: BatchSmoothAndPlot.ogs). This script uses the "Loess" function to smooth ratio traces and plots the smoothed traces on top of the original one. The "span" option of this function is adjusted for every measurement to achieve proper smoothing. Values close to 1 lead to extreme smoothing (signals are cut off) and values

close to 0 lead to noisy signals. The "span" is usually set to a value between 0.03 and 0.07. Use the preview function to optimise the value with 2-3 exemplary traces. Note value for the measurement and run script.
Inspect the overlay of smoothed and original trace to verify that the smoothed function follows the ratio trace.

3. Use "Peak Analyzer" to determine the peak height of all signals. Choose a ratio trace (not smoothed) of a cell that responded to all stimuli. Mark the beginning, centre, and end of each signal in the "Peak Analyzer". Choose peak centre and height as output and safe settings. Select all smoothed ratio traces and use batch analysis to determine all peak heights and centres.
4. Split heights and centres (Script: SplitHeightCenter.ogs) to individual sheets. Copy peak heights to an evaluation template in MS Excel. This template assigns the NP preference based on the response pattern of the respective cell.
Plot the peak centres into the ratio traces. Inspect every trace to verify that the centre matches the maximum of the peak. If it failed, assess the peak height manually and correct the value in the evaluation sheet. Also set values to "0" where no (validated) signal was elicited by a stimulus.

7.3.3 Semi-automatic quantification of IHC-stained area in histological sections of atherosclerotic plaques

1. Open an image of a section stained by IHC with Fiji. Set scale to 3.36 pixel/µm (5x objective, 2.5x mount). Use "enhance contrast" function to improve visibility of the plaque structure.
2. Use a polygon selection to mark the plaque and its cap region:
    a. Start at the luminal side of the plaque and follow the plaque until it merges with the media. Find the elastin fibre (not stained) that is not disrupted and closest to the luminal side. Follow this fibre to mark the inner border of the plaque. Close the selection, add as ROI and label as **"plaque 1"**.
    b. The cap is defined as the 30 µm luminal layer of the plaque. Duplicate the "plaque 1" ROI, change line thickness to 60 µm and change colour of this ROI. Check "Show all" and uncheck "Label". Now the inner border of the line is exactly 30 µm away from the border of the plaque (it is extended 30 µm in each direction). Use a polygon selection to draw a ROI along the inner border of this ROI until the media is reached. Continue the ROI at the luminal side. It does not need to follow the plaque border, but the complete cap must be enclosed in this ROI. Select this ROI and the ROI "plaque 1". Use "AND" to combine both ROIs to a new selection. Add selection as ROI and label **"cap 1"**. By using "AND", the cross section of both ROIs is created as selection. As the new ROI defines the inner border of the fibrous cap and the "plaque 1" ROI the outer border of the plaque, the cross section contains the complete cap.
    c. Repeat **(a)-(b)** with all plaques of the section. Save all **"plaque"** and **"cap"** ROIs and discard the rest. These ROIs will be used to quantify the total plaque and cap area, respectively (step **13**).
3. Process all stainings as described above.

Second, the parameters to semi-automatically mark the IHC+ area are determined.

4. Open 6-8 images of an IHC staining and the negative control in Fiji. Place a circular ROI in a tissue free region of the first image (the more central the better). Use the BIOP SimpleColorBalance plugin to perform a white balance of the image. Continue with the next image until all images are processed. This step is necessary for successful performance of the next step.
5. Use Fiji's "Color deconvolution" and select "H DAB". Fiji splits the image in a "haematoxylin" and a "DAB" channel. As no "haematoxylin" staining is performed, these images can be

discarded. The “DAB” channel contains the IHC-stained area (+ background) only as a “grey scale” image and can therefore be easily thresholded. Repeat this step with all open images.

6. Use the “Threshold” function to apply a threshold to the deconvoluted images:
    a. Select “Threshold” and use “Autothreshold” to get good starting parameters. Set the lower limit to “0” (the darkest value refers to the most intense staining). Adjust the upper limit until only IHC+ area is visible. It can be difficult to decide this in the deconvoluted images. Therefore, use the non-deconvoluted image and the negative control as reference. Note down the upper limit.
    b. Repeat step **(a)** with all deconvoluted images and take the previous upper limit as reference. Compare all upper limits. They should be similar. Chose a value in this range and test it on all images. If it is acceptable, verify this value with the negative control.
    c. Note the limits of the threshold, e.g., “0-185”.

Third, the parameters for the threshold are used to mark the IHC+ area with ROIs. All images are processed sequentially.

7. Open an IHC staining image in Fiji and perform steps **(5)-(6)**. For step **(6)** directly use the limits noted in **(6c)**.
8. Use the “Analyze Particles” to assess the stained area automatically. This function must be used several times to exclude holes within the staining and to include stained parts within these holes. The standard settings are: Size (pixel^2): 0-Infinity | Circularity: 0-1 | Show: Nothing | Add to Manager: checked. Additional settings must be included for some of the repetitions and are indicated accordingly:
    a. “Analyze particles” and select all ROIs in the ROI manager. Combine ROIs with “OR”, add combined ROI and label it **“area1”**. This will mark all stained area, including “holes” within the staining. Delete separate ROIs.
    b. Invert image and “Analyze particles” with the additional option “Exclude on edges” checked. Combine ROIs with “OR” as **“holes1”**. This will mark the holes within the stained area. Delete separate ROIs. It is important to select “exclude on edges” in this step only. Otherwise, unstained area touching the edge of the image will be included as stained area later.
    c. Invert image, select “holes1” and repeat step **(a)**. This will mark all stained area within the holes. Label the new ROI as **“area2”**. If nothing is selected (no staining within holes), continue with step **(e)**.
    d. Invert image, select “area2” and “Analyze particles”. Combine ROIs with “OR” as **“holes2”**. This will mark the holes within the inner stained area. Delete separate ROIs. If nothing is selected (no holes in the inner stained area), skip step **(f)** later. Invert image to restore the initial threshold image.
    e. Combine “area1” and “holes1” with “XOR” as **“staining1”**. This will exclude the holes from the stained area.
    f. Combine “area2” and “holes2” with “XOR” as **“staining2”**. This will exclude the holes from the inner stained area. If no “holes2” exist, use “area2” instead of “staining2” in the next step.
    g. Combine “staining1” and “staining2” with “OR” as **“IHC_staining”**. Discard all other ROIs and save. This ROI should contain only the stained area. For verification, choose a fill colour for the ROI and show in the original image. All stained area should be concealed by this ROI.
9. Repeat this procedure **(7)-(8)** with all images of stainings that were performed and recorded in parallel.

Fourth, the ROIs defining the plaque area are used to mark the IHC+ area in the plaque/cap only.

10. Open an image and the respective ROI sets created in step **(2)** (plaque/cap area) and in step **(8)** (IHC+ area). Combine “plaque 1” and “IHC_staining” as **“IHC_plaque 1”**. Combine “cap 1” and “IHC_staining” as **“IHC_cap 1”**. These ROIs mark the stained area within the plaque/cap only.
11. Repeat step (10) until all plaques of the given section are processed and save ROIs.
12. Repeat this procedure **(10)-(11)** with all images

Last, the IHC+ area is quantified and normalised to the plaque/cap area.

13. Open an image and the respective ROI set created in steps **(2) and (10)**. Set scale to 3.36 pixel/µm (5x objective, 2.5x mount). Select all ROIs (“plaque”, “cap”, “IHC plaque”, “IHC cap”) and use “Multi measure” to quantify the area of all ROIs and export data.
14. Import areas in MS Excel and calculate IHC+ area of the “core” and the total area of the “core”**.** This is exemplarily shown for the total area:

$$total\ area_{core}\ [\mu m^2\ ] = total\ area_{plaque}\ [\mu m^2\ ] - \ \ total\ area_{cap}\ [\mu m^2]$$

15. Normalise the IHC+ area to the total area of the respective structure. Below the calculation for the IHC+ cap area is described exemplarily. The calculations for the “complete plaque” and the “core” are performed accordingly.

$$IHC - positive\ area\ (cap)[\%] = \frac{IHC - positive\ area(cap)[\mu m^2]}{total\ area(cap)\ [\mu m^2]} \times 100\ [\%]$$

Own Publications

The presented work has contributed to the following publications:

Lehners, M., Feil, S., Schmidt, H. & Feil, R. CNP/GC-B-dependent cGMP signalling in VSMCs – a novel marker and antagonist of modulated VSMCs in atherosclerotic plaque development. *In preparation.*

Feil, R., Lehners, M., Stehle, D., & Feil, S. (2021). Visualising and understanding cGMP signals in the cardiovascular system. *Br J Pharmacol,* doi:10.1111/bph.15500

Lehners, M., Dobrowinski, H., Feil, S., & Feil, R. (2018). cGMP signaling and vascular smooth muscle cell plasticity. *J Cardiovasc Dev Dis, 5*(2), 20. doi:10.3390/jcdd5020020

The author has also presented his work on the following conferences:

Lehners, M. cGMP Signaling: Now Live and in Color. *Mini Symposium on "Live (and High-Resolution) Cell Imaging"*, Tübingen, July 2019

Dobrowinski, H., Lehners, M., Friebe, A., Feil, S., Feil, R. Regulation of VSMC growth and atherosclerosis by cGMP and fibronectin. *9th International Conference on cGMP Generators, Effectors and Therapeutic Implications,* Mainz, June 2019

Wolters, M., Lehners, M., Feil, R.: Watching cGMP signalling live and in colour. 70th *Mosbacher Kolloquium - High-Resolution Imaging of Cells and Molecules,* Mosbach, April 2019

Dobrowinski, H., Lehners, M., Michael, P., Schmidt, H., Feil, R. Shedding light on CNP-responsive vascular smooth muscle cells. *8th International Conference on cGMP Generators, Effectors and Therapeutic Implications,* Bamberg, June 2017

Lehners, M., Dobrowinski, H., Krämer, M., Stehle, D., Thunemann, M., Feil, R. (2015). Correlation of vascular smooth muscle cell phenotype and cGMP signalling. *7th International Conference on cGMP Generators, Effectors and Therapeutic Implications,* Trier, June 2015

Dobrowinski, H., Lehners, M., Kraemer, M., Thunemann, M., Feil, R. (2015). cGMP signaling and phenotypic modulation of vascular smooth muscle cells. *81st Annual Congress of the German Society for Experimental and Clinical Pharmacology and Toxicology,* Kiel, March 2015

Acknowledgements

First, I want to express my gratitude to Prof. Dr. Robert Feil, for giving me the opportunity to perform my doctoral thesis in his laboratory. I am very grateful for his and Dr. Susanne Feil's long-lasting and ongoing support, the excellent supervision, and the many scientific discussions.

Many thanks to all the people that contributed to this work. I thank Dr. Hyazinth Dobrowinski for the successful cooperations and Dr. Michael Paolillo for helping me establish *ex vivo* cGMP/FRET measurements in healthy arteries. Thank you Daniel Stehle and Michael Krämer for your early contributions while you were still Masters's students. Thank you Malte Roessing for your help in analysing data of atherosclerotic mice. Thank you, Maria T. Kristina Zaldivia PhD and Katrin Strobel for your valuable contributions to my experiments even though the data did not make it into this work.

I also want to acknowledge Prof. Dr. med. Andreas Peter in the "Zentrallabor des Universitätsklinikums Tübingen" for analysing the blood samples of atherosclerotic mice. Thank you, PD Dr. Hannes Schmidt (Eberhard Karls Universität Tübingen) and Prof. Dr. Andreas Friebe (Julius-Maximilians-Universität Würzburg) for providing antibodies and mice.

For her excellent technical assistance, I thank Barbara Birk. And for their support in the animal facility, I thank Dr. Susanne Feil, and all former and present animal care takers.

Thank you, past and present members of the Feil laboratory for all the interesting scientific and non-scientific discussions and for making me feel at home in this group. In particular, thank you Dr. Angelos Vachaviolos, Dr. Hyazinth Dobrowinski, Dr. Michael Paolillo, Daniel Stehle, and Michael Krämer for the many out-of-lab activities together. Thank you, Stefanie Peters, for all the bicycle tours which were sometimes longer than expected and thank you, PD Dr. Hannes Schmidt for broadening my cultural horizon, especially towards the east.

Thanks goes to Dr. Claus Lehners, Dr. Michael Paolillo, Dr. Susanne Feil, and Daniel Stehle for reading and commenting on my work.

Finally, I want to thank my mother Dr. Gudrun Lehners and my father Dr. Claus Lehners, who supported me a lot in the past months. Many thanks to all my friends and my family that made my time as a PhD student a great time.